T.R.
BOLU ABANT İZZET BAYSAL UNIVERSITY
INSTITUTE OF GRADUATE STUDIES
Department of Chemistry

SYNTHESIS AND CHARACTERIZATION OF VARIOUS BOROPHOSPHATE AND VANADATE MATERIALS

DOCTOR OF PHILOSOPHY

GÜLDEN ÖZEN KAHVECİ

ACADEMIC SUPERVISOR
Prof. Dr. Ayşe MORKAN

BOLU, OCAK - 2023

APPROVAL OF THE THESIS

SYNTHESIS AND CHARACTERIZATION OF VARIOUS BOROPHOSPHATE AND VANADATE MATERIALS submitted by **Gülden ÖZEN KAHVECİ** and defended before the Examining Committe Members listed below in partial fulfillment of the requirements for the degree of **Doctor of Philosophy** in **Department of Chemistry, Institute of Graduate Studies of Bolu Abant Izzet Baysal University in 5.01.2023** by

Examining Committee Members	**Signature**
Supervisor Prof. Dr. Ayşe MORKAN Bolu Abant Izzet Baysal University	.....
Member Prof. Dr. F. Devrim ÖZDEMİRHAN Bolu Abant Izzet Baysal University	.....
Member Assoc. Prof. Dr. Bahadır ALTINTAŞ Bolu Abant Izzet Baysal University	.....
Member Assoc. Prof. Dr. Mecit AKSU Duzce University	.....
Member Assoc. Prof. Dr. Abdulkadir ALLI Duzce University	.....

Prof. Dr. İbrahim KÜRTÜL

Director of Instıtute of Graduate Studies

ETHICAL DECLARATION

In this thesis dissertation that was properly prepared according to the Thesis Writing Rules of Bolu Abant İzzet Baysal University of the Institute of Graduates Studies, I hereby declare that;

- All data, information, and documents presented in the thesis were obtained in accordance with the academic and ethical rules,
- All data, documents, assessments, and results were presented in accordance with the scientific ethical and moral rules,
- All works that were benefitted in the thesis were appropriately cited,
- No alteration was made in the data used,
- Study presented in this thesis is original,

Otherwise, I declare that I accept the loss of all my rights in case any contradiction that may arise against me.

Based on the plagiarism report that was generated on the date of 03/02/2023 by using predetermined filtrations set by Directorate of Institute of Graduate Studies of the Turnitin programme, a plagiarism detection sofware, the similarity index detected was 20%.

_____

Gülden ÖZEN KAHVECİ

ABSTRACT

SYNTHESIS AND CHARACTERIZATION OF VARIOUS BOROPHOSPHATE AND VANADATE MATERIALS
PHD THESIS
GÜLDEN ÖZEN KAHVECİ
BOLU ABANT IZZET BAYSAL UNIVERSITY
INSTITUTE OF GRADUATE STUDIES
DEPARTMENT OF CHEMISTRY
(SUPERVISOR: PROF. DR. AYŞE MORKAN)
BOLU, JANUARY 2023
(xv + 151)

In this thesis, two different synthesis methods namely, Solid State and Solution Combustion Synthesis Methods were used.

First part of this study covers the synthesis of rare earth borophosphate compounds, $LnB(PO_4)_2$ (Ln= Nd, Ce, Pr, Sm, Eu, Yb, Tb, Ho, Tm, Lu) prepared by solid state method. The characterization studies were carried out by XRD, FT-IR, TG/DTA, SEM and EDX techniques. Monazite (Ln= Nd, Ce, Pr, Sm, Eu) and xenotime (Ln=Yb, Tb, Ho, Tm, Lu) type borophophates were successfully synthesized. From these compounds, $YbB(PO_4)_2$, $HoB(PO_4)_2$ and $LuB(PO_4)_2$ were indexed in tetragonal crystal system, space group: $I4_1/amd$. Their refined unit cell parameters were calculated as a=6.820(3) c=5.975(2), V=277.945 ($YbB(PO_4)_2$), a=6.891(5) c=6.031(7), V=286.46 ($HoB(PO_4)_2$) and a= 6.798(9) c= 5.962(6) V= 275.62 ($LuB(PO_4)_2$). The characteristic bands of PO_4 and BO_4 units of the obtained materials were examined with FT-IR.

In the second part of this work, the fabrication of pyrovanadates ($M_2V_2O_7$, M= Cu, Ni, Co, Zn, Mn) and orthovanadates ($M_3V_2O_8$, M= Cu, Ni, Co, Zn, Mn, Mg) was studied by solution combustion synthesis method. Characterization studies showed that the orthorhombic α-$Cu_2V_2O_7$, monoclinic β-$Cu_2V_2O_7$, α-$Zn_2V_2O_7$ and β-$Mn_2V_2O_7$ as single phase whereas $Co_2V_2O_7$ and $Ni_2V_2O_7$ pyrovanadates were produced as multiphase products. For the orthovanadate compounds, $Ni_3V_2O_8$ and $Co_3V_2O_8$ in orthorhombic structures were found as a single phase while in the synthesis process of $M_3V_2O_8$ containing Mg, Cu and Zn metals, the products were determined as mixture with pyrovanadates, $M_2V_2O_7$ (M=Mg, Cu, Zn). During the synthesis process of $Mn_3V_2O_8$ compound, α and β $Mn_2V_2O_7$ were obtained.

KEYWORDS: Borophosphate, Solid state method, Solution combustion synthesis method, Pyrovanadate, Orthovanadate.

ÖZET

ÇEŞİTLİ BORFOSFAT VE VANADAT MALZEMELERİN SENTEZİ VE KARAKTERİZASYONU
DOKTORA TEZİ
GÜLDEN ÖZEN KAHVECİ
BOLU ABANT İZZET BAYSAL ÜNİVERSİTESİ
LİSANSÜSTÜ EĞİTİM ENSTİTÜSÜ
KİMYA ANABİLİM DALI
(TEZ DANIŞMANI: PROF. DR. AYŞE ÜZTETİK MORKAN
BOLU, OCAK - 2023
(xv + 151)

Bu tezde, katı hal yöntemi ve çözeltide yanma sentezi yöntemi olmak üzere iki farklı sentez yöntemi kullanılmıştır.

Bu çalışmanın ilk bölümü, katı hal yöntemiyle hazırlanan nadir toprak borfosfat bileşiklerinin $LnB(PO_4)_2$ (Ln= Nd, Ce, Pr, Sm, Eu, Yb, Tb, Ho, Tm, Lu) sentezlerini kapsamaktadır. XRD, FT-IR, TG/DTA, SEM ve EDX yöntemleri ile karakterizasyon çalışmaları gerçekleştirilmiştir. Bu çalışma sonunda, monazite (Ln= Nd, Ce, Pr, Sm, Eu) ve xenotime (Ln=Yb, Tb, Ho, Tm, Lu) yapılı borfosfatlar başarılı bir şekilde elde edilmiştir. Bu bileşiklerden $YbB(PO_4)_2$, $HoB(PO_4)_2$ ve $LuB(PO_4)_2$, tetragonal kristal sistemde indekslenerek uzay grupları:$I4_1/amd$, birim hücre boyutları ise a=6.820(3) c=5.975(2), V=277.945 ($YbB(PO_4)_2$) ve a=6.891(5) c=6.031(7), V=286.46 ($HoB(PO_4)_2$), a= 6.798(9) c= 5.962(6) V= 275.62 ($LuB(PO_4)_2$) olarak hesaplanmıştır. Ayrıca elde edilen malzemelerin PO_4 and BO_4 birimlerinin karakteristik bantları FT-IR ile incelenmiştir.

Bu çalışmanın ikinci kısmında, çözeltide yanma sentezi yöntemi ile pirovanadatlar ($M_2V_2O_7$, M= Cu, Ni, Co, Zn, Mn) ve ortovanadatlar ($M_3V_2O_8$, M= Cu, Ni, Co, Zn, Mn, Mg) elde edilmiştir. Karakterizasyon çalışmaları, tek fazlı ortorombik α-$Cu_2V_2O_7$ (blossite) ve monoklinik β-$Cu_2V_2O_7$ (ziesite) faz geçişlerinin meydana geldiğini göstermiştir. Ayrıca monoklinik α-$Zn_2V_2O_7$ ve β-$Mn_2V_2O_7$ de saf olarak elde edilmiştir. $Co_2V_2O_7$ ve $Ni_2V_2O_7$ ise karışık faz olarak bulunmuşlardır. Ortovanadat bileşikleri için, ortorombik yapıdaki $Ni_3V_2O_8$ ve $Co_3V_2O_8$ saf halde bulunurken, $M_3V_2O_8$ in Mg, Cu ve Zn metallerini içerdiği ürünlerin pirovanadatlar $M_2V_2O_7$ (Mg, Cu ve Zn) ile karışım halinde oldukları belirlenmiştir. $Mn_3V_2O_8$ bileşiğinin sentez sürecinde, α-β $Mn_2V_2O_7$ yapıları elde edilmiştir.

ANAHTAR KELİMELER: Borfosfat, Katı hal metodu, Çözeltide yanma sentezi metodu, Pirovanadat, Ortovanadat.

TABLE OF CONTENTS

LIST OF FIGURES

Page

LIST OF TABLES

Page

LIST OF PICTURES

Page

LIST OF ABBREVIATIONS AND SYMBOLS

SCS **:** Solution Combustion Synthesis

XRD **:** X-ray Diffraction

FT-IR **:** Fourier Transform Infrared

TG/DTA **:** Thermogravimetry/Differencial Thermal Analysis

SEM **:** Scanning Electron Microscopy

EDX **:** Energy Dispersive X-ray

HMTA **:** Hexamethylenetetramine

HMDA **:** Hexamethylenediamine

ACKNOWLEDGEMENTS

I would like to express acknowledged to my supervisor Prof. Dr. Ayşe Morkan for her continuous encouragements, guidance and support throughout my research work.

I would also like to thank my friend Liska Fadliyani for her helps.

I'm grateful to my husband, Mahir KAHVECİ, my daughter Berilsu KAHVECİ and my parents Gönül and Hasan ÖZEN for their support whenever I need.

Finally, I would like to thank to BAP – 2012.03.03.511 for supporting this thesis and also acknowledge the Nobel İlaç San. Tic. A.Ş. for supporting to use of X-ray diffraction and FT-IR instruments.

1. INTRODUCTION

Borophosphate and vanadate compounds have been synthesized by many different methods until now. Some of these methods are solid state method, hydrothermal method, sol gel method, flux method, solution combustion synthesis (SCS) method etc. In our study, solid state method is used for borophosphates, solution combustion synthesis (SCS) method were preferred for vanadates.

1.1 Borophosphates

Borophosphates have drawn many attentions in the last decade due to their interesting properties which allow them to be used in various areas as redox catalysts, ion exchangers, and molecular sieves [1,2]. Due to their structural properties which includes a great variety of anionic partial structures pattern connections such as oligomers, isolated species chains, ring, and layers to frameworks with different ratio of Boron and phosphate [3].

Kniep et al. (1997), have determined a new group of isostructural borophophate which consist of only a one-dimensionally linked anionic partial structure [cited by 4, p.131]. This new borophospates is $M^{I}M^{II}(H_2O)_2[BP_2O_8].H_2O$ where M^{I} = Na, K and M^{II} = Mg, Mn, Fe, Co, Ni, Zn, respectively. The three-dimensional tetrahedral borophosphate compound open framework was also first synthesized by the same scientist in 1999 [5]. As reported by Kang et al., (2014), borophosphates compounds could be applied as microporous materials, such as $K[ZnBP_2O_8]$ and $A[ZnBP_2O_8]$ ($A=NH^{4+}$, Rb^{+}, Cs^{+}) because of their exceptional thermodynamic properties [cited by 6, p.131]. These compounds were synthesized according to the studies of Kniep et al. (1999) under mild hydrothermal conditions[cited by 5, p.131].

$Fe(H_2O)_2BP_2O_8.H_2O$, the first zeotype ferriborophosphate was reported by Yilmaz et al. (2000) with chiral tetrahedral framework topology[cited by 7, p.131].

Up to now, numerous borophosphates have been prepared by applying hydrothermal or solid-state methods. It was reported that under hydrothermal conditions, OH- and/or H_2O are contained in the structures.

$Ln_7O_6(BO_3)(PO_4)_2$ (Ln=La, Nd, Gd and Dy) which is the isomorphical rare earth consisted borophosphates were synthesized by Shi et al. (1997) and their vibrational spectra were examined [cited by 8, p.131].

Barium borophosphate, $BaBPO_5$ including isotopic compound was obtained by standard solid state reactions. The thermal decomposition and the crystal structure of $BaBPO_5$ were determined [9].

Two different methods, solid state reactions and hydrothermal method were applied in the preparation of The obtained compounds were compared and characterized [10].

A three-dimensional network of $Co_3[BPO_7]$ was synthesized via the flux method. The crystal structure analysis indicated the three metal consisted in this borophosphate such as tetrahedral P centers, triangular B centers and polyhedral Co centers were linked [11].

$(NH_4)(Fe(III)_{0.53}V(III)_{0.47}[BP_2O_8(OH)]$ and $(NH_4)M(III)[BP_2O_8(OH)]$ (M=V or Fe), the isostructural chain borophosphates were prepared by hydrothermal methods [12]. The $\{(NH4)_xCo_{(3-x)/2)}\}(H_2O)_2[BP_2O_8]$. $(1-x)H_2O$ ($x \approx 0.5$) which is known as a borophosphate hydrate was also synthesized by mild hydrothermal conditions (T = 170ºC) [13]. $LiCd(H_2O)_2[BP_2O_8].H_2O$ was also obtained hydrothermally and the crystal structure of this compound was reported [14].

The $NH_4Cd(H_2O)_2(BP_2O_8).0.72H_2O$ was also first fabricated by Ge et al. (2005). The properties and structures of this borophosphate were also investigated [cited by 15, p.132]. Two different single crystals $Mg(H_2O)_2[B_2P_2O_8(OH)_2].H_2O$ and $Mg_2(H_2O)(BP_3O_9(OH)_4]$ were also successfully synthesized for the first time under hydrothermal conditions [16].

$M^{II}(H_2O)_2[B_2P_2O_8(OH)_2].H_2O$ (M^{II} = Fe, Co, Ni), three novel isotypic transition metal borophosphates were obtained by hydrothermal route [17].

Yilmaz et al. (2005), synthesized the new borophospates with chiral tetrahedral topology. These two novel borophosphates were reported, where Co(II) and Mn(II) substituted to $(H)_{0.5}M_{1.25}(H_2O)_{1.5}[BP_2O_8].H_2O$ [cited by 18, p.132].

Another borophosphate compound, $(NH_4)_xMn_{(3-x)/2)}(H_2O)_2[BP_2O_8]$. $(1-x)H_2O$ was also well investigated by Birsoz et al. (2007) using a mild hydrothermal route. This compound is known to be the first sample of a borophosphate which consist of NH_4^+ and Mn^{2+}. Because of its open-framework structure, it is reported that this borophosphate might be used as ion exchangers, molecular sieves or catalyst [cited by 19, p.132].

Xiong et al. (2007) have been succeeded the synthesis and characterizatios of one dimensional structure of two sodium borophosphates, $Na_3B_6PO_{13}$ and $Na_3BP_2O_8$. These new borophosphates were prepared for the first time using low-temperature molten salts techniques [cited by 20, p.132].

Solid state NMR investigations have been succeed in the preparation of $K_3[BP_3O_9(OH)_3]$, $NH_4[ZnBP_2O_8]$, and $Rb_3[B_2P_3O_{11}(OH)_2]$. The local environments in the three crystalline model compounds have also been characterized [21].

$SrFe[BP_2O_8(OH)_2]$ was first prepared successfully by Menezes et al. (2009). This borophospate was determined to be in an unbranched trimeric oligomer. Also, it represents the novel borophosphates where a divalent (M^{II}) and a trivalent (M^{III}) cation balanced the anionic partial structure charge [cited by 22, p.132].

Zhao et al. (2009) have been accomplished the synthesis of two new isotypic 3D diamond-like framework anhydrous borophosphates compounds, $KMBP_2O_8$ (M=Sr, Ba) via high temperature solution growth (HTSG) [cited by 23, p.132].

Yang et al. (2010) have succeeded in obtaining the new $Pb^{II}_4\{Co_2[B(OH)_2P_2O_8](PO_4)_2\}Cl$ via hydrothermal method containing both Pb^{2+} cations and Cl^- anions. The crystal structure and characterization of the compound were also studied [cited by 24, p.132].

$Fe_2BP_3O_{12}$ and $In_2BP_3O_{12}$ anhydrous borophosphates have been attained under solid state method and their structural features were investigated [25].

The synthesis, structure, and physical characterization of $K_3Ln[OB(OH)_2]_2[HOPO_3]_2$ (Ln=Yb, Lu) which is known to be the hydrated rare-earth borate phosphates, were prepared under mild hydrothermal synthesis conditions firstly [26].

Three novel isostructural transition metal borophosphates in organo templated were prepared successfully. The borophosphates are, $(C_3H_{12}N_2)[FeB_2P_3O_{12}(OH)]$ noted as FeBPO-CJ30A, $(C_4H_{12}N_2)[FeB_2P_3O_{12}(OH)]$ noted as FeBPO-CJ30B and $(C_3H_{12}N_2)[MnB_2P_3O_{12}(OH)]$ noted as MnBPO-CJ30 [27].

Wang et al. (2012) were reported the first sample of varied alkali-metal anhydrous borophosphates by using solid state method. These four new anhydrous borophosphates are $Li_2Cs_2B_2P_4O_{15}$, $LiK_2BP_2O_8$, $Li_3K_2BP_4O_{14}$ and $Li_3Rb_2BP_4O_{14}$.

It is also stated that all the compound except $LiK_2BP_2O_8$, define two unusual anionic partial structures [cited by 28, p.133].

Using molten hydrated flux method a new $Cu_3[B_2P_3O_{12}(OH)_3]$ have been synthesized by Duan et al. (2014) and its magnetism property was also determined. It was reported that the combination of isolated PO_4 tetrahedral and two different types of polymeric chains resulting on the formation of the three-dimensional framework of this compound [cited by 29, p.133].

Li et al. (2013) have been synthesized the first $KPbBP_2O_8$ by using the top seed growth method from a K_2O-PbO-B_2O_3-P_2O_5 system [cited by 30, p.133].

Hasegawa and Yamane (2014) have been reported the single crystals of lithium borophosphate, $Li_3BP_2O_8$ and characterized the electrical properties [cited by 31, p.133].

$(NH_4)_2(C_4H_{12}N_2)[Co_2B_4P_6O_{24}(OH)_2].H_2O$ have been reported firstly with the 3D anionic partial borophosphatic network formed by the introduction of the varied templates of NH_4^+ and piperazine using hydrothermal method by Liu et al. (2011). Pure $Na_5[B_2P_3O_{13}]$ was reported to synthesize with microwave-assisted and hydrothermal method by Hauf et al., (1998) [cited by 32,33, p.133].

1.2 Vanadates

According to Cotton et al. (1999), vanadate is a compound that consists of the highest oxidation state of vanadium oxianion is +5. The simplest of vanadate ion is in tetrahedral structure which known as orthovanadate, VO_4^{3-} e.g. sodium orthovanadate which found to be strong base (pH>13) in V_2O_5 solution. Most vanadates are brittle and occur in small crystals and heavy and can be classified into three catagories metavanadates, pyrovanadates and orthovanadates [34].

1.2.1 Pyrovanadates

Pyrovanadate compounds with the general formula $X_2Y_2O_7$ structures are classified two different categories, depending on the *Y-O-Y* angle of the anions $Y_2O_7^{n-}$. These structures are known as “thortveitite” ($Sc_2Si_2O_7$) and the other is “dichromate” ($K_2Cr_2O_7$) structures. The fundamental distinction between these two structures is based on the arrangement of the two linked YO_4 groups and the *Y-O-Y* angle between them. In the thortveitite structure the $Y_2O_7^{n-}$ anion is staggered with the *Y-O-Y* angle of ~180º, while in the dichromate structure, the $Y_2O_7^{n-}$ anion appears in an eclipsed conformation as the *Y-O-Y* angle is found around 130º.

Many pyrovanadate compounds ($Ca_2V_2O_7$, $Cu_2V_2O_7$, $Sr_2V_2O_7$, $Co_2V_2O_7$, $Ni_2V_2O_7$, $Mg_2V_2O_7$, $Mn_2V_2O_7$ and $Zn_2V_2O_7$) have been obtained by different methods. The crystal structures of these transition metal pyrovanadates are determined as $Mg_2V_2O_7$, $Mn_2V_2O_7$, $Cu_2V_2O_7$ and $Zn_2V_2O_7$ in thortveitite structure while $Co_2V_2O_7$ and $Ni_2V_2O_7$ found to be crystallize in dichromate structure [35].

The structure of pyrovanadates could be also varies according to its transition metal. It is state that $Co_2V_2O_7$ and $Ni_2V_2O_7$ have only one polymorph where as $Mn_2V_2O_7$, $Cu_2V_2O_7$ and $Zn_2V_2O_7$ have more than one polymorph. The structural form of these pyrovanadates could be α-form, β-form or γ-form. According to He Z. et al. (2009) the V-O-V angle of pyrovanadates crystal structure $(V_2O_7)^{4-}$ anion is approximately 117.5° (Figure 1.1) [cited by 36, p.133].

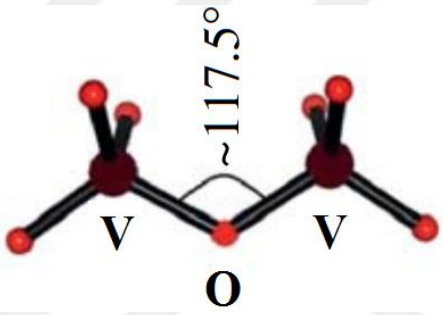

Figure 1.1. Structure and V-O-V angle of pyrovanadate anion

Crystal structures and magnetic properties of $M_2V_2O_7$ (M = Co, Ni and Cu) compounds were also investigated by Touaiher et al., (2004). It is reported that Ni-compound is antiferromagnetic, Co compound is ferromagnetic. The two varities of $Cu_2V_2O_7$ compounds are observed to have different magnetic properties: the β-$Cu_2V_2O_7$ is antiferromagnetic whereas α-$Cu_2V_2O_7$ is canted antiferromagnetic [cited by 35, p.133].

$Mn_2V_2O_7$ single crystals were prepared by using hydrothermal synthesis. In this work, Liao J. H. et al. (1996) were identified structural changes (α-β phase transition) of $Mn_2V_2O_7$. They showed that owing to the bending of V-O-V moieties, the structure of α-$Mn_2V_2O_7$ different from the β-$Mn_2V_2O_7$.The magnetic properties of α-$Mn_2V_2O_7$ was also determined and behave as antiferromagnetic at room temperature [37]. Further studies of $Mn_2V_2O_7$ was also done of these pyrovanadate magnetic properties. It is reported that α-β $Mn_2V_2O_7$ exhibits the anisotropy antiferromagnetic behavior [38]. $ZnMV_2O_7$ (M=Cu, Ni, Cu) have been prepared via

solid state method and it observed that these $ZnMV_2O_7$ are found to be in antiferromagnetic compounds [39].

In this studies, two pyrovanadates were observed which are blossite (α-$Cu_2V_2O_7$) and Ziesite (β-$Cu_2V_2O_7$). α-$Cu^{2+}{}_2V^{5+}{}_2O_7$ is an anhydrous copper vanadate mineral called as Blossite [40]. Blossite and ziesite were discovered by two mineralogist Donald F. Bloss and Hughes J.M. and Birnie R.W. (1980), respectively. Blossite was found alongside with several high-temperature minerals such as ziesite (β-$Cu_2V_2O_7$), mcbirneyite, fingerite ($Cu_{11}O_2(VO_4)_6$, and stoiberite [41,42]. Ziesite (β-$Cu_2V_2O_7$) minerals that was discovered in Izalco Volcano, El Salvador was presented in Figure 1.2.

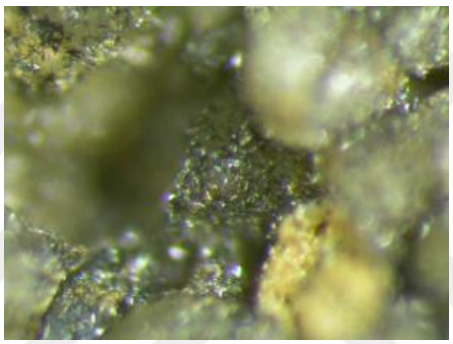

Figure 1.2. Ziesite (β-$Cu_2V_2O_7$) (Izalco Volcano, El Salvador)

Brisi and Molinari (1958) was studied the CuO-V_2O_5 binary system and identified it first synthetic compound. It is reported that Blossite, α-$Cu_2V_2O_7$ is transformed into ziesite, β-$Cu_2V_2O_7$ at higher temperature. These two minerals are observed in two different crystal structure which are α-$Cu_2V_2O_7$ in orthorhombic crystals form and β-$Cu_2V_2O_7$ in monoclinic crystal form. Blossite and Ziesite have similar physical properties and consist of same chemical composition [cited by 43, p.134]. The phase diagram of the system is also investigated by Fluery P. (1966) and five melting compounds between the CuO and V_2O_5 end members were observed. In the studies of Cu-V complex oxide on the aerobic oxidation of isobutane, it is showed that the catalytic activity of the complexes are decreased in the order CuO, V_2O_5, $Cu_2V_2O_7$ > CuV_2O_6 > $Cu_3V_2O_8$ > $Cu_5V_2O_{10}$. The rate formation of the isobutene are also reported to be decreased in the order $Cu_2V_2O_7$ > CuV_2O_6 > V_2O_5 > $Cu_3V_2O_8$ > $Cu_5V_2O_{10}$ > CuO at 623K. Anionic groups of pyrovanadates, $[V_2O_7]^{4-}$ in blossite, α-$Cu_2V_2O_7$ are showed parallel to (100) planes.

Adjacent (100) planes of tetrahedra are linked by Cu atoms in five fold coordination with oxygen. Cu atoms not shown. (Figure 1.3) [40,44,51].

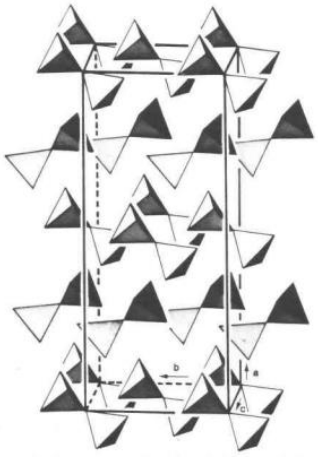

Figure 1.3. Arrangement of $[V_2O_7]^{4-}$ anionic groups in blossite, α-$Cu_2V_2O_7$

$Cu_2V_2O_7$ has three polymorphs; α-$Cu_2V_2O_7$, β-$Cu_2V_2O_7$ and γ-$Cu_2V_2O_7$, which are similar in structure but differ in the kinetics of their formation. Their transformations are reversible [40].

Table 1.1. Crystal Symmetry of $Cu_2V_2O_7$ Polymorphs

Structure	α-$Cu_2V_2O_7$	β-$Cu_2V_2O_7$	γ-$Cu_2V_2O_7$
Crystal Symmetry	Orthorombic	Monoclinic	Triclinic
Unit cell parameters	a = 20.645Å b = 8.383Å c = 6.442Å	a = 7.685Å b = 8.077Å c = 10.09Å	a = 5.087Å b = 5.823Å c = 9.402Å
	-	β = 110.27°	α= 99.780º β=97.253º γ= 97.202°
	Z=8	Z=2	Z=2
Space group	*Fdd2*	*C2/c*	*P1*

The phase transition between the α-β (blossite-ziesite) copper vanadate phases occurs approximately 710°C [46]. Table 1.1 represents the crystal symmetry of different kinds $Cu_2V_2O_7$ polymorph α-$Cu_2V_2O_7$ [45], β-$Cu_2V_2O_7$ [46], γ-$Cu_2V_2O_7$ [40].

Copper vanadate ($Cu_2V_2O_7$) nanoparticles were synthesized by a simple thermal decomposition method and investigated their electrochemical sensing property [47].

Transition metal pyrophosphates, pyroarsenates and pyrovanadates (X=3d-transition metal Ni, Co, Cu; Y=P, As, V) adopt the thortveitite structure but on cooling undergo the dichromate structure. The magnetic properties and magnetic structures of the transition metal pyroarsenates $M_2As_2O_7$ (M=Ni, Co, Mn) were investigated by magnetic susceptibility measurements [48].

$Cu_2V_2O_7$ was obtained by a solid-state method and its magnetic properties were studied by Ponomarenko et al. (2000). They saw that the inverse magnetic susceptibility of $Cu_2V_2O_7$ is depend on the temperature [cited by 49, p. 134].

Due to its applications in mobile and satellite communications areas, microwave dielectric materials have been widely researched. $Cu_2V_2O_7$ effect on the microwave dielectric properties of BiTaO4 ceramics was studied by Kim et al., (2001). It is observed that the dielectric constant is slightly changed with the increase of $Cu_2V_2O_7$ content [cited by 50, p. 134].

In the anaerobic oxidation of isobutane over Cu-V complex oxides, high oxidizing activity of V_2O_5, CuV_2O_6 and $Cu_2V_2O_7$ were observed. At the beginning of the reaction (within 30 min.), formation of the CO_2 occured rapidly but sharply decreased. Formation of isobutene reached a maximum at 30-45 min. and then decreased until 180 min. $Cu_2V_2O_7$ should be applicable in a thin-layer reactor in which isobutane and oxygen are supplied to opposite sides of a thin-layer catalyst [51].

Magnetic and thermal properties of β-$Cu_{2-x}Zn_xV_2O_7$ (x = 0, 0.05, 0.1, 0.15, 0.2, 0.3, 2) were investigated [52].

Sanchez-Andujar et al. (2011) have synthesized $M_2V_2O_7$ (M^{2+}=Co^{2+} and Cu^{2+}) divanadates. They reported dielectric behavior of this divanadates. In the $Cu_2V_2O_7$, due to the existence of weak ferromagnetism in a polar crystal structure, magnetodielectric couplings were observed. In the $Co_2V_2O_7$, the magnetodielectric effect occurs because of the magnetic anisotropy of Co^{2+} cations, which resulting in different arrangement of magnetic: a noncollinear arrangement inside the chains and magnetostriction which caused electrical polarization [cited by 53, p.135].

The study of $Cu_2V_2O_7$ were also done by Camargo L.P. et al. (2020) via combustion synthesis method by mixing two different solution of A

($Cu(NO_3)_2.3H_2O$ and citric acid dissolved in HNO3 solution) and B (citric acid and NH_4VO_3 in distilled water) which then evaporated to form gel-like solution at 80°C for 32 h. The $Cu_2V_2O_7$ were obtained after annealed at 400°C for 1 h. Different crystal structure were observed in the preparation of $Cu_2V_2O_7$ using various fuel such as citric acid, glycine and urea. It reported that the highest proportion of β-$Cu_2V_2O_7$ was observed by the used of urea fuel, highest specific surface area found by citric acid fuels and the most gas evaporates was observed by the used glycine fuel. According to the XRD results there is no single-phase $Cu_2V_2O_7$ were obtained and all the fuels produced multi-phase $Cu_2V_2O_7$, $Cu_{0.55}V_2O_5$, V_2O_5 and CuV_2O_6 [cited by 54, p.135].

The effect of non magnetic Mg and magnetic Co ion on the structural, dielectric and magnetic properties of α-$Cu_2V_2O_7$ have been examined. It stated the α-$Cu_2V_2O_7$ was discovered in the honeycomb like structure that is formed by CuO_5 polyhedra which attached to two mutually perpendicular spin chains that is isolated by pyrovanadate ion containing edge-sharing VO_4 tetrahedra [55]. Furthermore, Tsirlin A A. et al. (2010) has also studied the microscopic model and the band structure of β-$Cu_2V_2O_7$, based on its theoretical calculation it is also found that the β-$Cu_2V_2O_7$ mignt be consider as a spin-1/2 anisotropic honeycomb lattice model [cited by 56, p.135].

Structural characterization of the $(Zn_{2-x}Cu_x)V_2O_7$ solid solutions were investigated by Schindler and Hawthorne (1999) and they show that the solid-solution series between α-$Zn_2V_2O_7$ and β-$Cu_2V_2O_7$ is complete and there is no phase transition [cited by 57, p.135].

Kataev et al. (2004) have investigated the magnetic exchange in a low-dimensional complex oxide $(Cu, Zn)_2V_2O_7$ [cited by 58, p.135].

$Ni_2V_2O_7$ thin films were synthesized by using a physical vapor deposition technique [59].

$[Ni(NH_3)_6][VO(O_2)_2(NH_3)]_2$ compound was prepared and after thermal decomposition of this compound up to 600˚C, $Ni_2V_2O_7$ and V_2O_5 solid products were obtained [60].

The pyrovanadates, $M_2V_2O_7$ (M=Mn, Co, Ni, Cu and Zn) were investigated for the oxidative dehydrogenation of isobutane from 300˚C to 450˚C. $Ni_2V_2O_7$ was the most stable pyrovanadate according to Almukhlifi and Burns (2015). It reported the catalytic performance data was investigated by using pyrovanadate phases β-

$Mn_2V_2O_7$, $Co_2V_2O_7$, $Ni_2V_2O_7$, α-$Cu_2V_2O_7$ and α-$Zn_2V_2O_7$. In these transition metals the most active catalyst is $Ni_2V_2O_7$ [61].

Monoclinic $Ni_2V_2O_7$ and triclinic $FeVO_4$ vanadium transition metal oxides were obtained a very simple physical vapour deposition technique and they have been studied in thin-film form [62].

He Z. and Ueda Y. (2008) have synthesized β-$Mn_2V_2O_7$ single crystals via flux method. The honeycomb-like structure of $Mn_2V_2O_7$ was reported and exhibits two forms such as α-form (a low-temperature) and β-form (high temperature) [cited by 63, p.136].

The convertible phases transition of α and β $Mn_2V_2O_7$ structure were investigated by He Z. et al. (2008). They found that martensitic-like transformation which is known as thermoelastic solid-solid phase transition at first order is occupied by lattice deformation at critical temperature. These martensitic transformation from austenite (monoclinic β-phase) to martensite (triclinic α-phase) and they noted that martensitic-like transformation observed in $Mn_2V_2O_7$ was found to be independent of magnetic fields, heating/cooling rates, and frequencies. It also stated that the different arrangement of plane which paralel to honeycomb-like structure is the most significant differences between these to phases, (001) plane and (110) in β-phase and α-phase, respectively [cited by 64, p.136].

Krasnenko T. I. and Rotermel M. V. (2013) have studied thermally activated $Mn_2V_2O_7$ structural deformation at temperature between -180-1000˚C. They showed that under normal atmospheric pressure, $Mn_2V_2O_7$ can be crystallized in two polymorphic forms: triclinic α-$Mn_2V_2O_7$ and monoclinic β-$Mn_2V_2O_7$ [cited by 65, p.136].

$Sr_2V_2O_7:Eu^{3+}$ and $Ba_2V_2O_7:Eu^{3+}$ nanophosphors have been prepared via solution combustion synthesis with urea fuel. It showed to possess red-emitting property owing to their luminescent properties attractive to a wide range of potential applications in electronic devices [66].

Eu doped calcium pyrovanadate nanoparticles ($Ca_2V_2O_7:Eu^{3+)}$ which are excellent red emitting phosphors have been synthesized using combustion process [67].

Polycrystalline metavanadates $M_2V_2O_7$ (M=Ca, Sr, and Ba) as a new vanadate phosphor system were synthesized by a solid-state method and their photoluminescent properties were investigated [68].

Vanadium compounds (AVO_4, A=Bi, Fe, Cr and $Co_2V_2O_7$) have been prepared to exemined its structure and thermal expansion properties. At room temperature both $BiVO_4$ and $Co_2V_2O_7$ are monoclinic structure. Crystal structure of $CrVO_4$ and $FeVO_4$ are orthorombic and triclinic, respectively [69].

Single-phase $Co_2V_2O_7$ were synthesized by solid state method and calcined at various temperatures in the interval of 150^{o}C from 150^{o}C to 450^{o}C for 24 h. Followed by further annealing process at 600^{o}C for 1 week and the final product was obtained at 700^{o}C for 24 h [70].

1.2.2 Orthovanadates

Conventionally the orthovanadate anion is a tetrahedron containing four equivalent oxygen atoms and represented with single double bond. For this reason it can be arranged as resonance form (Figure 1.4).

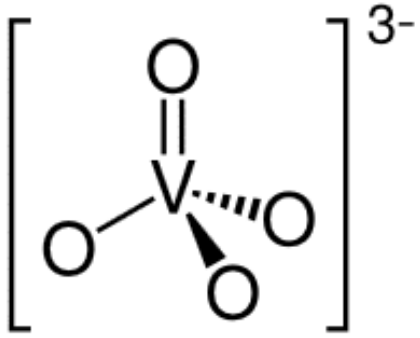

Figure 1.4. Structure of the orthovanadate anion

The compound with general formula of $M_3V_2O_8$, (M=divalent metal) are known to have orthorhombic structures with various Kagome staircase lattice. The alkaline earth metal orthovanadates have been investigated because of their interesting transport, ferroelectric properties, and use in solid-state lasers. Furthermore, these types of orthovanadates have found potential usage in television tubes, luminescent lamp coatings and flat panel displays [71-75].

Kagome type lattice or also known as kagome staircase structure have attracted attentions due to its unique magnetic for creating quantum-spin-liquid states. The Kagome structure is consisted of edge-sharing of octahedra MO_6 which detached by non-magnetic VO_4 in tetrahedral. Anisotropic variation of the ideal kagome net was represented by buckled planes of corner sharing isosceles triangle

from magnetic ions [76]. The Kagome net can be accomplished in some spin like as spin-5/2, spin-3/2 ans spin-1 showing the frustrated magnetic geometric. The reduction on the symmetry of kagome staircase geometry lowered the degree of frustration which resulting in the low ordered of magnetic structure and attractive magnetic properties [77].

$Cu_3V_2O_8$ have been synthesized by many researchers due to its great photocatalytic, electrochemical properties and reversible phase transition consequent to temperature increase. The phase transition is expected to happen at range of 450-550^oC; α-$Cu_3V_2O_8$ (453-510^oC), β-$Cu_3V_2O_8$ (535-545^oC) and γ-$Cu_3V_2O_8$ (>545^oC) [78].

The Cupper vanadates compound was also succesfully synthesized by three different methods which are in-situ co-precipitation, wet chemical and ex-situ co-precipitation. It reported that the solvent, temperature and time are affected the morphology and the particle sized of the as-obtained product. The mixture of monoclinic-$Cu_3V_2O_8$ and monoclinic-$Cu_2V_2O_7$ were obtained during the preparation process for all methods [79].

Rahni S G and Kakhki R M (2019), have been succeed in the preparation of $Cu_3V_2O_8$ by a green synthesis method with *moringa* seed's extract. The effect of initial concentration, the pH, light illumination and the amount of used catalyst were examined. It is also reported that the as-obtained products can be applied as adsorption and photodegradation as organic pollutant [cited by 80, p.137].

Kagome-like layers of $Ni_3V_2O_8$ were prepared by flux method. It is reported that the octahedral arrangement of NiO_6 are isolated with VO_4 tetrahedra. The Magnetic and heat capacity measurement of this compound presenting a very good magnetic property. The crystal growth of the $Ni_3V_2O_8$ was analyzed and best quality of product was acquired by the mixture of $SrCO_3$ and V_2O_5 which then calcined at 900^oC for 40 h. the grinding and the reheating process were done to obtained single-phase $Ni_3V_2O_8$[81]. The morphologies of this synthesized product have also been investigated. The pillar-like morphology was detected in a closed crucible and the plate like morphology was observed upon high vertical temperature in open crucible [82].

Multiferroic material has synthesized by preparing the $Ni_3V_2O_8$ using sputter deposition method using various substrates. The multiferroic film of $Ni_3V_2O_8$ was obtained after annealing at 900^oC for 16 h [83].

The two isostructural kagome staircase compounds, $Ni_3V_2O_8$ and $Co_3V_2O_8$ were prepared by solid state reaction with NiO, CoO and V_2O_5 as starting materials. Both Ni and Co compounds were firstly heated at 800^oC for a day. Further heating was applied at 1050^oC (2 days) for Co compound and the at 900^oC (1 day) for Ni compound [84].

The effect of Mg^{2+} and Co^{2+} doping in the kagome staircase compound was investigated. $Ni_3V_2O_8$, $Ni_{3-3x}Co_{3x}V_2O_8$ and $Co_{3-3x}Mg_{3x}V_2O_8$ were prepared and the chemical disorder in the compounds caused by Mg^{2+} and Co^{2+} reportly to affect the magnetocrystalline properties of the Kagome system [85].

Due to its great properties as excellent magnetic anisotropy, magnetic phase transition and low temperature ferroelectricity, another well known Kagome staircase compound, $Co_3V_2O_8$ was also successfully synthesized and characterized. It was prepared by microwave method and introduced to microwave treatment (2.45GHz750W) for 10 mins. The final product was crystallized in cubic system [86].

A high-quality Mg doped $Co_3V_2O_8$ has been obtained by applying the optical floating zone technique. The final product was acquired after three times of annealing process applied. Firstly, the annealing process was done at 935^oC for a day followed by 950^oC and 975^oC for a day, respectively [87].

Single phase $Ni_3V_2O_8$ has also been grown via the flux method. The physical, magnetic properties and the phase transition of $Ni_3V_2O_8$ were determined [88].

The phase diagram of magnetic compositon-temperature of Kagome mixed type $(Co_xNi_{1-x})_3V_2O_8$ were examined by applying single crystal heat capacity and neutron powder diffraction. The changed on the magnetic structure was observed twice below 5.5K. Both antiferromagnetic and ferromagnetic reflections of the orthovanadate were detected in the diffraction pattern and these behaviors are affected by different concentration of cobalt substitution [89].

The precipitation method has also applied in the preparation of $Ni_3V_2O_8$ and the as prepared product was obtained after annealed at 500^oC for 3 h. Before annealing process, the unknown phase was detected which might be the vanadium oxide/hydroxide. The structure of single-phase nickel orthovanadate is in orthorhombic crystal structure and the particle size is reported to be in the range of 20-50 nm [90].

Kagome staircase compound, $Co_3V_2O_8$ and $Ni_3V_2O_8$ have been analyzed and their magnetic phase diagram has been determined. For $Co_3V_2O_8$, there is no critical magnetization behavior at zero fields and different antiferromagnetic and ferromagnetic structured are presented [91].

The reactions occurring in the solid state of $FeVO_4$ in $Ni_2V_2O_7$ and $Ni_3V_2O_8$ were investigated by using conventional sintering method. Different compositions of FeVO4 were applied and affected the final products [92].

$Ni_3V_2O_8$ and $Mg_3V_2O_8$ have been synthesized via flameless oxy-combustion technique where $VOSO_4$, $NiSO_4$ and $MgSO_4$ are used as vanadate, nickel and magnesium sources. The as-prepared product was obtained at 1300^{o}C. During the preparation process the MgO and NiO was also observed at first which then transform to $Mg_2V_2O_7$, $Mg_3V_2O_8$ and $Ni_3V_2O_8$ after reacting with V_2O_7 [93].

Co-precipitation method was applied in the preparation of $Ni_3V_2O_8$ and $Co_3V_2O_8$ which known as high pseudocapacitive material. It is reported that $Ni_3V_2O_8$ and $Co_3V_2O_8$ have a excellent specific capacitance and higher rate capability/exceptional cycle stability, respectively. These two orthovanadates were successfully combined by growing the cobalt orthovanadates on nickel orthovanadates compound. By these two orthovanadates combination, superb electrochemical performance materials was obtained [94].

Solid state reaction method were used in the preparation Raw material $Co_3V_2O_8$ for crystal growth. The homogenized mixture was calcined at 900^{o}C (40 h) and followed by several regrinding and reheating process. The $Co_3V_2O_8$ Crystal growth was also done done by using V_2O_5, $SrCO_3$ and $BaCO_3$ as flux, separately and kept the mixture for 10 h at 1000^{o}C. During this process $Co_2V_2O_7$ is found as a second phase [95].

Hierarchiral $Co_3V_2O_8$ mesoporous microsphere has been successfully acquired via co-precipitation method followed by post annealing treatment. The as-prepared $Co_3V_2O_8$ was obtainen at 450^{o}C (8 h) with 2^{o}C/min heating rate. It reported that the $Co_3V_2O_8$ conveya high reversible capacity, exceptional rate capability, and high cyclebility [96].

Zhang Q, et al. (2017), have reported the fabrication of hexagonal pyramid crystal of $Co_3V_2O_8$ by hydrothermal method (200^{o}C for 12 h). The heating treatment was also done to construct the 3D-stucture. To maintain the original

morphologies of the compound it heated at 550°C and orthorhombic-$Co_3V_2O_8$ phase were observed [97].

The magnetic and dielectric properties of $Co_3V_2O_8$ were compared with the $Ni_3V_2O_8$. The preparation of $Co_3V_2O_8$ was carriedout by solid state reaction method. The final product was acquired at 1000°C for 12 h. It revealed that the magnetocapacitance of Co compound are different with Ni ones as Ni has positive magnetocapasitance while Co compound has negative magnetocapacitance [98].

$Co_3V_2O_8$ has two magnetic phase transition and composed of spin-3/2 in the kagome staircase system. The magnetic phase transition observed at 11 K indicated to antiferromagnetic phase of Co^{2+} and at below 6 K the ferromagnetic phase of Co^{2+} [99].

Various metal orthovanadates, $M_3V_2O_8$ (M=Zn, Mg, C and Sr) have been synthesized by applying combustion methods. Metal nitrate was used as the oxidizing agent and urea as reducing agent. It showed that the $Zn_3V_2O_8$ were obtained at approximately 770°C while at lower temperature (500°C and 600°C) the $Zn_2V_2O_7$ was predominated. The final $Zn_3V_2O_8$ from combustion were correlated with some synthesis method (hydrothermal, solid-state and sol-gel method). It revealed that $Zn_3V_2O_8$ were obtained after calcining at 750°C for 12 h [100].

Facile green precipitation method were used in the fabrication of single crystal $Zn_3V_2O_8$. The as-prepared products obtained at 70°C for 3 h and followed by the calcination process at 450°C for 3 h. The clectrochemical and structural characterization of single phase $Zn_3V_2O_8$ were investigated [101].

The synthesis of $Mn_3V_2O_8$ was first fabricated in flux under the controlled conditions. MnO, V_2O_5 and MoO_3 were used as flux and oxygen partial pressure was applied to forbit the oxidation and reduction of Mn^{2+} and V^{5+} during the process of crystallization. The $Mn_3V_2O_8$ undergo ferromagnetic behavior and found in orthorhombic phase. It also stated that the preparation of $Mn_3V_2O_8$ via solid state method was not successfully as some impurities (MnO and $Mn_2V_2O_7$) were formed [102].

The optical, mechanical and urthe electronical properties of the Kagome staircase compounds, Ni_3V_2O8 and $Mn_3V_2O_8$ were reported. The band gap of these two compounds is found in a d-d character and the Eg value is 0.77eV for $Mn_3V_2O_8$ and 1.58eV for $Ni_3V_2O_8$. It also disclosed that Ni-containing compound is harder stiffness than Mn-containing compound [103].

$Mn_3V_2O_8$ noted to crystallize into two arrangements upon changing in temperature as low temperature-$Mn_3V_2O_8$ which crystallize in orthorhombic structure and high temperature-$Mn_3V_2O_8$ which crystallize in tetragonal structure. The high temperature-$Mn_3V_2O_8$ was reported to be form at temperature above ~946^oC. The synthesis of low temperature-$Mn_3V_2O_8$ was carried out by solid state method and the $Mn_3V_2O_8$ powder was obtained at 800^oC (15 h). It described there are two magnetic phases transition observed in low temperature $Mn_3V_2O_8$ such as antiferromagnetic order below ~25 K which result in high degree of spin frustration and by further cooling below ~17K the released of spin frustration is detected [104]. The low temperature-$Mn_3V_2O_8$ has also been reported by applying the same method. The pressure-induced on the structural performance of the compound was characterized by Raman and XRD measurement of the obtained product [105].

Two metal orthovanadates, $Zn_3V_2O_8$ and $Mg_3V_2O_8$ have been prepared via solid state method and their optical properties were examined. The compounds were gained at different temperature as $Zn_3V_2O_8$ (750^oC, 12h) and $Mg_3V_2O_8$ (950^oC, 12h). The yellow luminescent color was observed in these compounds showing the broad band emission at 410-900 nm. It also recorded that the value of η in $Zn_3V_2O_8$ is higher than in $Mg_3V_2O_8$ [106].

Polycrystalline $Mg_3V_2O_8$ was fabricated via solid-state reaction method by using MgO and V_2O_5. The reduction of polycrystalline $Mg_3V_2O_8$ compound by hydrogen in the range of 560-800^oC was completed and the transformation of orthorhombic phase into cubic phase $Mg_3V_2O_8$ was identified. The pure $Mg_3V_2O_8$ were attained at 920^oC where as multiphase $Mg_3V_2O_8$ with $Mg_3V_2O_6$ was detected at 620^oC [107].

Magnesium vanadates are known to be a great catalyst in the formation of isobutene. The catalytic activity order on the formation of isobutene at 400-450^oC was reported as $Mg_2V_2O_7$> $Mg_3V_2O_8$>$Cu_2V_2O_7$ [108].

The catalytic activity of three magnesium vanadate phases, MgV_2O_6, $Mg_2V_2O_7$ and $Mg_3V_2O_8$ in propane oxydehydrogenation were determined. Theothoborates were synthesized via solid sate route and the end products were attained at different temperatures such as MgV_2O_6 (700^oC, 24 h), $Mg_2V_2O_7$ (700oC, 17 h) and $Mg_3V_2O_8$ (800^oC, 15 h). it also stated that $Mg_3V_2O_8$is the least selective and active catalyst, compared to metavanadates and pyrovanadate [109].

Strontium and barium orthovanadates, $Sr_3V_2O_8$ and $Ba_3V_2O_8$, exhibit intense rare earth activated luminescence and when optimized will have intensity of luminescence approaching that of commercially used YVO_4 rare-earth materials [70]. Because of their excellent microwave dielectric properties, barium orthovanadate has been studied for use as microwave filters and antennas [110].

$M_3V_2O_8$ (M=Ca, Sr, and Ba) orthovanadates have been synthesized by a solid-state metathesis approach initiated by microwave energy [111].

Thermal stability and cathodoluminescence properties of five potassium strontium vanadates: $KSr(VO_3)_3$, $K_2Sr(VO_3)_4$, $K_4Sr(VO_3)_6$, $K_6Sr(VO_3)_8$, and $KSrVO_4$ have been reported [112].

Eu doped strontium orthovanadate, $Sr_3(VO_4)_2$: Eu^{3+} nanopowders was prepared by citric acid combustion synthesis. The effect of of some parameters such as fuel/nitrates ratio, amount of boric acid, annealing temperatures on the physical chemical and optical properties of the $Sr_3(VO_4)_2$ powder products were investigated [113].

The Solution Combustion Synthesis or SCS has been applied in the fabrication of various inorganic nanopowders due to its time and energy effectiveness, simplicity, and cost efficiency. Solution combustion synsthesis is known for its self-sustained exothermic oxidation-reduction reaction that is completed by the presence of fuels and oxidizer in aqueous solutions. The commonly used oxidizers are metal nitrates and ammonium nitrates while the commonly used fuels are glycine, urea, sucrose, glucose, citric acid, carbohydrazide, HMTA, HMDA and etc. The role of fuels during the synthesis is not only to generate heat but also as a complexing agent in metal-complexes formation to enhance the solubility level of the reactants and avoid the formation of metal ion precipitation during the evaporation process [66,111,113]. Gelatin was used as fuel for the first time in SCS and was reported to be a good dispersing agent and able to inhibits particle agglomeration [114].

Ammonium nitrate and urea was used as an oxidizer and reducer, respectively in the preparation of Zn_2SiO_4 via solution combustion synthesis method. The starting materials are applied in stoichiometric ratio and dissolved in the minimum amount of distilled water. The mixture was pre-heated at 500^oC and ignited at 450^oC. It reported that the entire process to obtain the as-prepared product

was accomplished within few minutes. Combustion synthesis was the most suitable method of preparing the phosphor [115].

The redox reaction mixture is generally prepared in stoichiometric proportion which is determined by appying the oxidizing and reducing valancies of the related oxidizer and reducer. It calculated that the oxidizing valence of the divalent metal is -10, trivalent metal is -15 and the reducing valancies of urea is +6, carbohydrazide is +8 and diformly hydrazide is +8 [116].

Solution combustion synthesis can be devided into two stages process such as the gel formation and the self-ignition stage. The amount of fuel used during the preparation should be considered as important parameter. The gel formation is the initial process where all the starting materials, fuel and oxider are homogeneously mixed. The ignition process is the process that takes place after the formation of gel which exhibits in flame or fire. There are also two phenomenons that occur during the combustion process: combustion heat utilization and evolution of gas. The generation of combustion heat improves the crystallinity and provides the formation of high purity product. The evolution of gas known as N_2, CO_2 and H_2O prevents the increase in temperature during this process. It also worth noting that high temperature could affect the characteristics of the final product and the desired product has 0.5 to 5.0 μm particle size due to fast reaction time [117-119].

SCS has also attracted tremendous attention because of its ability to produce high purity products that exceptionally have great sintering properties, low distribution of particle size and excellent surface area. Many metal vanadates have also been synthesized with SCS method, for example Eu^{3+} doped $Sr_2V_2O_7$ and $Ba_2V_2O_7$ [66], $Ca_2V_2O_7$:Eu^{3+} [67], and $Zn_3V_2O_8$ [100].

2. AIM AND SCOPE OF THE STUDY

Boron compounds have attracted many attentions for the past decades due to its unique properties, for this reason the synthesis of Lanthanide Borophosphates, $LnB(PO_4)_2$ was done in this study. Various rare-earth (Ln =Nd, Ce, Pr, Sm, Eu, Yb, Tb, Ho, Tm, Lu) borophosphates have been synthesized via solid state methods. The structural, morphology and thermal properties of these borophosphates were characterized.

Due to the low crystalinity of the vanadate compounds, the solid-state reactions take longer time compare to combustion method. Owing to its simplicity and time effiency, solution combustion method was applied in the second part of this study. The preparation of pyro ($M_2V_2O_7$) and orthovanadates ($M_3V_2O_8$) with various metals (Cu, Ni, Co, Zn, Mn and Mg) and different fuels (urea, glycine, carbohydrazide, HMTA and HMDA) were perfomed. Phase transitions of vanadate compounds were also determined.

3. MATERIALS AND METHODS

3.1 Chemicals

The following chemicals were used in the synthesis of the products:

NH_4VO_3: Merck (pure ≥%99.00)

V_2O_5: Merck (pure ≥%99.00)

CON_2H_4: Merck (pure %99.00-%100.5)

$C_2O_2NH_5$: Merck (pure ≥%99.00)

$C_6H_{12}N_4$: Merck (pure ≥%99.00)

CH_6N_4O: Aldrich (pure %98.00)

$C_6N_2H_{16}$: Merck (pure ≥%99.00)

$Cu(NO_3)_2.3H_2O$: Kimetsan (pure %99.35)

$Ni(NO_3)_2.6H_2O$: Merck (pure ≥%99.00)

$Co(NO_3)_2.6H_2O$: Merck (pure ≥%99.00)

$Zn(NO_3)_2.6H_2O$: Carlo Erba (pure %97.50)

$Mn(NO_3)_2.4H_2O$: Merck (pure %98.50)

$Mg(NO_3)_2.6H_2O$: Merck (pure ≥%99.00)

$Tb(NO_3)_2.5H_2O$: Aldrich (pure %99.99)

$Ce(NO_3)_2.6H_2O$: Aldrich (pure ≥%99.00)

$Pr(NO_3)_2.6H_2O$: Aldrich (pure %99.90)

$Tm(NO_3)_2.4H_2O$: Aldrich (pure %99.90)

Nd_2O_3: Merck (pure ≥%99.00)

Eu_2O_3: Merck (pure ≥%99.00)

Sm_2O_3: Merck (pure ≥%99.00)

Lu_2O_3: Aldrich (pure %99.90)

Yb_2O_3: Merck (pure ≥%99.00)

Ho_2O_3: Aldrich (pure %99.80)

H_3BO_3: Merck (pure ≥%99.00)

$NH_4H_2PO_4$: Merck (pure ≥%99.00)

$(NH_4)_2HPO_4$: Merck (pure ≥%99.00)

KBr : Spectroscopic grade was used in IR pellets preparation. It was dried at 180^oC about 2 hours before using.

3.2 Instrumentation

3.2.1 Xray Powder Diffractometer (XRD)

Rigaku miniflex X-Ray diffractometer powder were used to provide the structural properties of the prepared products using CuKα (30-40kV, 10-20mA, λ=1,54056Å) in the range of 2θ= 5-70º. The least square refinement procedure of unit cell parameters were determined by using Jana2006. The XRD Patterns presented in this work was plottet by Gnuplot program and were checked with the ICDD Data Card.

3.2.2 Fourier Transform Infrared Spectrophotometer (FT-IR)

The Fourier Transform Infrared (FT-IR) spectra were recorded using Digilab-Excalibur series 600 microwatt and Perkin Elmer FT-IR Spectrometer Spectrum Two in the region of 4000-400cm^{-1}. The spectra of the product were obtained by preparing the KBR pellet using 1:150 (wt/wt) of product to KBr ratio.

3.2.3 Thermogravimetry/Differential Thermal Analyzer (TG/DTA)

TG/DTA analysis was measured in the range of room temperature to 1300ºC using Perkin Elmer Pyris 1 instrument.

3.2.4 Scanning Electron Microscopy (SEM)/ Energy Dispersive Xray Analyzer (EDX)

Powder morphology and size of the product were observed by SEM photograph at 20 kV with a Jeol JSM 6390 LV equipped with an energy dispersive x-ray analyzer (EDX).

3.2.5 Furnaces

All the products were synthesized by using Nuve MF 1200 and Nobertherm B180 furnaces.

3.3 Experimental Procedures

3.3.1 Solid-State Reaction of $LnB(PO_4)_2$ (Ln:Nd, Yb, Ce, Pr, Sm, Eu, Tb, Ho, Tm, Lu)

$LnB(PO_4)_2$ (Ln:Nd, Yb, Ce, Pr, Sm, Eu, Tb, Ho, Tm, Lu) were synthesized by using solid state method. These products were prepared by weighing the stoichiometric amounts of reactants separately as below reactions and grinding together in an agate mortar, then heating at different temperatures (600-1200ºC) for 7 hours. At the end of each heating period, samples were taken from these mixtures for X-ray diffraction and IR analysis.

$Ln_2O_3 + 4(NH_4)_2HPO_4 + 2H_3BO_3 \rightarrow 2LnB(PO_4)_2 + 8NH_3 + 6H_2O$

(Ln=Nd, Yb, Sm, Eu, Ho, Lu)

$Ln(NO_3)_3.6H_20 + 2NH_4H_2PO_4 + H_3BO_3 \rightarrow LnB(PO_4)_2 + 3NH_3 + 9H_2O + 2NO_2 + {}^5/_2O_2$

(Ln:Ce, Pr)

$Tb(NO_3)_3.5H_20 + 2NH_4H_2PO_4 + H_3BO_3 \rightarrow TbB(PO_4)_2 + 3NH_3 + 8H_2O + 2NO_2 + {}^5/_2O_2$

$Tm(NO_3)_3.4H_20 + 2NH_4H_2PO_4 + H_3BO_3 \rightarrow TmB(PO_4)_2 + 3NH_3 + 7H_2O + 2NO_2 + {}^5/_2O_2$

3.3.2 Solution Combustion Synthesis of $M_2V_2O_7$ (M=Cu, Ni, Co, Zn, Mn)

$M_2V_2O_7$ (M=Cu, Ni, Co, Zn, Mn) powders were prepared by the solution combustion synthesis (SCS) method using urea or glycine as the fuel. $M(NO_3)_2.nH_2O$ and V_2O_5 were taken as starting materials in the stoichiometric amounts besides urea/glycine and made into a homogeneous solution with distilled water. The mixture was heated on a hot plate approximately at 80°C with uniform stirring. The resulted solution was dehydrated slowly and gradually converted into the viscous before the formation of a gel. The gel was transferred to a furnace at 400°C. On rapid heating the mixture evaporates and ignites.

3.3.3 Solution Combustion Synthesis of $M_3V_2O_8$ (M=Cu, Ni, Co, Zn, Mn, Mg)

$M_3V_2O_8$ was synthesized by combustion method. Stoichiometric amounts of the starting reagents $M(NO_3)_2.nH_2O$, V_2O_5 or NH_4VO_3 and fuels [CON_2H_4 (urea) $C_2O_2NH_5$ (glycine), $C_6H_{12}N_4$ (HMTA), CH_6N_4O (Carbohydrazide) or $C_6N_2H_{16}$ (HMDA)] were dissolved in minimum quantity of deionized water. The mixture was heated until foam was formed. The thermal dehydration of this solution on a hot plate resulted in viscous liquids. Then this mixture was transferred to a furnace at 400°C and the process was completed in about 5 minutes.

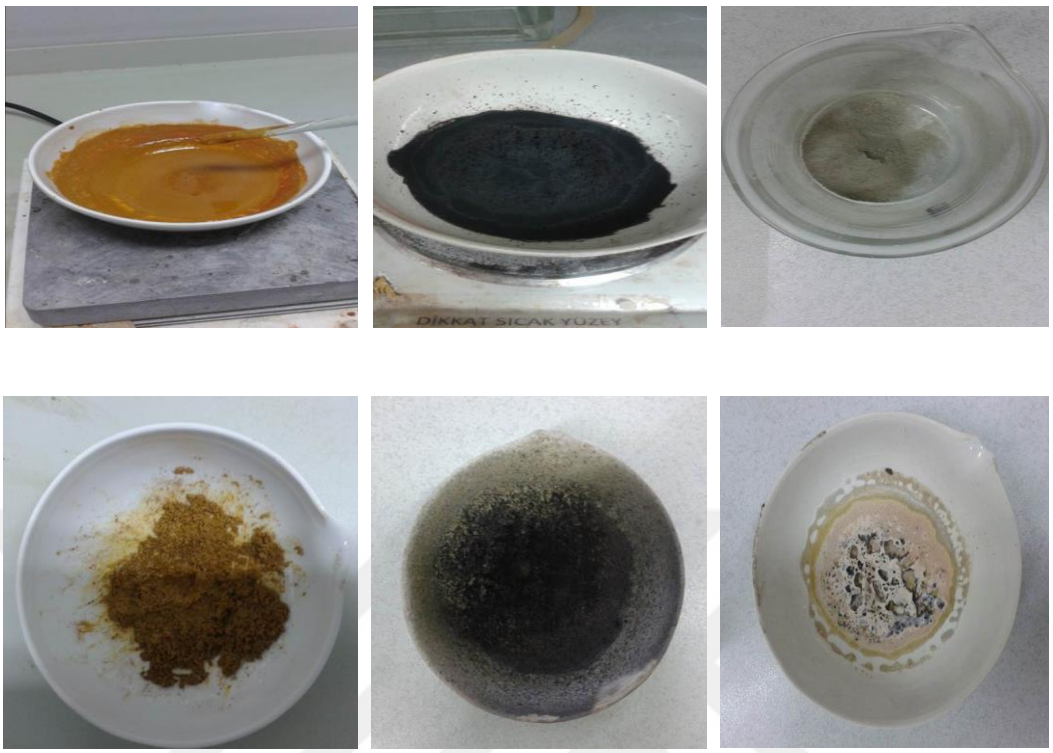

Picture 3.1. The examples of precursor gels and as-prepared products of vanadate compounds

4. RESULTS

4.1 Solid State Reactions for the Synthesis of Some New Rare Earth Borophosphates, $LnB(PO_4)_2$ (Ln=Nd, Yb, Ce, Pr, Sm, Eu, Tb, Ho, Tm, Lu)

The stoichiometric mixtures of reactants with respect to the equations given below were heated between 600-1200^oC for about 7 hours. The expected reactions are;

$$Ln_2O_3 + 4(NH_4)_2HPO_4 + 2H_3BO_3 \rightarrow 2LnB(PO_4)_2 + 8NH_3 + 6H_2O$$

(Ln=Nd, Yb, Sm, Eu, Ho, Lu)

$$Ln(NO_3)_3.6H_20 + 2NH_4H_2PO_4 + H_3BO_3 \rightarrow LnB(PO_4)_2 + 3NH_3 + 9H_2O + 2NO_2 + {}^5/_2O_2$$

(Ln:Ce, Pr)

$$Tb(NO_3)_3.5H_20 + 2NH_4H_2PO_4 + H_3BO_3 \rightarrow TbB(PO_4)_2 + 3NH_3 + 8H_2O + 2NO_2 + {}^5/_2O_2$$

$$Tm(NO_3)_3.4H_20 + 2NH_4H_2PO_4 + H_3BO_3 \rightarrow TmB(PO_4)_2 + 3NH_3 + 7H_2O + 2NO_2 + {}^5/_2O_2$$

First part of the study was done to examine whether the amount of boron evaporated or not evaporated, the boric acid was used in normal proportions and also increased by 25% and 50% proportions and benchmarking studies were performed. For this study, Nd and Yb rare earths were used.

At the end of the study boric acid in different proportions were the same in all of the structures of compounds prepared using boron phosphate.

4.1.1 Xray Powder Diffraction Studies for Ln: Nd, Ce, Pr, Sm, Eu, Yb, Tb, Ho, Tm, Lu Compounds

The products obtained at different temperatures were subjected to X-ray powder diffraction analysis after each heating process. The diffraction patterns observed for $NdB(PO_4)_2$ and $YbB(PO_4)_2$ compounds are given in Figures 4.1 and 4.8 respectively.

In the analysis of XRD patterns of the products obtained between 600-1000^oC unreacted Nd_2O_3 (ICDD Card No: 21-0579), Yb_2O_3 (ICDD Card No: 41-1106), $NdPO_4$ (ICDD Card No: 83-0654), $YbPO_4$ (ICDD Card No: 45-0530), $Nd(PO_3)_3$ (ICDD Card No: 27-0322), $Yb(PO_3)_3$ (ICDD Card No: 35-0356) and BPO_4 (ICDD Card No: 34-0132) were observed. Depending on the powder data

and infrared spectra which will be discussed later, the following reaction could be considered (Ln: Nd, Yb);

$2Ln_2O_3 + 8(NH_4)_2HPO_4 + 4H_3BO_3 \rightarrow 4BPO_4 + Ln_2O_3 + LnPO_4 + Ln(PO_3)_3 + 16NH_3 + 18H_2O$ **(equation 1)**

At 1000°C, examination of the XRD pattern showed that $LnPO_4$ with xenotime and monazite structures were found together with weak BPO_4. Here the amount of the BPO_4 is higher in our reactions using excess H_3BO_3.

Since the diffraction lines belong to $Ln(PO_3)_3$ and unreacted Ln_2O_3 become quite weak.

The following reaction was suggested;

$Ln(PO_3)_3 + Ln_2O_3 \rightarrow 3LnPO_4$ **(equation 2)**

Therefore, the final reaction could be written as follows:

$2Ln_2O_3(s) + 8(NH_4)_2HPO_4 + 4H_3BO_3 \rightarrow 4BPO_4(s) + 4LnPO_4(s) + 16NH_3(g) + 18H_2O(g)$

At 1100°C, since the diffraction lines for BPO_4 disappeared in the powder data, it was decided that the below reaction was produced;

$LnPO_4 + BPO_4 \rightarrow LnB(PO_4)_2$ **(equation 3)**

Because of the similarities of the d-lines for the obtained compounds with those of the xenotime and monazite $LnPO_4$ (Ln: Yb, Nd), it was predicted that the formation of monazite structure with the tentative formula $NdB(PO_4)_2$ and xenotime structure with $YbB(PO_4)_2$.

Based on these reactions, the different rare-earth compounds have been used in the preparation of $LnB(PO_4)_2$; Ce, Pr, Sm, Eu, Tb, Ho, Tm, Lu compounds. Similar to Nd-containing borophosphate compound Ce, Pr, Sm, and Eu are observed in monazite structure while Tb, Ho, Tm, Lu compounds structure are found in xenotime structure which similar to Yb-containing compound.

The XRD patterns of Nd (various composition of H_3BO_3 were applied zero-excess, 25% and 50%), Ce, Pr, Sm, and Eu monazite type structure were presented in Figure 4.1-4.7. At lower temperature Ln_2O_3, $LnPO_4$, $Ln(PO_3)_3$ (Ln: Nd, Ce, Pr, Sm, Eu) and BPO_4 were detected and with further heating these compounds were disappeared and single phase monazite $LnB(PO_4)_2$ (Ln: Nd, Ce, Pr, Sm, Eu) structure were obtained.

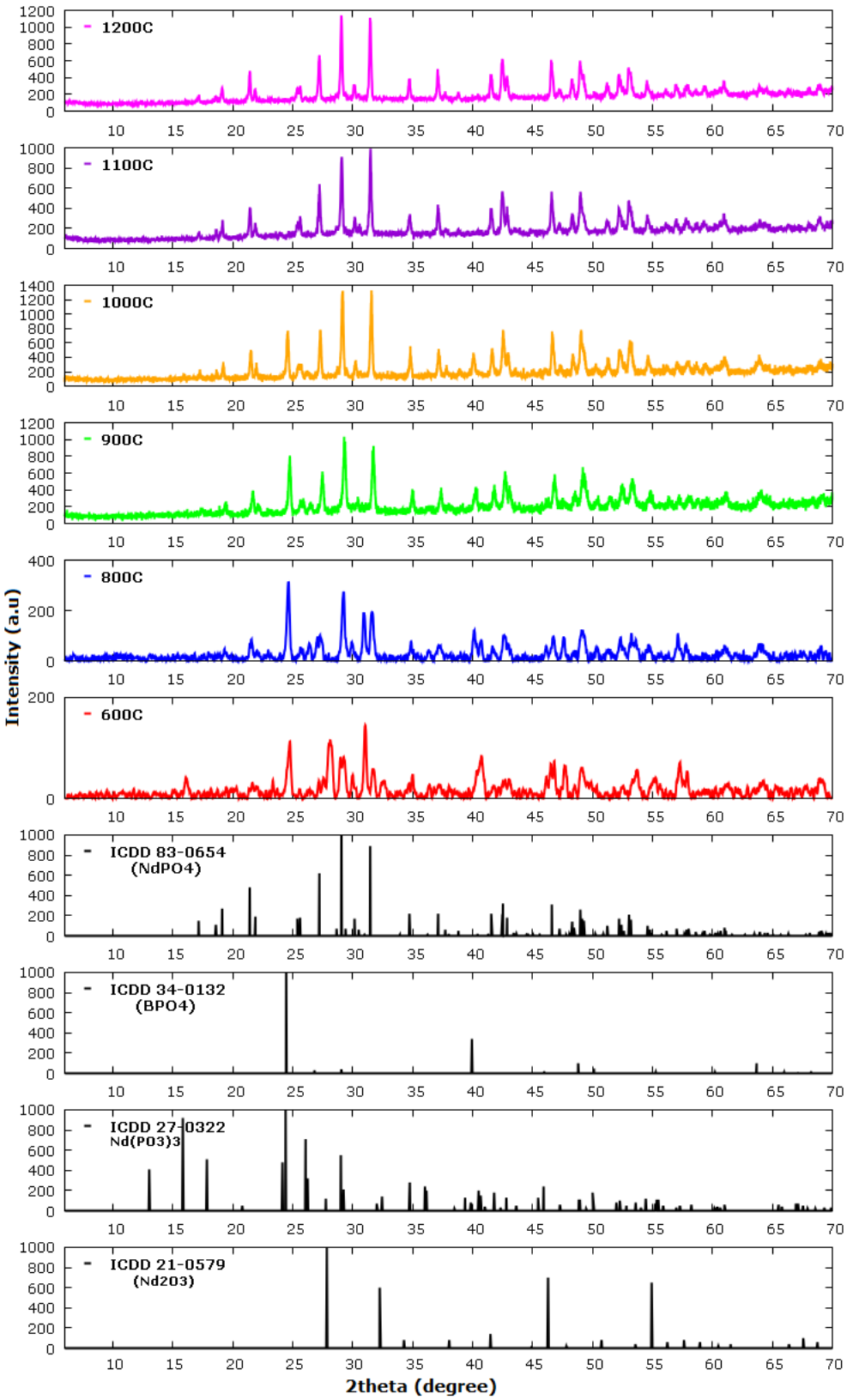

Figure 4.1. XRD pattern of $NdB(PO_4)_2$.

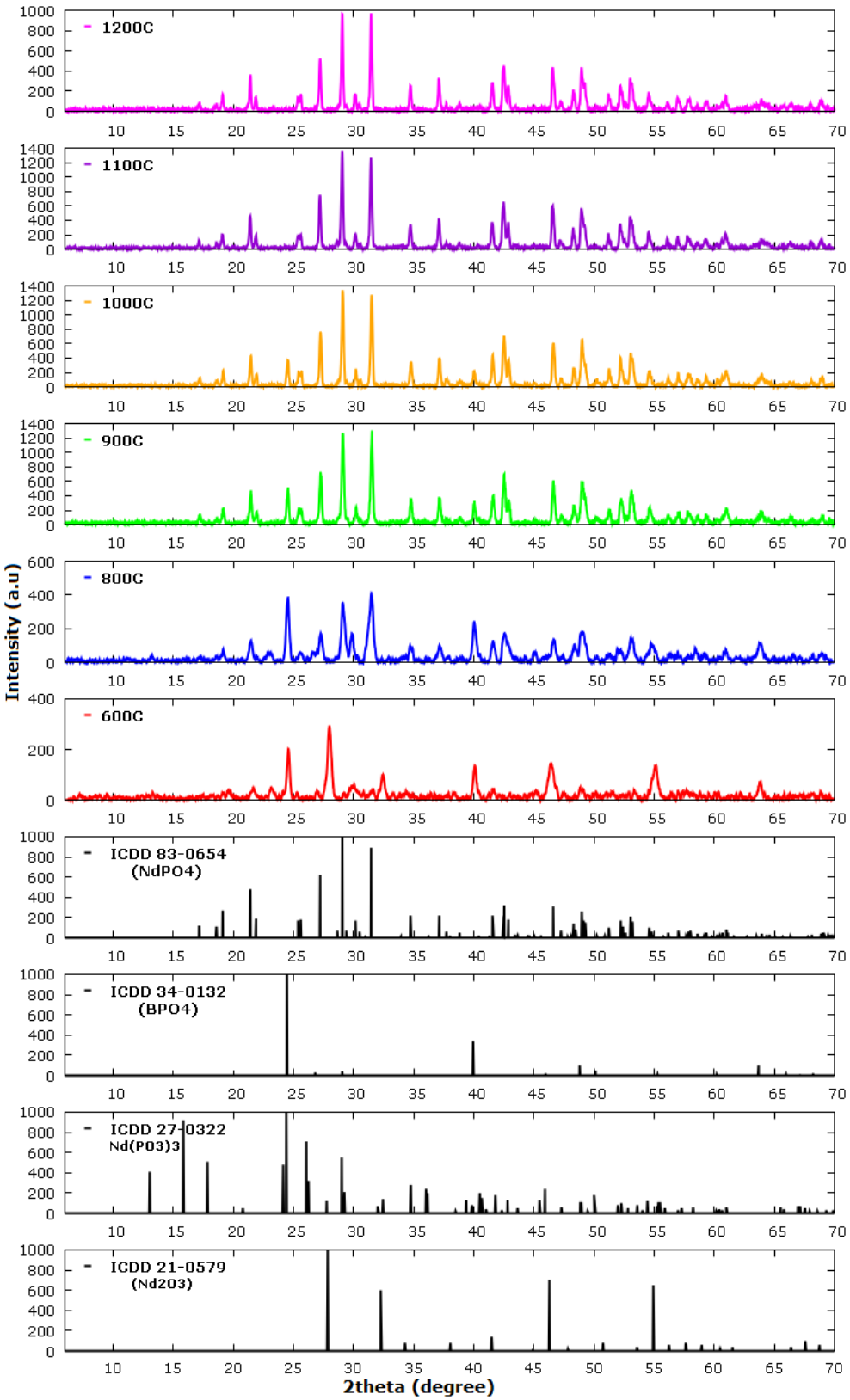

Figure 4.2. XRD patterns of $NdB(PO_4)_2$ (25% excess of H_3BO_3).

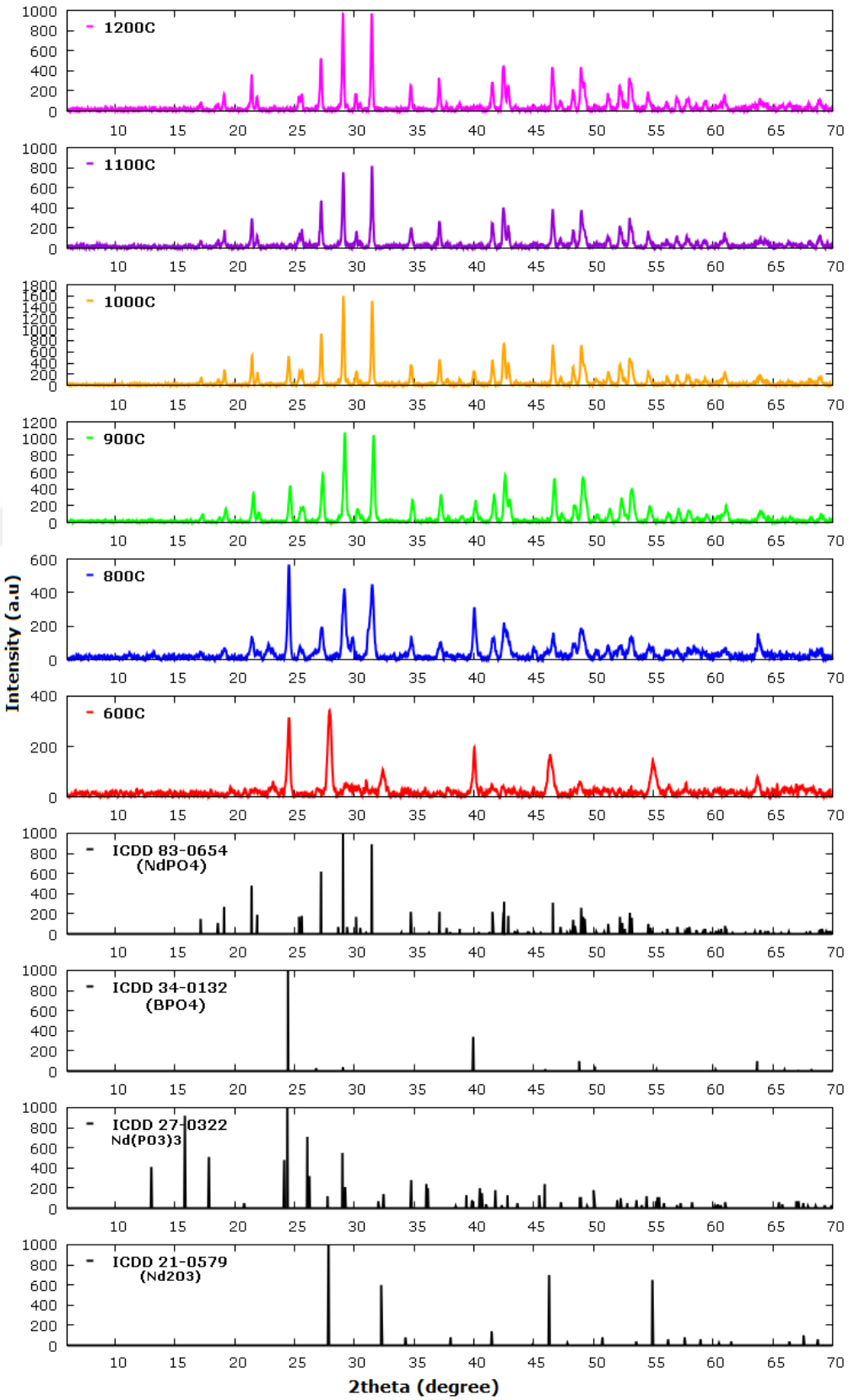

Figure 4.3. XRD pattern of $NdB(PO_4)_2$ (50% excess of H_3BO_3).

To determine the existence of boron in our sample, different amount of H_3BO_3 proportion were used (0%, 25% and 50%) for $NdB(PO_4)_2$ and its shown that BPO_4 compound were detected the most at 1000°C in the excessed one. By heating at the higher temperature, BPO_4 compound was reacted with the $NdPO_4$ after this reaction $NdB(PO_4)_2$ was formed. Since the formation of $NdB(PO_4)_2$ were acquired at 1100°C for all amount of H_3BO_3, The formation of monazite $LnB(PO_4)_2$ was predicted to observes since there is d-line similarities of the compound with the $LnPO_4$ (Ln= Nd, Ce, Pr, Sm, Eu). The synthesis of the other lanthanide compounds was done by zero excess of H_3BO_3. In the analysis of XRD patterns of the products obtained between 600-1000°C unreacted Ce_2O_3 (ICDD Card No: 23-1048), Pr_2O_3 (ICDD Card No: 22-0880), Sm_2O_3 (ICDD Card No: 15-0813), Eu_2O_3 (ICDD Card No: 34-0392), $CePO_4$ (ICDD Card No: 83-0652), $PrPO_4$ (ICDD Card No: 83-0653), $SmPO_4$ (ICDD Card No: 83-0655), $EuPO_4$ (ICDD Card No: 83-0656), $Ce(PO_3)_3$ (ICDD Card No: 33-0336, $Pr(PO_3)_3$ (ICDD Card No: 33-1077), $Sm(PO_3)_3$ (ICDD Card No: 52-1762), $Eu(PO_3)_3$ (ICDD Card No: 34-1453) and BPO_4 (ICDD Card No: 34-0132) were observed.

At 1000°C, examination of the XRD pattern showed that $LnPO_4$ (Ln=Ce, Pr, Sm, Eu) with monazite structures were found together with weak BPO_4.

At 1100°C, since the diffraction lines for BPO_4 disappeared in the powder data, it was decided that the below reaction was produced;

$LnPO_4 + BPO_4 \rightarrow LnB(PO_4)_2$

Because of the similarities of the d-lines for the obtained compounds with those of the monazite $LnPO_4$ (Ln=Ce, Pr, Sm, Eu), they were predicted that the formation of monazite structures with the tentative formulas $CeB(PO_4)_2$, $PrB(PO_4)_2$ $SmB(PO_4)_2$ and $EuB(PO_4)_2$. The XRD patterns of these products are presented below (Figure 4.4-4.7).

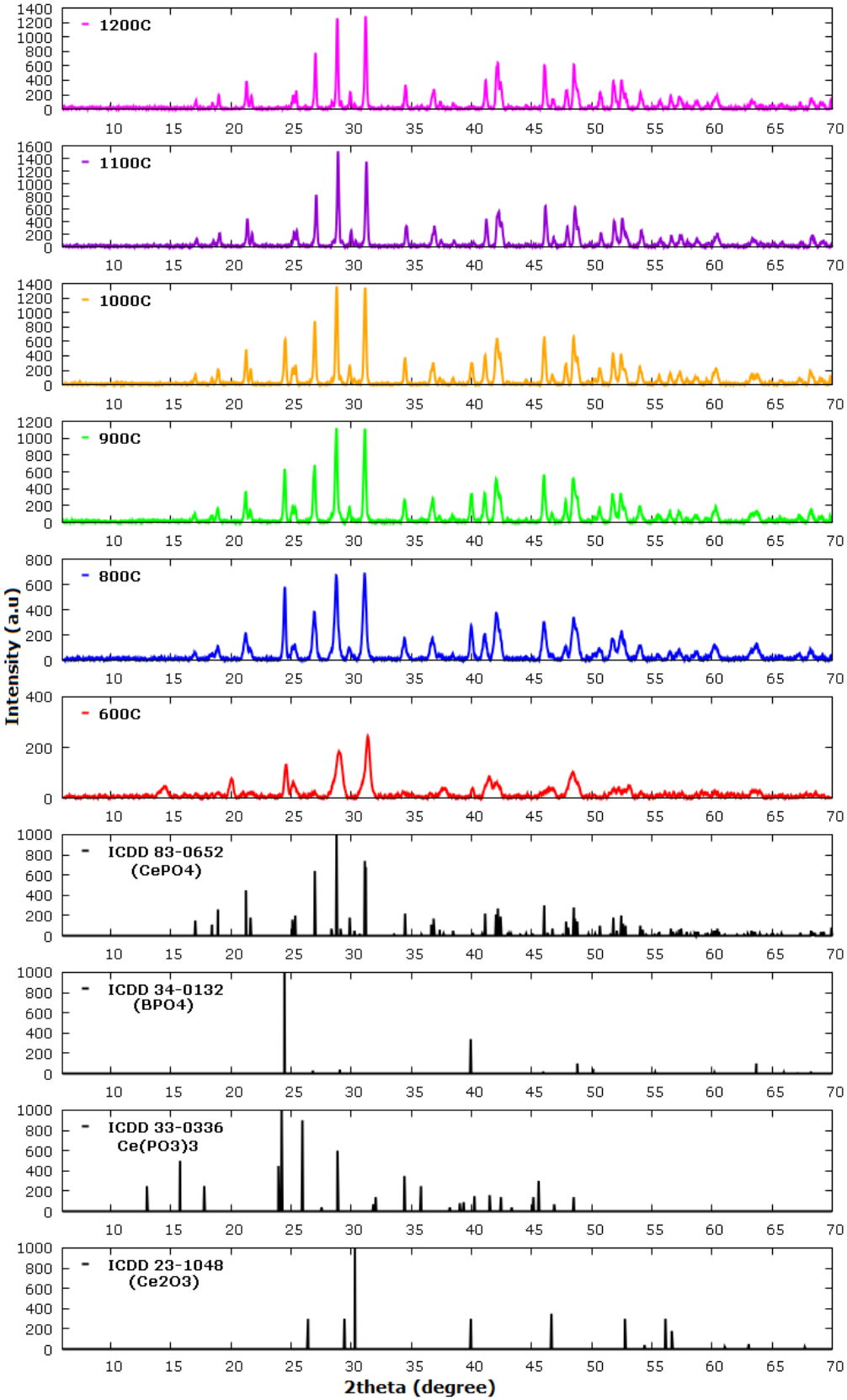

Figure 4.4. XRD pattern of $CeB(PO_4)_2$.

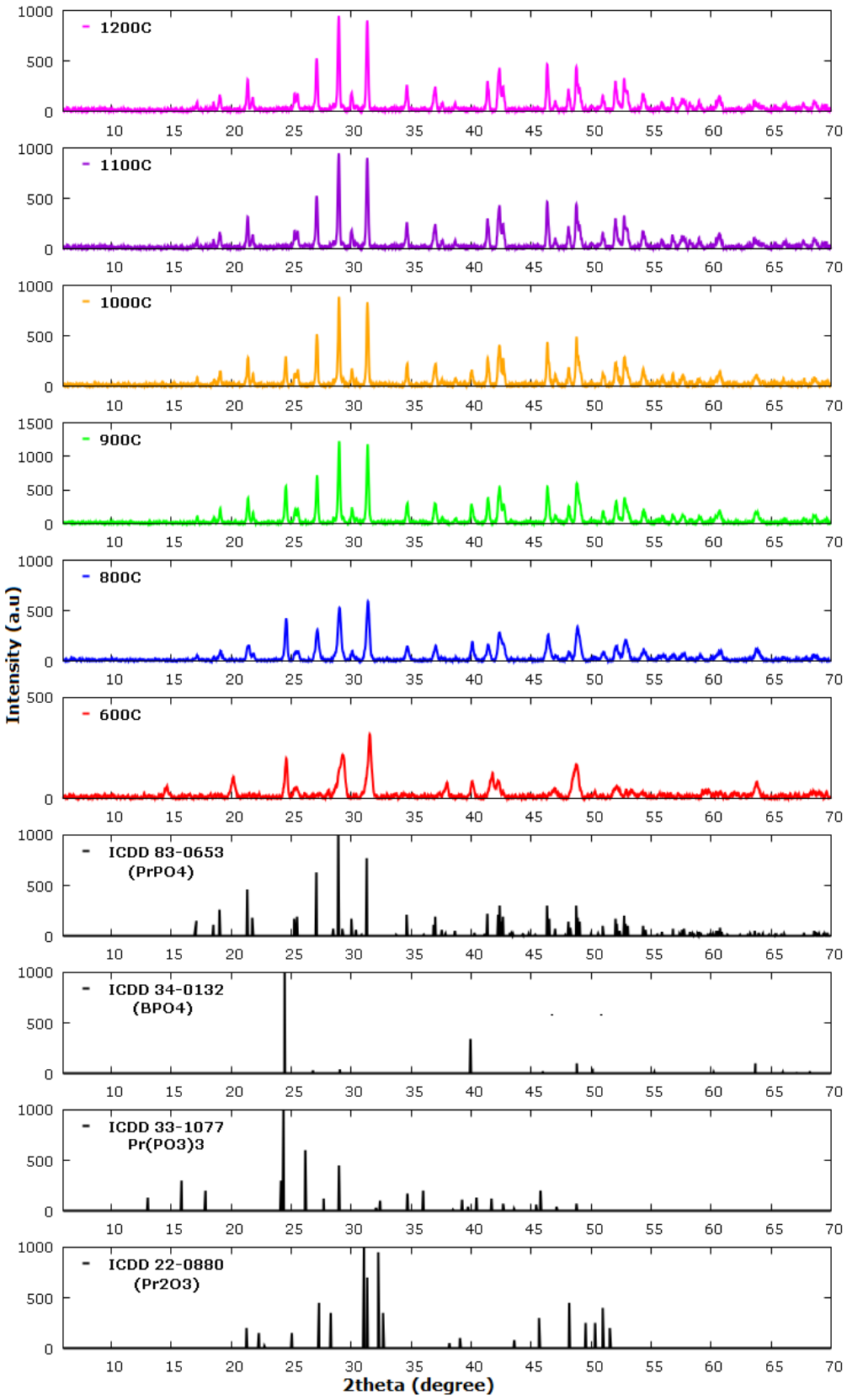

Figure 4.5. XRD pattern of $PrB(PO_4)_2$.

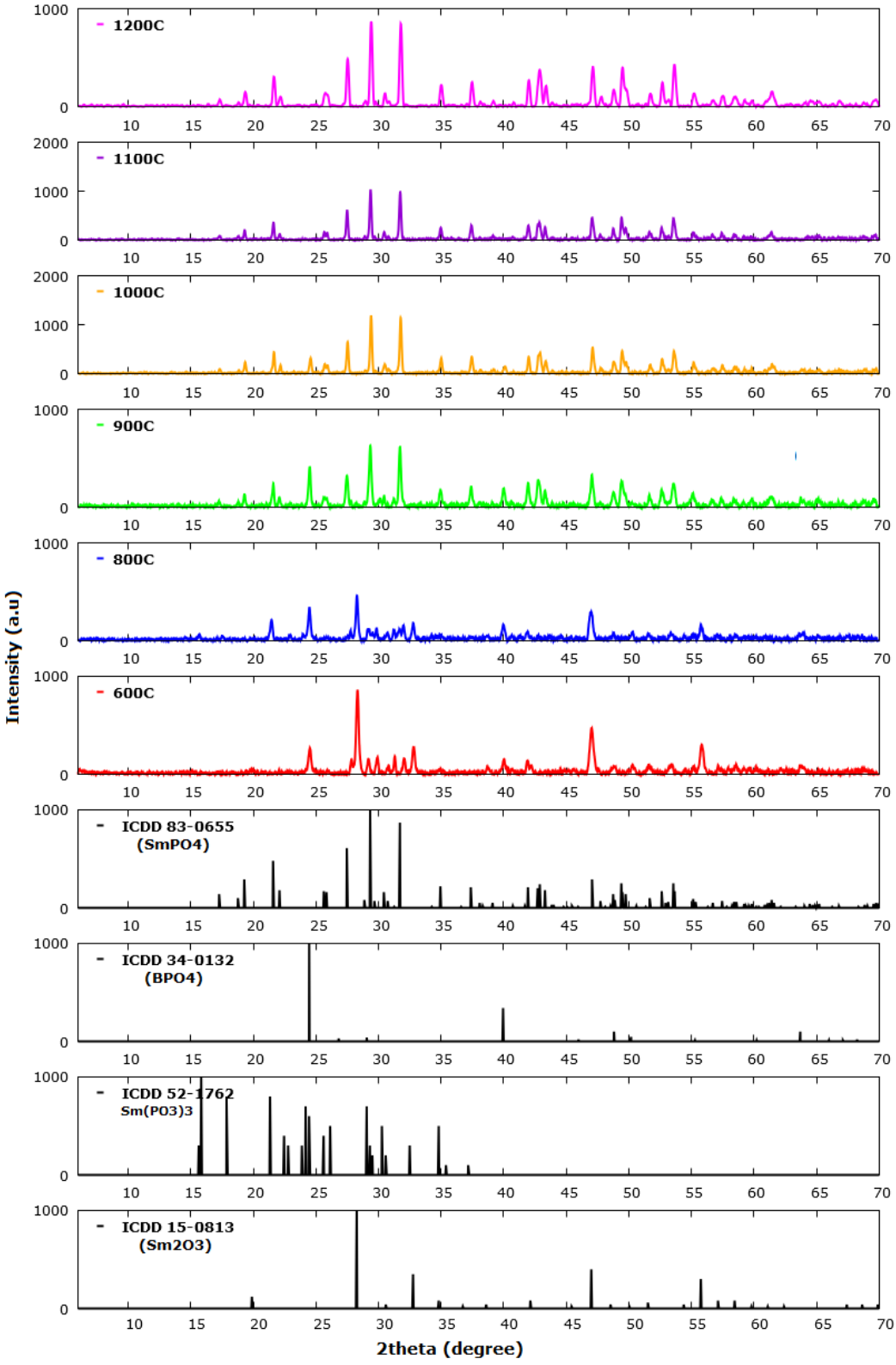

Figure 4.6. XRD pattern of $SmB(PO_4)_2$.

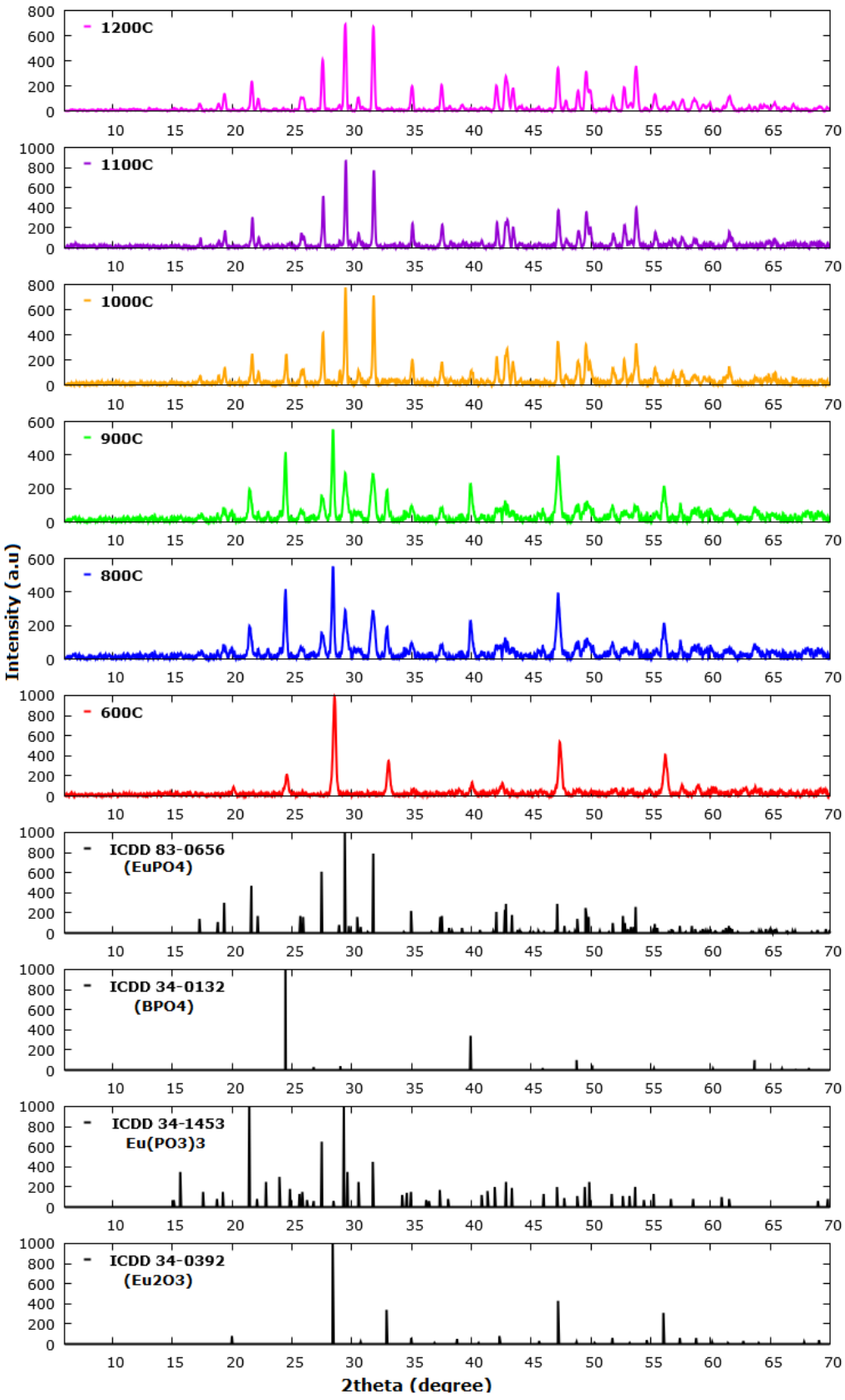

Figure 4.7. XRD pattern of $EuB(PO_4)_2$.

The various composition of H_3BO_3 were also applied in the fabrication of $YbB(PO_4)_2$ to confirm the presence of boron compound in our sample. Based on the XRD data, the BPO_4 are detected at 1000^oC for 25% and 50% excess of boric acid (2θ=~23^o). By further heating (>1000^oC) pure xenotime structure of $YbB(PO_4)_2$ were attained for all synthesized compounds(Figure 4.8-4.10).

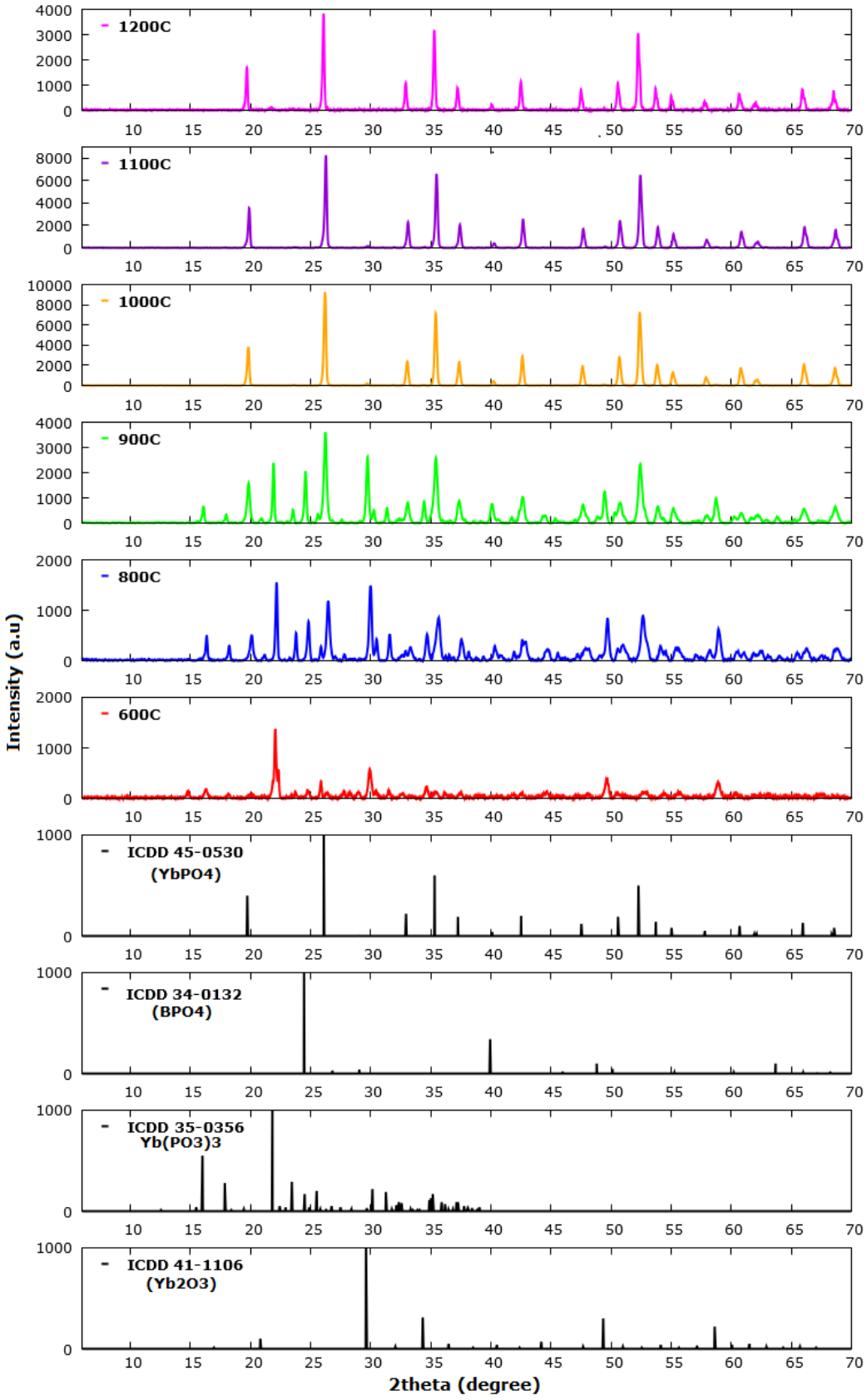

Figure 4.8. XRD pattern of $YbB(PO_4)_2$.

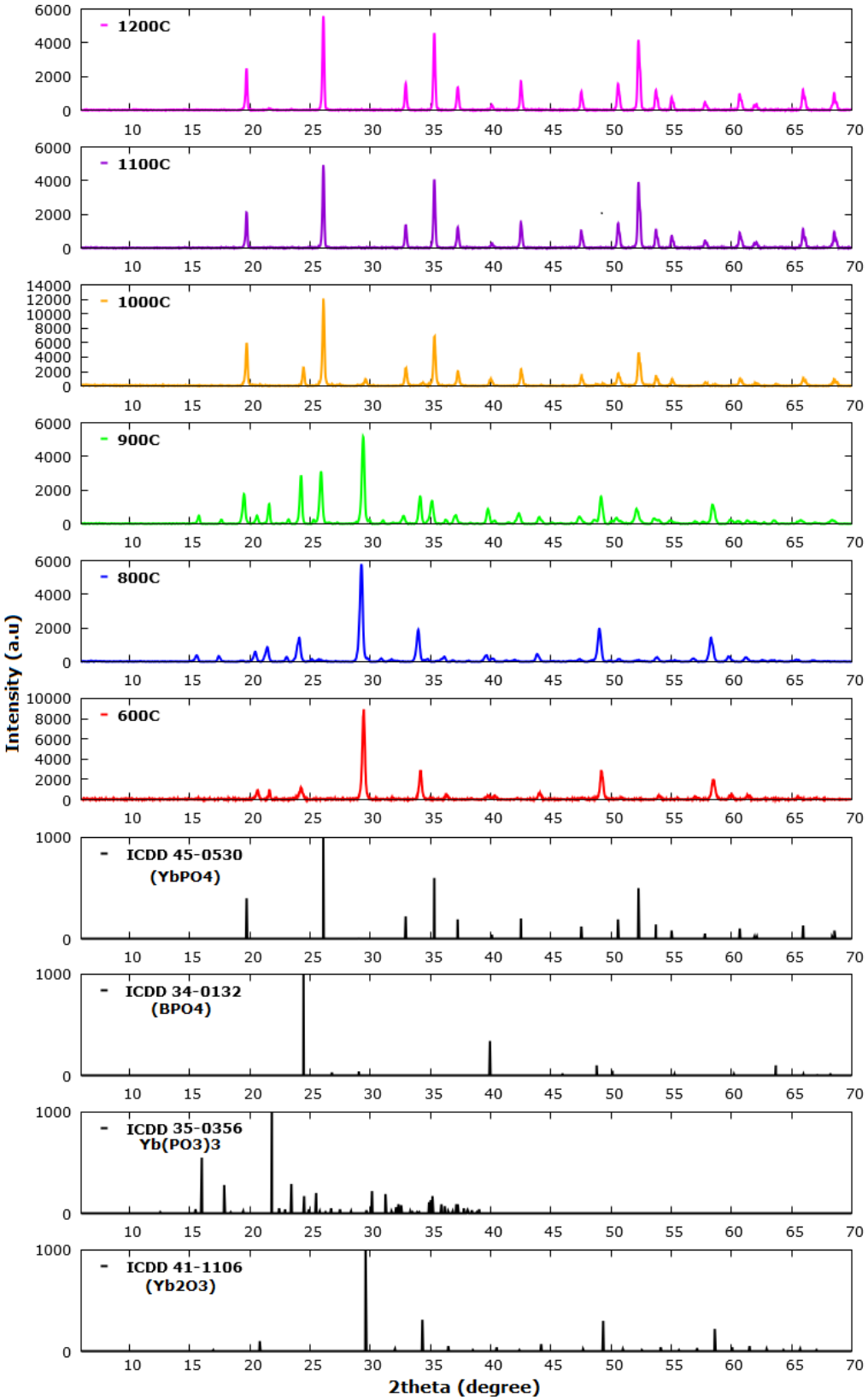

Figure 4.9. XRD pattern of $YbB(PO_4)_2$ (25% excess of H_3BO_3).

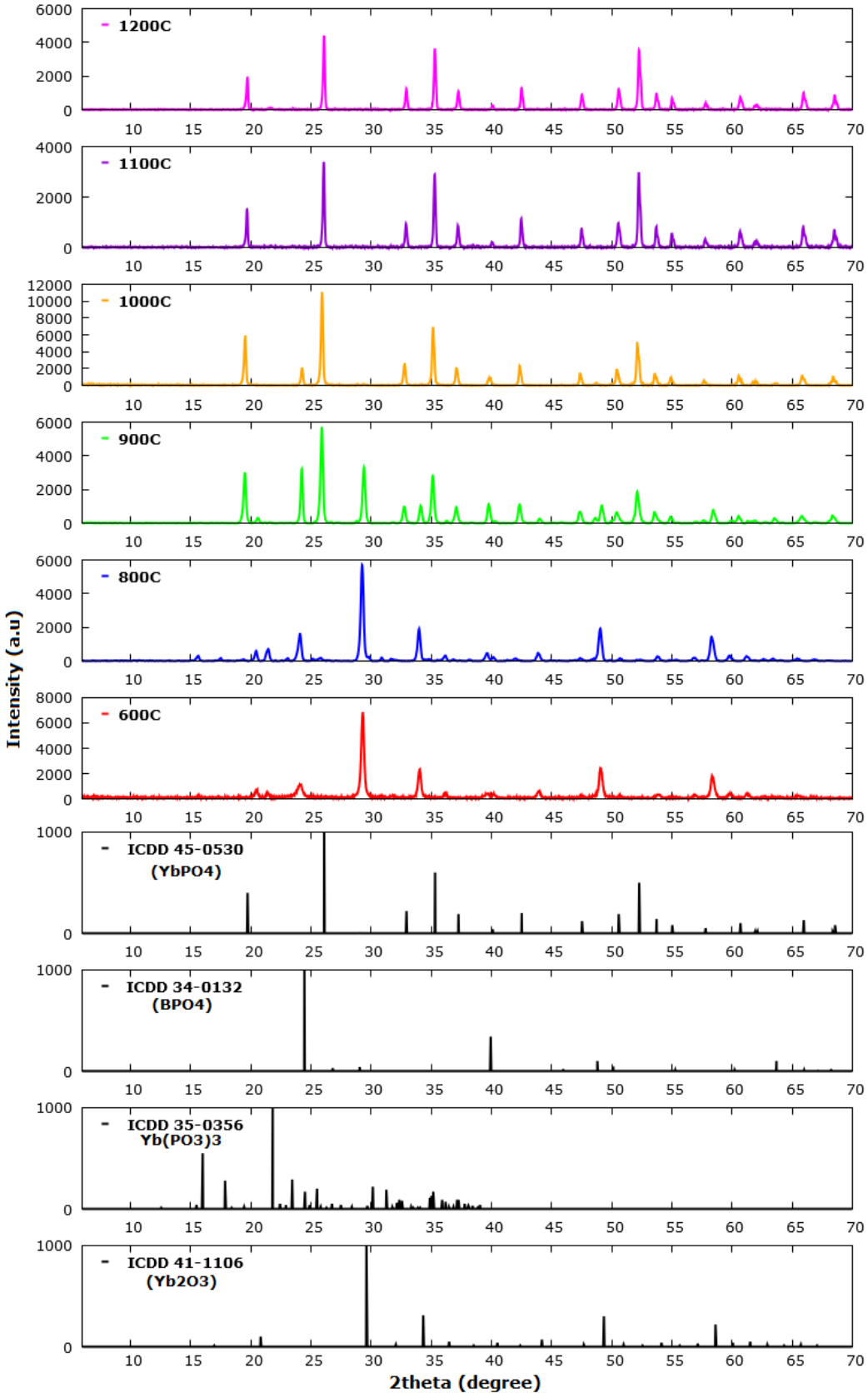

Figure 4.10. XRD pattern of $YbB(PO_4)_2$ (50% excess of H_3BO_3).

Similar to $YbB(PO_4)_2$ compound, xenotime structure of Tb, Ho, Tm, Lu-containing $LnB(PO_4)_2$ were prepared. According to their XRD data (Figure 4.11-4.14) the formation of $LnB(PO_4)_2$ were not completed since there are some extra peak which belongs to Ln_2O_3, $LnPO_4$, $Ln(PO_3)_3$ (Ln: Tb, Ho, Tm, Lu) were detected. In the analysis of XRD patterns of the products obtained between 600-1000^oC unreacted Tb_2O_3 (ICDD Card No: 43-1032), Ho_2O_3 (ICDD Card No: 43-1018), Tm_2O_3 (ICDD Card No: 43-1034), Lu_2O_3 (ICDD Card No: 43-1021), $TbPO_4$ (ICDD Card No: 83-0659), $HoPO_4$ (ICDD Card No: 83-0661), $TmPO_4$ (ICDD Card No: 83-0663), $LuPO_4$ (ICDD Card No: 83-0665), $Tb(PO_3)_3$ (ICDD Card No: 35-0296, $Ho(PO_3)_3$ (ICDD Card No: 52-1763), $Tm(PO_3)_3$ (ICDD Card No: 52-1759), $Lu(PO_3)_3$ (ICDD Card No: 35-0399) and BPO4 (ICDD Card No: 34-0132) were observed. Single phase lanthanide borophosphates with higher crystalinity were successfully obtained by further heating at 1100^oC. Due to its identical d-line of the obtained compound with the $LnPO_4$, the formation of $LnB(PO_4)_2$ were predicted (Ln: Yb, Tb, Ho, Tm, Lu).

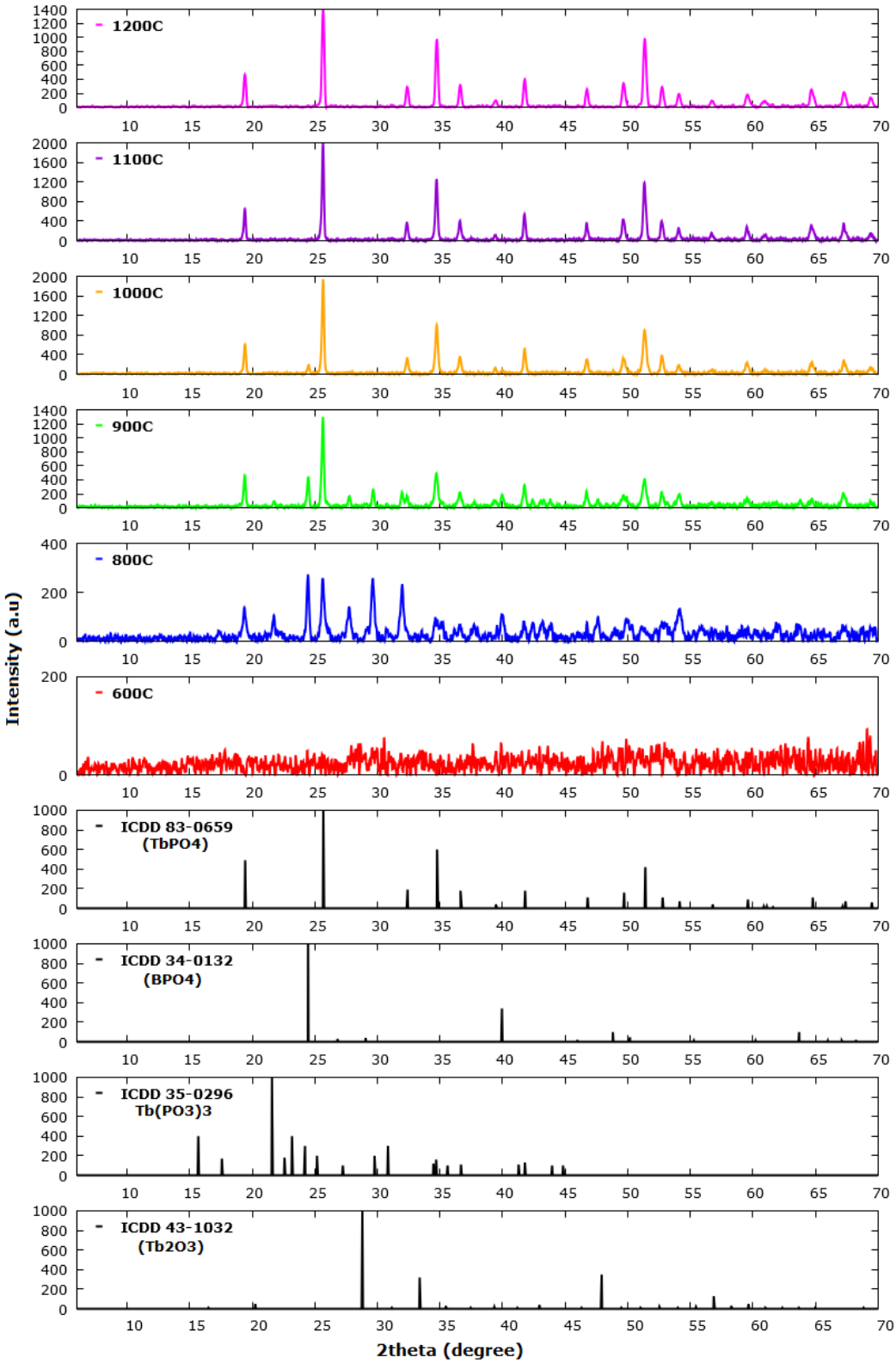

Figure 4.11. XRD pattern of $TbB(PO_4)_2$.

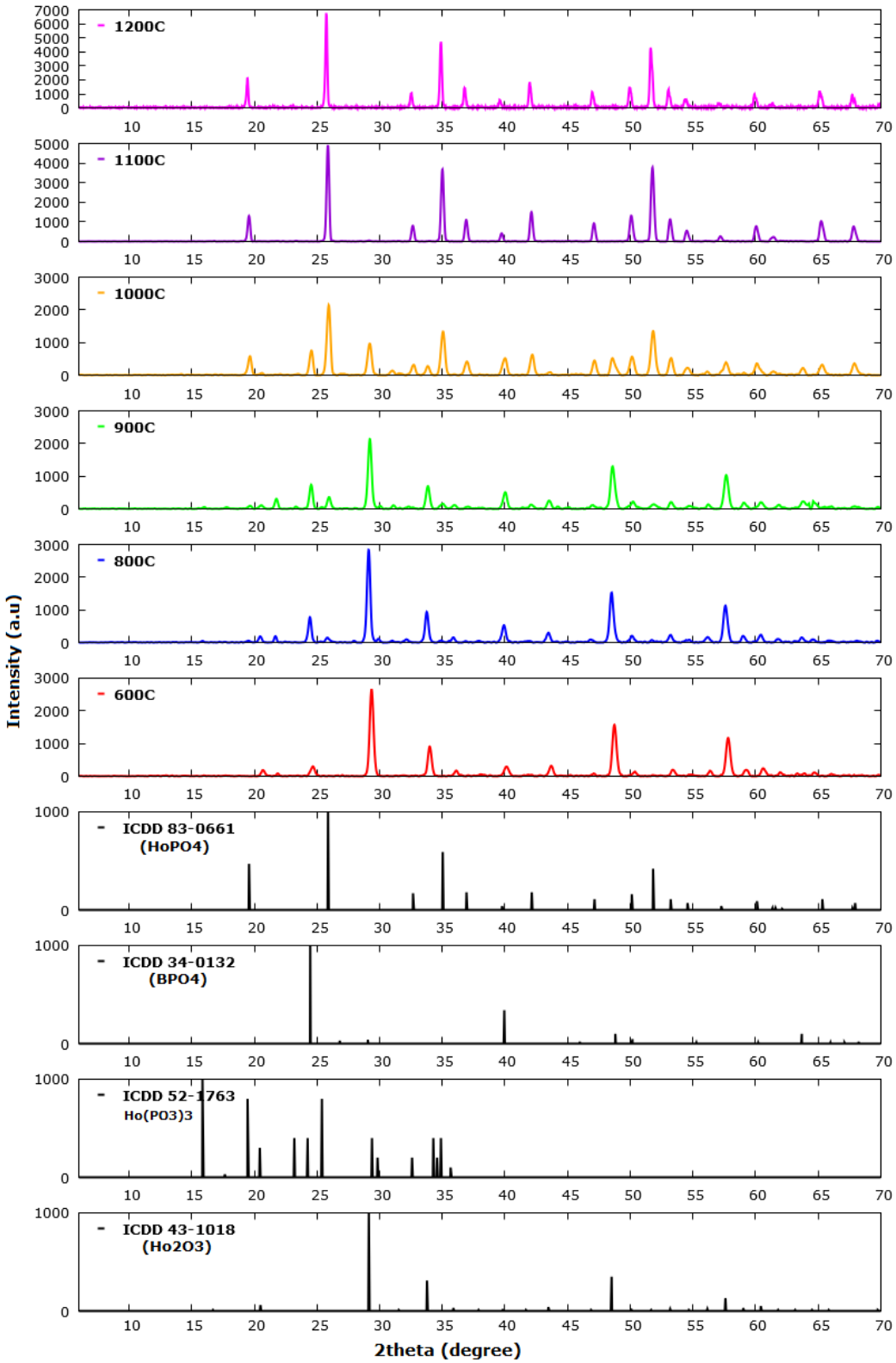

Figure 4.12. XRD pattern of $HoB(PO_4)_2$.

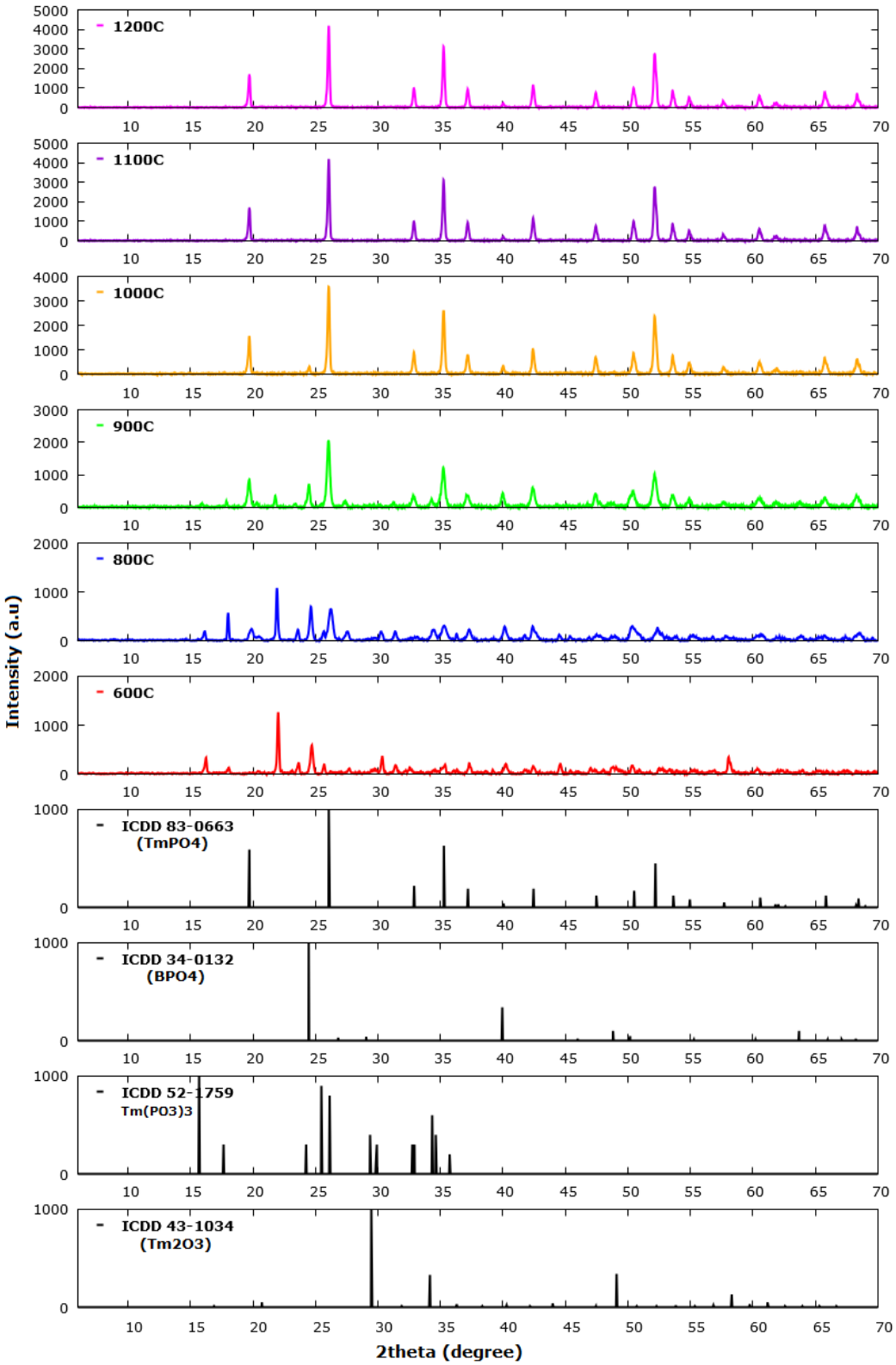

Figure 4.13. XRD pattern of $TmB(PO_4)_2$.

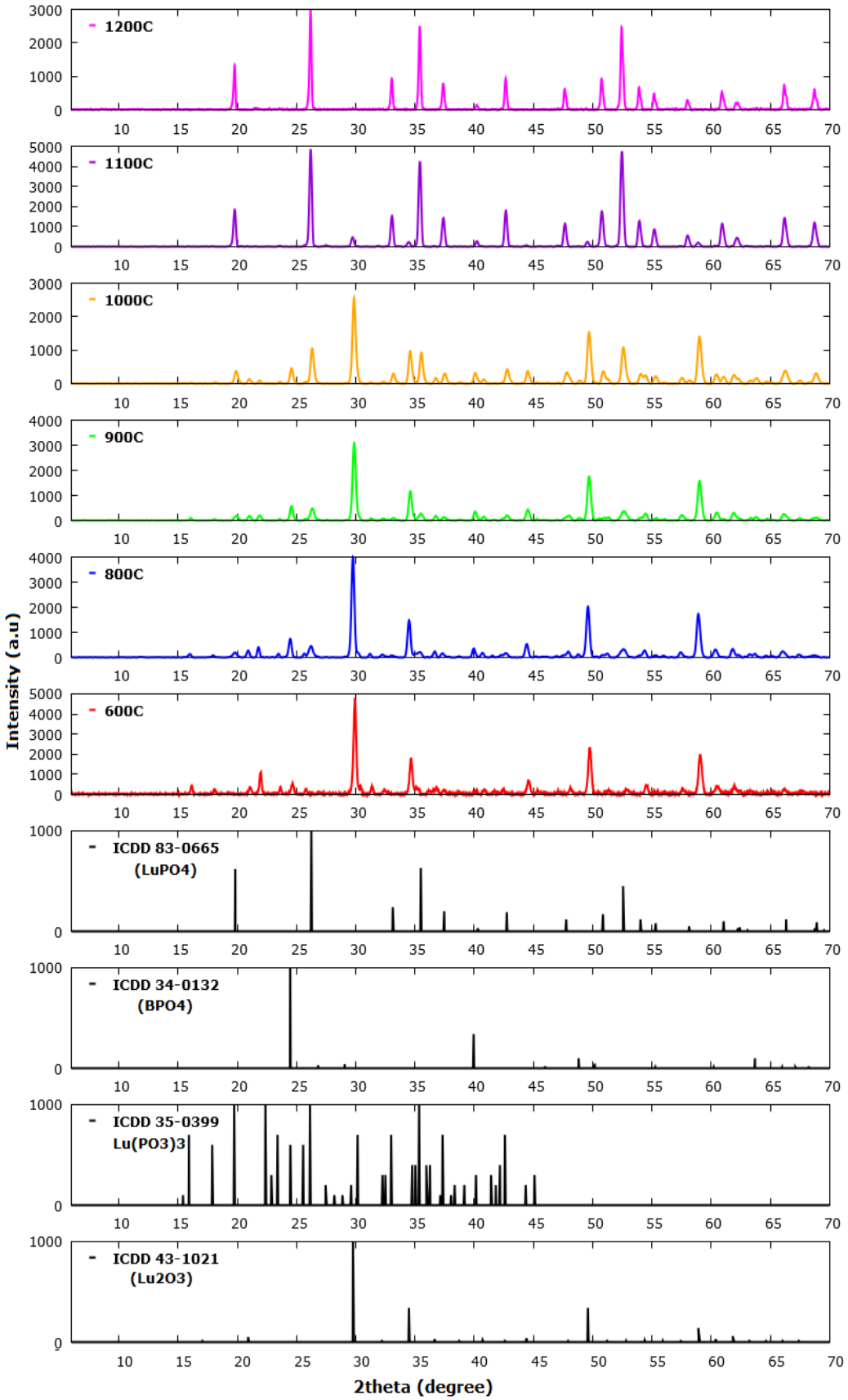

Figure 4.14. XRD pattern of $LuB(PO_4)_2$.

4.1.1.1. The Refinement Studies of Some Xenotime Rare-Earth Borophosphates

The refinement studies of xenotime structure borophosphates $LnB(PO_4)_2$ (Ln=Yb, Ho and Lu) were examined. Indicated by our indexing and refinement studies, The structure of the $YbB(PO_4)_2$ compound is shown to be xenotime. The indexing data was given in Table 4.1 and the unit cell parameters were calculated as tetragonal with a= 6.820(3) c= 5.975 (2) V= 277.945 space grup: I41/amd. The refinement pattern was given in Figure 4.15.

Table 4.1. The Indexing Data of $YbB(PO_4)_2$

I/I_o	hkl	d_{obs} (Å)	d_{calc}(Å)	$YbPO_4$ XRD data (ICDD: 45-0530)	
				d_{values}	I/I_o
44	1 0 1	4.496	4.945	4.492	40
100	2 0 0	3.4088	3.4103	3.4090	100
31	2 1 1	2.7145	2.7168	2.7160	22
84	1 1 2	2.5384	2.5336	2.5390	60
28	2 2 0	2.4100	2.4115	2.4110	19
9	2 0 2	2.2452	2.2473	2.2460	4
33	3 0 1	2.1248	2.1249	2.1240	30
24	1 0 3	1.9114	1.9119	1.9110	12
32	3 2 1	1.8021	1. 8035	1.8030	19
81	3 1 2	1.7478	1.7488	1.7480	50
27	4 0 0	1.7043	1.7051	1.7040	14
19	2 1 3	1.6671	1.6677	1.6670	8
13	4 1 1	1.5936	1.5943	1.5940	5
23	4 2 0	1.5247	1.5250	1.5240	10
10	3 0 3	1.4982	1.4939	1.4970	2
11	0 0 4	1.4930	1.4901	1.4930	2
27	3 3 2	1.4154	1.4157	1.4150	13
24	3 2 3	1.3678	1.3682	1.3680	8

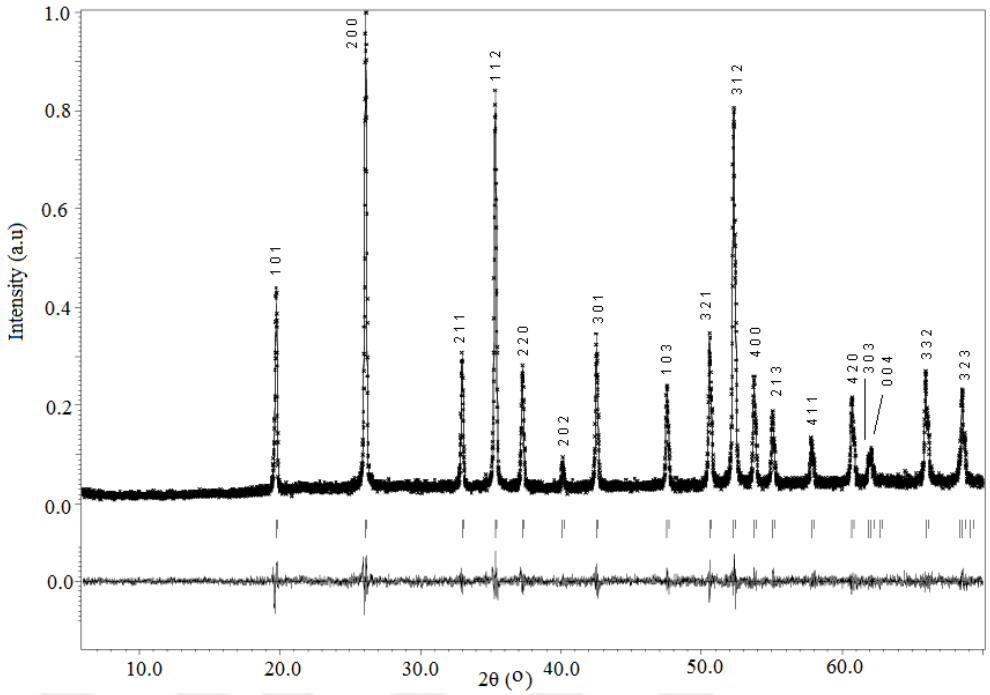

Figure 4.15. Refinement Pattern of $YbB(PO_4)_2$ at 1100°C.

The Indexing data (Table 4.2) and refinement pattern of $HoB(PO_4)_2$ (Figure 4.16) was also determined and calculated. It shown that unit cell parameters of $HoB(PO_4)_2$ are a= 6.891(5) c= 6.031(7) V= 286.46 space group: $I4_1/amd$. The inset shows as the superposition of the observed (dots) and the calculated (line) in the refinement patterns.

Table 4.2. The Indexing Data of $HoB(PO_4)_2$

I/I_o	hkl	d_{obs} (Å)	d_{calc}(Å)	XRD data of $HoPO_4$ JCPDS 83-0661	
				d_{values}	I/I_o
32	101	4.56	4.54	4.53	47
100	200	3.450	3.450	3.430	100
19	211	2.751	2.744	2.731	17
72	112	2.570	2.564	2.559	59
25	220	2.442	2.437	2.431	18
13	202	2.273	2.270	2.264	4
30	301	2.150	2.150	2.142	18
21	103	1.9333	1.9302	1.9260	11

27	321	1.8247	1.8221	1.8180	16
68	312	1.7685	1.7664	1.7630	42
24	400	1.7251	1.7229	1.7190	11
15	213	1.6857	1.6840	1.6800	7
11	411	1.6133	1.6108	1.6070	4
20	420	1.5429	1.5410	1.5380	9
10	303	1.5145	1.5093	1.5100	2
24	332	1.4317	1.4301	1.4270	11
20	323	1.3825	1.3819	1.3820	2
15	204	1.3793	1.3781	1.3780	7
15	431	1.3446	1.3437	1.3410	6

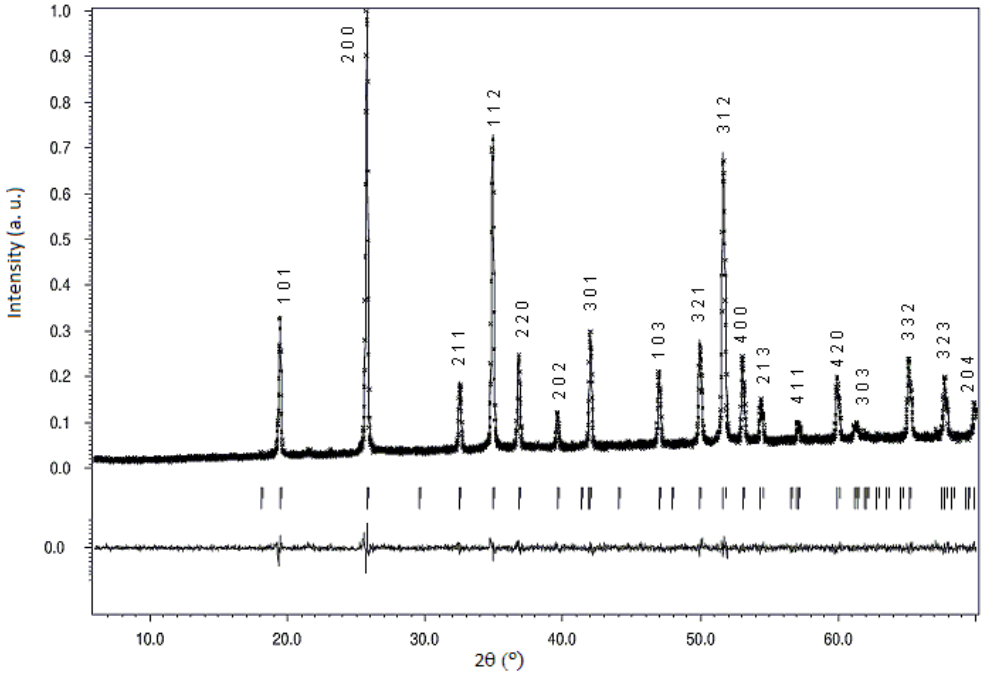

Figure 4.16. Refinement Pattern of the $HoB(PO_4)_2$ compound at 1200ºC.

The refinement studies of $LuB(PO_4)_2$ were also carried out and the calculated unit cell are described as a= 6.798(9) c= 5.962(6) V= 275.62 space group: $I4_1/amd$. The indexing data and refinement pattern are shown in Table 4.3 and Figure 4.16, respectively. In the refinement pattern, the inset shows the superposition of the observed (dots) and the calculated (line) patterns.

Table 4.3. The Indexing Data of $LuB(PO_4)_2$

I/I_o	hkl	d_{obs} (Å)	d_{calc}(Å)	XRD data of $LuPO_4$ (JCPDS 83-0665)	
				d_{values}	I/I_o
50	101	4.48	4.48	4.47	62
100	200	3.400	3.400	3.391	100
37	211	2.709	2.708	2.702	24
88	112	2.533	2.533	2.527	63
30	220	2.404	2.404	2.398	20
10	202	2.243	2.242	2.236	3
36	301	2.118	2.119	2.113	19
27	103	1.9084	1.9078	1.9030	12
36	321	1.7971	1.7980	1.7940	17
87	312	1.7440	1.7439	1.7400	45
29	400	1.6993	1.6998	1.6960	12
22	213	1.6634	1.6637	1.6590	8
16	411	1.5891	1.5894	1.5860	5
24	420	1.5197	1.5203	1.5170	10
14	303	1.4932	1.4944	1.4900	3
14	004	1.4906	1.4907	1.4870	4
31	332	1.4111	1.4081	1.4080	12
23	323	1.4082	1.3680	1.3650	3
27	204	1.3651	1.3619	1.3620	9

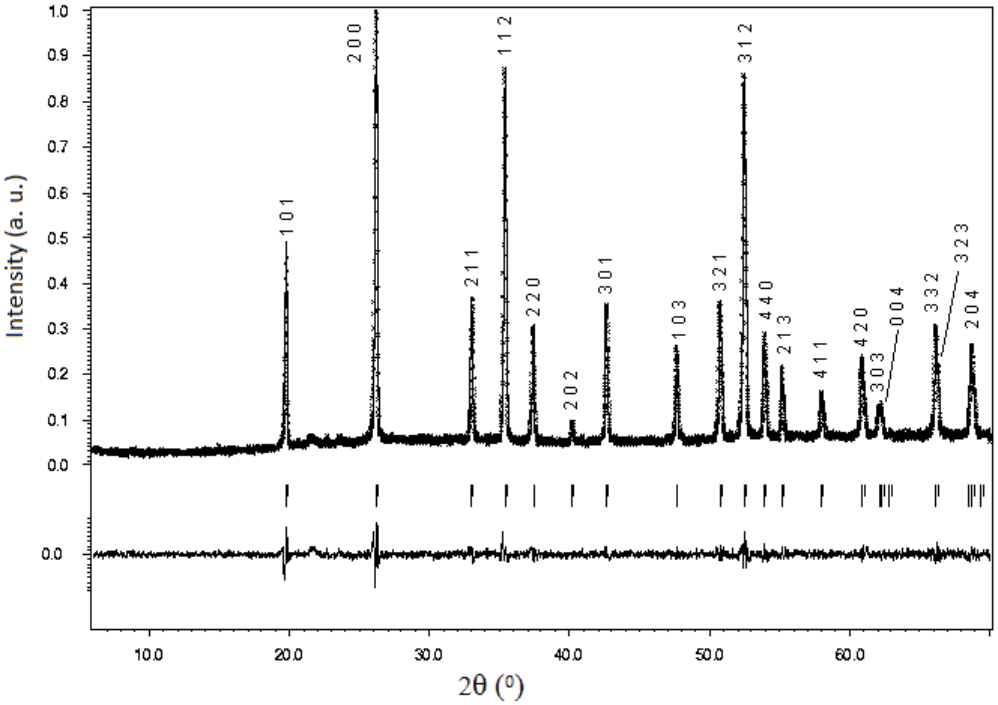

Figure 4.17. Refinement Pattern of the $LuB(PO_4)_2$ compound at 1200ºC.

4.1.2 Infrared Spectroscopy Studies for Ln: Nd, Ce, Pr, Sm, Eu, Yb, Tb, Ho, Tm, Lu Compounds

The infrared spectra of the products obtained by solid state reaction method at 600-1200^{o}C for monazite type structure $LnB(PO_4)_2$ (Ln: Nd, Ce, Pr, Sm, Eu) were presented in Figure 4.18 to Figure 4.24.

The infrared spectra of the compounds was measured in the range 400-4000 cm^{-1}. The absortion band assigned at >1000^{o}C are in a good accordance to the literature data as the band in the range of 1000-1250 cm^{-1} is associated to asymmetric stretching mode, The symmetric strecthing mode was assigned between 900-1000cm^{-1} whereas the asymmetric and symmetric bending mode are observed at 500-700cm^{-1} and 300-500$cm^{-1,}$ respectively [120]. The broad absorption band at around 3600-3000^{o}C detected at lower temperatures is assigned to the hydroxyl group of water molecule. The vibrational bands of BPO_4, $LnPO_4$ and $Ln(PO_3)_3$, Ln_2O_3 (Ln: Ce, Pr, Nd, Sm, Eu) were also observed at low temperatures (600-900°C).

The IR absorbtion bands of $Ln(PO_3)_3$ and Ln_2O_3 disappeared at high temperatures (after 1000°C), thus attributing to the formation of $LnB(PO_4)_2$. In these compounds, the boron atoms have tetrahedral coordination since the typical bands are situated in the 1000-850cm^{-1} range. The stretching modes of a free PO_4^{-1} anion with Td symmetry have four internal modes of vibrations which are $\upsilon_3(PO_4)$=1107, 1024; $\upsilon_1(PO_4)$=954, $\upsilon_4(PO_4)$=576; $\upsilon_2(PO_4)$=482 cm^{-1}. These vibrational wave numbers are in reasonable agreement with the experimental absorption bands for the obtained products.)

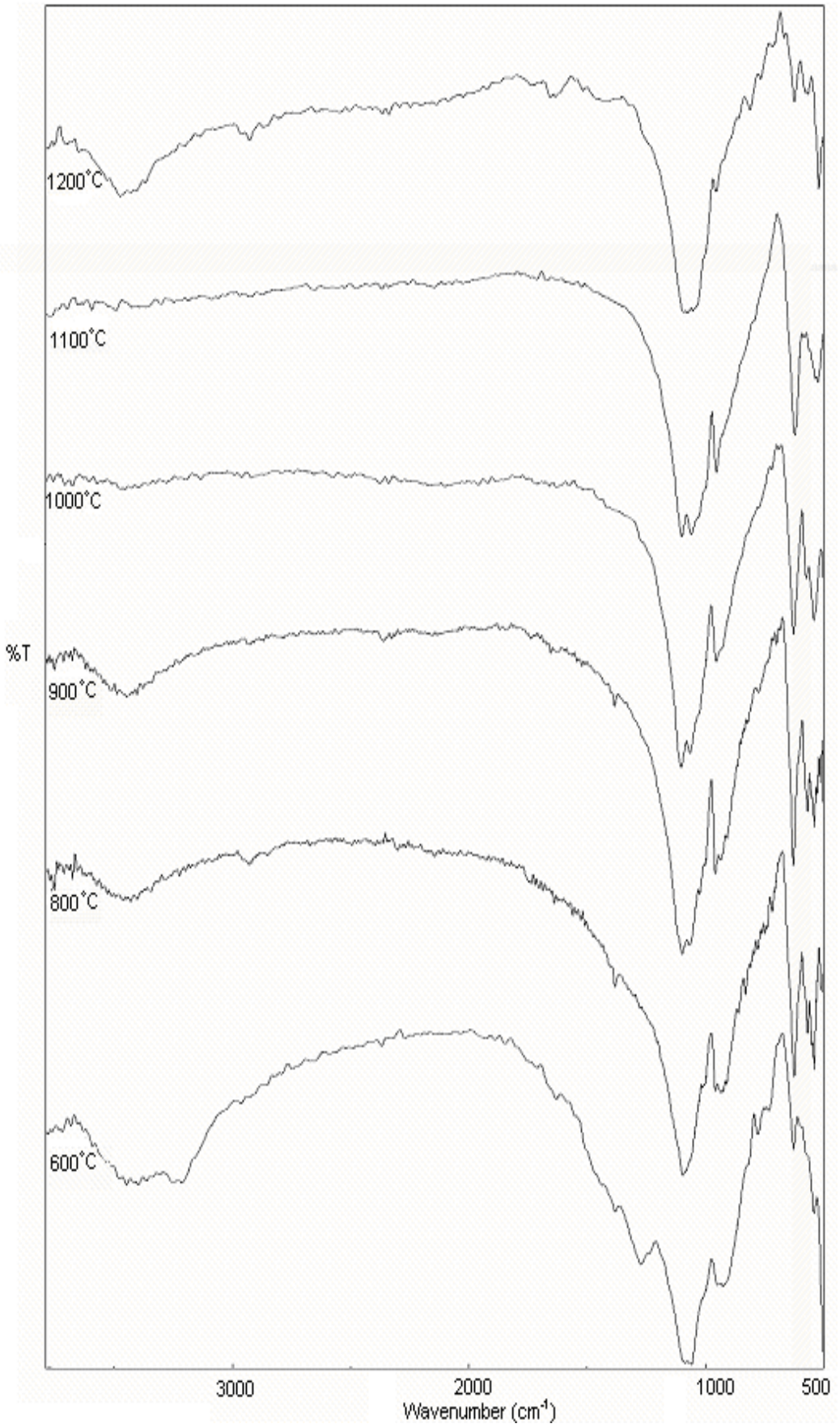

Figure 4.18. IR Spectra of $NdB(PO_4)_2$.

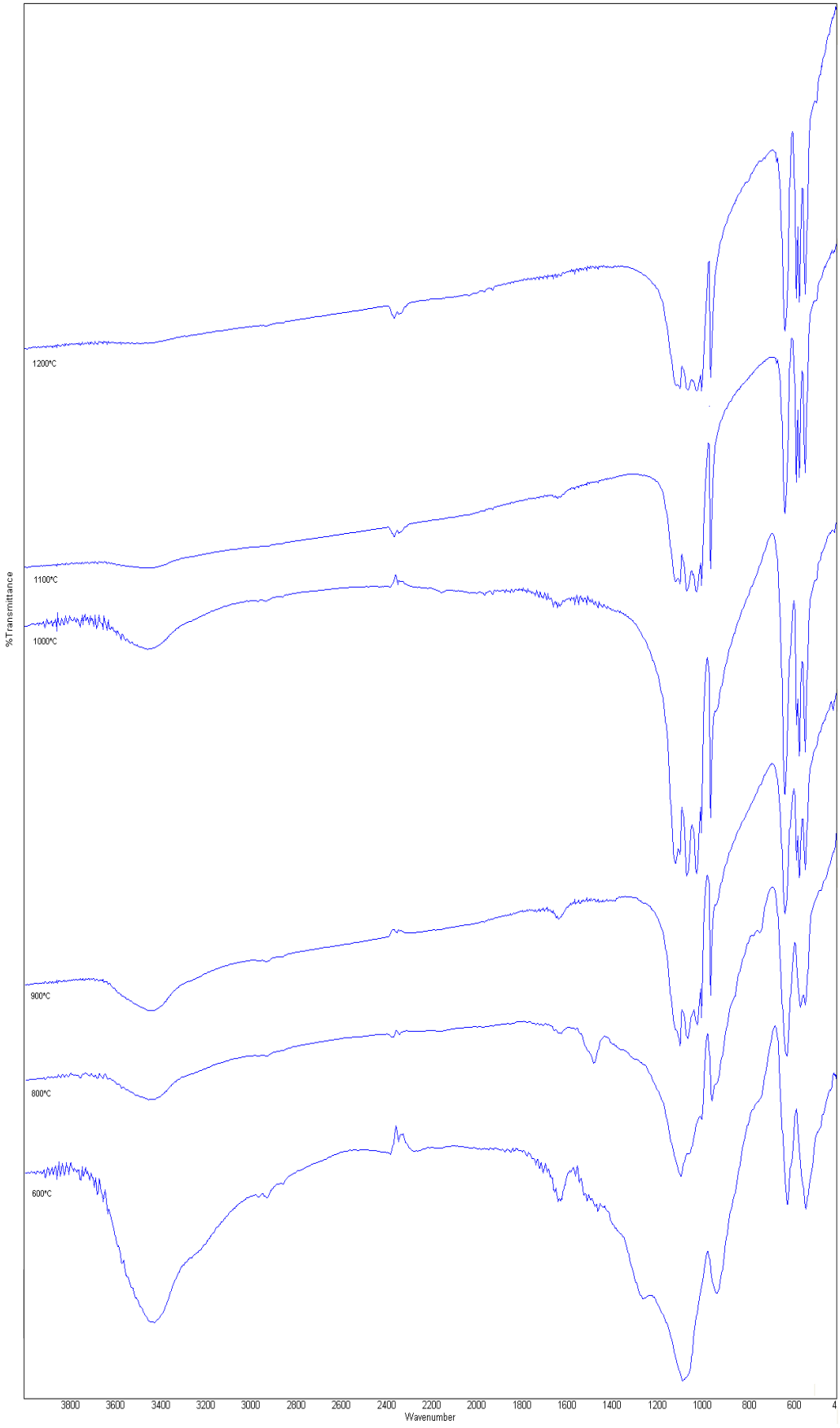

Figure 4.19. IR Spectra of $NdB(PO_4)_2$ (25% excess of H_3BO_3).

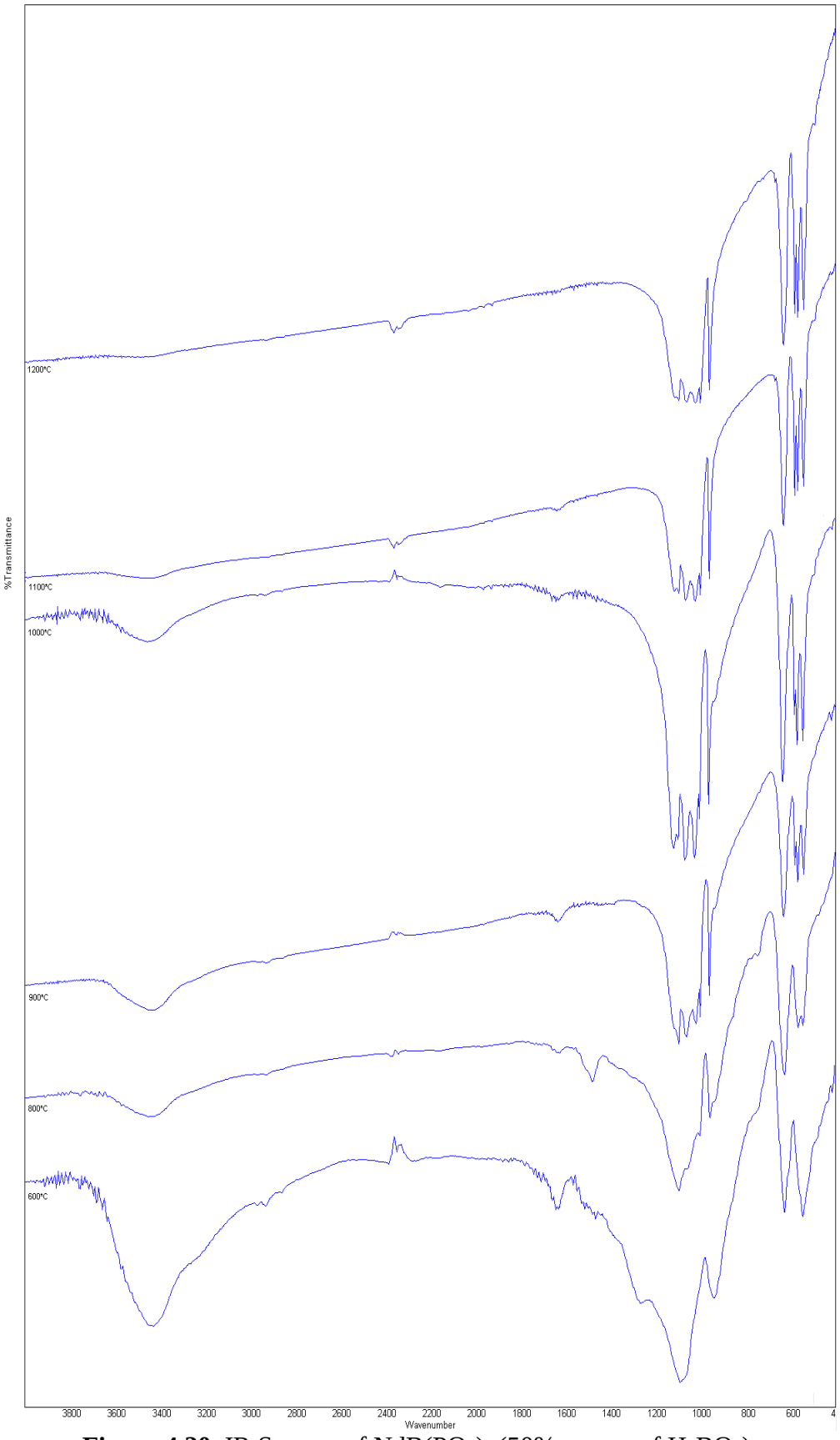

Figure 4.20. IR Spectra of $NdB(PO_4)_2$ (50% excess of H_3BO_3).

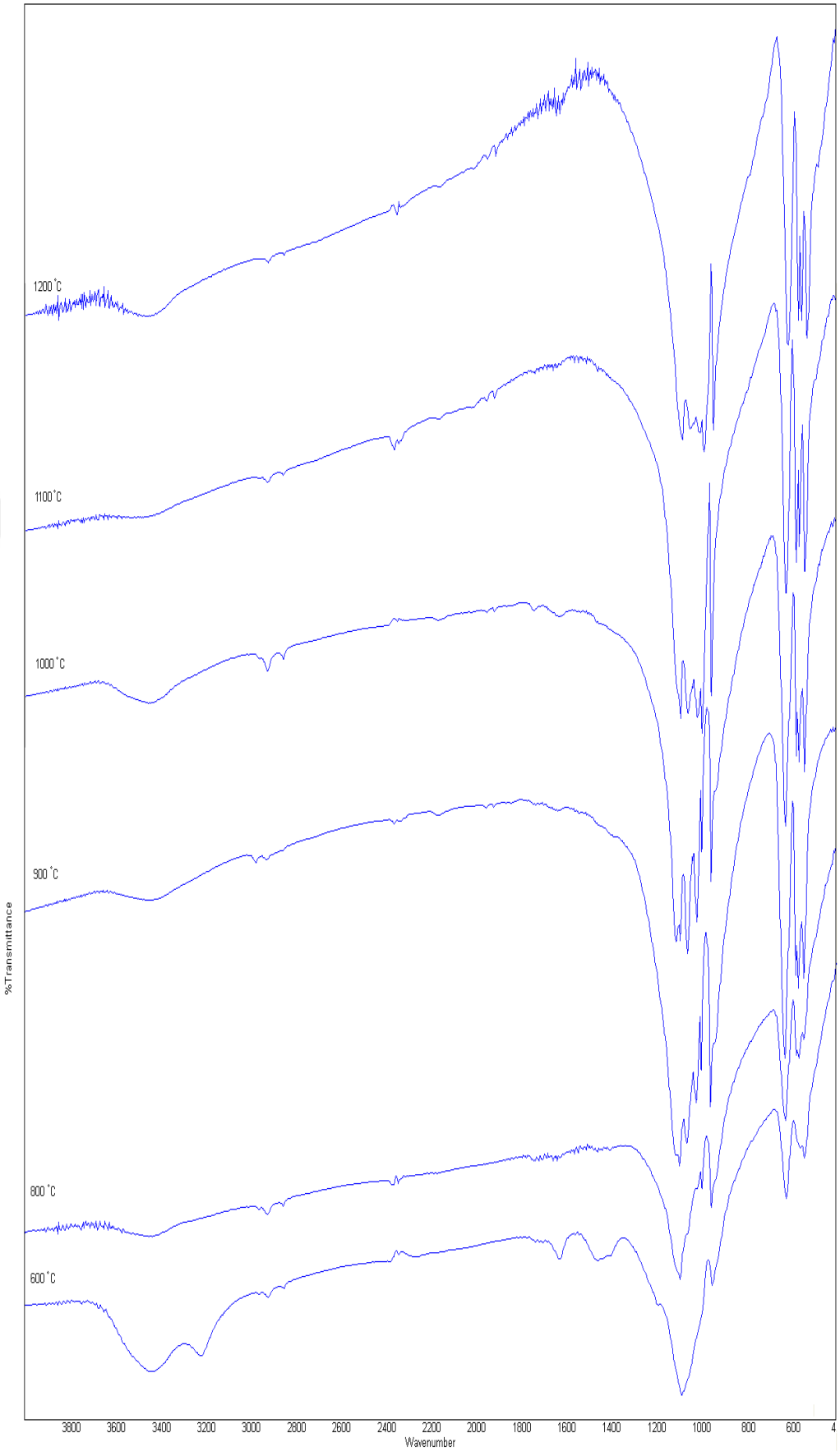

Figure 4.21. IR Spectra of $CeB(PO_4)_2$.

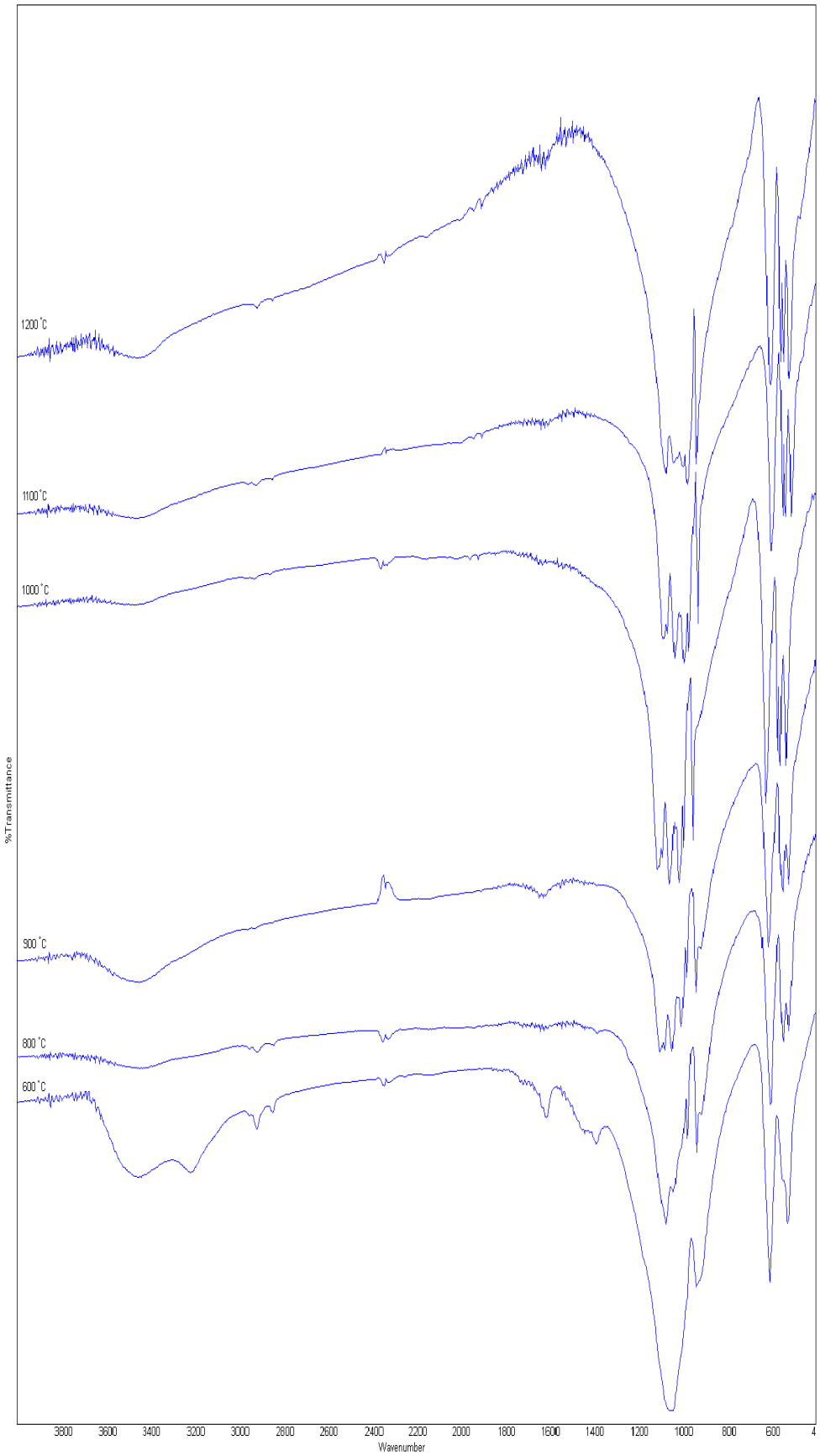

Figure 4.22. IR Spectra of $PrB(PO_4)_2$.

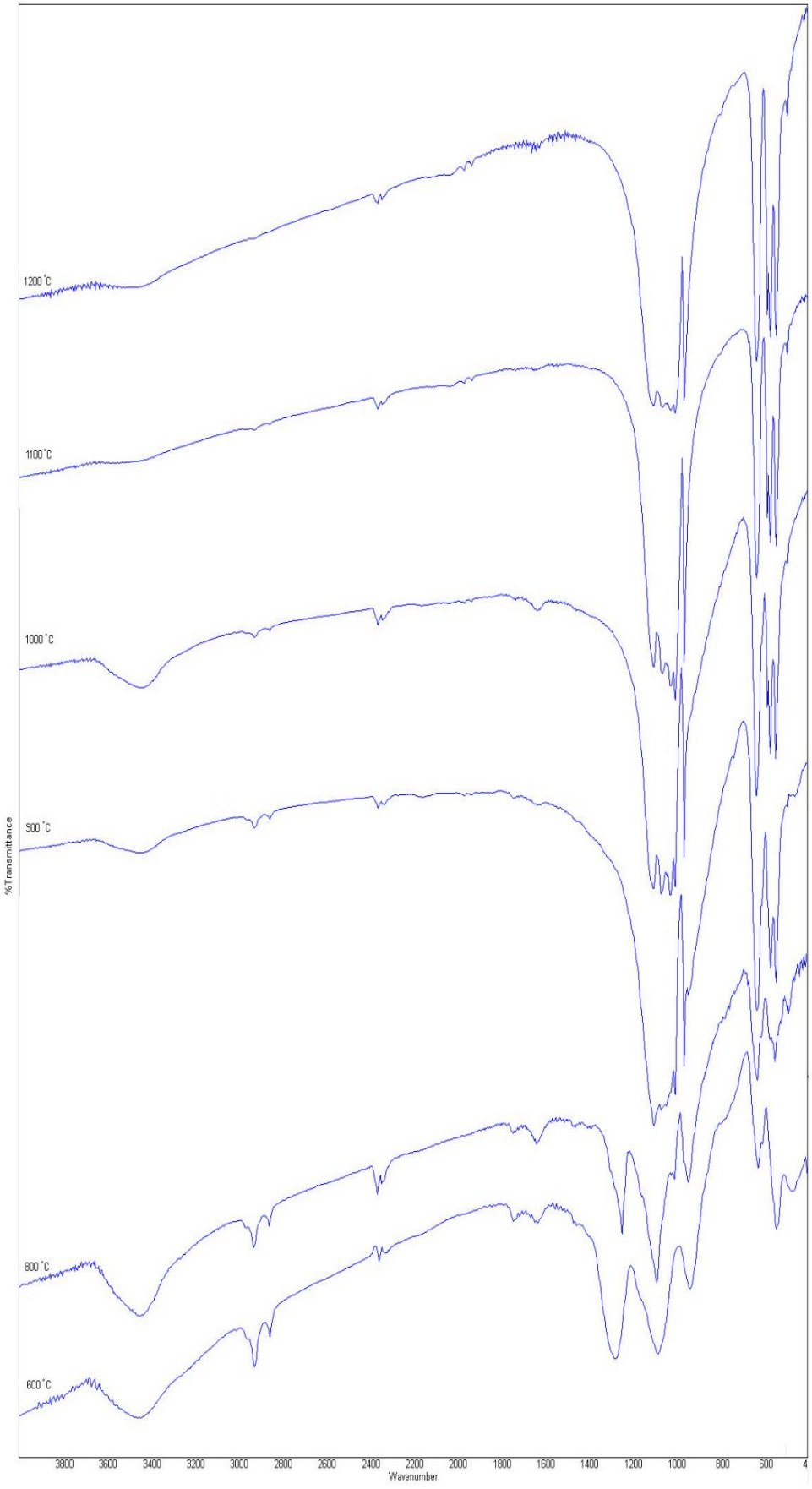

Figure 4.23. IR Spectra of $SmB(PO_4)_2$.

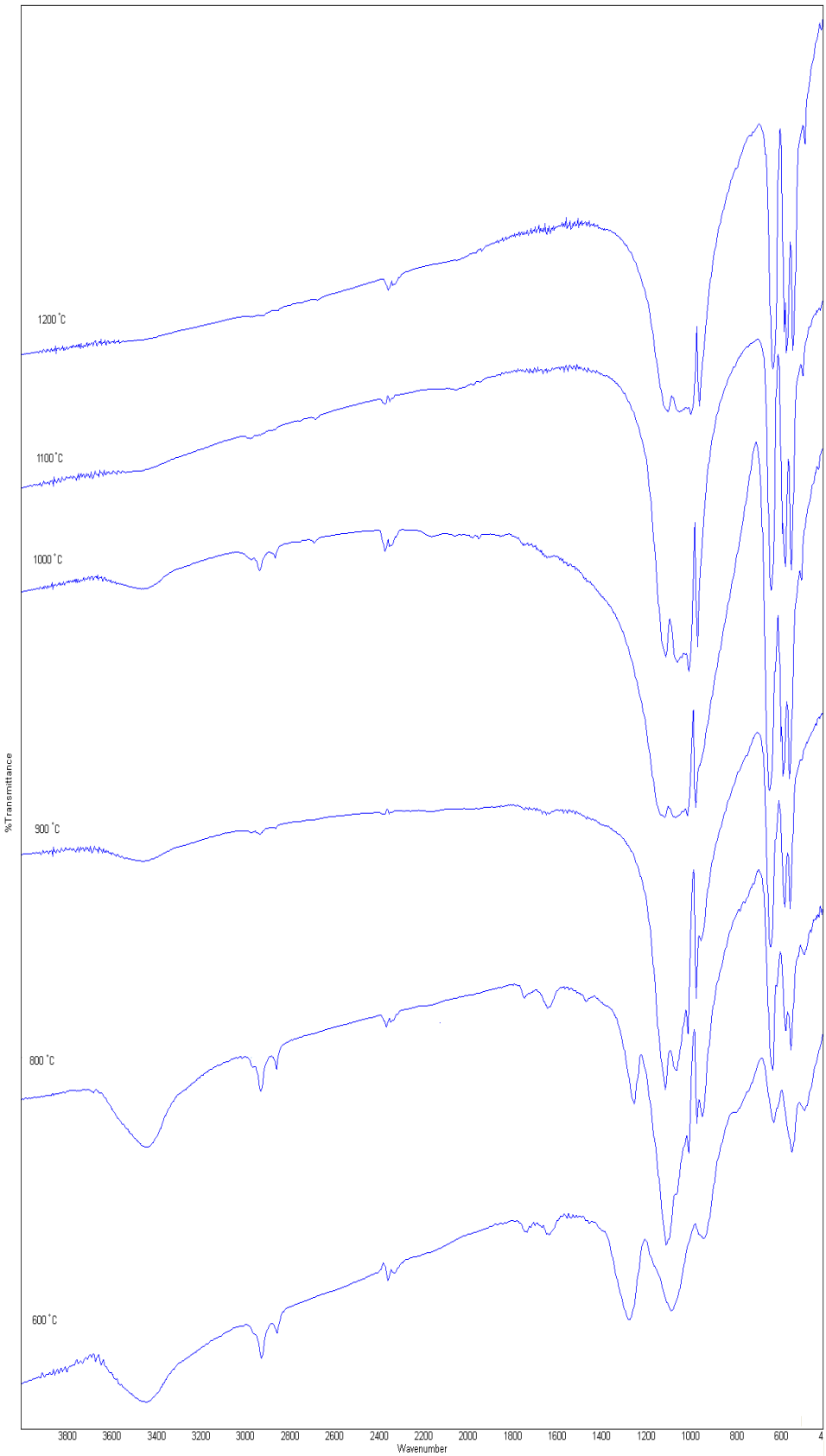

Figure 4.24. IR Spectra of $EuB(PO_4)_2$.

The xenotime type structure $LnB(PO_4)_2$ (Ln: Yb, Tb, Ho, Tm, Lu) obtained at different temperatures were also characterized by FT-IR Spectroscopy to determined their bond variations. The measurement was carried out between 4000-400^oC. It found that at the strong broad absorption band observed at around 3000 cm^{-1} is attributed to O-H group stretching vibration which then disappeared after further heating at higher temperatures. The bands belong to $Ln(PO_3)_3$ and Ln_2O_3 were observed at 600-900^oC. According to our FT-IR spectra, the band belongs to PO_4 were detected at around 1100 cm^{-1}, 930 cm^{-1} 630 cm^{-1} and 560 cm^{-1}. The bands assigned at 930 cm^{-1}, 630 cm^{-1} and 580 cm^{-1} identify the presence of BO_4.

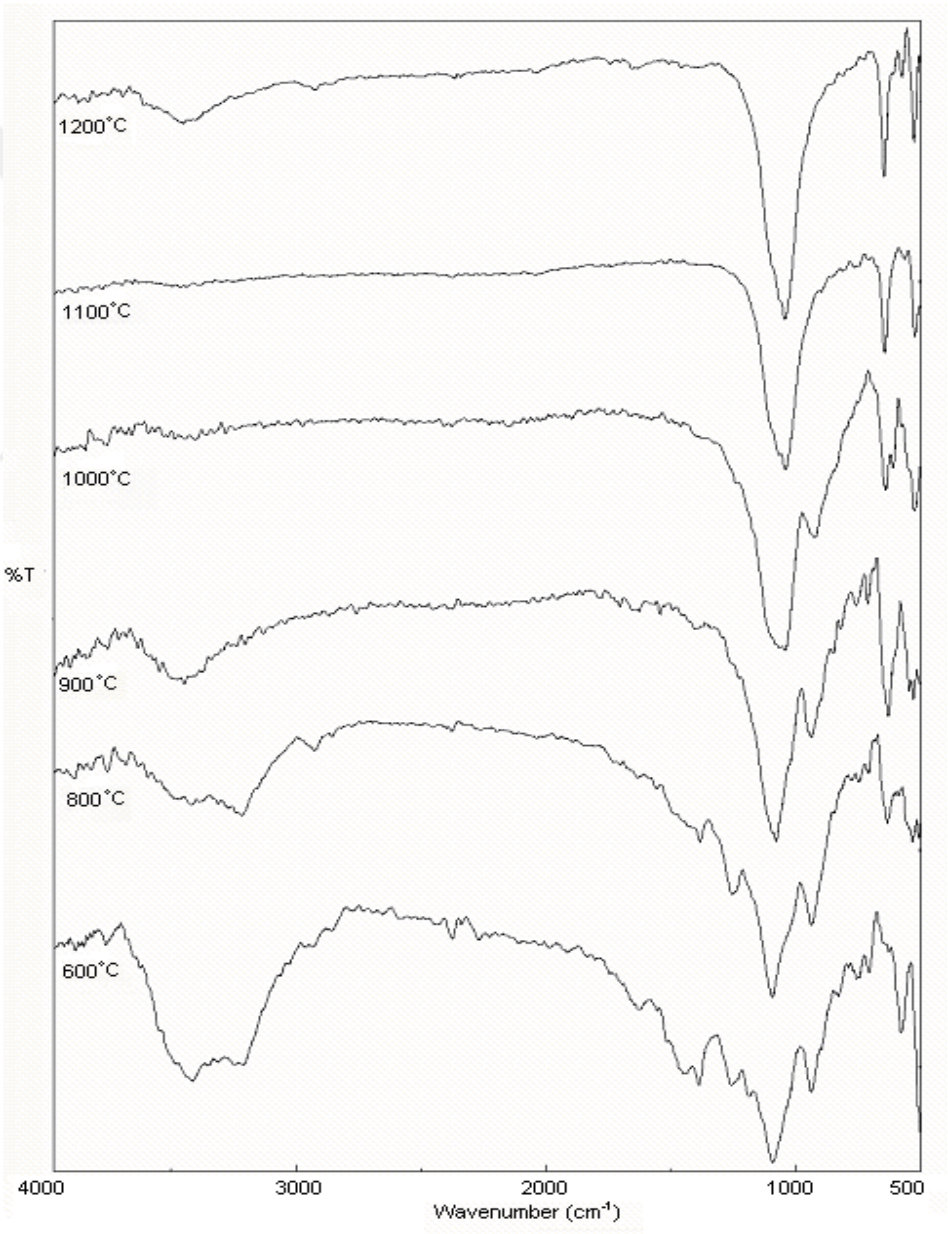

Figure 4.25. IR Spectra of $YbB(PO_4)_2$.

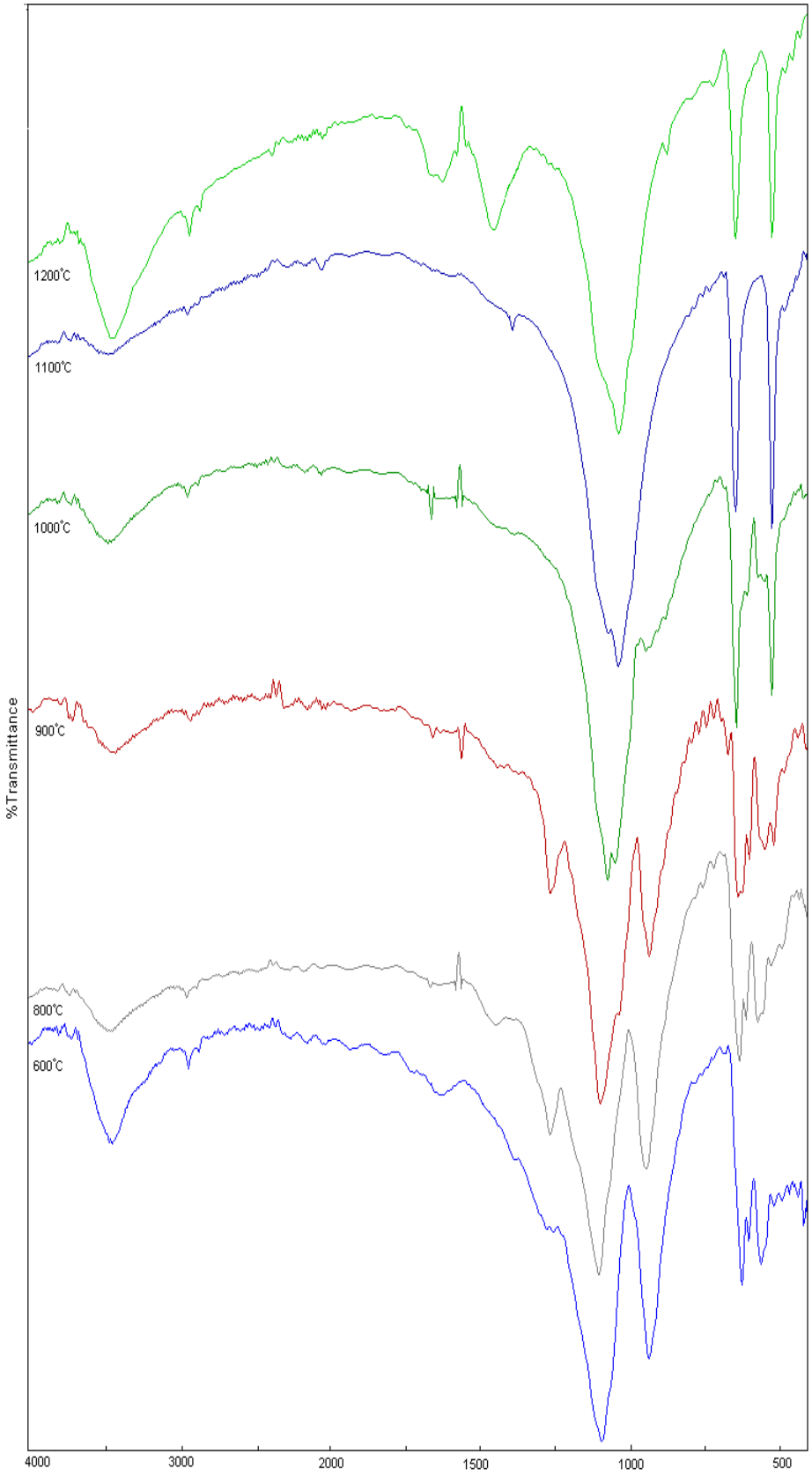

Figure 4.26. IR Spectra of $YbB(PO_4)_2$(25% excess of H_3BO_3).

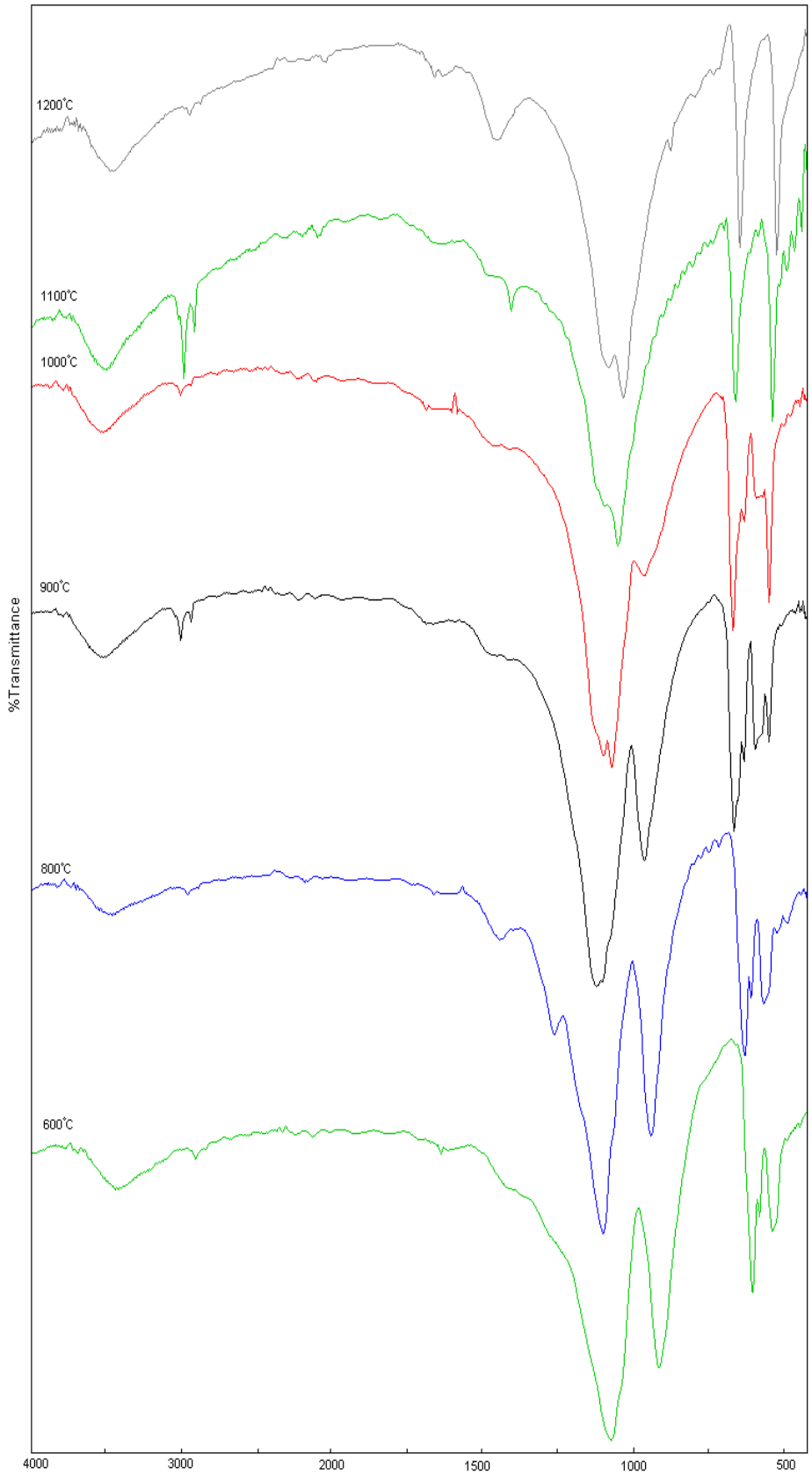

Figure 4.27. IR Spectra of $YbB(PO_4)_2$(50% excess of H_3BO_3).

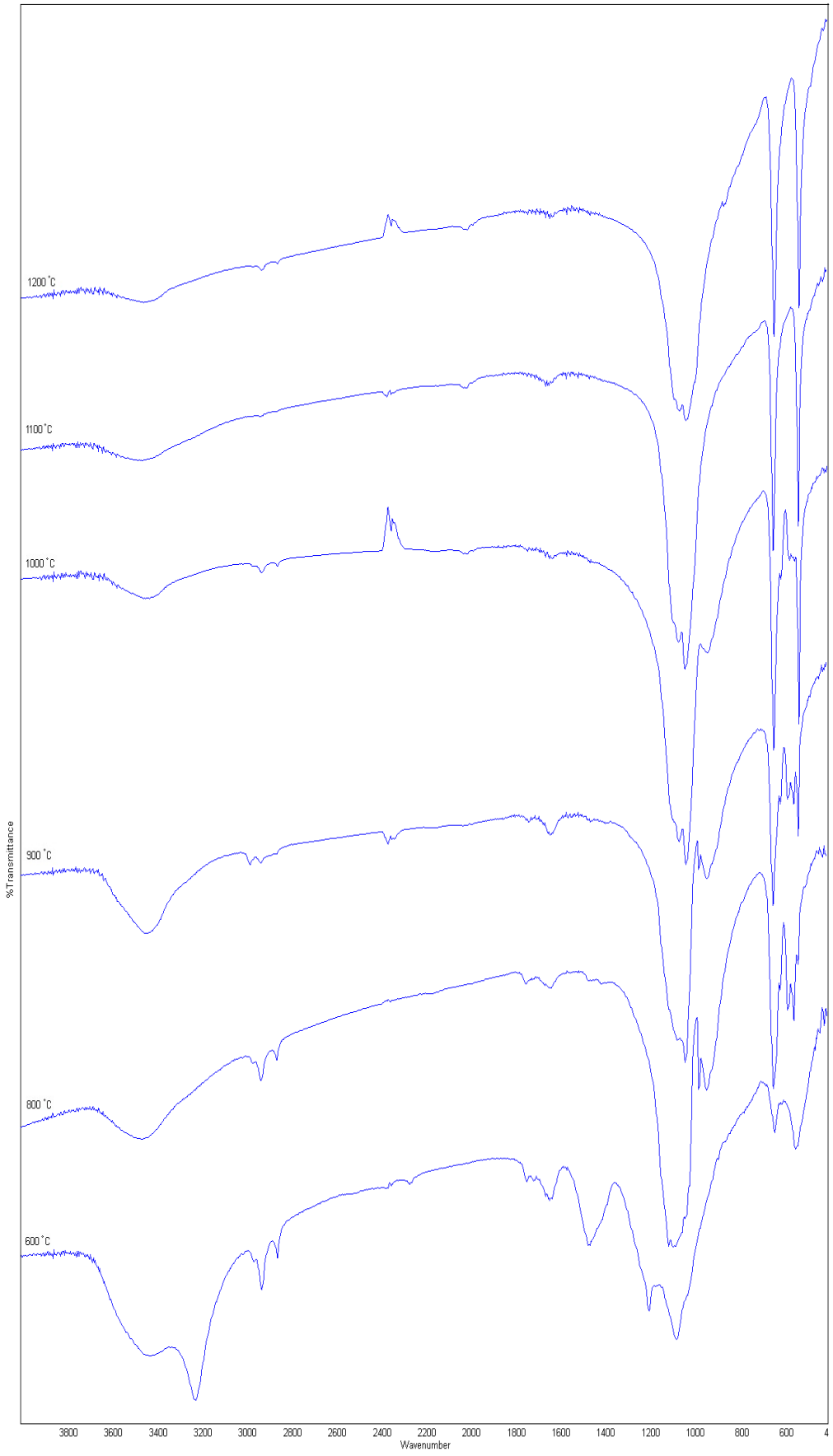

Figure 4.28. IR Spectra of $TbB(PO_4)_2$.

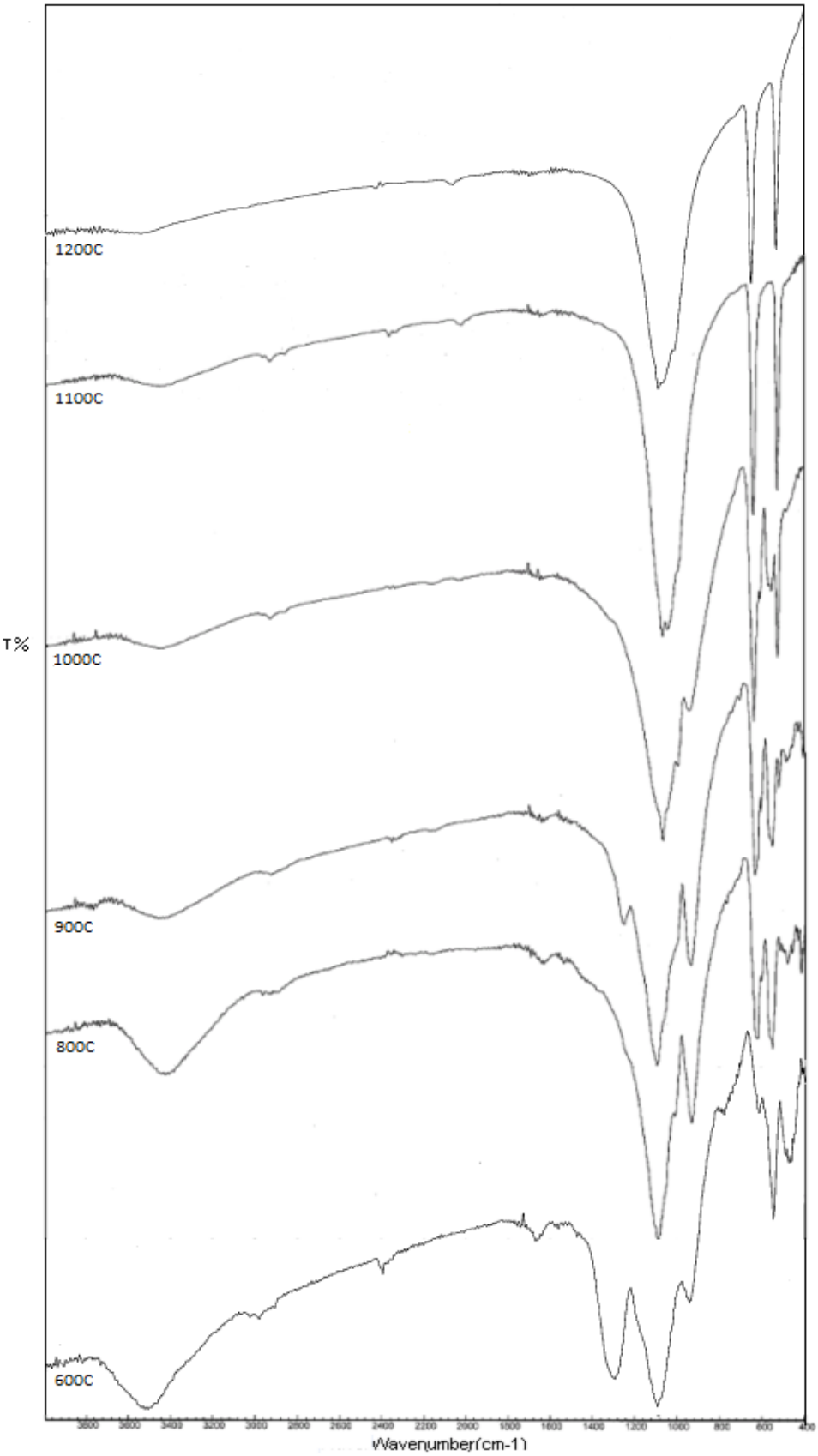

Figure 4.29. IR Spectra of $HoB(PO_4)_2$.

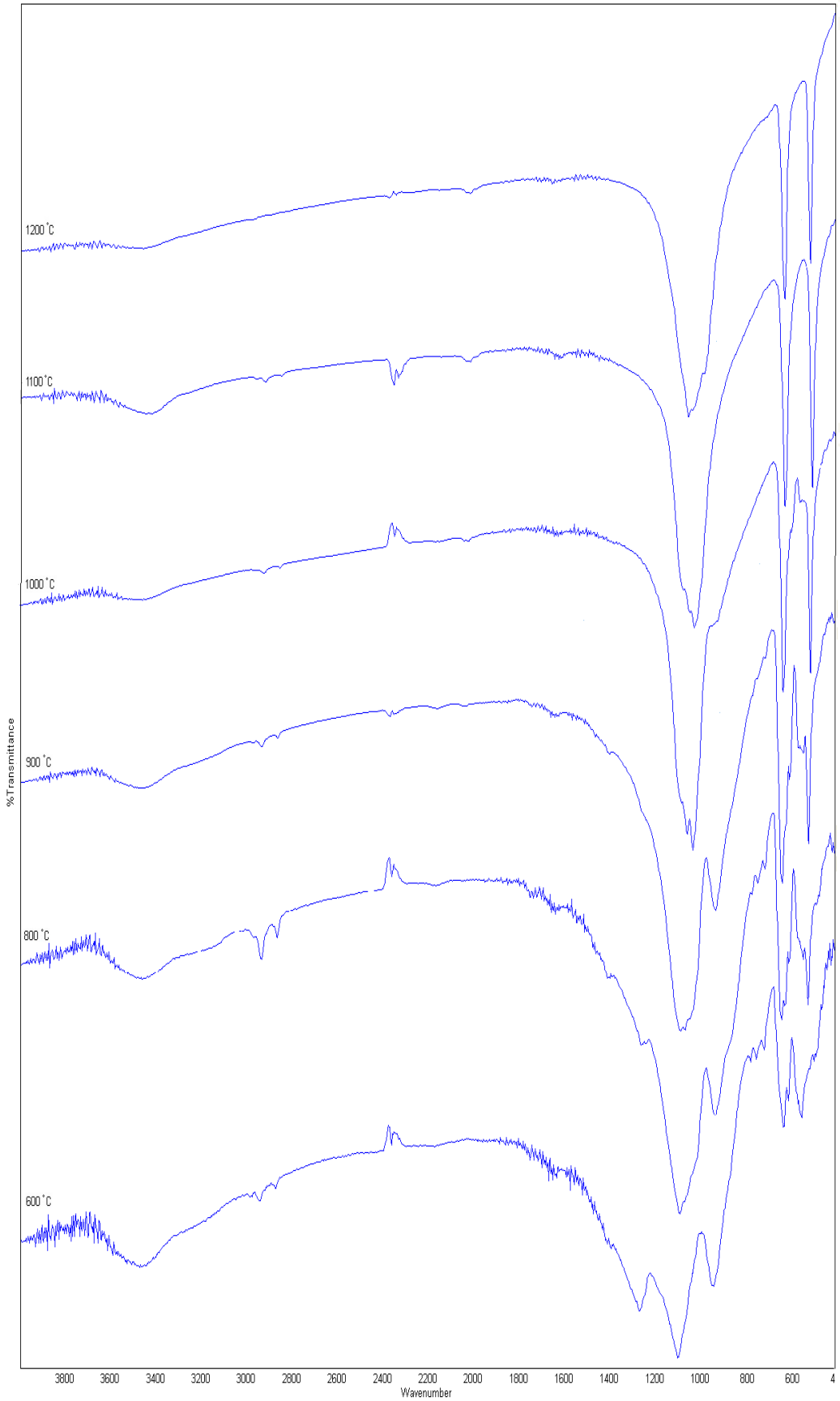

Figure 4.30. IR Spectra of $Tm(PO_4)_2$.

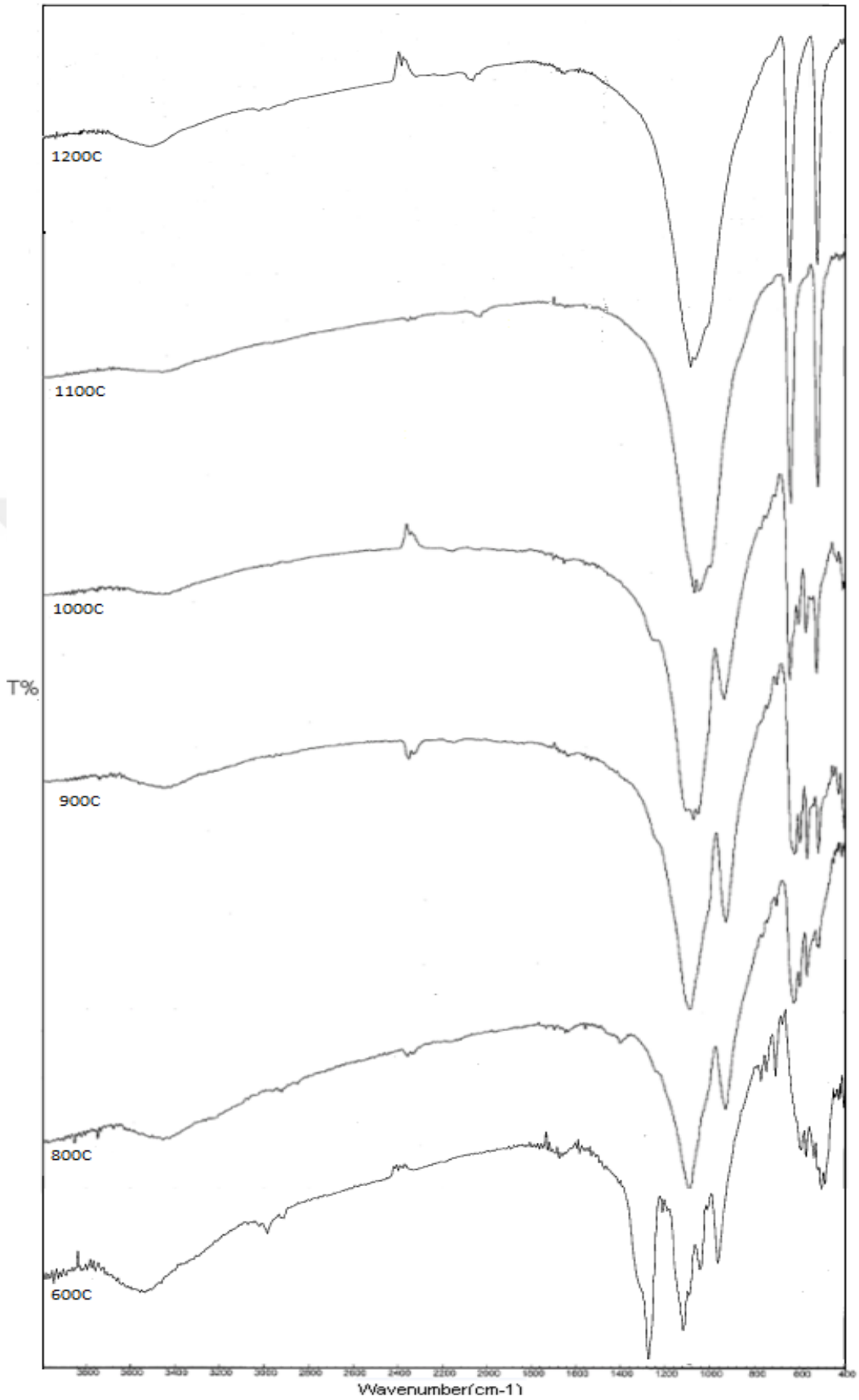

Figure 4.31. IR Spectra of $Lu(PO_4)_2$.

As shown in the figures above, dispite of their different structures all $LnB(PO_4)_2$ absorption bands are detected at the same frequencies. The IR absorption bands and the assignments for the vibrational frequencies of the products at 1100°C and 1200°C are present in Table 4.4.

Table 4.4. IR data of $LnB(PO_4)_2$ (Ln: Ce, Pr, Nd, Sm, Eu, Tb, Ho, Tm, Yb, Lu)

Frequency υ(cm^{-1})	**Assignments**
1100-1000	υ_3 PO_4
970-940	υ_3 BO_4, υ_1 PO_4
635-620	υ_4 PO_4, υ_3 BO_4
580 (weak)	υ_4 BO_4
566-525	υ_2 PO_4

4.1.3 TG/DTA Studies for $LnB(PO_4)_2$ (Ln: Yb, Ho and Lu)

The simultaneous TG/DTA curves of the $LnB(PO_4)_2$ (Ln: Yb, Ho and Lu) are given in Figure 4.32 to Figure 4.34. The curves indicate that there is no weight loss and endothermic or exothermic peak observed from 20 to 1400°C. Thus, it could be said that all compounds are thermodynamically stable within these temperature ranges.

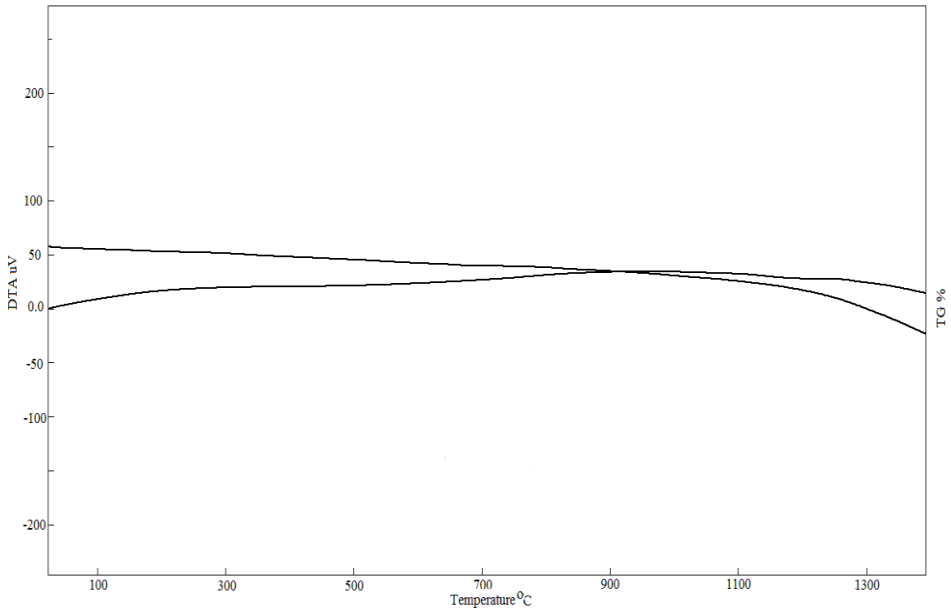

Figure 4.32. TG/DTA Curve of $YbB(PO_4)_2$.

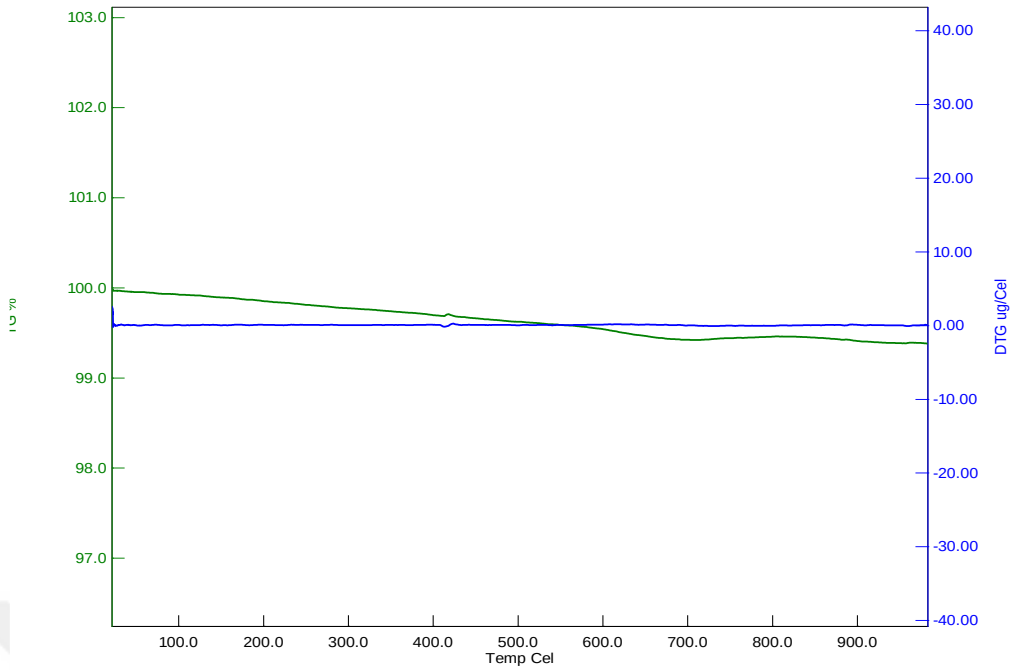

Figure 4.33. TG/DTA Curve of $HoB(PO_4)_2$.

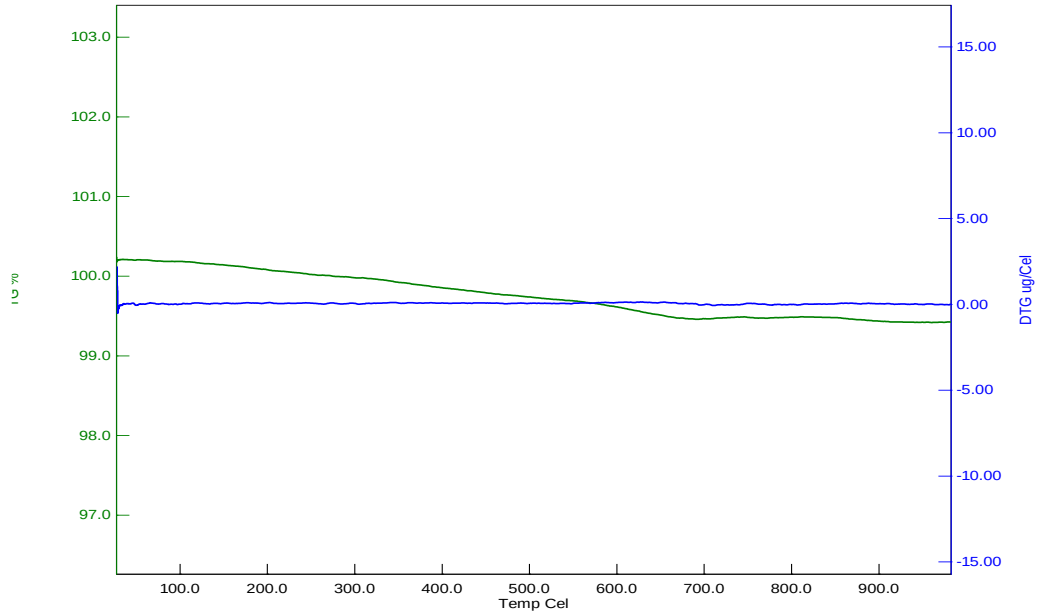

Figure 4.34. TG/DTA Curve of $LuB(PO_4)_2$.

4.1.4 SEM (Scanning Electron Microscopy) and EDX (Energy Dispersive X-ray) Studies for $LnB(PO_4)_2$ (Ln= Ho and Lu)

The morphology of rare earth Ho and Lu containing $LnB(PO_4)_2$ obtained at 1200^oC was examined by SEM measurements up to 10μm. All the samples exhibit distributions of particle size over a wide range. The shape of the particles is regular. From the SEM images, similar morphologies were observed for $HoB(PO_4)_2$ and $LuB(PO_{4)2}$ along with the nanosized particle formation. The presence of related

elements of the desired products such as Ln (Ln=Ho and Lu), B, P and O were determined in the EDX analysis. The SEM images and EDX of representative samples are shown in Figure 4.35 and Figure 4.36.

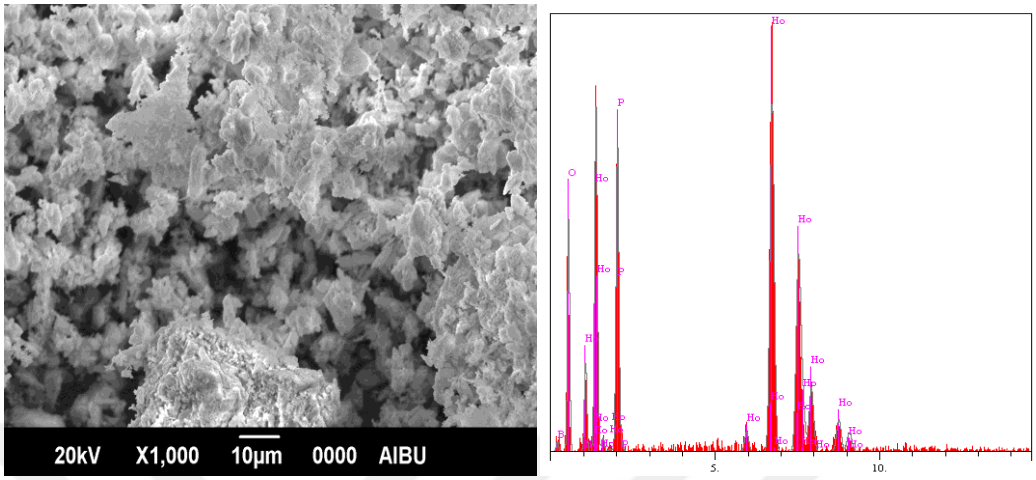

Figure 4.35. SEM Images and EDX of the $HoB(PO_4)_2$ at 1200°C.

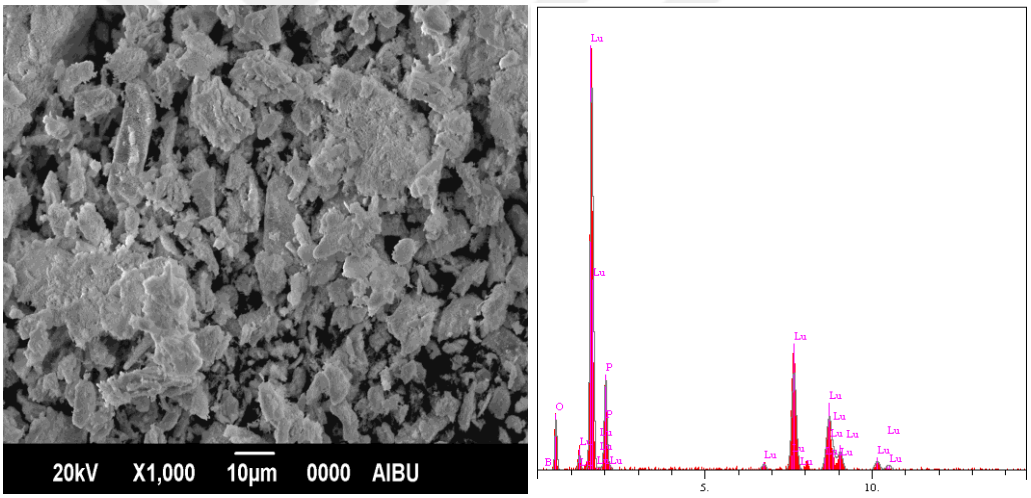

Figure 4.36. SEM Images and EDX of the $LuB(PO_4)_2$ at 1200°C.

4.2 Solution Combustion Synthesis of Metal Pyrovanadates (Metal=Cu, Ni, Co, Zn, Mn)

4.2.1 Solution Combustion Synthesis Method for the Production of Copper Pyrovanadate with Urea Fuel

$Cu_2V_2O_7$ was synthesized by combustion method. Stoichiometric amounts of the starting reagents $Cu(NO_3)_2.3H_2O$, V_2O_5 and CON_2H_4 were dissolved in minimum quantity of deionized water. The mixture was heated until foam was formed. The thermal dehydration of this solution on a hot plate resulted in viscous liquids. Then dark green mixture was transferred to a furnace at 400°C and the process was completed in about 5 minutes. After this process dark brown powder

was formed. Further heatings were done at interval of 50°C between 450-800°C about one hour. Based on the literature, in order to discover α-$Cu_2V_2O_7$ the annealing process was also carried out at 670°C [121,122]. Each heating samples were taken from initial 400°C sample and the structure of this product was examined by using X-ray powder diffraction and IR analysis. The expected reaction was:

$$6Cu(NO_3)_2.3H_2O + 3V_2O_5 + 10CON_2H_4 \rightarrow 3Cu_2V_2O_7 + 10CO_2 + 16N_2 + 38H_2O$$

4.2.1.1 X-Ray Powder Diffraction Studies of Copper Pyrovanadate with Urea Fuel

As it is known that $Cu_2V_2O_7$ has three polymorphs which are α-$Cu_2V_2O_7$, β-$Cu_2V_2O_7$, γ-$Cu_2V_2O_7$ and undergo a reversible phase transition at related temperatures changes [40]. α-$Cu_2V_2O_7$ were synthesized at 680 °C about 72 hours by using solid state method [121].

Slobodin B V and Samigullina R F (2010) has also synthesized the β-$Cu_2V_2O_7$ at 500 °C for 260 hours with intermediate grindings by using nitrate route and α-$Cu_2V_2O_7$ at 660 °C for 150 hours with intermediate grindings by using citrate route [cited by 122, p.141]. The phase transition between α-β phase were also reported to happen at 710°C [76].

In our studies, two crystallographic forms α and β-$Cu_2V_2O_7$ were obtained. All the diffraction peaks of 400°C and 800°C products are compatible with β-$Cu_2V_2O_7$ (ziesite) (ICDD No. 73-1032) that characterize to monoclinic structure of $Cu_2V_2O_7$. At 800°C, pure β-$Cu_2V_2O_7$ was succesfully acquired with very high intensity approximately 8000cps. The formation of α-$Cu_2V_2O_7$ was started to form 650°C as all the peak were detected except for 2θ=27.758°. By the further heating at 670°C, the formation of single phase α-$Cu_2V_2O_7$ (blossite) was confirmed as it suitable to ICDD No. 70-0831 which belongs to orthorhombic $Cu_2V_2O_7$. At the other temperatures α- $Cu_2V_2O_7$ and β-$Cu_2V_2O_7$ was found as mixture (Figure 4.37).

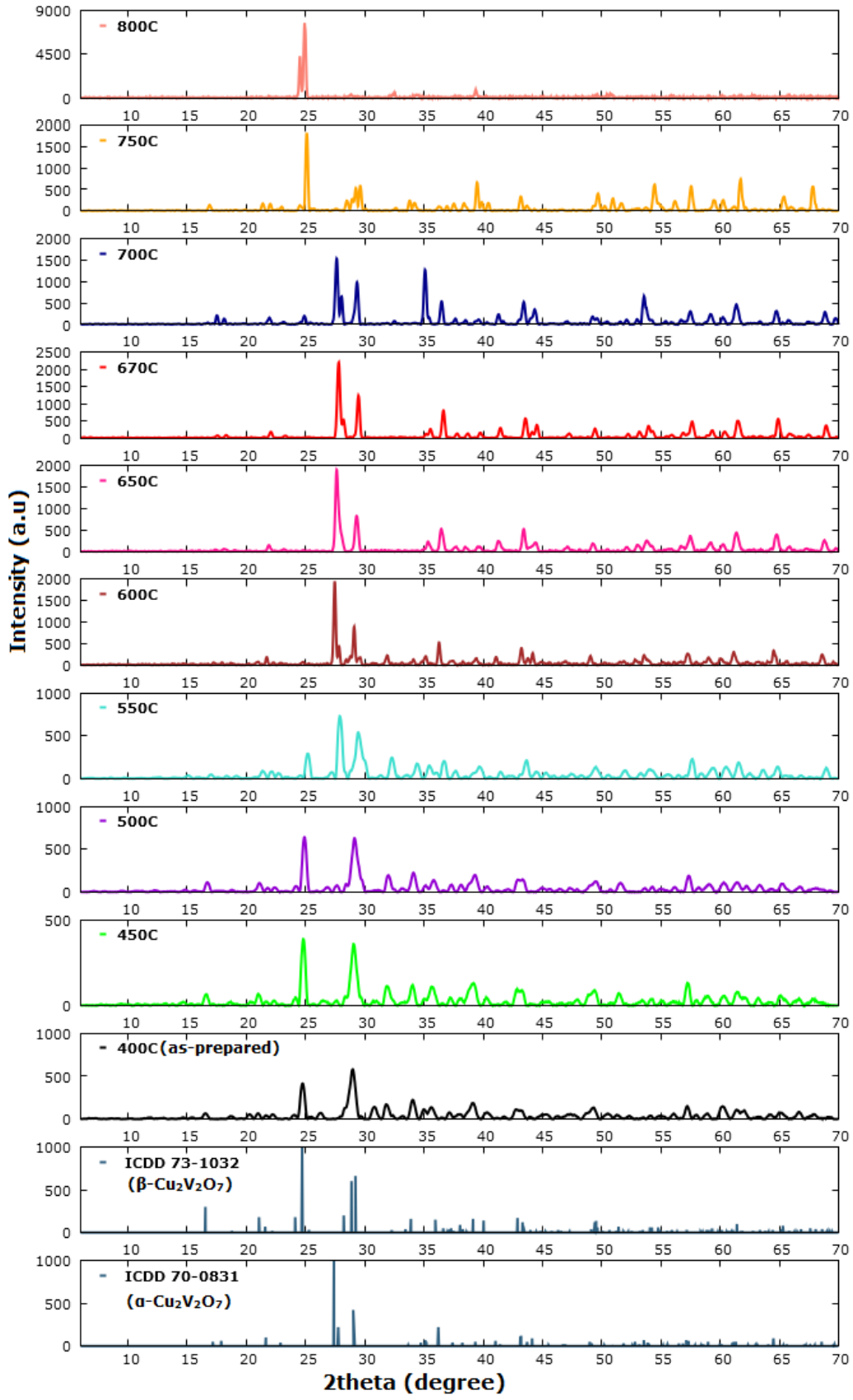

Figure 4.37. XRD patterns of $Cu_2V_2O_7$ product with urea fuel.

4.2.1.2 Infrared Spectroscopy Studies of Copper Pyrovanadate with Urea Fuel

The structural information of the $Cu_2V_2O_7$ was further identified by the FT-IR spectroscopy as shown in Figure 4.38. The FT-IR spectra of the $Cu_2V_2O_7$ was acquired in the range of 400-4000cm^{-1}. The infrared bands of desired products were found at 3435, 1634, 1385,1119, 943, 828, 713 and 551 cm^{-1}. The bands observed at 3435 and 1634cm^{-1} correspond to stretching vibration and bending vibration of absorbed-water molecules. The band at 943cm^{-1} indicates the antisymmetric stretching vibrations of VO_3. The band 828 corresponds to symmetric stretching vibrations of VO_3. The band at 713cm^{-1} belongs to the antisymmetric stretching of bridging V-O-V units and the band at 551cm^{-1} is corresponding to the symmetric stretching mode of V-O-V units [46].

The FT-IR spectra in our studies showed a great agreement with the literature as presented in Table 4.5.

Table 4.5. IR data of α-$Cu_2V_2O_7$ and β-$Cu_2V_2O_7$

Asssignments	**Frequencies υ(cm^{-1})**	
	α-$Cu_2V_2O_7$	**β-$Cu_2V_2O_7$**
asymmetric stretching VO_3	943	942
symmetric stretching VO_3	849	811
asymmetric stretching of bridging V-O-V	717	714
symmetric stretching of bridging V-O-V	567	557
O-H stretching and bending	3450, 1620	3450, 1620

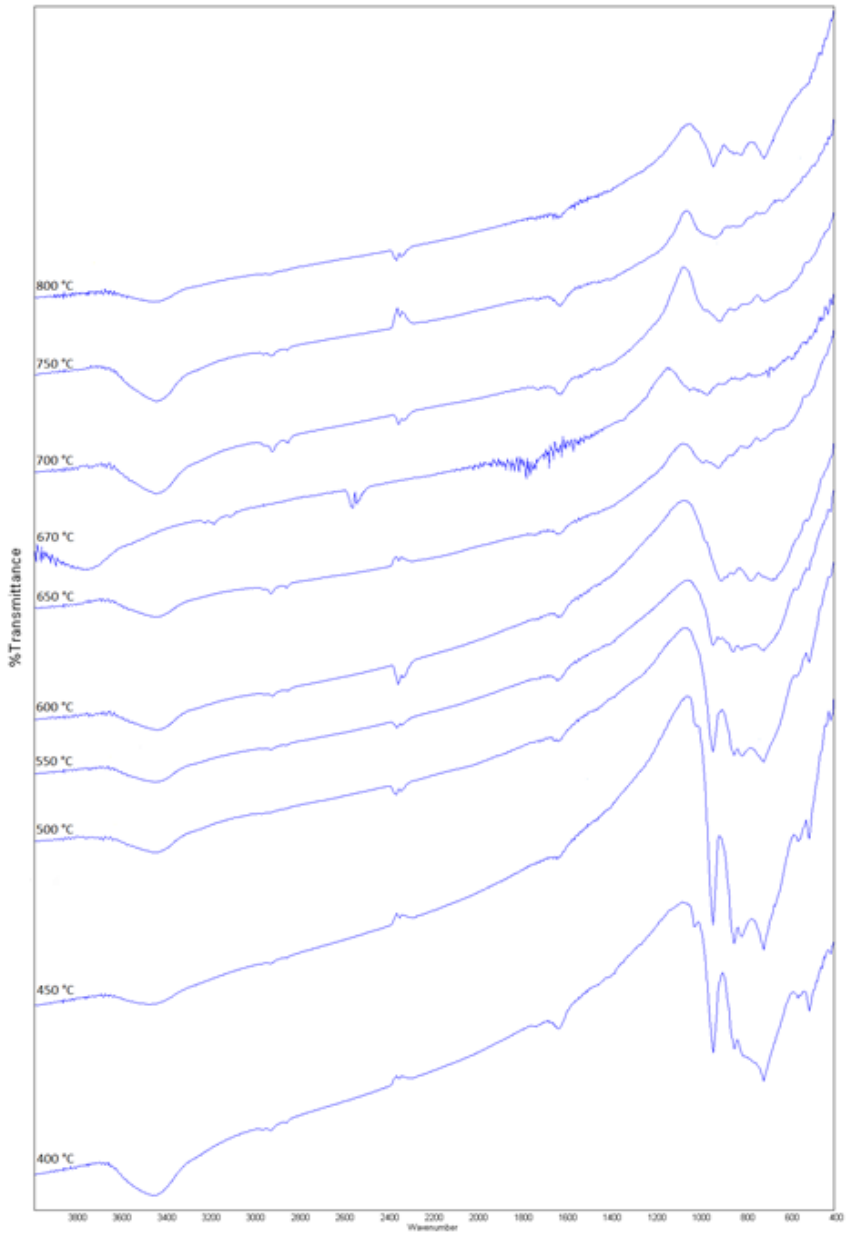

Figure 4.38. IR Spectra of $Cu_2V_2O_7$ product with urea fuel.

4.2.1.3 TG/DTA Studies of Copper Pyrovanadate with Urea Fuel

Figure 4.39 showed the TG/DTA curve of the $Cu_2V_2O_7$ from room temperature up to 1300°C. TGA/DTA was carried out to determine the phase transition of $Cu_2V_2O_7$. The curve indicated that the phase transition started to observe at around 600°C. The peak belongs to water molecules were noticed at 550°C, the α-$Cu_2V_2O_7$ at 670°C and β-$Cu_2V_2O_7$ at 800°C.

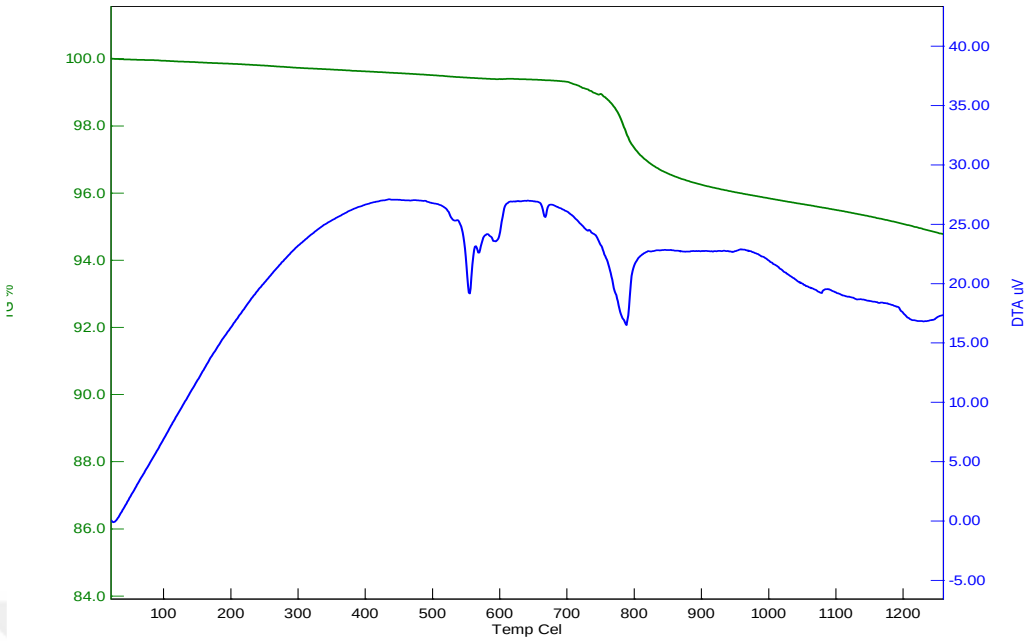

Figure 4.39. TG/DTA Curve of $Cu_2V_2O_7$ product with urea fuel

4.2.2 Solution Combustion Synthesis Method for the Production of Copper Pyrovanadate with Glycine Fuel

In this combustion reaction, glycine was used as fuel. The mixture was heated up to foam was formed. Then the viscous liquids were obtained transferred to a furnace at 400°C and the process was completed in about 5 minutes. After this process black powder was formed. Further heatings were done at 450-500-550-600-650-670-700 and 800°C about one hour. Each heating samples were taken from initial 400°C sample and the structure of this product was investigated by using X-ray powder diffraction and IR analysis. The expected reaction was:

$9Cu(NO_3)_2.3H_2O + 4.5V_2O_5 + 10C_2O_2NH_5 \rightarrow 4.5Cu_2V_2O_7 + 20CO_2 + 14N_2 + 52H_2O$

4.2.2.1 X-Ray Powder Diffraction Studies of Copper Pyrovanadate with Glycine Fuel

In figure 4.40, multiphase α-$Cu_2V_2O_7$ and β-$Cu_2V_2O_7$ were found between the 400°C-550°C. Unlike urea fuel which form single phase α-$Cu_2V_2O_7$ at 670°C, α-$Cu_2V_2O_7$ was failed to obtain by using glycine fuel at 600°C-670°C because additional peak that belongs to CuV_2O_6 was observed (ICDD Card No:45-1054). The transformation of obtained compound to β-$Cu_2V_2O_7$ were acquired at 800°C and identical to ICDD Card No. 73-1032.

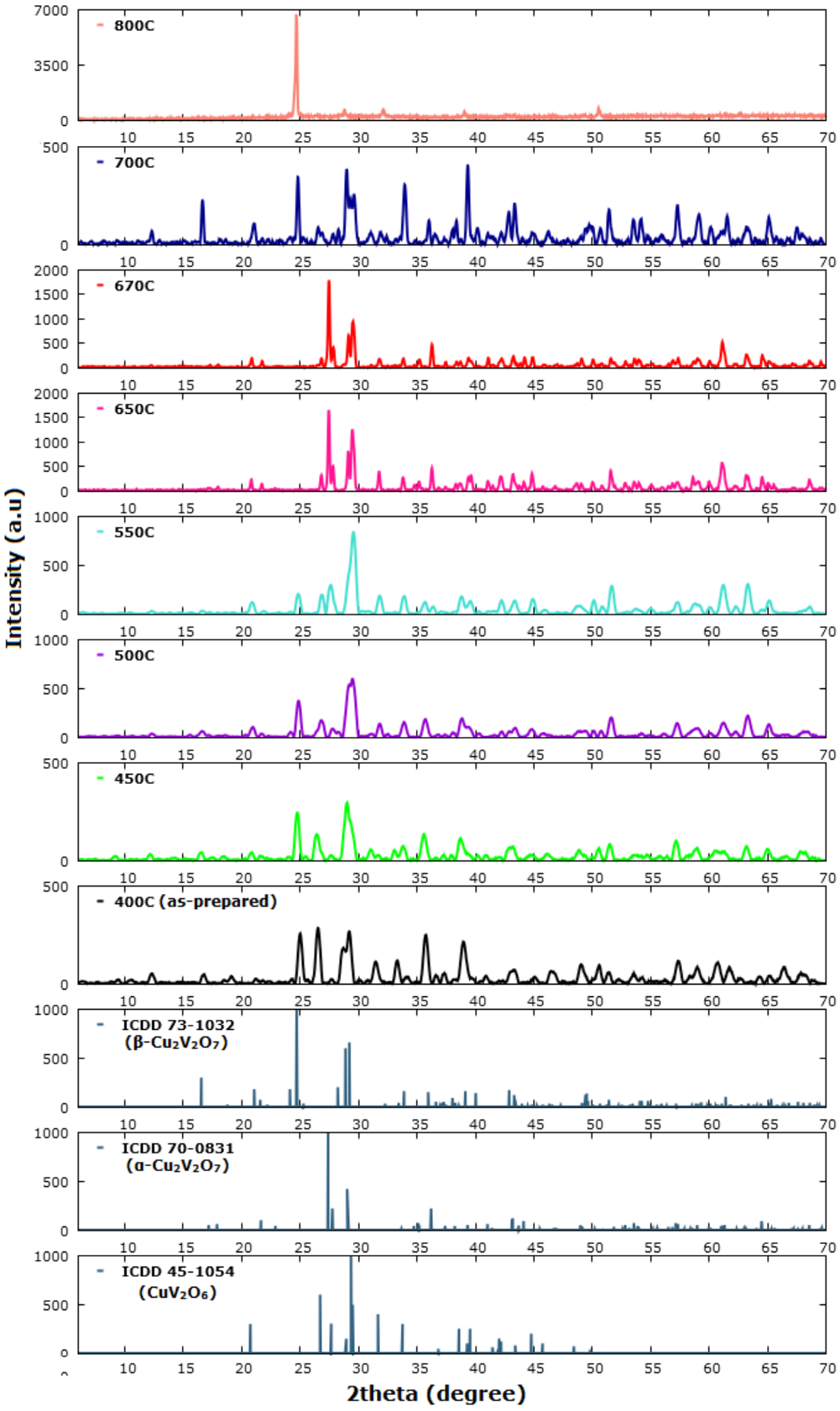

Figure 4.40. XRD patterns of $Cu_2V_2O_7$ product with glycine fuel

4.2.2.2 Infrared Spectroscopy Studies of Copper Pyrovanadate with Glycine Fuel

The structural information of $Cu_2V_2O_7$ with glycine as fuel was further identified by the FT-IR spectroscopy as shown in Figure 4.41. The FT-IR spectra of $Cu_2V_2O_7$ were acquired in the range of 400-4000cm^{-1} and the band vibration of β-$Cu_2V_2O_7$ shows a comparable results with the one synthesized by urea fuel. The infrared data of β-$Cu_2V_2O_7$ is presented in Table 4.6.

Table 4.6. IR data of β-$Cu_2V_2O_7$ at 800^{o}C

Asssignments	**Frequencies υ(cm^{-1})**
asymmetric stretching VO_3	940
symmetric stretching VO_3	845
asymmetric stretching of bridging V-O-V	714
symmetric stretching of bridging V-O-V	560
O-H stretching and bending	3450, 1634

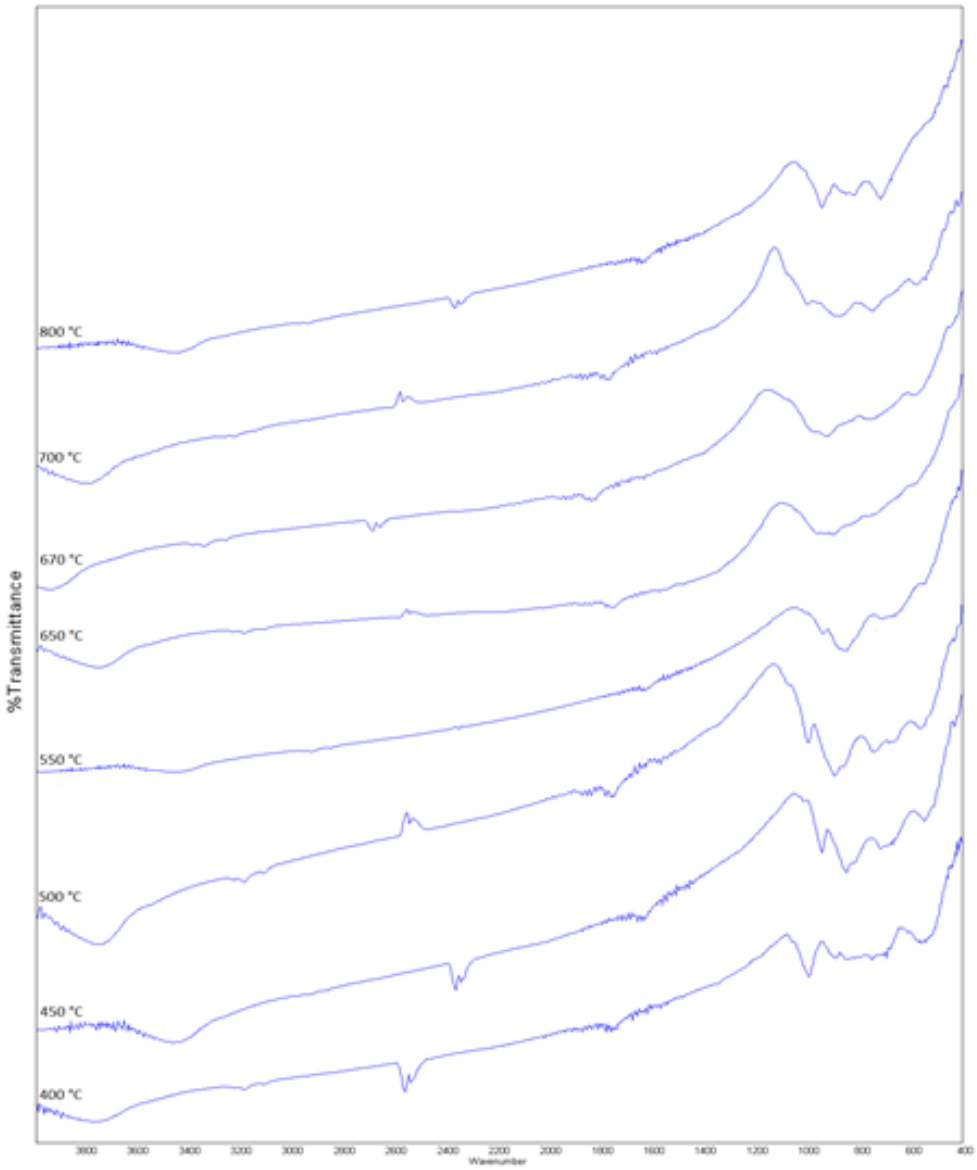

Figure 4.41. IR Spectra of $Cu_2V_2O_7$ product with glycine fuel

4.2.2.3 TG/DTA Studies of Copper Pyrovanadate with Glycine Fuel

TG/DTA curve of the $Cu_2V_2O_7$ was examined at the temperature between room temperature up to 1300 ^oC. The curve shows that the water molecules is presented at 650^oC.

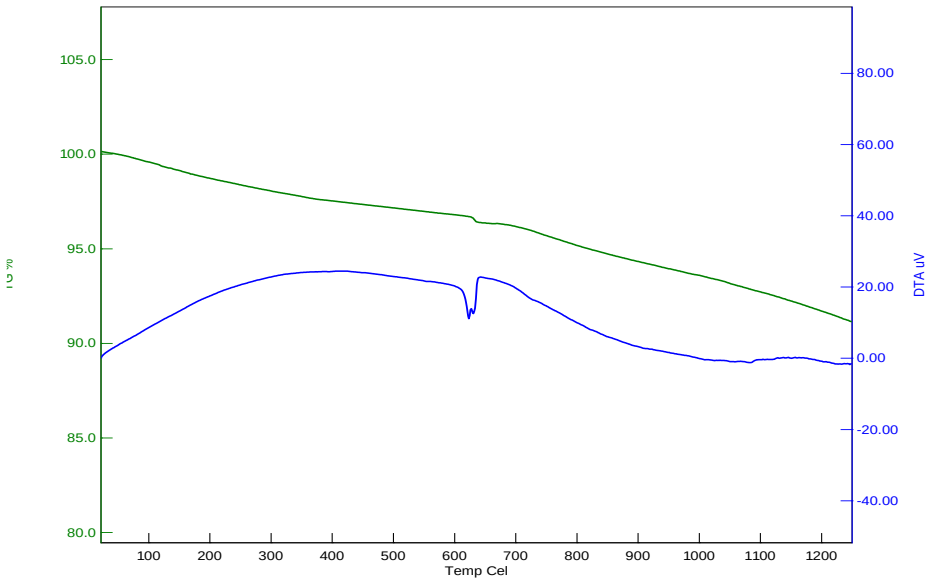

Figure 4.42. TG/DTA Curve of $Cu_2V_2O_7$ product with glycine fuel

4.2.3 Solution Combustion Synthesis Method for the Production of Nickel Pyrovanadate with Urea Fuel

In this work, we wanted to synthesis $Ni_2V_2O_7$ by using the combustion method. $Ni(NO_3)_2.6H_2O$, V_2O_5 and CON_2H_4 were mixed and dissolved with small amount of water. Then heated by stirring on hot plate. When gel formation started, mixture was transferred to a furnace at 400°C. Combustion reaction resulted in about 5 minutes. After this process brown powder was formed. This powder was heated at 600°C and 900°C about one hour. Each heating samples were taken from initial 400°C sample. All these products were examined by using X-ray powder diffraction and IR analysis. The expected reaction was:

$6Ni(NO_3)_2.6H_2O + 3V_2O_5 + 10CON_2H_4 \rightarrow 3Ni_2V_2O_7 + 10CO_2 + 16N_2 + 56H_2O$

4.2.3.1 X-Ray Powder Diffraction Studies of Nickel Pyrovanadate with Urea Fuel

The XRD Pattern of $Ni_2V_2O_7$ obtained at 400°C, 600°C and 900°C were determined as shown in Figure 4.43. It showed that the peaks assign to $Ni_3V_2O_8$ were detected alongside $Ni_2V_2O_7$ at 600°C and 900°C. ($Ni_2V_2O_7$; ICDD No. 38-0285 and $Ni_3V_2O_8$; ICDD No:74-1484).

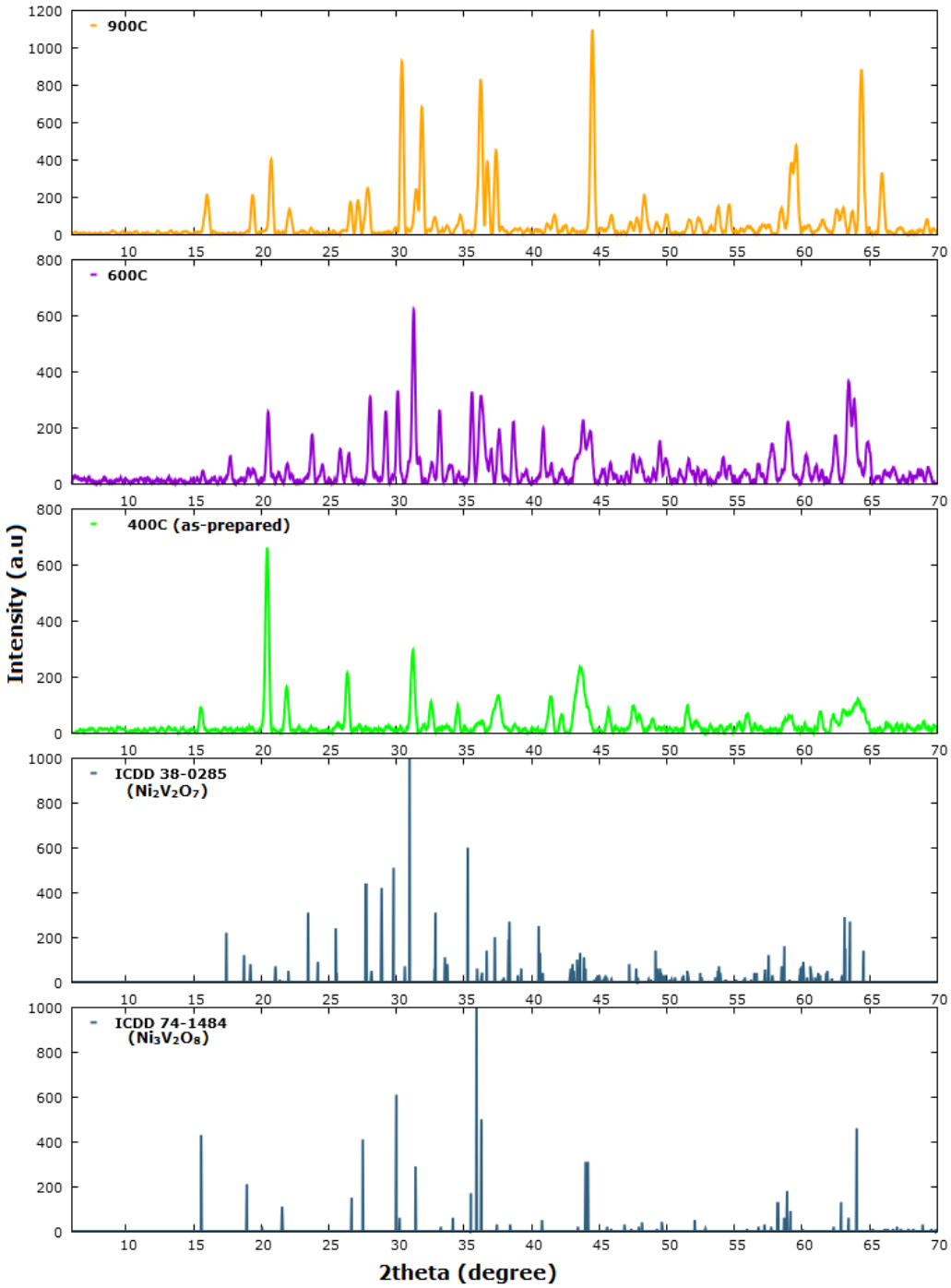

Figure 4.43. XRD patterns of $Ni_2V_2O_7$ product with urea fuel

4.2.3.2 Infrared Spectroscopy Studies of Nickel Pyrovanadate with Urea Fuel

The FT-IR spectra of the $Ni_2V_2O_7$ were measured in the range of 400-4000cm^{-1}. As shown in Figure 4.44, the essential peak of V-O-V that described the presence of pyrovanadates (~720 nm^{-1}) was not identified. Supported by the XRD data results, the synthesis of the single phase $Ni_2V_2O_7$ was unsuccessful.

Table 4.7. IR data of $Ni_2V_2O_7$ at 600^oC

Asssignments	**Frequencies υ(cm^{-1})**
asymmetric stretching VO_3	944
symmetric stretching VO_3	815
asymmetric stretching of bridging V-O-V	-
symmetric stretching of bridging V-O-V	579
O-H stretching and bending	3450, 1640

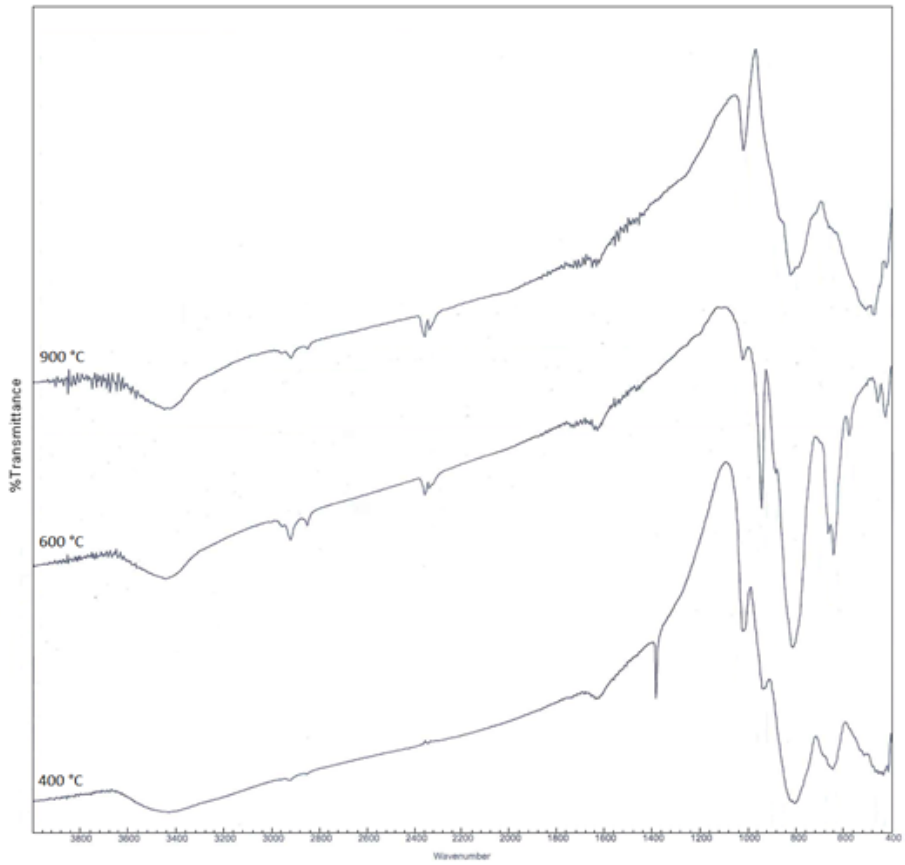

Figure 4.44. IR Spectra of $Ni_2V_2O_7$ product with urea fuel

4.2.3.3 TG/DTA Studies of Nickel Pyrovanadate with Urea Fuel

Figure 4.45 shows the TG/DTA curve of the $Ni_2V_2O_7$ that was identified from room temperature to 1300^oC. The curve indicated that there are two exothermic peaks at 570^oC, 650^oC and one endothermic peak were observed at 900^oC. In accordance to TG/DTA data, the formation of $Ni_2V_2O_7$ might occurs at 900^oC but unfortunately in our studies pure $Ni_2V_2O_7$ was failed to obtained and further studies should be done.

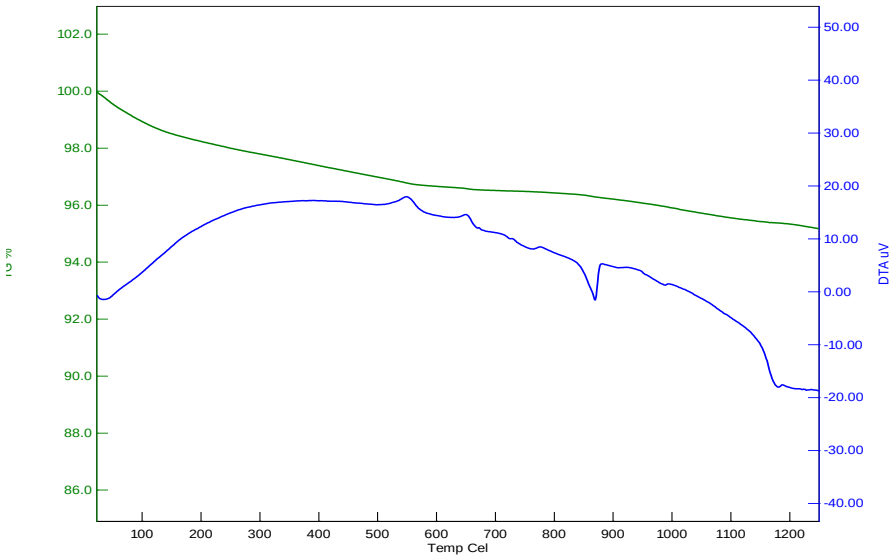

Figure 4.45. TG/DTA of $Ni_2V_2O_7$ product with urea fuel.

4.2.4 Solution Combustion Synthesis Method for the Production of Cobalt Pyrovanadate with Urea Fuel

$Co_2V_2O_7$ compound was prepared by the combustion method. For this purpose stoichiometric amounts of $Co(NO_3)_2.6H_2O$, V_2O_5 and CON_2H_4 were mixed, dissolved with water and heated on hot plate. After gel formation began, the mixture was transferred to a furnace for combustion reactions at 400°C in about 5 minutes. Black powder was formed after this treatment. This powder was separately heated at 600°C and 900°C for approximately one hour. The obtained samples were characterized by using X-ray powder diffraction and IR analysis. The expected reaction was:

$$6Co(NO_3)_2.6H_2O + 3V_2O_5 + 10CON_2H_4 \rightarrow 3Co_2V_2O_7 + 10CO_2 + 16N_2 + 56H_2O$$

4.2.4.1 X-Ray Powder Diffraction Studies of Cobalt Pyrovanadate with Urea Fuel

The XRD analysis showed that the peak observed at 600^{o}C were compatible with $Co_2V_2O_7$ (ICDD No: 70-1189) but only one additional peak at $2\theta=35.990^o$ was observed which belongs to $Co_3V_2O_8$. By further heating at 900^{o}C the multiphase compound were also determined.

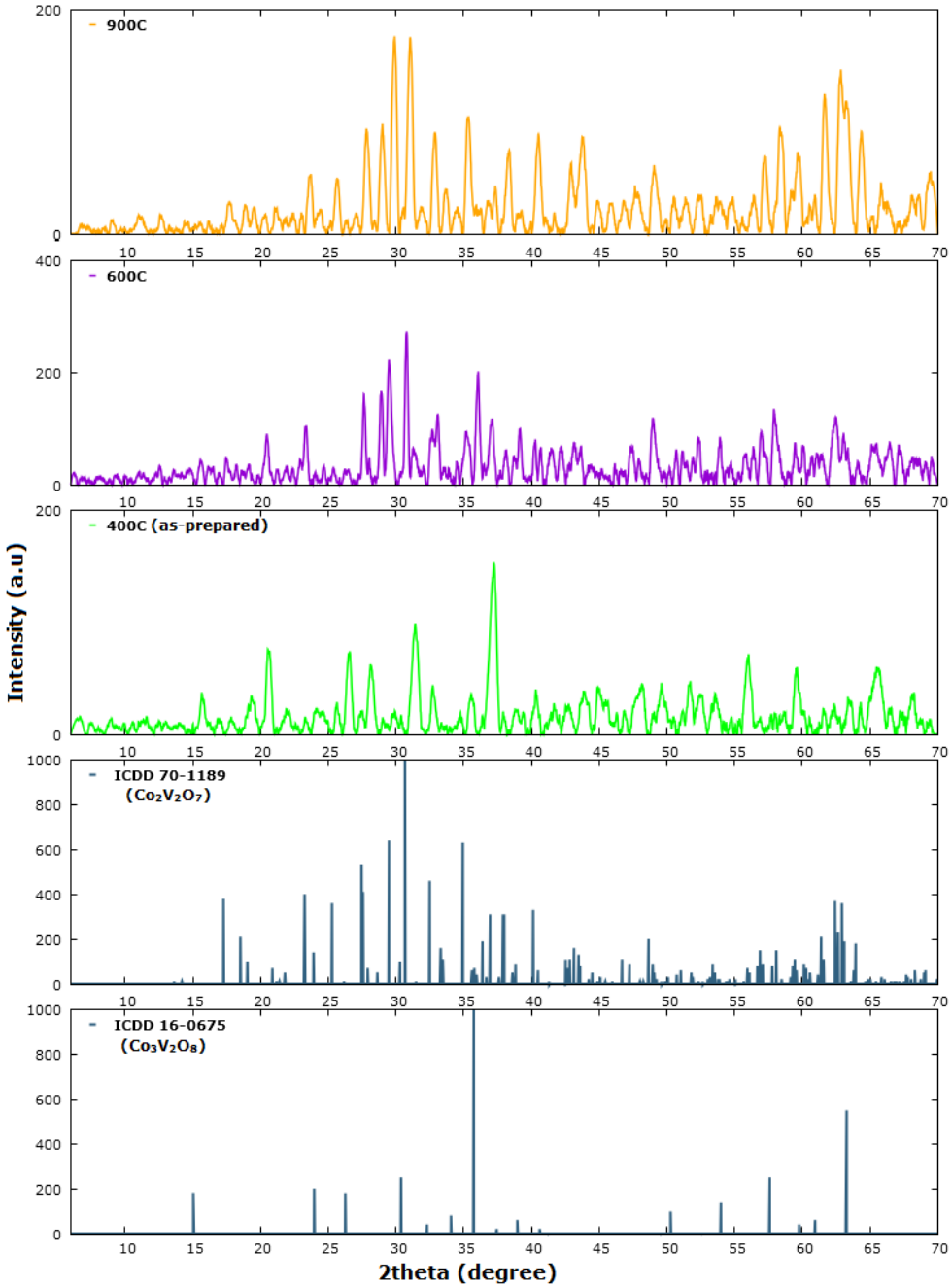

Figure 4.46. XRD patterns of $Co_2V_2O_7$ product with urea fuel.

4.2.4.2 Infrared Spectroscopy Studies of Cobalt Pyrovanadate with Urea Fuel

The FT-IR spectrum of the $Co_2V_2O_7$ at 600^{o}C shows the bands 3440, 1620, 1021, 956, 929, 867, 848, 792, 710, 659, 558, 467 and 418cm^{-1} (Figure 4.47). The absorption at 3440cm^{-1} and 1620cm^{-1} are assigned to the stretching and bending vibration of the hydrogen bond OH groups of the absorbed water. The band at

418cm^{-1} in the spectrum belongs to the stretching mode of the inorganic Co-O. The vibration bands in the range of 956-848cm^{-1} are attributed to the antisymmetric and the symmetric stretching vibrations of VO_3. The bands in the range of 792-558cm^{-1} correspond to the antisymmetric and the symmetric stretching vibrations of V-O-V units.

Table 4.8. IR data of $Co_2V_2O_7$ at 600^{o}C

Asssignments	**Frequencies υ(cm^{-1})**
asymmetric stretching VO_3	956
symmetric stretching VO_3	848
asymmetric stretching of bridging V-O-V	710
symmetric stretching of bridging V-O-V	558
O-H stretching and bending	3440, 1620

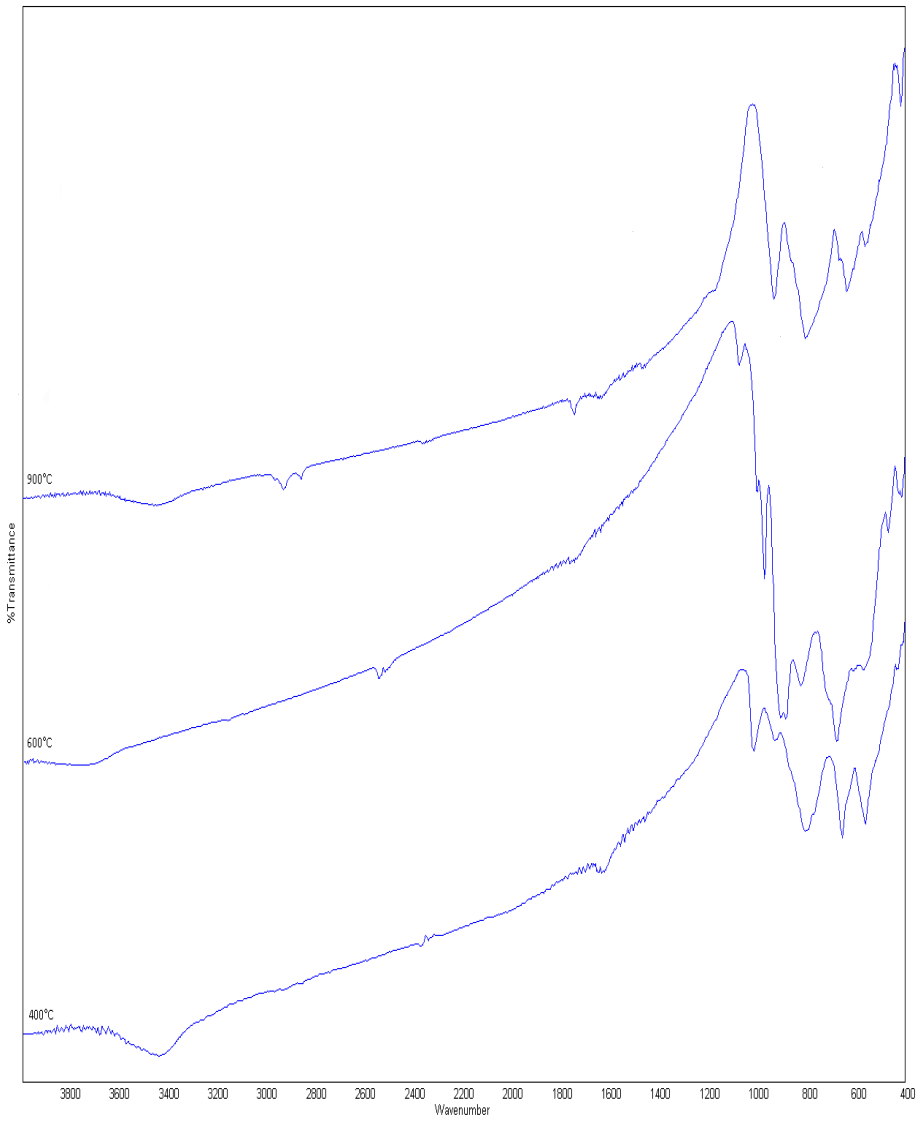

Figure 4.47. IR Spectra of $Co_2V_2O_7$ product with urea fuel.

4.2.4.3 TG/DTA Studies of Cobalt Pyrovanadate with Urea Fuel

The TG/DTA curve of the $Co_2V_2O_7$ was examined at the temperature between room temperature to 1300^oC. The curve indicates that there are three endothermic peaks were indexed at 680^oC, 770^oC and 910^oC.

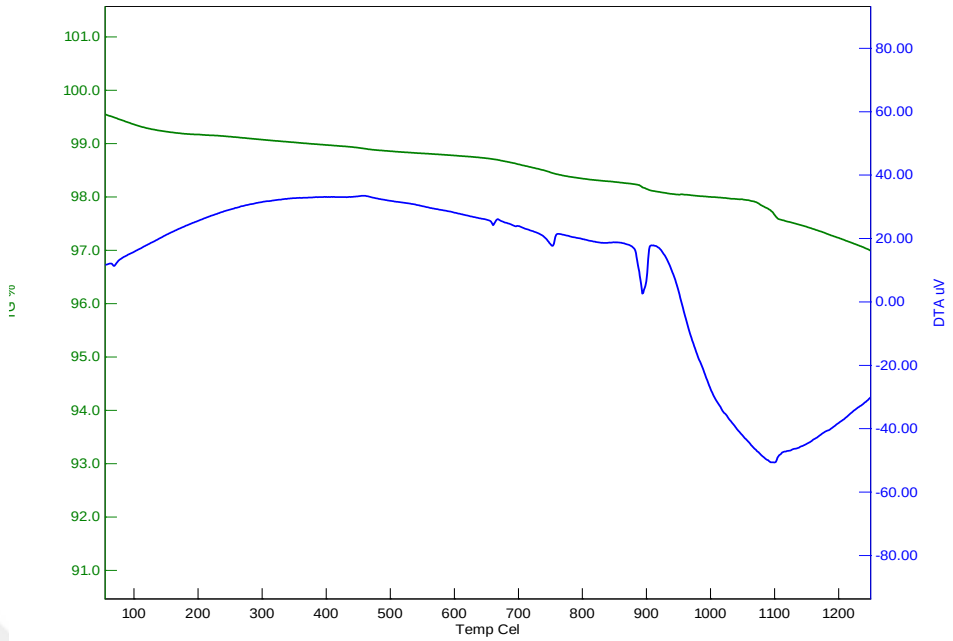

Figure 4.48. TG/DTA of $Co_2V_2O_7$ product with urea fuel.

4.2.5 Solution Combustion Synthesis Method for the Production of Zinc Pyrovanadate with Urea Fuel

The $Zn_2V_2O_7$ powder was synthesized by using the combustion method. Zn nitrate hexahydrate ($Zn(NO_3)_2.6H_2O$), vanadium pentoxide (V_2O_5) were used as starting materials. Urea (CON_2H_4) was added as a fuel. Stoichiometric amounts of these chemicals were mixed and grinded in an agate mortar. Obtained homogenous mixture was dissolved with small amount of water. Then heated by stirring on hot plate. When gel formation started, mixture was transferred to a furnace at 400°C. Combustion reaction resulted in about 5 minutes. After this process brown-yellow mixture powder was formed. This powder was heated at various temperatures of 650°C and 900°C about one hour. Each heating samples were taken from initial 400°C sample. All these products were examined by using X-ray powder diffraction and IR analysis.

$6Zn(NO_3)_2.6H_2O + 3V_2O_5 + 10CON_2H_4 \rightarrow 3Zn_2V_2O_7 + 10CO_2 + 16N_2 + 56H_2O$

4.2.5.1 X-Ray Powder Diffraction Studies of Zinc Pyrovanadate with Urea Fuel

$Zn_2V_2O_7$ has known to have two polymorphs which are α- β- $Zn_2V_2O_7$. The Figure 4.49 showed the XRD patterns of the samples synthesized at different initial combustion temperatures of 400, 650 and 900°C. It revealed that at 400°C, two

small peaks at (2θ= 29.180° and 31.700°) belongs to $Zn_4V_2O_9$ (ICDD No:77-1757) were observed. Single phase monoclinic α-$Zn_2V_2O_7$ (ICDD card 70-1532) was successfully fabricated at 650°C and higher crystallinity product was obtained at 900°C. In our work, there is no impurity phases were observed at 650°C and 900°C.

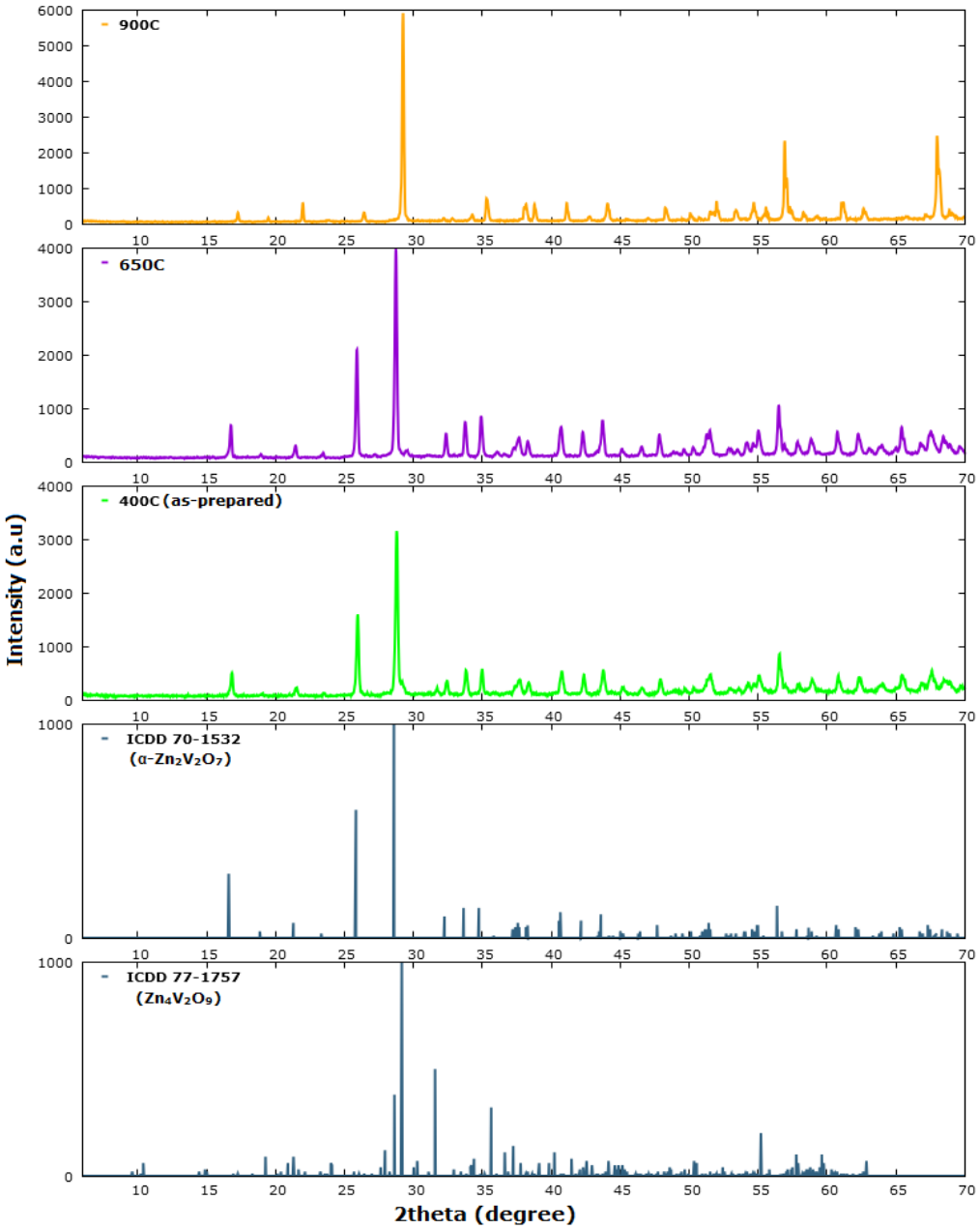

Figure 4.49. XRD patterns of $Zn_2V_2O_7$ product with urea fuel.

4.2.5.2 Infrared Spectroscopy Studies of Zinc Pyrovanadate with Urea Fuel

The Figure 4.50 shows the Fourier transform infrared spectra of our Zn vanadate synthesis work. At 650^{o}C, the spectra show absorption peaks at 927, 793, 757, 718, 592 and 471cm^{-1}. According to Frederickson L.D. and Hausen D.M. (1963) pyrovanadates seem to be identifiable as a class or group, by virtue of lower frequency absorption band groups [124]. The vibration bands in the range of 927-757cm^{-1} are attributed to the antisymmetric and the symmetric stretching vibrations of VO_3. The bands in the range of 718-471cm^{-1} correspond to the antisymmetric and the symmetric stretching vibrations of V-O-V units. The band at 417cm^{-1} is associated to the Zn-O stretching vibration. Table 4.8 represents the detailed information of the observed bands.

Table 4.9. IR data of $Zn_2V_2O_7$ at 650^{o}C

Asssignments	**Frequencies υ(cm^{-1})**
asymmetric stretching VO_3	927
symmetric stretching VO_3	793
asymmetric stretching of bridging V-O-V	718
symmetric stretching of bridging V-O-V	592

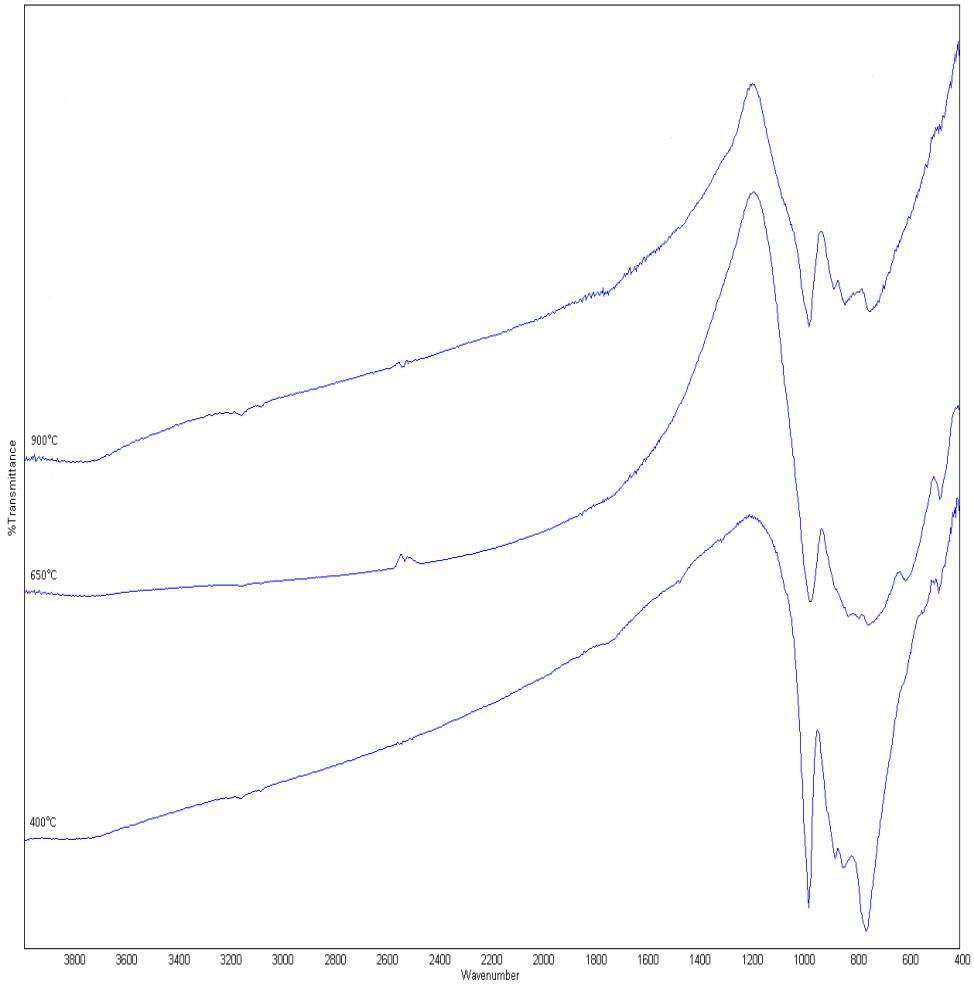

Figure 4.50. IR Spectra of $Zn_2V_2O_7$ product with urea fuel.

4.2.6 Solution Combustion Synthesis Method for the Production of Manganese Pyrovanadate with Urea Fuel

Manganese pyrovanadate $Mn_2V_2O_7$ was prepared by combustion synthesis method from $Mn(NO_3)_2.4H_2O$, V_2O_5 and CON_2H_4, taken in the desired ratio. Obtained homogenous mixture was dissolved with small amount of water. Then heated by stirring on hot plate. When gel formation started, mixture was transferred to a furnace at 400°C. After this process combustion reaction resulted in about 5 minutes and black powder was formed. This powder was heated at 650°C, 900°C, 950°C, 1000°C and 1050°C about one hour. Each heating samples were taken from initial the as-prepared product at 400°C. All these products were examined by using X-ray powder diffraction and IR analysis. The predicted reaction was;

$6Mn(NO_3)_2.4H_2O + 3V_2O_5 + 10CON_2H_4 \rightarrow 3Mn_2V_2O_7 + 10CO_2 + 16N_2 + 44H_2O$

4.2.6.1 X-Ray Powder Diffraction Studies of Manganese Pyrovanadate with Urea Fuel

The Figure 4.51 represented the two crystallographic forms α and β-$Mn_2V_2O_7$. At 400-650°C, multiphase of α-$Mn_2V_2O_7$ and β-$Mn_2V_2O_7$ peaks were seen. It was observed that at 900 °C and 950 °C, one peak belonged to α-$Mn_2V_2O_7$ (2θ=28.310°) and the other peaks were compatible with β-$Mn_2V_2O_7$ (ICDD No: 89-0484). At 1000°C pure monoclinic β-$Mn_2V_2O_7$ was synthesized but its intensity was very low. To obtain the higher intensity product, the heating process was applied at 1050°C but α-$Mn_2V_2O_7$ and β-$Mn_2V_2O_7$ were found as mixture.

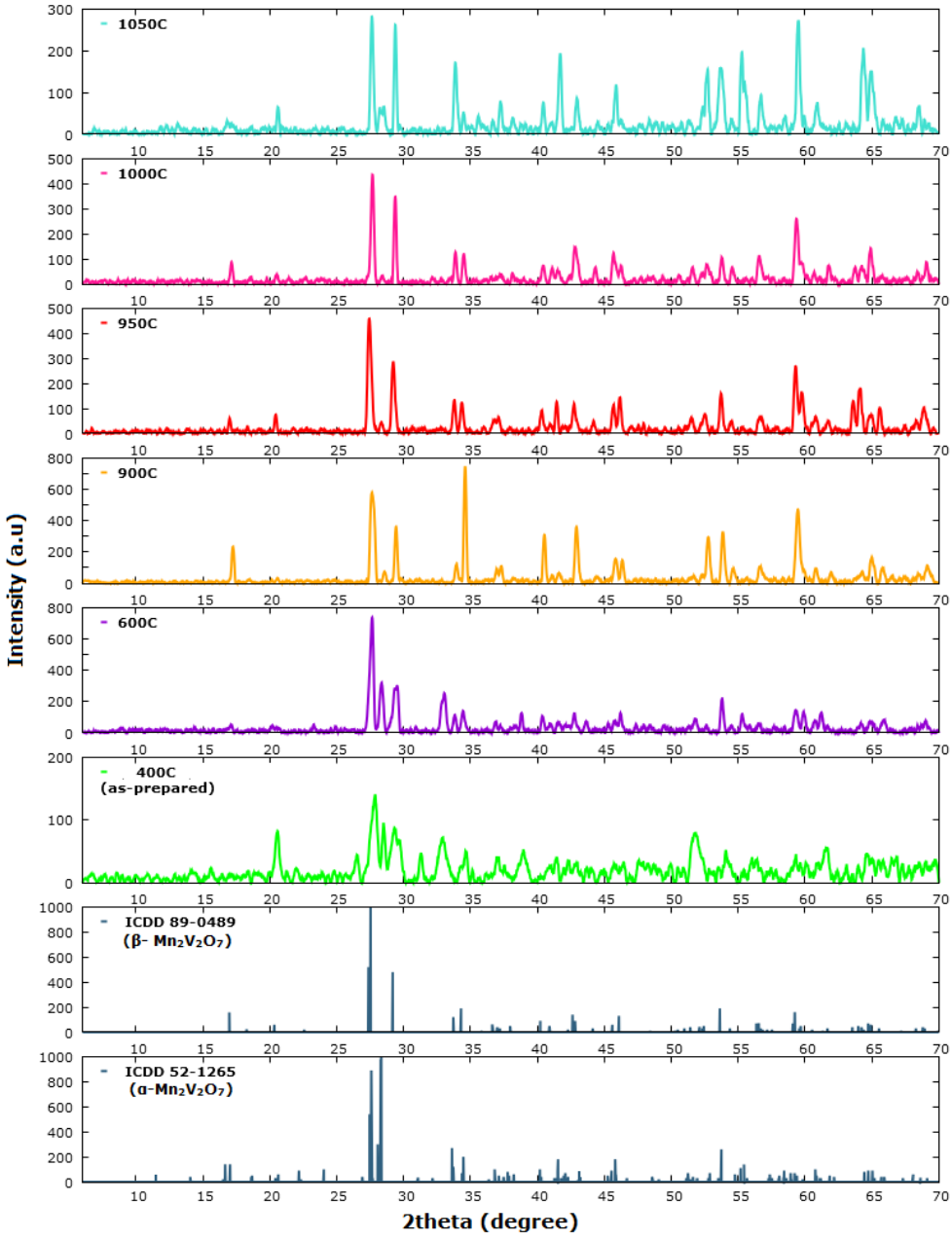

Figure 4.51. XRD patterns of $Mn_2V_2O_7$ product with urea fuel.

4.2.6.2 Infrared Spectroscopy Studies of Manganese Pyrovanadate with Urea Fuel

The FT-IR spectra of the $Mn_2V_2O_7$ were shown in Figure 4.52. The characteristics bands vibration of 1000^oC are reported as 3450, 1630, 955, 888, 841, 793 and 725cm^{-1}. The bands observed at 3450 and 1630cm^{-1} correspond to stretching vibration and bending vibration of hydroxyl group of absorbed-water molecules.The band at 955cm^{-1} and 841cm^{-1} are assigned to the antisymmetric and symmetric stretching vibrations of VO_3, respectively. The band at 538 cm^{-1} is attributed to the symmetric stretching of bridging V-O-V units whereas the band at 725cm^{-1} is corresponded to the antisymmetric stretching mode of V-O-V units.

Table 4.10. IR data of $Mn_2V_2O_7$ at 1000^oC

Asssignments	**Frequencies υ(cm^{-1})**
asymmetric stretching VO_3	956
symmetric stretching VO_3	848
asymmetric stretching of bridging V-O-V	710
symmetric stretching of bridging V-O-V	558
O-H stretching and bending	3440, 1620

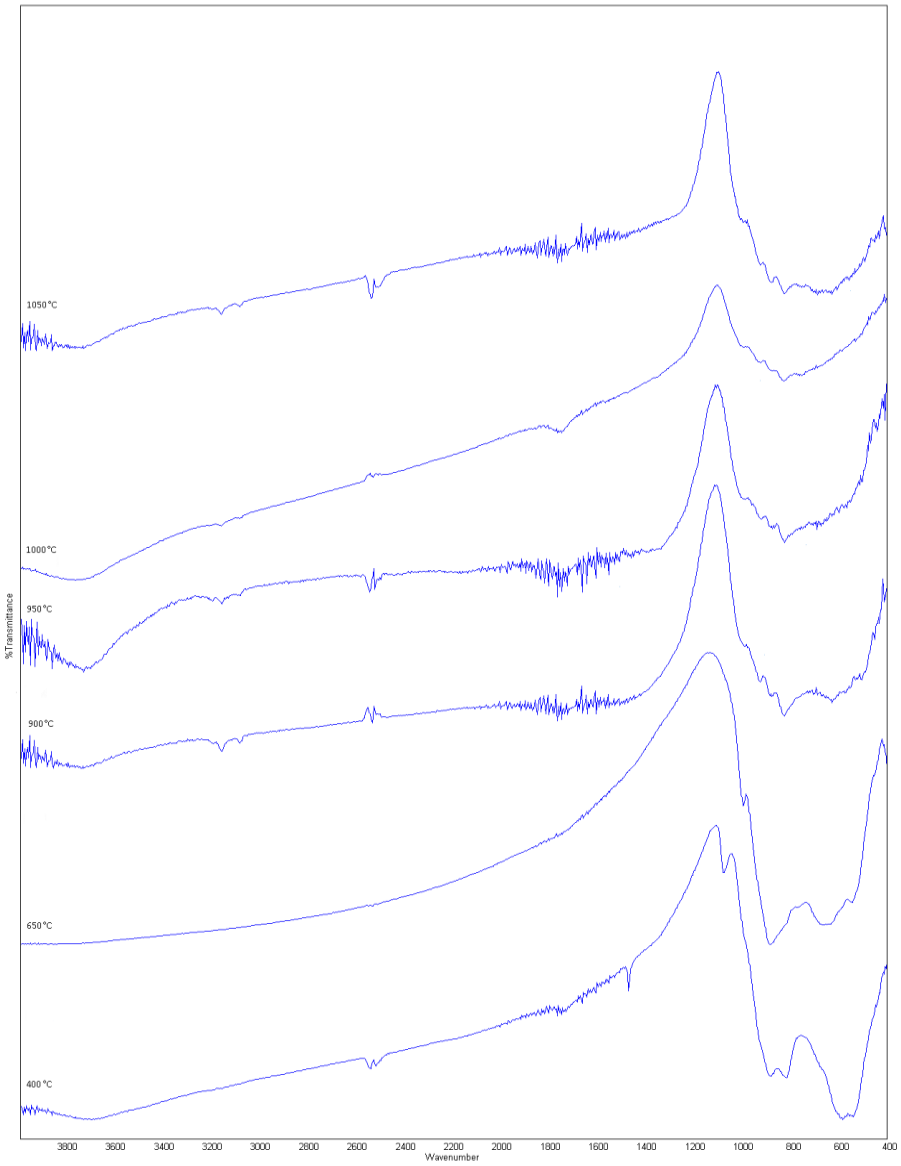

Figure 4.52. IR Spectra of $Mn_2V_2O_7$ product with urea fuel.

4.3 Solution Combustion Synthesis of Metal Orthovanadates (Metal=Cu, Ni, Co, Zn, Mn, Mg)

4.3.1 Solution Combustion Synthesis Method for the Production of Copper Orthovanadate with Urea Fuel and V_2O_5 as Starting Reagents

Combustion method was used to synthesize the $Cu_3V_2O_8$. Stoichiometric amounts of the starting reagents $Cu(NO_3)_2.3H_2O$, V_2O_5 and CON_2H_4(urea) were dissolved in a minimum quantity of deioned water. The mixture was heated until foam was formed. Then the mixture was transferred to a furnace at 400°C and the process was completed in about 5 minutes. After this process dark brown powder was formed. Further heatings were done at 500-650-700-750 and 800°C about one

hour. Each heating samples were taken from initial 400°C sample and the structure of this product was examined by using X-ray powder diffraction and IR analysis. The expected reaction was:

$6Cu(NO_3)_2.3H_2O + 2V_2O_5 + 10CON_2H_4 \rightarrow 2Cu_3V_2O_8 + 10CO_2 + 16N_2 + 38H_2O$

4.3.1.1 X-Ray Powder Diffraction Studies of Copper Orthovanadate with Urea Fuel

Figure 4.53 showed the XRD patterns of triclinic structure of $Cu_3V_2O_8$. The XRD data of the products were compared to ICCD Card No 49-0689. At 400 ^oC and 500^oC, multiphase product with $Cu_3V_2O_8$ were obtained as some peaks that belongs to β-$Cu_2V_2O_7$ (ICCD No: 73-1032) were observed. At 650 ^oC and 700 ^oC, validated to our previous pyrovanadate studies, the β-$Cu_2V_2O_7$ were transformed into α-$Cu_2V_2O_7$. The $Cu_3V_2O_8$, α-$Cu_2V_2O_7$ and very small amount of β-$Cu_2V_2O_7$ reflections were identified in this heating temperature. At 750 ^oC, the reflections that refer to $Cu_3V_2O_8$ were predominated but could not be obtained in pure form as some peaks belonging to β-$Cu_2V_2O_7$ were also observed. At 800^oC, complete transformation of $Cu_3V_2O_8$ to β-$Cu_2V_2O_7$ were shown since all the reflections have a greet agreement with ICCD No: 73-1032.

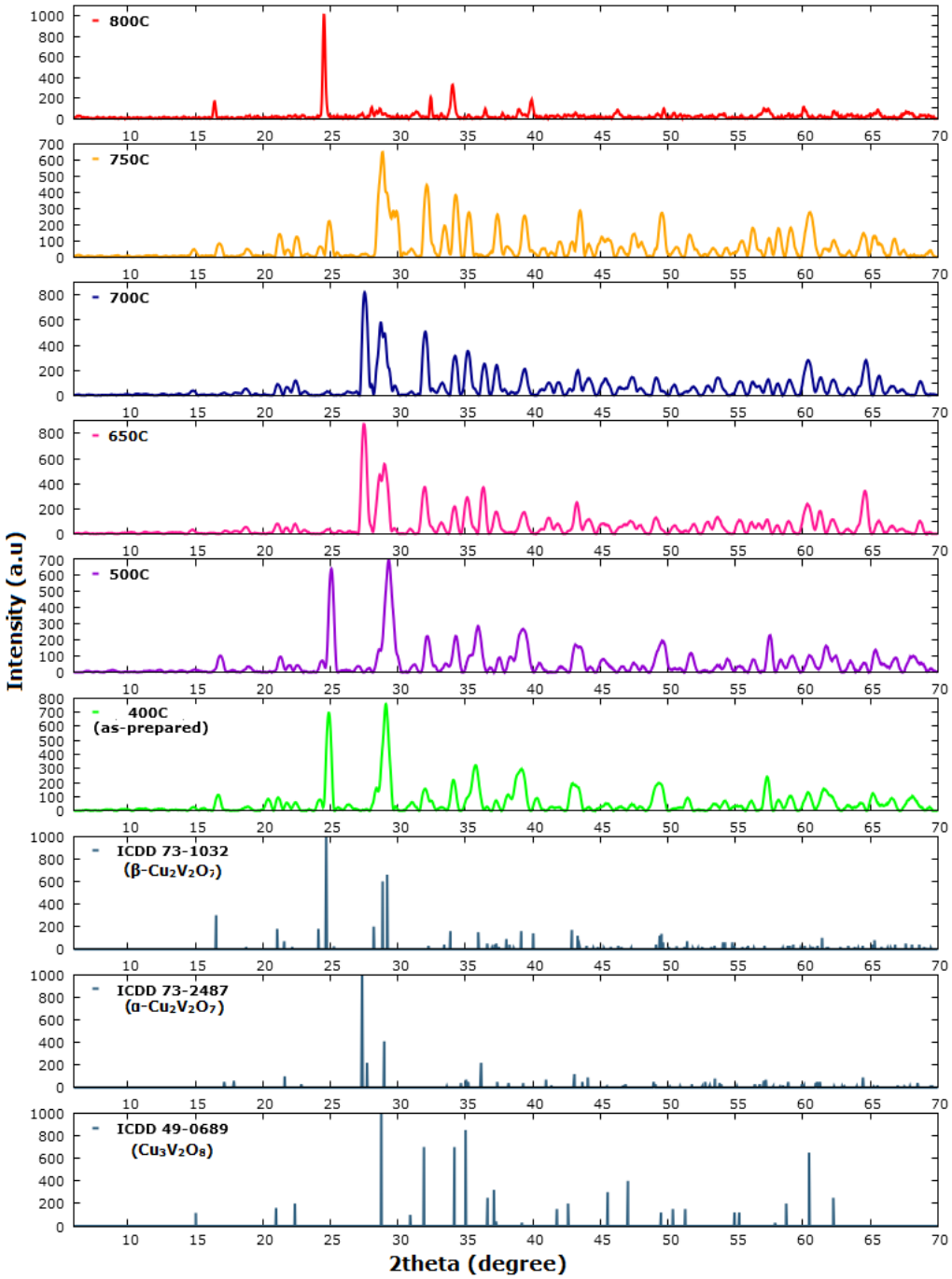

Figure 4.53. XRD patterns of $Cu_3V_2O_8$ product with urea fuel and V_2O_5 as starting reagents.

4.3.1.2 Infrared Spectroscopy Studies of Copper Orthovanadate with Urea Fuel and V_2O_5 as Starting Reagents

The FT-IR spectra of the $Cu_3V_2O_8$ obtained at different temperature were measured in the range of 400–4000 cm^{-1}. Frederickson L.D. and Hausen D.M. (1963) reported that the infrared absorption bands of orthovanadates are between 936-254 cm^{-1} [124]. According to FT-IR spectrum of the product obtained at 750^oC

(Figure 4.54), the vibration band at 3430cm^{-1} and 1630cm^{-1} identifies the stretching and bending vibrations of hydroxyl group of water molecules, respectively. The vibration bands between 920-430nm^{-1} refer to the vibration modes of octahedral CuO_6 and tetrahedral VO_4. The characteristic vibration bands that specify the formation of orthovanadates were observed. The band at 771 cm-1 is assigned to V-O vibration, the band at 570 cm-1 is refered to metal stretching vibration in the tetrahedral arragenment and the one determined at 430 cm^{-1} is associated to Cu-O stretching vibration in the octahedral arrangement.

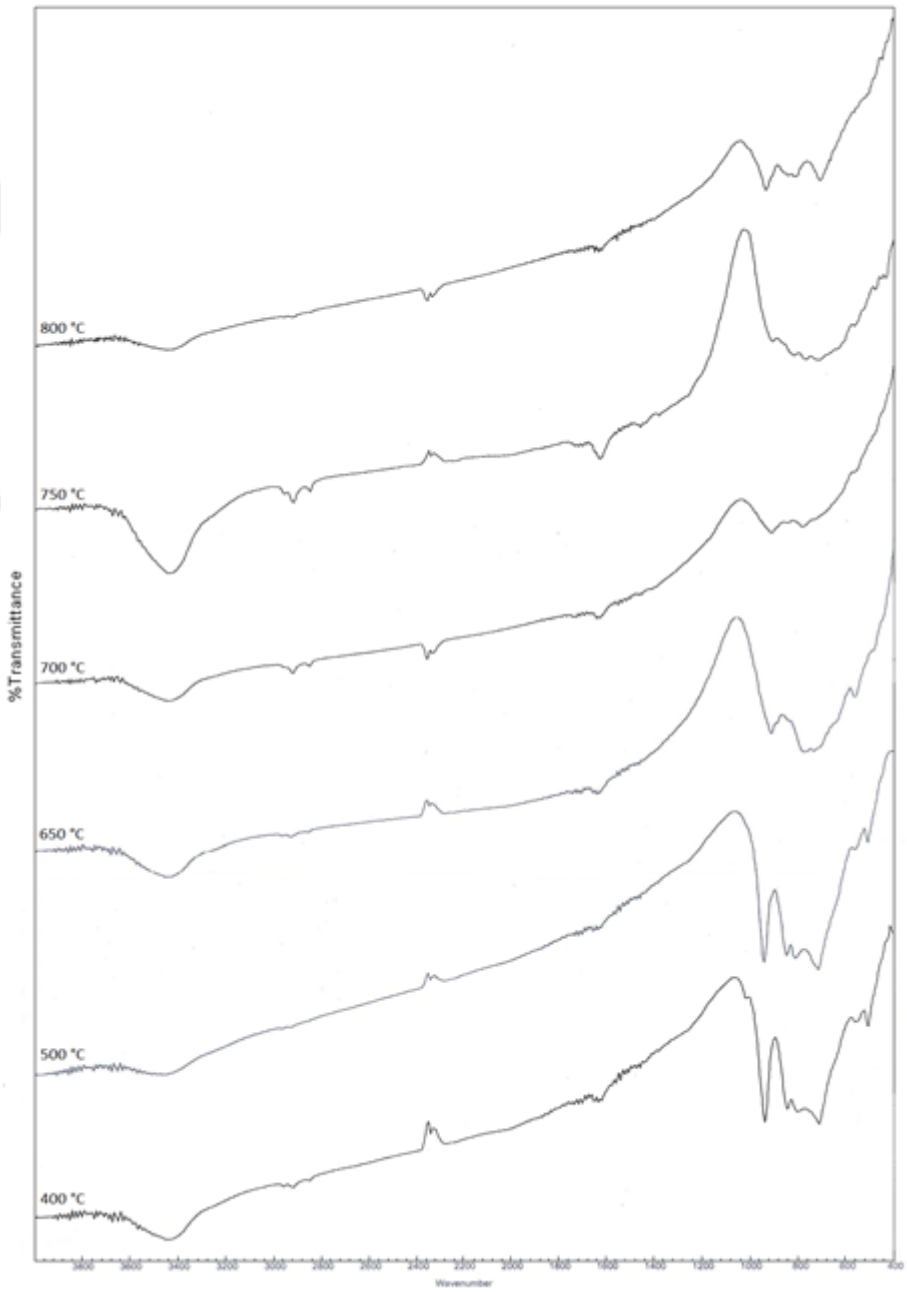

Figure 4.54. IR Spectra of $Cu_3V_2O_8$ product with urea fuel and V_2O_5 as starting reagents at different temperatures

4.3.1.3 TG/DTA Studies of Copper Orthovanadate with Urea Fuel and V_2O_5 as Starting Reagents

TG/DTA studies of the $Cu_3V_2O_8$ were done in the rate from room temperature to 1300°C. The study was carried out to determine the phase transition of the synthesized product. In TG analysis, the weight loss of the product was identified at 700-800°C. From the DTA results, endothermic peaks were found at 550°C, 750°C, 800°C, 1100 and 1200°C which specify the phase transition of the compound.

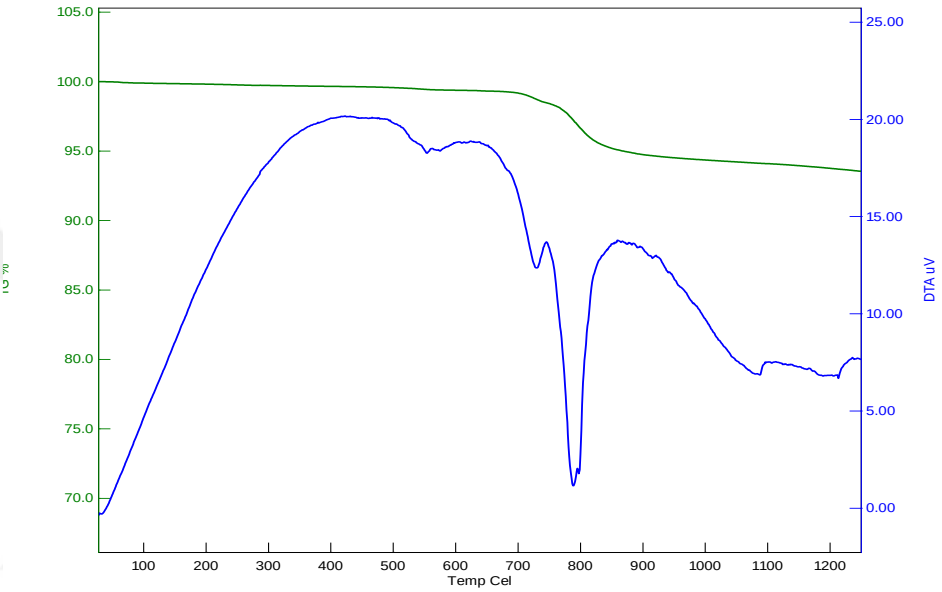

Figure 4.55. TG/DTA Curve of $Cu_3V_2O_8$ product with urea fuel and V_2O_5 as starting reagents.

4.3.2 Solution Combustion Synthesis Method for the Production of Copper Orthovanadate with Urea Fuel and NH_4VO_3 as starting reagents

$Cu_3V_2O_8$ was synthesized by using NH_4VO_3 starting material instead of V_2O_5. Stoichiometric amounts of the starting reagents $Cu(NO_3)_2.3H_2O$, NH_4VO_3 and CON_2H_4 were dissolved in a minimum quantity of deioned water. Then the mixture was heated until foam was formed and transferred to a furnace at 400°C. The process was completed in about 5 minutes and black powder was formed. After this process further heatings were done at 500-600-710 and 900°C about one hour. Each heating samples were taken from initial 400°C sample and the structure of this product was examined by using X-ray powder diffraction and IR analysis. The expected reaction was:

$6Cu(NO_3)_2.3H_2O + 4NH_4VO_3 + 10CON_2H_4 \rightarrow 2Cu_3V_2O_8 + 24NH_3 + 10CO_2 + 12NO_2 + 10H_2O + 3O_2$

4.3.2.1 X-Ray Powder Diffraction Studies of Copper Orthovanadate with Urea Fuel and NH_4VO_3 as starting reagents

The XRD patterns of $Cu_3V_2O_8$ were showed at Figure 4.56. According to the study reports, it is seen that $Cu_3V_2O_8$ could not be obtained. At 400^oC and 500^oC, β-$Cu_2V_2O_7$ was found, where as the peaks that assign to α-$Cu_2V_2O_7$ and β-$Cu_2V_2O_7$ was observed at 600^oC and 700 ^oC. At 900^oC, the compound was completely converted to β-$Cu_2V_2O_7$ and all the peaks has a good accordance to ICDD No: 73-1032 which belongs to monoclinic β-$Cu_2V_2O_7$.

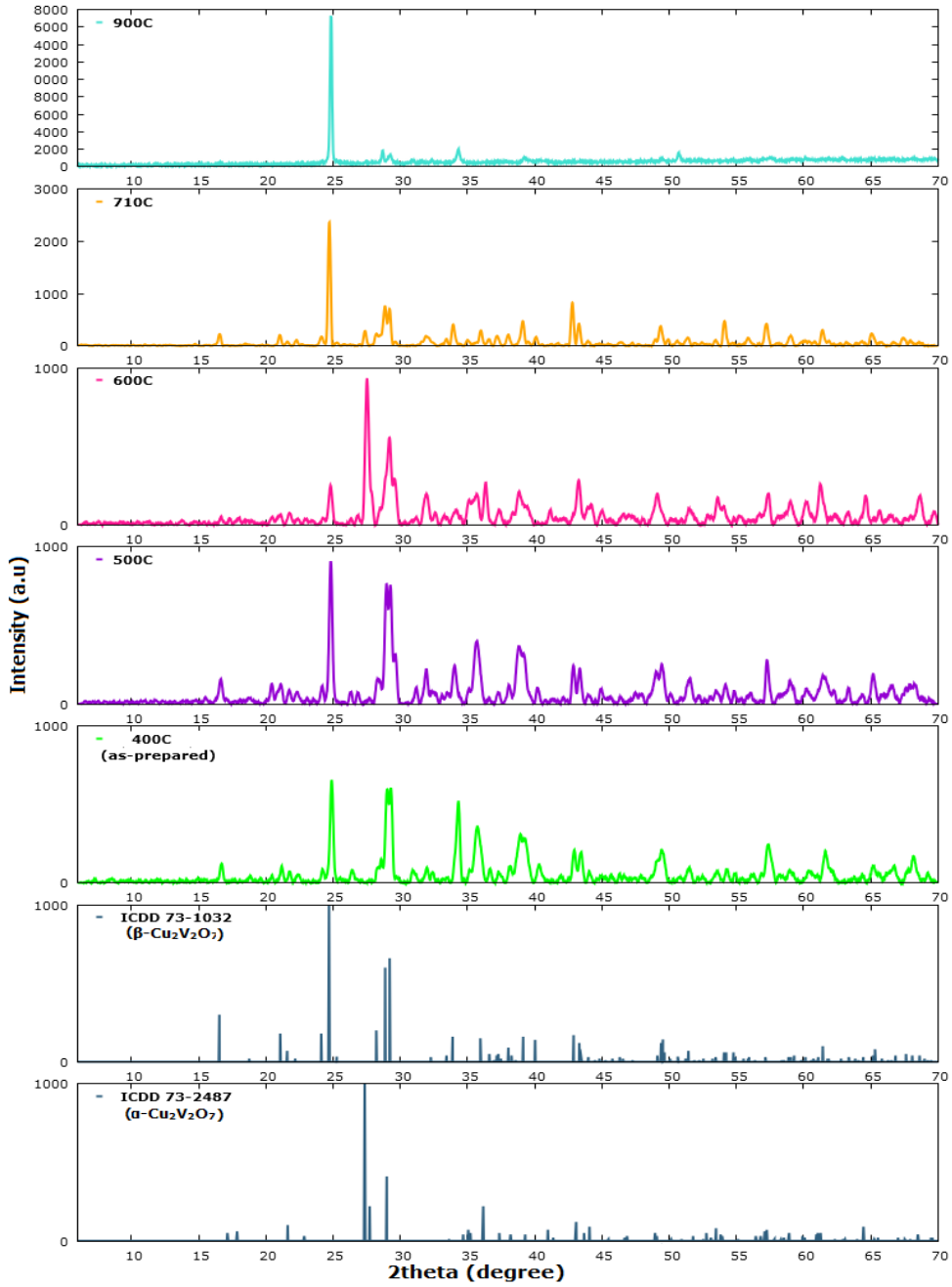

Figure 4.56. XRD patterns of $Cu_3V_2O_8$ product with urea fuel and NH_4VO_3 as starting reagents**.**

4.3.2.2 Infrared Spectroscopy Studies of Copper Orthovanadate with Urea Fuel NH_4VO_3 as Starting Reagents

The structural FT-IR spectra of the $Cu_3V_2O_8$ were presented at Figure 4.57. According to the study reports, it is confirmed that single phase $Cu_3V_2O_8$ was failed to synthesized. The strong absorption band at 717 cm-1 belongs to V-O-V bond of V_2O_7 was observed in the FT-IR Data.

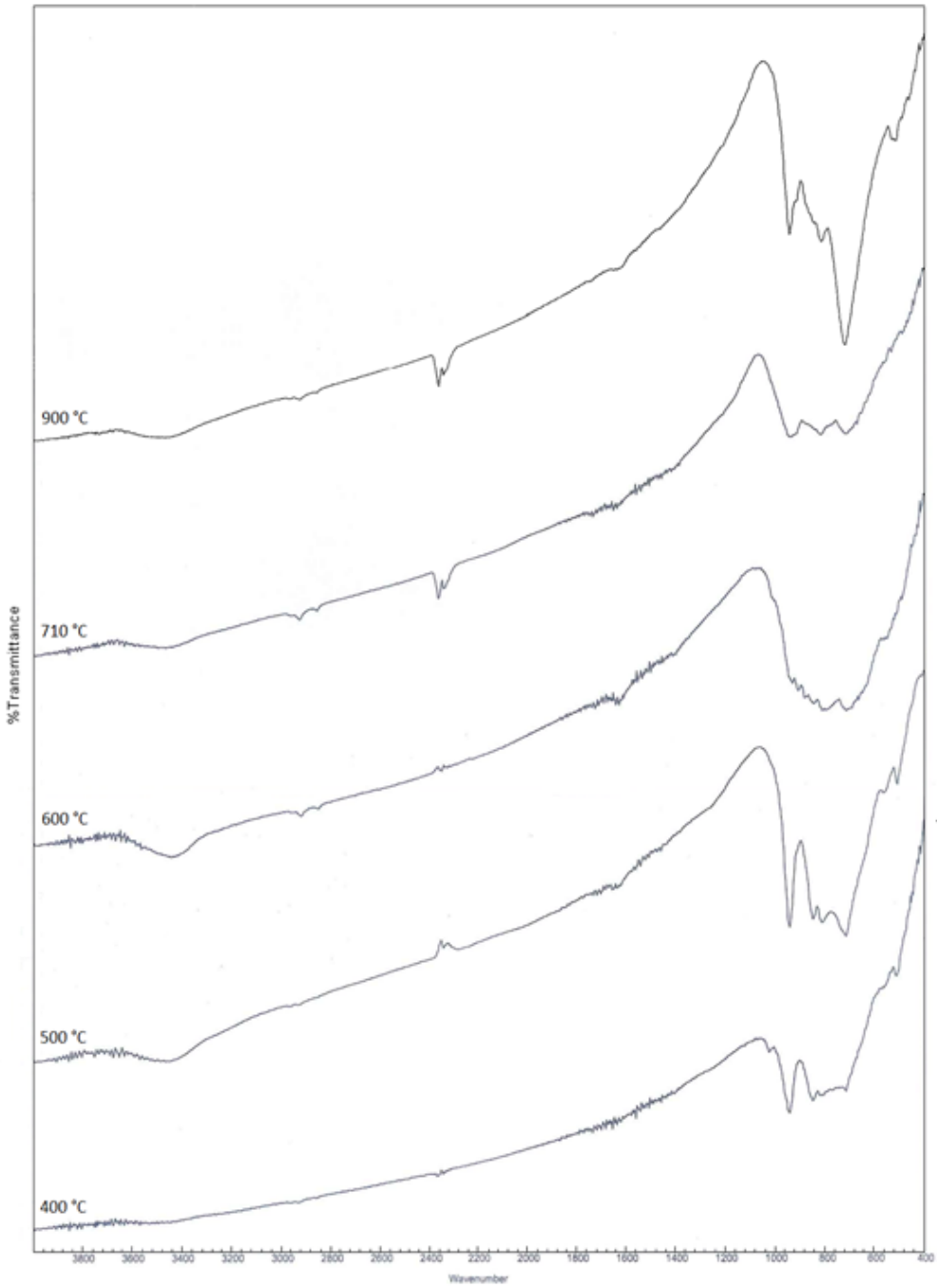

Figure 4.57. IR Spectra of $Cu_3V_2O_8$ product with urea fuel and NH_4VO_3 as starting reagents.

4.3.3 Solution Combustion Synthesis Method for the Production of Copper Orthovanadate with Glycine Fuel and V_2O_5 as Starting Reagents

The synthesis of $Cu_3V_2O_8$ was also done by solution combustion method using V_2O_5 as starting reagent and instead of urea, glycine was used as fuel. The homogeneous mixtures were prepared by dissolving stoichiometric proportion of $Cu(NO_3)_2.3H_2O$, V_2O_5 and $C_2O_2NH_5$(glycine) in minimum amount of distilled

water. The mixture was heated until the gel-like solution was obtained and was put in the furnace for five minutes at 400°C. After this ignition process the product was inseparable from evaporating dish. For this reason, further heating process could not be done. The expected reaction reported as below;

$9Cu(NO_3)_2.3H_2O + 3V_2O_5 + 10\ C_2O_2NH_5 \rightarrow 3Cu_3V_2O_8 + 20CO_2 + 14N_2 + 52H_2O$

4.3.4 Solution Combustion Synthesis Method for the Production of Nickel Orthovanadate with Glycine Fuel

The preparation of $Ni_3V_2O_8$ by applying solution combustion method was done using glycine as fuel. Two different starting reagent was used during this process which are V_2O_5 and NH_4VO_3. The stoichiometric amount of $Ni(NO_3)_2.6H_2O$, V_2O_5 or NH_4VO_3 and $C_2O_2NH_5$ were dissolved in small amount of deionized water. The homogeneous mixture was allowed to evaporates under continous stirring. After the precursor-gel formed, it was introduced to furnance at 400°C for 5 minutes. The further heating process at 400°C and 900°C was done to get a best desired products. The as-synthesized product was observed to be in a black colour which then light green colour changed after further heating at 900°C.The properties of the products were analyzed by using X-ray powder diffraction and IR analysis. The expected reaction are presented as:

With V_2O_5,

$9Ni(NO_3)_2.6H_2O + 3V_2O_5 + 10\ C_2O_2NH_5 \rightarrow 3\ Ni_3V_2O_8 + 20CO_2 + 14N_2 + 79H_2O$

With NH_4VO_3,

$6Ni(NO_3)_2.6H_2O + 6NH_4VO_3 + 10C_2O_2NH_5 \rightarrow 3Ni_3V_2O_8 + 20CO_2 + 30NH_3 + 46H_2O + 4NO_2 + 24O_2$

4.3.2.3 X-Ray Powder Diffraction Studies of Nickel Orthovanadate with Glycine Fuel

The multiferroic film of $Ni_3V_2O_8$ was synthesized previously by using sputter deposition method and the product was obtained at 900°C for 16 h [83]. In the other literature, it was reported that as prepared-$Ni_3V_2O_8$ was prepared at 800°C for a day and the further heating was carried out at 900°C to attain the $Ni_3V_2O_8$ [84]. In our work, the $Ni_3V_2O_8$ was successfully obtained at 900°C in shorter annealing time, 1 hour.

To determined the structural properties of $Ni_3V_2O_8$, the XRD studies were done. Figure 4.58 represent the XRD patterns that were prepared by **V_2O_5** starting reagent. It showed that high crystalinity orthorhombic $Ni_3V_2O_8$ was steadily formed as all the reflections are in a great agreement to ICDD Card No: 74-1484.

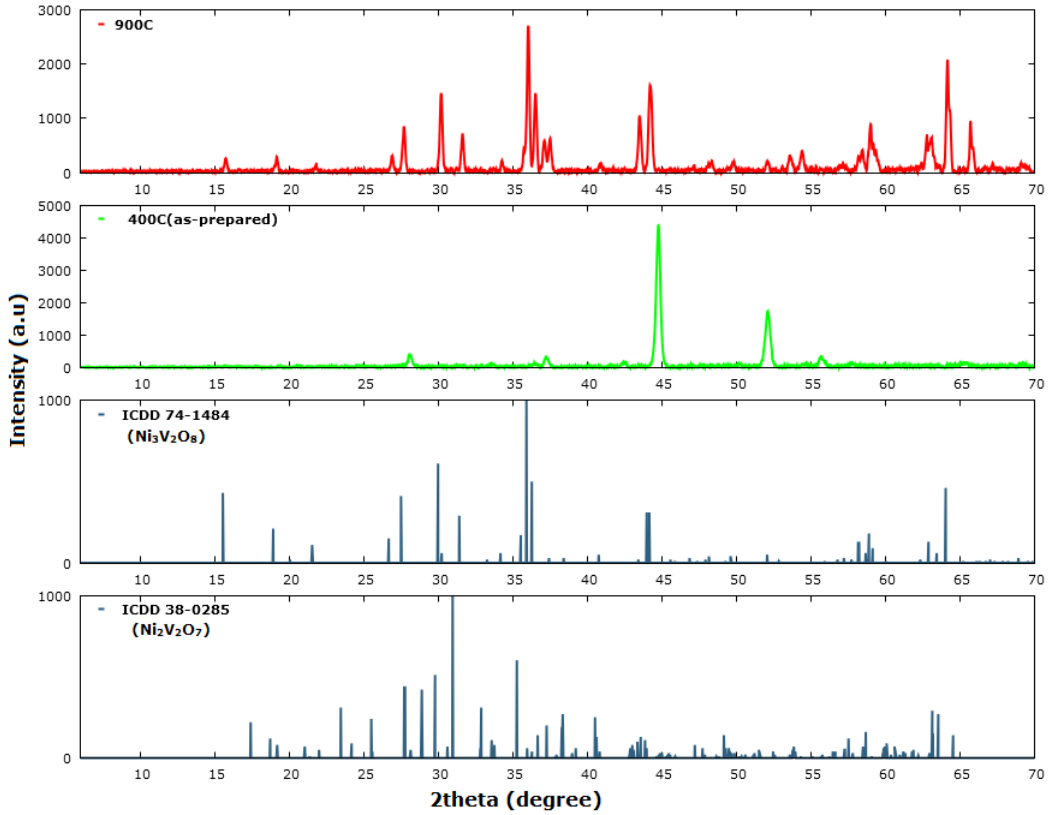

Figure 4.58. XRD patterns of $Ni_3V_2O_8$ as-prepared product and 900^{o}C with glycine fuel and V_2O_5 as starting reagent

For the product fabricated by **NH_4VO_3** shown in Figure 4.59, all the reflections were belonged to $Ni_3V_2O_8$ except for the reflection at around 2θ=44.110^o which is not dissociated as the previous reflection observed in the XRD data of V_2O_5 reagent (ICDD No: 74-1484).

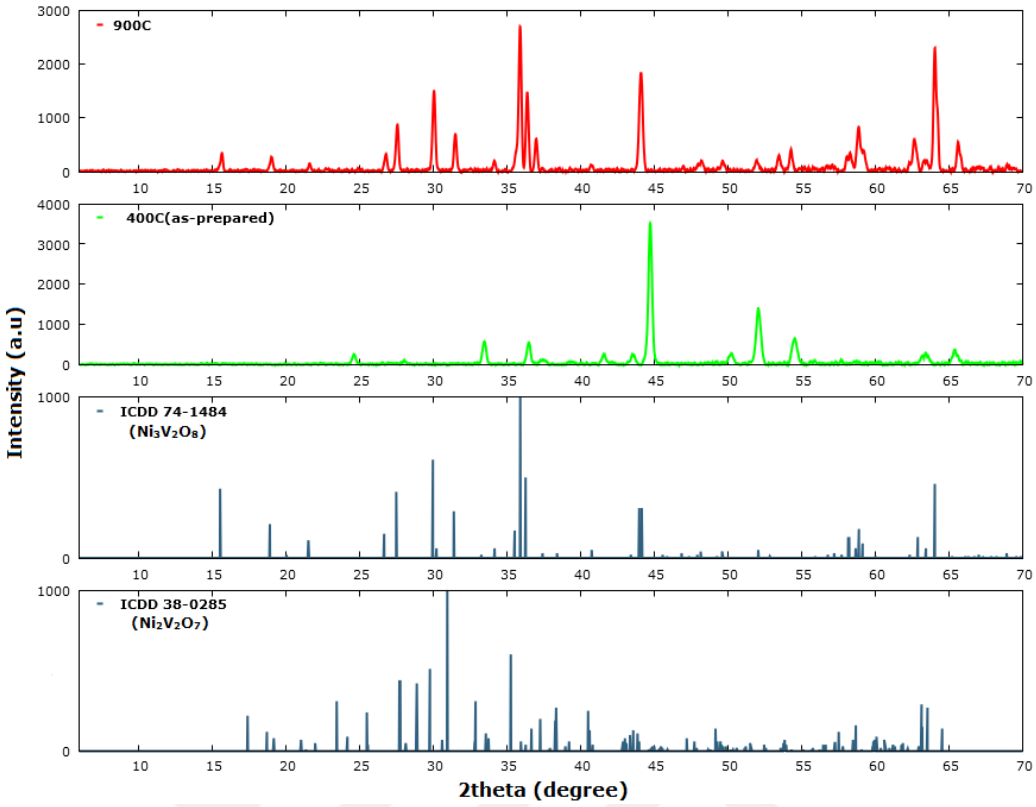

Figure 4.59. XRD patterns of $Ni_3V_2O_8$ as-prepared product and 900°C with glycine fuel and NH_4VO_3 as starting reagent.

4.3.2.4 Infrared Spectroscopy Studies of Nickel Orthovanadate with Glycine Fuel

The FT-IR spectra of $Ni_3V_2O_8$ obtained at 900°C were shown in Figure 4.60 and 4.61. The characteristic bands that specify to the formation of orthovanadates, 936-454 cm^{-1} bands were determined [79]. The The band at The strong band of Ni-O stretching vibration in the tetrahedral site was observed at aroung 600-500 cm^{-1} and weak band of Ni-O stretching vibration at the octahedral site was identified in the range 450-385 cm^{-1}[86].

Table 4.11. The IR assignment data of $Ni_3V_2O_8$ with glycine fuel

Asssignments	**Frequency υ(cm^{-1})**	
	V_2O_5	**NH_4VO_3**
stretching of V-O	828	826
Ni-O at Td stretching (strong)	650	657
Ni-O at Oh stretching (weak)	424	424

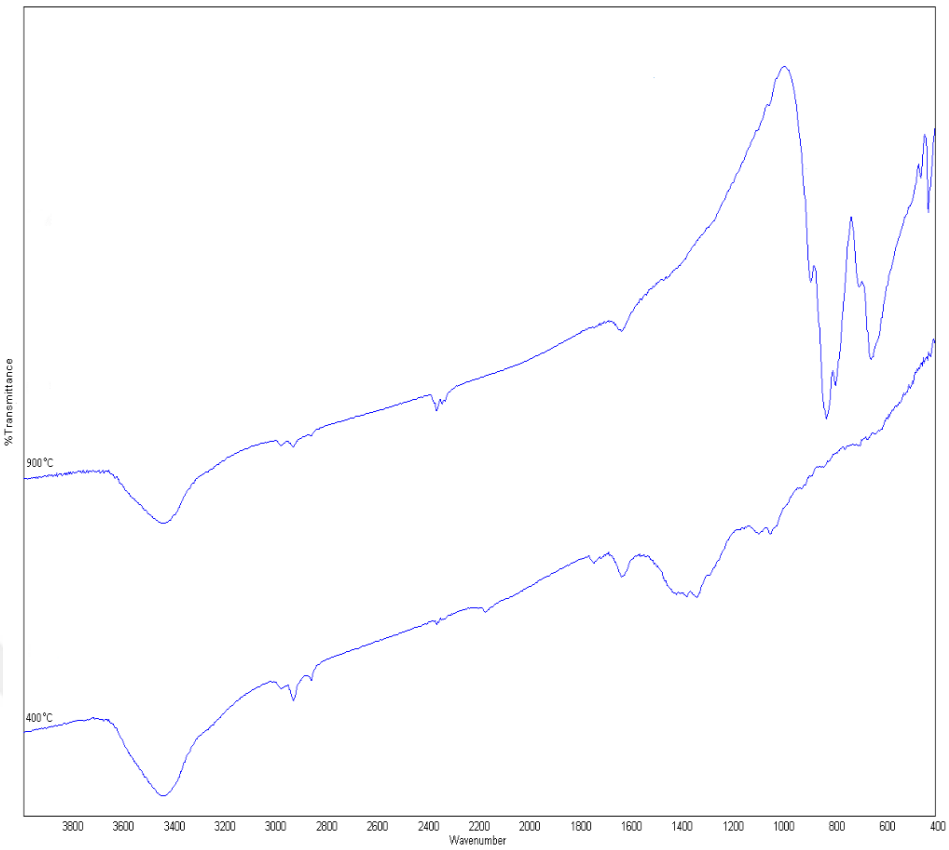

Figure 4.60. IR Spectra of of $Ni_3V_2O_8$ as-prepared product and 900ºC with glycine fuel and V_2O_5 as starting reagent.

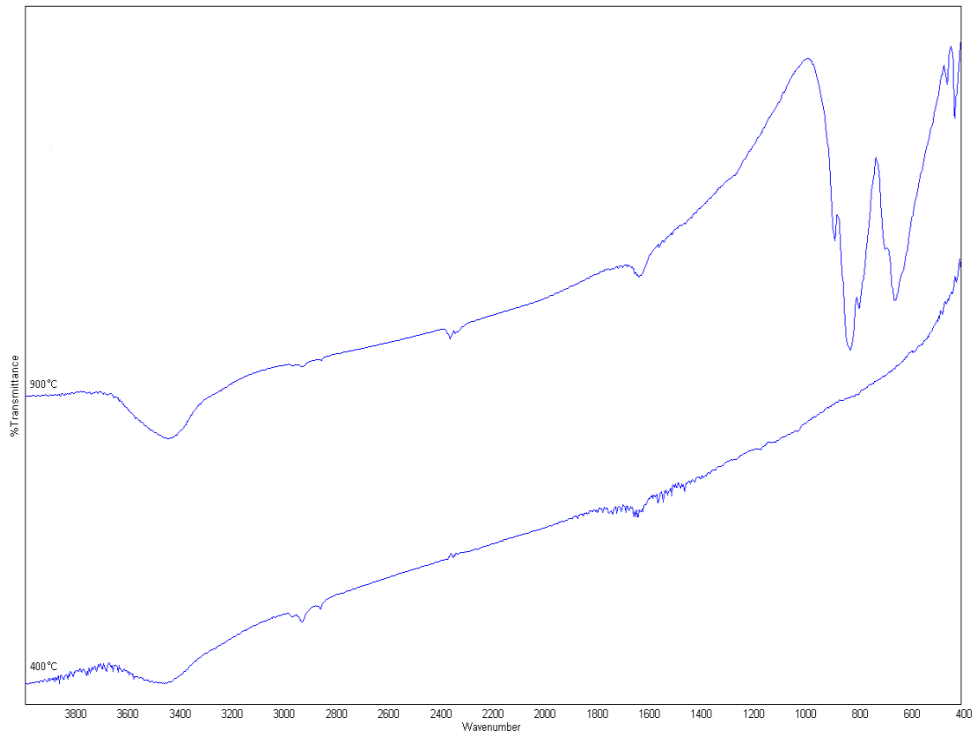

Figure 4.61. IR Spectra of of $Ni_3V_2O_8$ as-prepared product and 900ºC with glycine fuel and NH_4VO_3 as starting reagent.

4.3.2.5 TG/DTA Studies of Nickel Orthovanadate with Glycine Fuel

The TG/DTA curve of $Ni_3V_2O_8$ prepared with V_2O_5 were presented in Figure 4.62. In DTA analysis, the water loss was observed at ~85^oC and small endothermic peak was also detected at ~900^oC. This result also concluded that the compound is thermally stable.

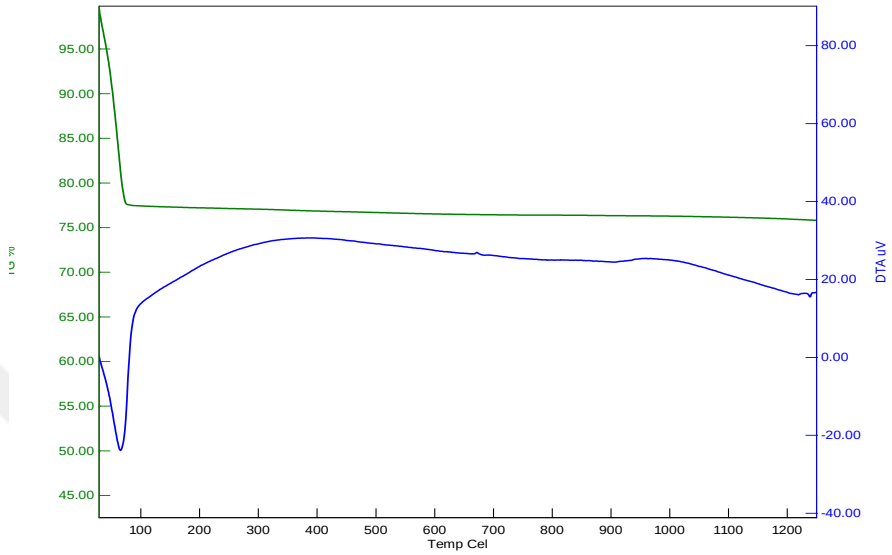

Figure 4.62. TG/DTA Curve of $Ni_3V_2O_8$ product with urea fuel.

4.3.5 Solution Combustion Synthesis Method for the Production of Nickel Orthovanadate with Urea Fuel

The synthesis of $Ni_3V_2O_8$ via solution combustion method with urea as fuel were done. Two different starting reagent was used during this process which are V_2O_5 and NH_4VO_3. The stoichiometric amount of $Ni(NO_3)_2.6H_2O$, V_2O_5 or NH_4VO_3 and CON_2H_4 were dissolved in minimum amount of distilled water and heated until the viscous solution observed. The solution was tranferred to furnance at 400^oC for 5 minutes and the further heating process at 400^oC and 900^oC was applied. The dark green colour of as-prepared product were changed to brownish green colour at 900^oC. The properties of the products were characterized by using X-ray powder diffraction and IR analysis. The expected reaction are presented as:

With V_2O_5,

$6Ni(NO_3)_2.6H_2O + 2V_2O_5 + 10CON_2H_4 \rightarrow 2\ Ni_3V_2O_8 + 10CO_2 + 16N_2 + 56H_2O$

With NH_4VO_3,

$6Ni(NO_3)_2.6H_2O + 4NH_4VO_3 + 10CON_2H_4 \rightarrow 2Ni_3V_2O_8 + 10CO_2 + 24NH_3 + 32H_2O + 12NO_2 + O_2$

4.4.1.1 X-Ray Powder Diffraction Studies of Nickel Orthovanadate with Urea Fuel

In Figure 4.63, the XRD patterns of $Ni_3V_2O_8$ that were prepared by V_2O_5 starting reagent. The results were compared with ICDD No:74-1484 which belongs to orthorhombic $Ni_3V_2O_8$. The multiphase products with $Ni_2V_2O_7$ (ICDD No:38-0285) were found at 900°C. Two small peak of $Ni_2V_2O_7$ with a very poor intensities were observed at around 2θ= 29.130° and 31.180°.

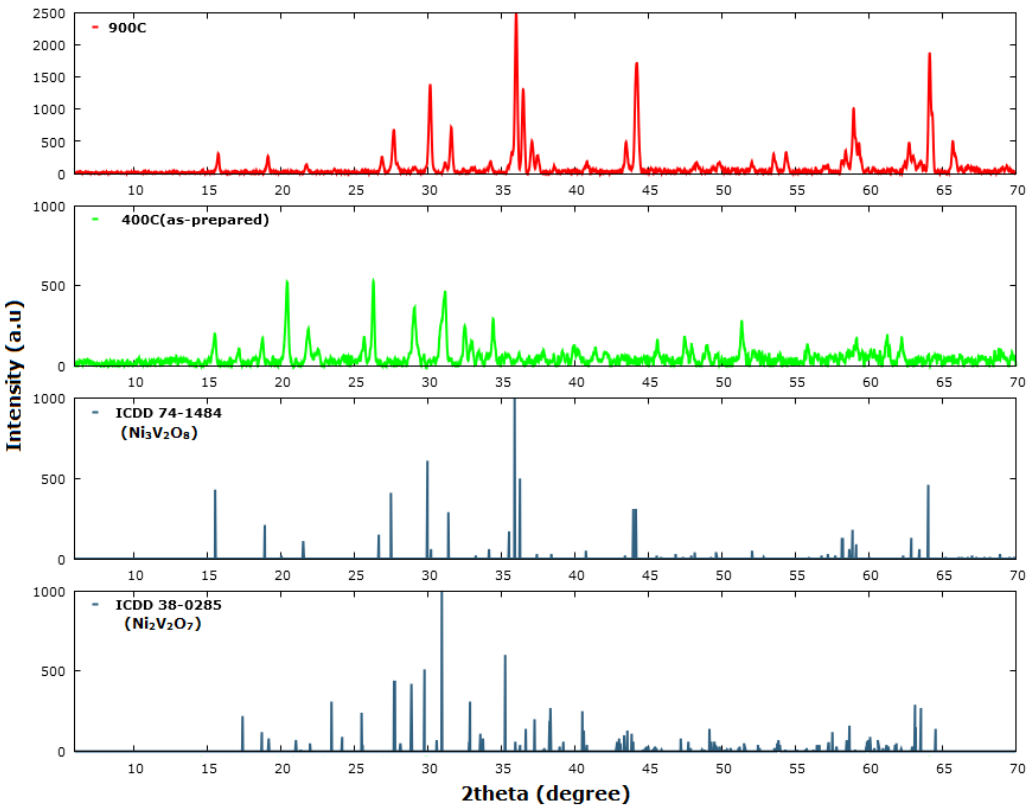

Figure 4.63. XRD patterns of $Ni_3V_2O_8$ as-prepared product and 900°C with urea fuel and V_2O_5 as starting reagent.

Slightly different from the V_2O_5 result, instead of two peaks there is only one peak with high intensity was observed at 2θ=44.360° in the XRD pattern of $Ni_3V_2O_8$ synthesized with NH_4VO_3 (ICDD No:74-1484). Two peaks that refer to $Ni_2V_2O_7$(ICDD No:38-0285) were also observed at 2θ=29.260° and 2θ=31.310° (Figure 4.64).

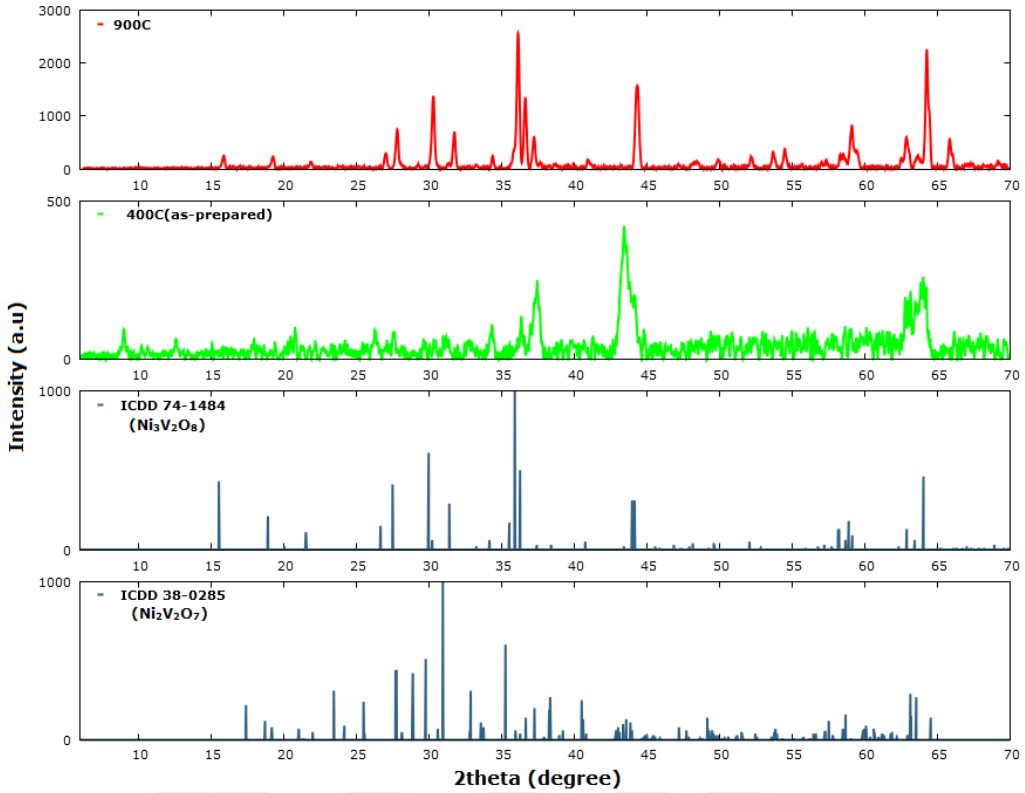

Figure 4.64. XRD patterns of $Ni_3V_2O_8$ as-prepared product and 900°C with urea fuel and NH_4VO_3 as starting reagent.

4.4.1.2 Infrared Spectroscopy Studies of Nickel Orthovanadate with Urea Fuel

The structural The FT-IR spectra of $Ni_3V_2O_8$ obtained at 900°C were presented (Figure 4.65 and 4.66). The characteristic bands that specify to the vibration band of octahedral NiO_6 and tetrahedral VO_4 were found in the range of 450-385 cm^{-1} and 936-454 cm^{-1} were reported, respectively [86]. In our work, the bands that belongs to $Ni_3V_2O_8$ as described in the literature was observed (Table 4.12) but due to the mixture with $Ni_2V_2O_7$ the band that characterized to asymmetric stretching of VO_3 at 943 cm^{-1} and symmetric stretching of V-O-V at 570 cm^{-1} were identified.

Table 4.12. The IR assignment data of $Ni_3V_2O_8$ with urea fuel

Asssignments	**Frequency υ(cm^{-1})**	
	V_2O_5	**NH_4VO_3**
stretching of V-O	816	827
Ni-O at Td stretching (strong)	642	653
Ni-O at Oh stretching (weak)	427	425

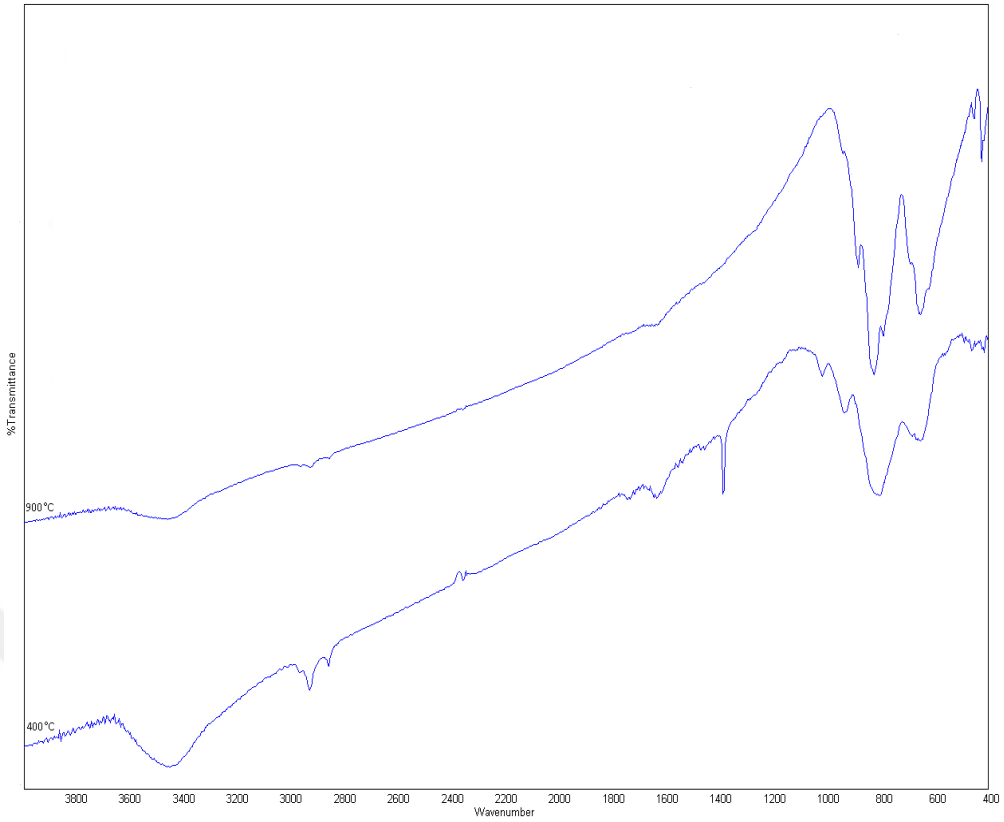

Figure 4.65. IR Spectra of of $Ni_3V_2O_8$ as-prepared product and 900°C with urea fuel and V_2O_5 as starting reagent.

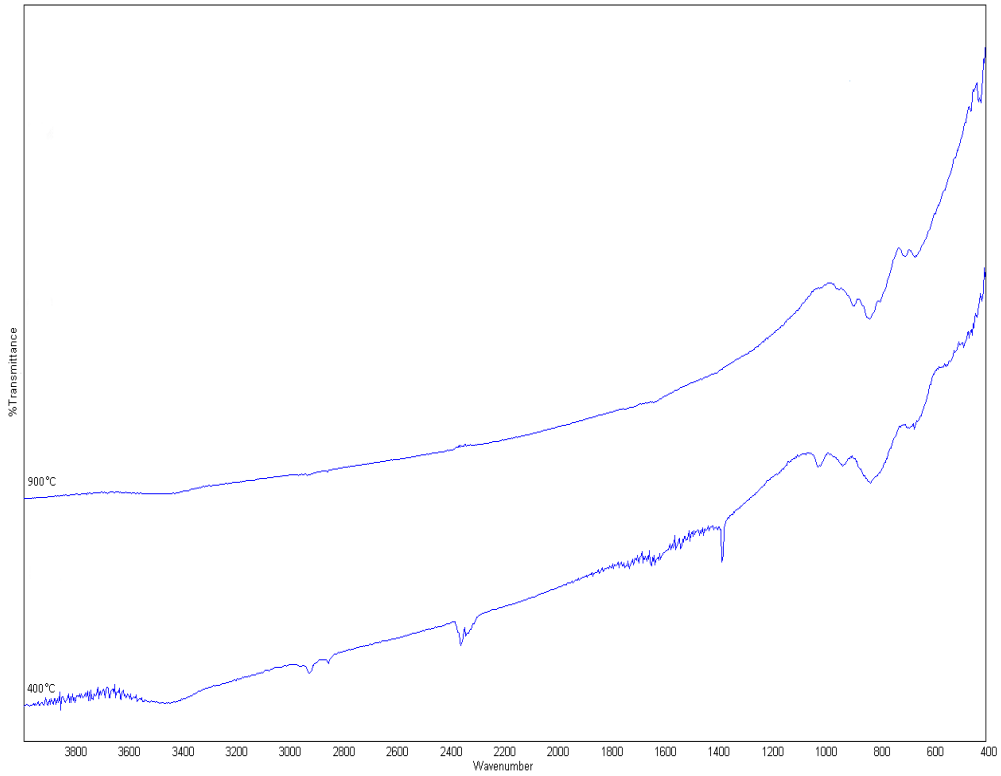

Figure 4.66. IR Spectra of of $Ni_3V_2O_8$ as-prepared product and 900°C with urea fuel and NH_4VO_3 as starting reagent.

4.3.6 Solution Combustion Synthesis Method for the Production of Nickel Orthovanadate with HMTA Fuel

Stoichiometric composition of $Ni(NO_3)_2.6H_2O$, V_2O_5 and $C_6H_{12}N_4$ were used to synthesized the $Ni_3V_2O_8$ by solution combustion method. The mixture of starting materials were dissolved in small amount of distilled water and allow to evaporated until the gel-like solution was observed. The annealing process were carried out at 400°C and 900°C. The colour changed during the annealing process was noticed from black powder to brownish green powder. The as-synthesized and the product obtained at 900°C were analyzed by X-Ray Diffraction, FT-IR Spectrometer and TG/DTA analysis. The expected reaction is:

$18Ni(NO_3)_2.6H_2O + 6V_2O_5 + 5\ C_6H_{12}N_4 \rightarrow 6Ni_3V_2O_8 + 30CO_2 + 28N_2 + 138H_2O$

4.5.1.1 X-Ray Powder Diffraction Studies of Nickel Orthovanadate with HMTA Fuel

The structural properties of orthorhombic $Ni_3V_2O_8$ prepared by using HMTA were shown in Figure 4.67. The $Ni_3V_2O_8$ is predominated and observed in a excellent agreement with ICDD Card No. 74-1484. The only different is one sharp peak was observed at 2θ=43.950°. Two additional peaks belongs to $Ni_2V_2O_7$(ICDD No:38-0285) were detected at around 2θ=29.010° and 2θ=31.040°.

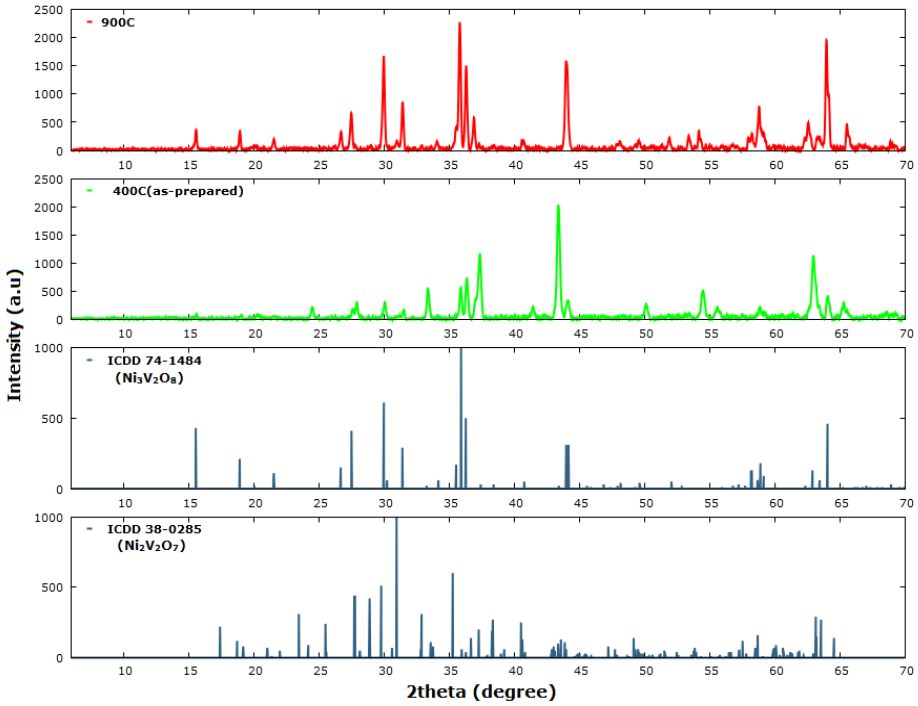

Figure 4.67. XRD patterns of $Ni_3V_2O_8$ as-prepared and 900°C product with HMTA fuel.

4.5.1.2 Infrared Spectroscopy Studies of Nickel Orthovanadate with HMTA Fuel

The band that characterized the vibration of VO_4 of $Ni_3V_2O_8$ were recognized at the FT-IR data obtained at 900°C (Figure 4.68). The weak absorption peak of $Ni_2V_2O_7$ were detected at 943 cm-1 which is attributed to antisymmetric stretching of VO_3. The vibration bands that assigned to $Ni_3V_2O_8$ as presented in Table 4.13.

Table 4.13. The IR assignment data of $Ni_3V_2O_8$ with HMTA fuel

Asssignments	**Frequency υ(cm^{-1})**
stretching of V-O	827
Ni-O at Td stretching (strong)	648
Ni-O at Oh stretching (weak)	415

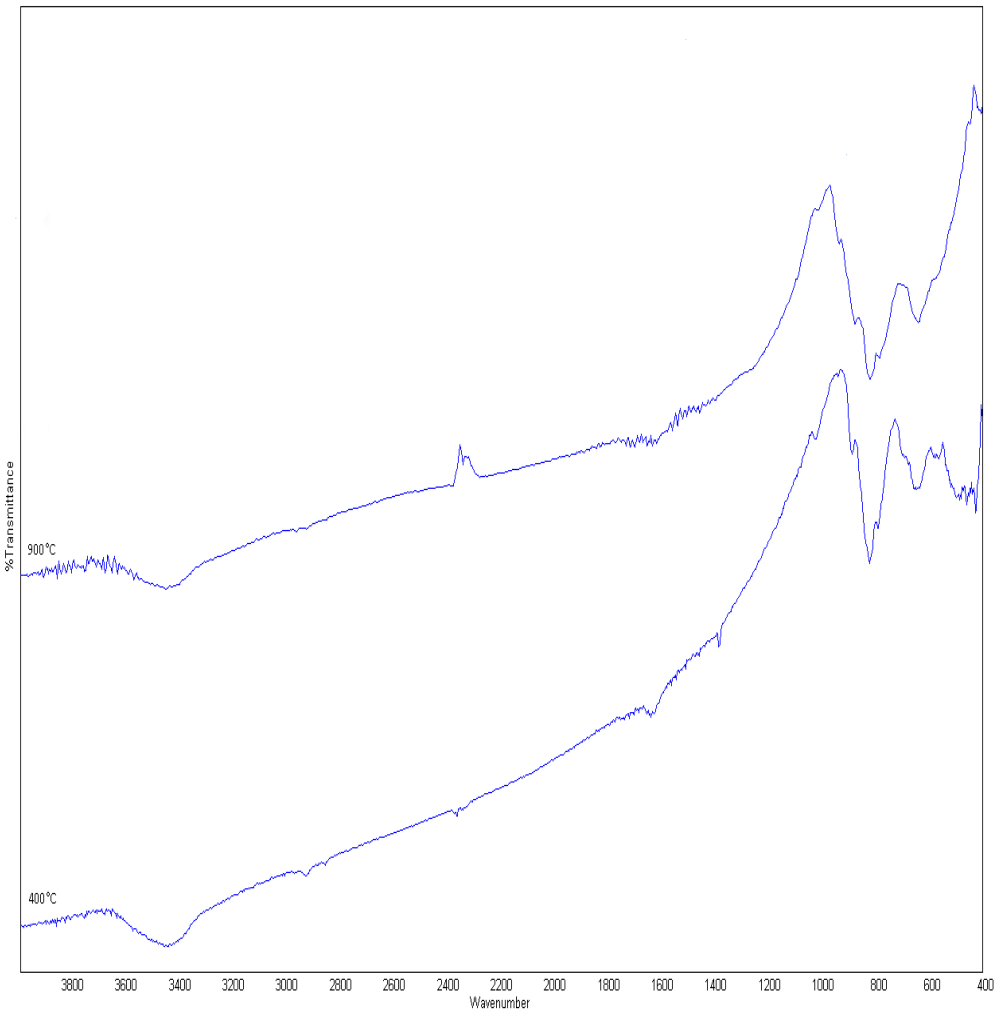

Figure 4.68. IR Spectra of $Ni_3V_2O_8$ product with HMTA fuel.

4.5.1.3 TG/DTA Studies of Nickel Orthovanadate with HMTA Fuel

TG/DTA analysis of the as-synthesized $Ni_3V_2O_8$ were done in the rate of room temperature to 1300^oC (Figure 4.69). There in no weight loss examined in the TG analysis and only one endothermic peak that described the phase transition of the compound was detected at ~1280^oC in DTA analysis.

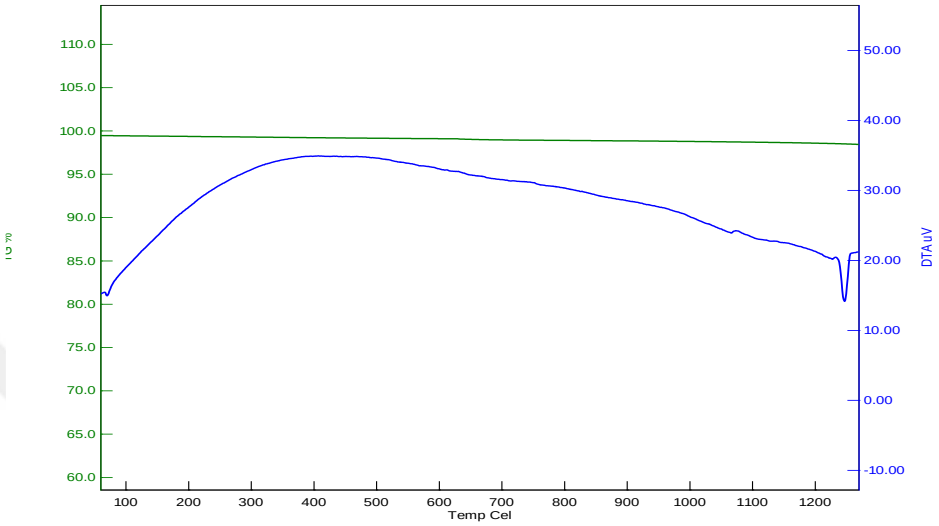

Figure 4.69. TG/DTA Curve of $Ni_3V_2O_8$ product with HMTA fuel

4.3.7 Solution Combustion Synthesis Method for the Production of Cobalt Orthovanadate with Different Fuels (Urea, Glycine and HMTA)

The fabrication of $Co_3V_2O_8$ has been done by undergo the solution combustion method. Stoichiometrtic amount of reactants; $Co(NO_3)_2.6H_2O$, V_2O_5 and fuels were dissolved in minimum volume of distilled water. In the preparation of this orthovanadates three different fuels (urea, glycine and HMTA) were applied. The mixture was allowed to evaporated until the viscous gel were formed. The gel was introduced to the pre-heated furnace at 400^oC for 5 minutes. Further heating process was carried out and different annealing temperature were applied for each fuels.

The predicted reactions are presented as;

With urea fuel;

$6Co(NO_3)_2.6H_2O + 2\ V_2O_5 + 10CON_2H_4 \rightarrow 2Co_3V_2O_8 + 10CO_2 + 16N_2 + 56H_2O$

With glycine fuel;

$9Co(NO_3)_2.6H_2O + 3V_2O_5 + 10C_2O_2NH_5 \rightarrow 3Co_3V_2O_8 + 20CO_2 + 14N_2 + 79H_2O$

With HMDA fuel;

$18Co(NO_3)_2.6H_2O + 6V_2O_5 + 5C_6N_4H_{12} \rightarrow 6Co_3V_2O_8 + 30CO_2 + 28N_2 + 138H_2O$

By using urea fuel, the products were obtained in black colour and the as-synthesized products were heated at 400°C and 900°C. There is no color changed observed in this $Co_3V_2O_8$ synthesis. Due to its low intensity detected in the XRD patterns (Figure 4.70) which expected the low crystallinity of products, 25% excess of urea fuel was also applied. It revealed that, no distinct different was observed by the excess of urea fuel.

The annealing process of as-prepared $Co_3V_2O_8$ obtained by glycine fuels was done at 400°C, 900°C and 950°C. There is no changed in powder products were identified at the higher temperatures.

Two different heating temperatures were also applied in order to for the best desired produts of $Co_3V_2O_8$. The as-obtained products synthesized by HMTA fuel was annealed at 400°C and 900°C. The color charged of the product was also not examined under heating at higher temperatures.

All the properties of these products were characterized by XRD diffraction, IR Spectrometer and TG/DTA analysis and presented in sections below.

4.5.7.1 X-Ray Powder Diffraction Studies of Cobalt Orthovanadate with Urea Fuel

The XRD studies of the obtained product were carried out at the range of $2\theta=5^o$-70^o. All the pattern analyzed and compared attentively by ICDD Card No: 70-1393 which belongs to orthorhombic $Co_3V_2O_8$.

Figure 4.70 represent the XRD patterns of $Co_3V_2O_8$ prepared with **urea fuel**. It clearly seen that the intensity of the orthorhombic $Co_3V_2O_8$ obtained at 900°C was very low. All the peak was compatible with the ICDD data card and only one peak located in the $2\theta=15.415^o$ were not detected.

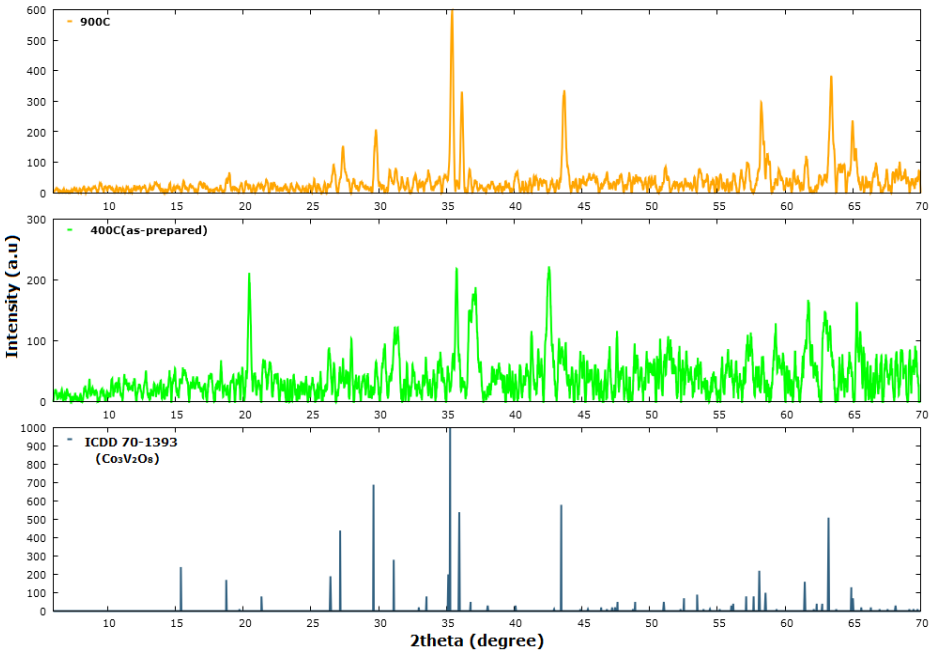

Figure 4.70. XRD patterns of $Co_3V_2O_8$ product with urea fuel.

As mentioned, to acquired a high crystallinity products and to accomplished the best result, the synthesis of $Co_3V_2O_8$ was repeated with **25% excess of urea**. The XRD Patterns of the product revealed that there is no difference in the intensity. It also showed that the peak at around $2\theta=18.764^o$ disappeared along with the appearance of peak at $2\theta=15.415^o$ (Figure 4.71).

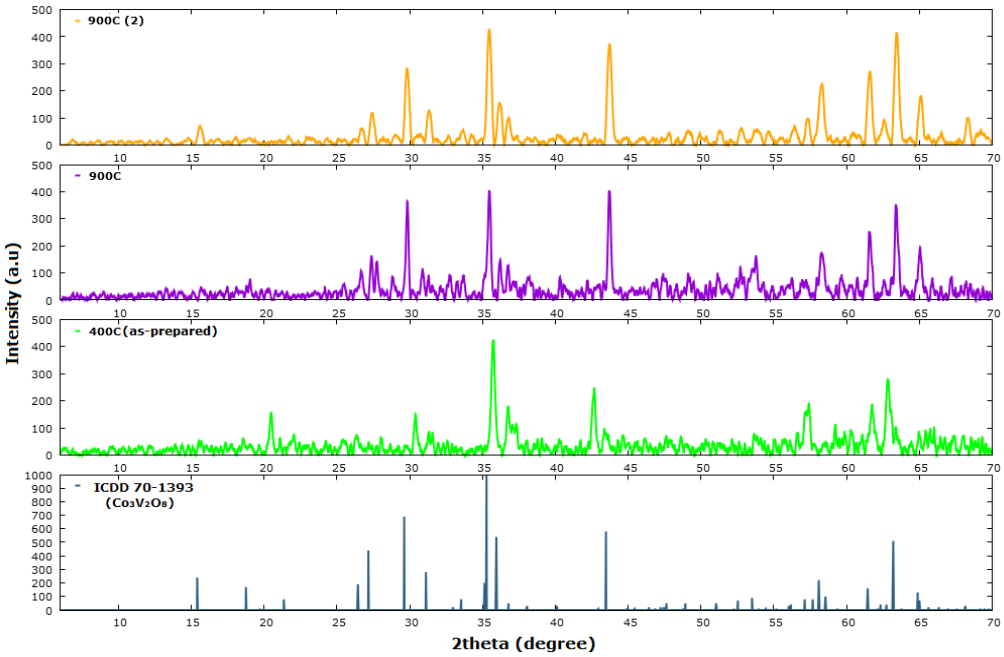

Figure 4.71. XRD patterns of $Co_3V_2O_8$ product with 25% excess of urea fuel.

The XRD patterns of $Co_3V_2O_8$ synthesized with the **glycine fuels** were also shown in Figure 4.75 and was correlated to ICDD No. 70-1393. In comparison to the product acquired by urea fuels, the products with glycine has a higher intensity. In more addition, it observed that some peaks of $Co_3V_2O_8$ are disappeared at 950^oC which confirmed the formation of $Co_3V_2O_8$ at lower temperature. All the peaks of product obtained at 900^oC are compatible with the orthorhombic structure of $Co_3V_2O_8$.

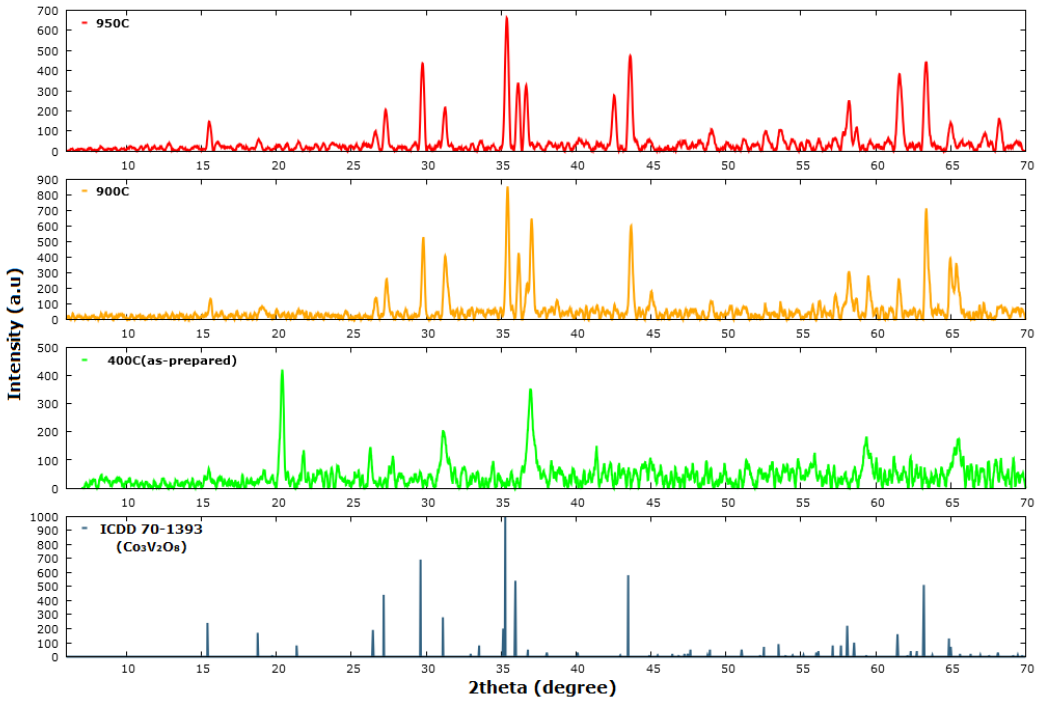

Figure 4.72. XRD patterns of $Co_3V_2O_8$ product with glycine fuel.

All the peaks related to orthorhombic structure of were detected in the XRD pattern of $Co_3V_2O_8$ product obtained at 900^oC with **HMTA**, except for one peak at 2θ=15.415^o. In more additions, there are also three low intensity additional peaks of secondary phase at 2θ= 10.750 ^{o}, 28.900 ^{o}, 54.590^o were observed.

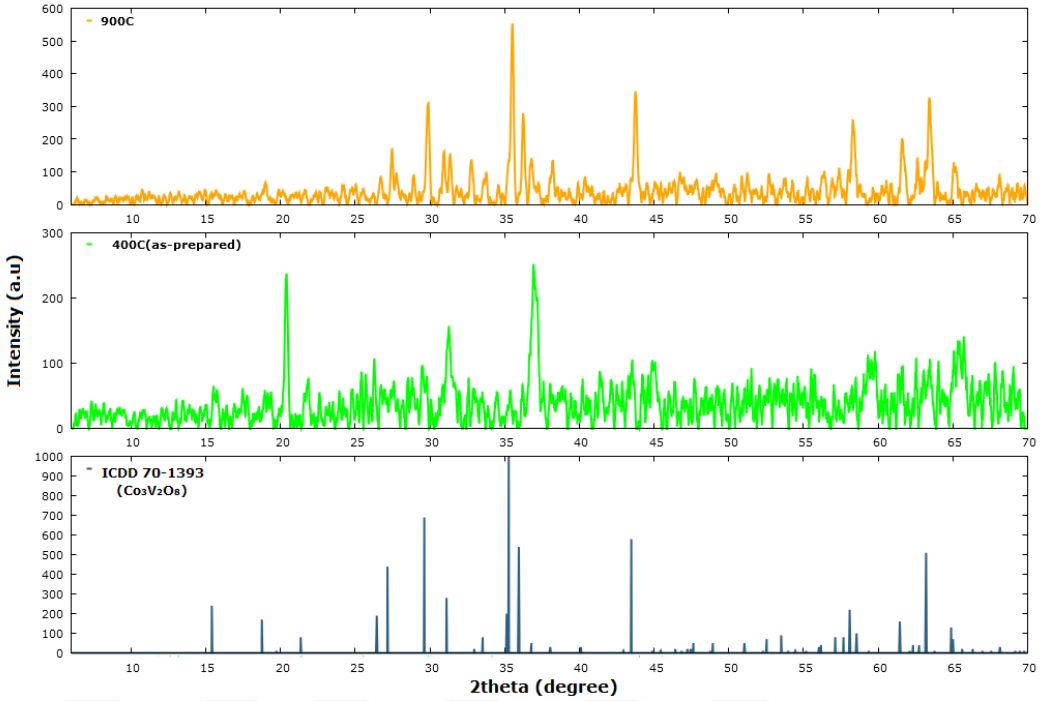

Figure 4.73. XRD patterns of $Co_3V_2O_8$ product with HMTA fuel.

4.5.7.2 Infrared Spectroscopy Studies of Cobalt Orthovanadate with Different Fuels (Urea, Glycine, HMTA)

The FT-IR Spectra of all $Co_3V_2O_8$ prepared with different fuels were presented in Figure 4.74 to 4.77. It was reported that all spectra identified at 900°C have a compatible data with the literature as all the absorption peaks were observed in a range of 936-454 cm^{-1}[86]. All characteristic bands of $Co_3V_2O_8$ are listed in Table 4.14.

Table 4.14. The IR assignment data of $Co_3V_2O_8$

Asssignments	**Frequency υ(cm^{-1})**			
	Urea		**Glycine**	**HMTA**
	Non-excess	25%excess		
stretching of V-O	817	820	824	815
Co-O at Td stretching (strong)	647	642	670	634
Co-O at Oh stretching (weak)	417	411	410	410

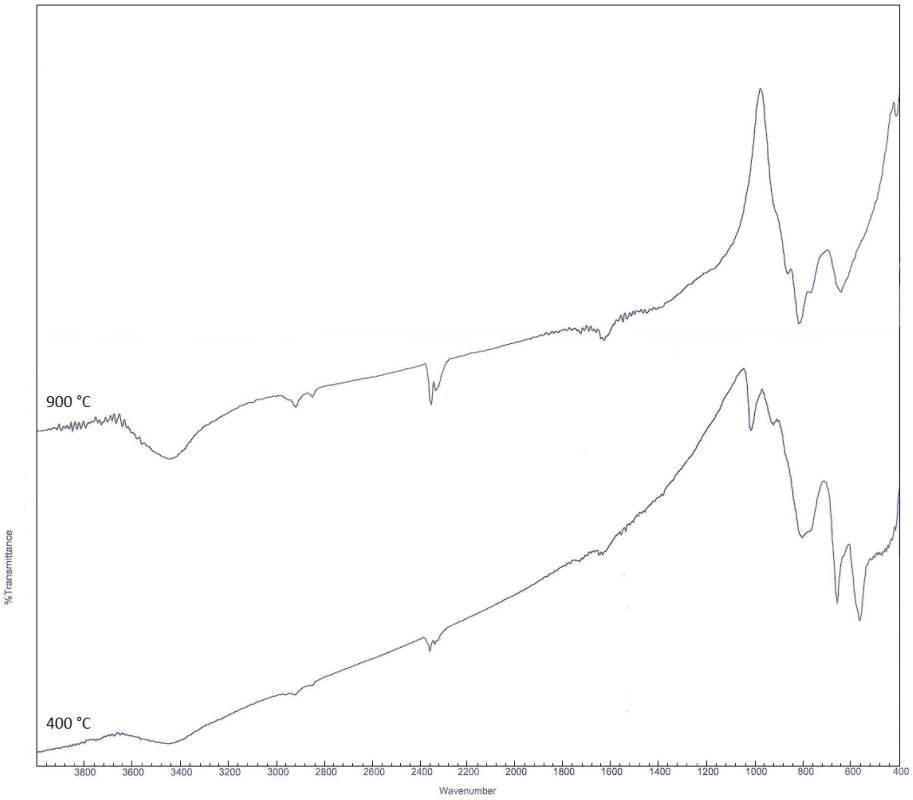

Figure 4.74. IR Spectra of $Co_3V_2O_8$ product with urea fuel

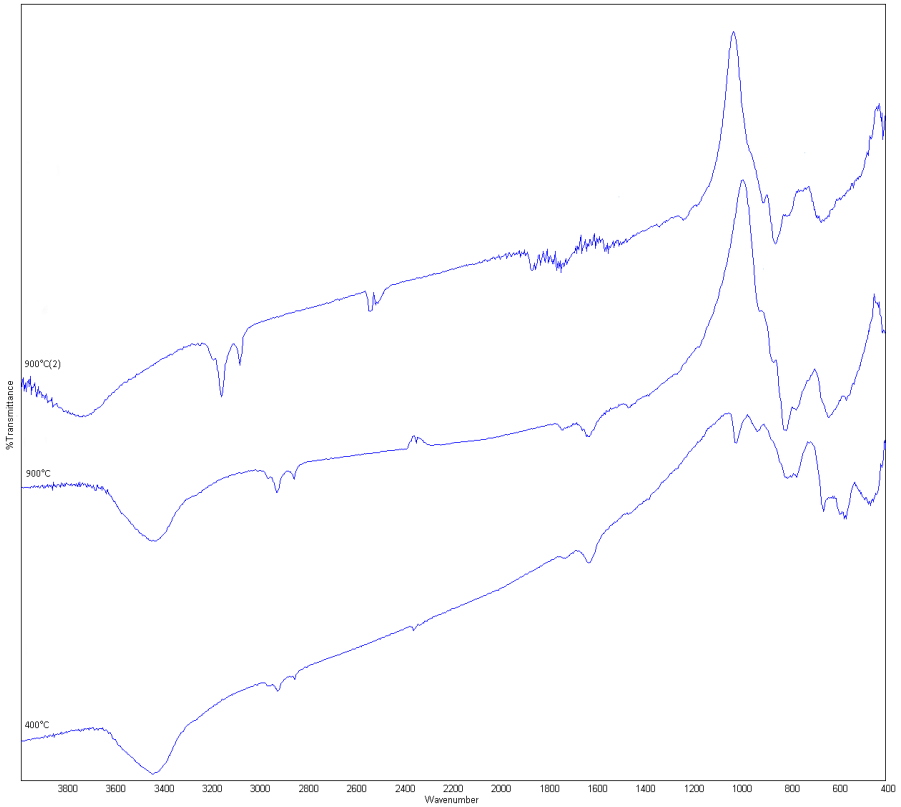

Figure 4.75. IR Spectra of $Co_3V_2O_8$ product with 25%excess of urea fuel.

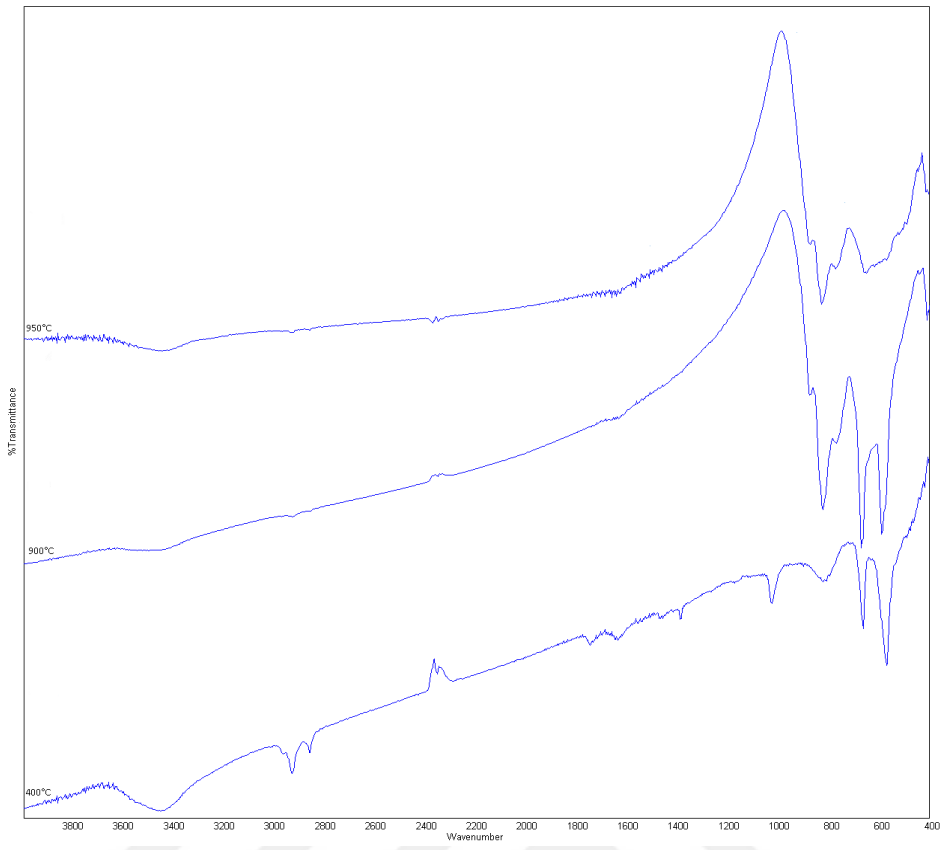

Figure 4.76. IR Spectra of $Co_3V_2O_8$ product with glycine fuel.

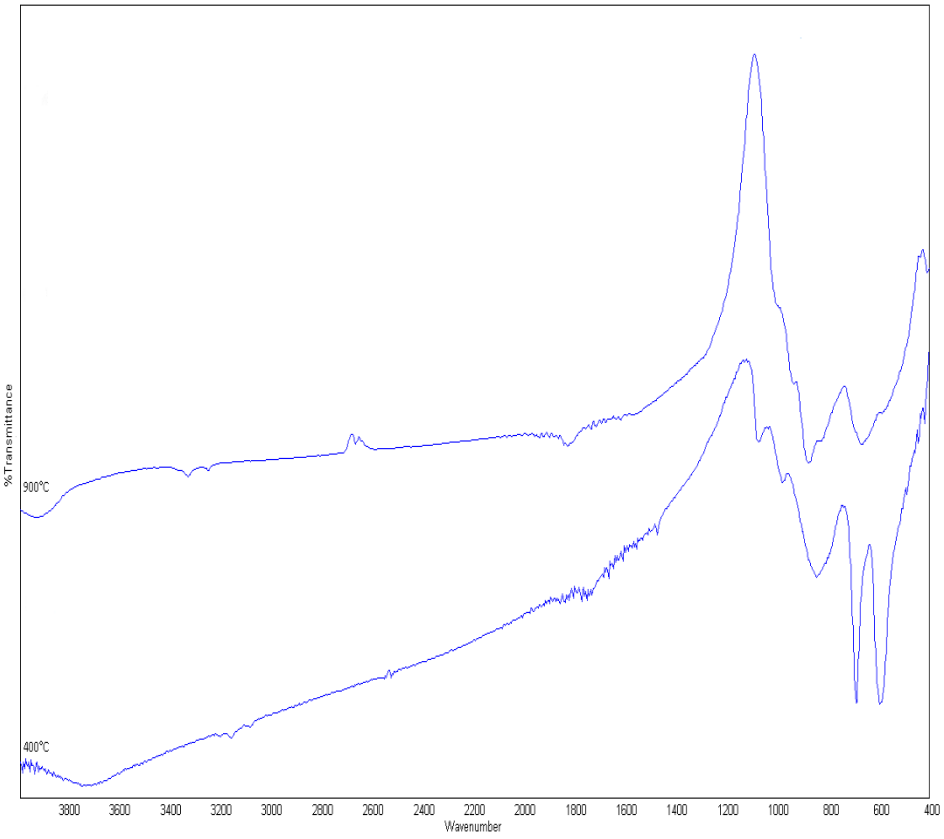

Figure 4.77. IR Spectra of $Co_3V_2O_8$ product with HMTA fuel.

4.5.7.3 TG/DTA Studies of Cobalt Orthovanadate with Different Fuels (Urea, Glycine and HMTA)

Figure 4.78 to 4.80 represent the TG/DTA data analysis of as-prepared $Co_3V_2O_8$ with different fuels. The TG/DTA analysis were carried out in the rate of room temperature to 1300°C.

In DTA analysis of products obtained by **urea fuel**, one endothermic peak at 1130° were determined.

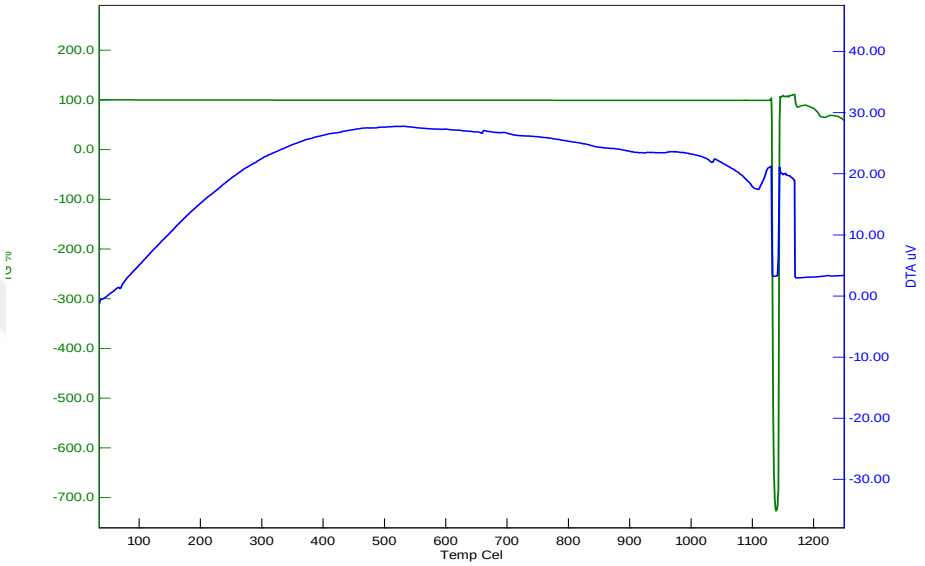

Figure 4.78. TG/DTA Curve of $Co_3V_2O_8$ product with urea fuel

Two endothermic peaks that defined the phase transition of $Co_3V_2O_8$ were examined at 850°C and 1150°C in DTA analysis of products synthesized with **glycine fuel**. The compound was also thermally stable (Figure 4.77).

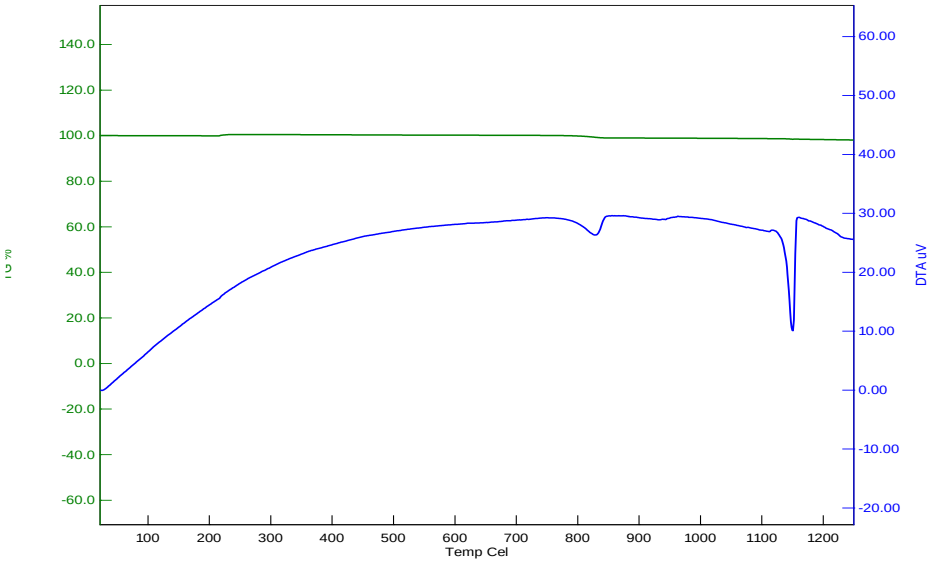

Figure 4.79. TG/DTA Curve of $Co_3V_2O_8$ product with glycine fuel.

Three endothermic peaks were identified at 800°C, 900°C and 1050°C which specified the phase transition of the product acquired by **HMTA fuel**. Hence, the product was also thermally stable (Figure 4.80).

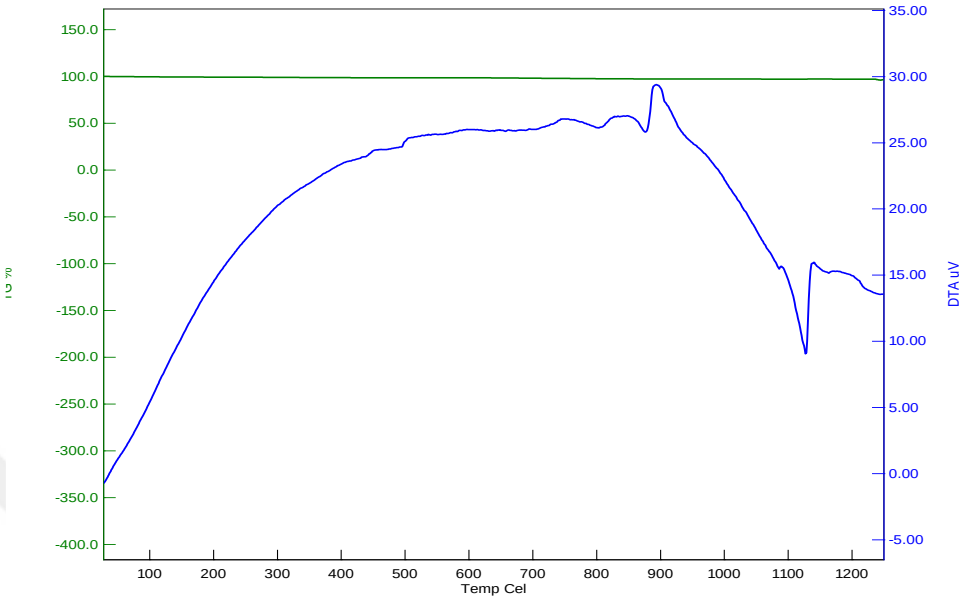

Figure 4.80. TG/DTA Curve of $Co_3V_2O_8$ product with HMTA fuel.

4.3.8 Solution Combustion Synthesis Method for the Production of Zinc Orthovanadate with Different Fuels (Urea, Glycine, Carbohydrazide and HMDA)

The same method was also applied in the preparation of $Zn_3V_2O_8$. Stoichiometric amount starting materials $Zn(NO_3)_2.6H_2O$, V_2O_5 and fuels (urea, glycine, carbohydrazide and HMDA) were dissolved in moderate amount of water. The homogeneous mixture was allowed to evaporated until the precursor gel was observed. The gel was directly transfered to pre-heated at 400°C for 5 minutes. The calcination process was of each products obtained from different fuels were carried out at different temperatures. The structural properties, band variations and thermal properties of products were characterized by X-ray Diffraction, IR Spectrophotometer and TG/DTA analysis, respectively. The expected reactions are presented;

With urea fuel;

$6Zn(NO_3)_2.6H_2O + 2V_2O_5 + 10CON_2H_4 \rightarrow 2Zn_3V_2O_8 + 10CO_2 + 16N_2 + 56H_2O$

With glycine fuel;

$9Zn(NO_3)_2.6H_2O + 3V_2O_5 + 10C_2O_2NH_5 \rightarrow 3\ Zn_3V_2O_8 + 20CO_2 + 14N_2 + 79H_2O$

With carbohydrazide fuel;

$12Zn(NO_3)_2.6H_2O + 4V_2O_5 + 15CH_6N_4O \rightarrow 4Zn_3V_2O_8 + 15CO_2 + 42N_2 + 117H_2O$

With HMDA fuel;

$12Zn(NO_3)_2.6H_2O + 4V_2O_5 + 3C_6N_2H_{16} \rightarrow 4Zn_3V_2O_8 + 18CO_2 + 15N_2 + 96H_2O$

The sythesis of $Zn_3V_2O_8$ with all fuels (**urea, glycine, carbohydrazide and HMDA**) were prepared as the explained procedures but single phase of desired product were not obtained at 400^{o}C as reported in XRD patterns shown in Figure 4.81 to 4.84. The annealing process of **urea and glycine** synthesized product were done at 500^{o}C, 750^{o}C, 850^{o}C and 900^{o}C for one hour. While the annealing process of **carbohydrazide and HMDA** were carried out only at 750^{o}C and 850^{o}C. After 850^{o}C, $Zn_3V_2O_8$ was decomposed to $Zn_2V_2O_7$ and $Zn_4V_2O_9$[125].

For all fuels, further studies were done according to Luitel N H. et al, literature to obtain pure $Zn_3V_2O_8$[cited by 100, p.139]. Instead of 400^{o}C the ignition process was done at 530^{o}C for 5 minutes as described in literature. Only for urea fuel, as-synthesized substance was heated at 700^{o}C. Due to presence of secondary phase detected at 530^{o}C and 700^{o}C (Figure 4.85) the additional heating was not applied to other fuels.

The characterization studies of all prepared products were done using XRD diffraction, IR Spectrometer and TG/DTA analysis.

4.6.1.1 X-Ray Powder Diffraction Studies of Zinc Orthovanadate with Different Fuels (Urea, Glycine, Carbohydrazide, and HMDA)

$Zn_3V_2O_8$ known to has two crystallographic forms; α-$Zn_3V_2O_8$, low temperature form and β-$Zn_3V_2O_8$, high temperature form. The phase transition between these two forms are reversible and take place at around 795°C. The structure of α-$Zn_3V_2O_8$ was determined in orthorhombic structure while the β-$Zn_3V_2O_8$ crystal structure has not been identified due to its steady decomposition into two solid phases of $Zn_4V_2O_9$ and β-$Zn_2V_2O_7$ [125].

The XRD Patterns of all $Zn_3V_2O_8$ synthesized with different fuels were presented in the Figure 4.81 to Figure 4.84. All the products were compared to $Zn_3(VO_4)_2$ (ICDD No: 34-0378), β-$Zn_3(VO_4)_2$ (ICDD No: 19-1468), $Zn_2V_2O_7$ (ICDD No:38-0251) and $Zn_4V_2O_9$ (ICDD No: 77-1757).

Figure 4.81 represent the XRD pattern of the products acquired by **urea fuel**. It showed that at 400°C as-prepared substance and 500°C 1h substance, $Zn_2V_2O_7$ was examined. The formation of $Zn_3V_2O_8$ was started to obtained at 750°C and residual substance of $Zn_2V_2O_7$ was shown. The decomposition of $Zn_3V_2O_8$ into $Zn_4V_2O_9$ and $Zn_2V_2O_7$ was confirmed at ≥850°C.

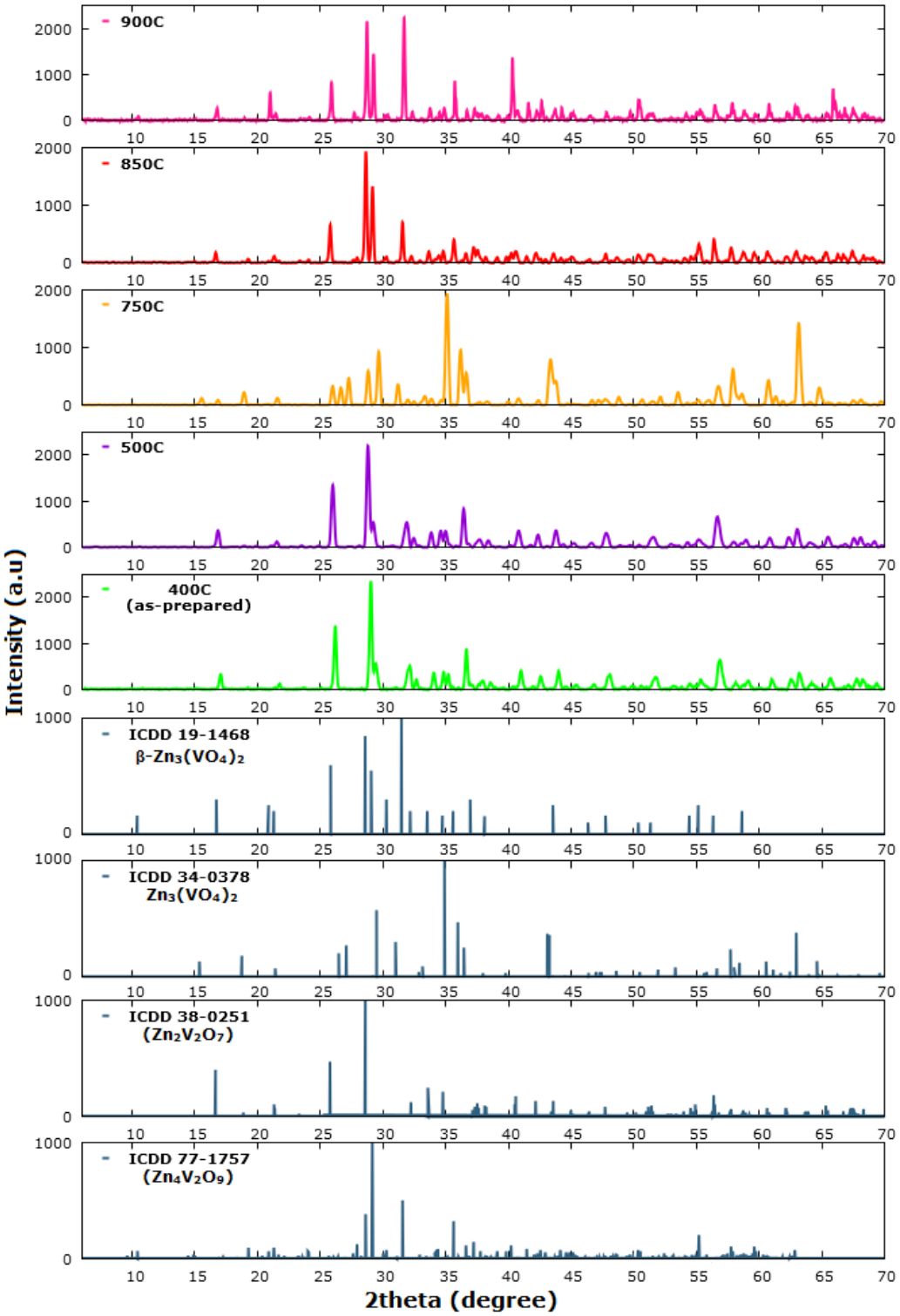

Figure 4.81. XRD patterns of $Zn_3V_2O_8$ product with urea fuel.

XRD pattern of the products synthesized by **glycine fuel** was shown in Figure 4.82. The multiphase products ($Zn_3V_2O_8$, β-$Zn_3V_2O_8$ and $Zn_2V_2O_7$) were identified at 400°C 5 minutes. $Zn_2V_2O_7$ was observed in small quantity compared to the other phases.

At 500°C and 750°C, the mixture of $Zn_3V_2O_8$ and $Zn_2V_2O_7$ were found and at higher temperature the decomposition reaction of $Zn_3V_2O_8$ into $Zn_4V_2O_9$ and $Zn_2V_2O_7$ was determined.

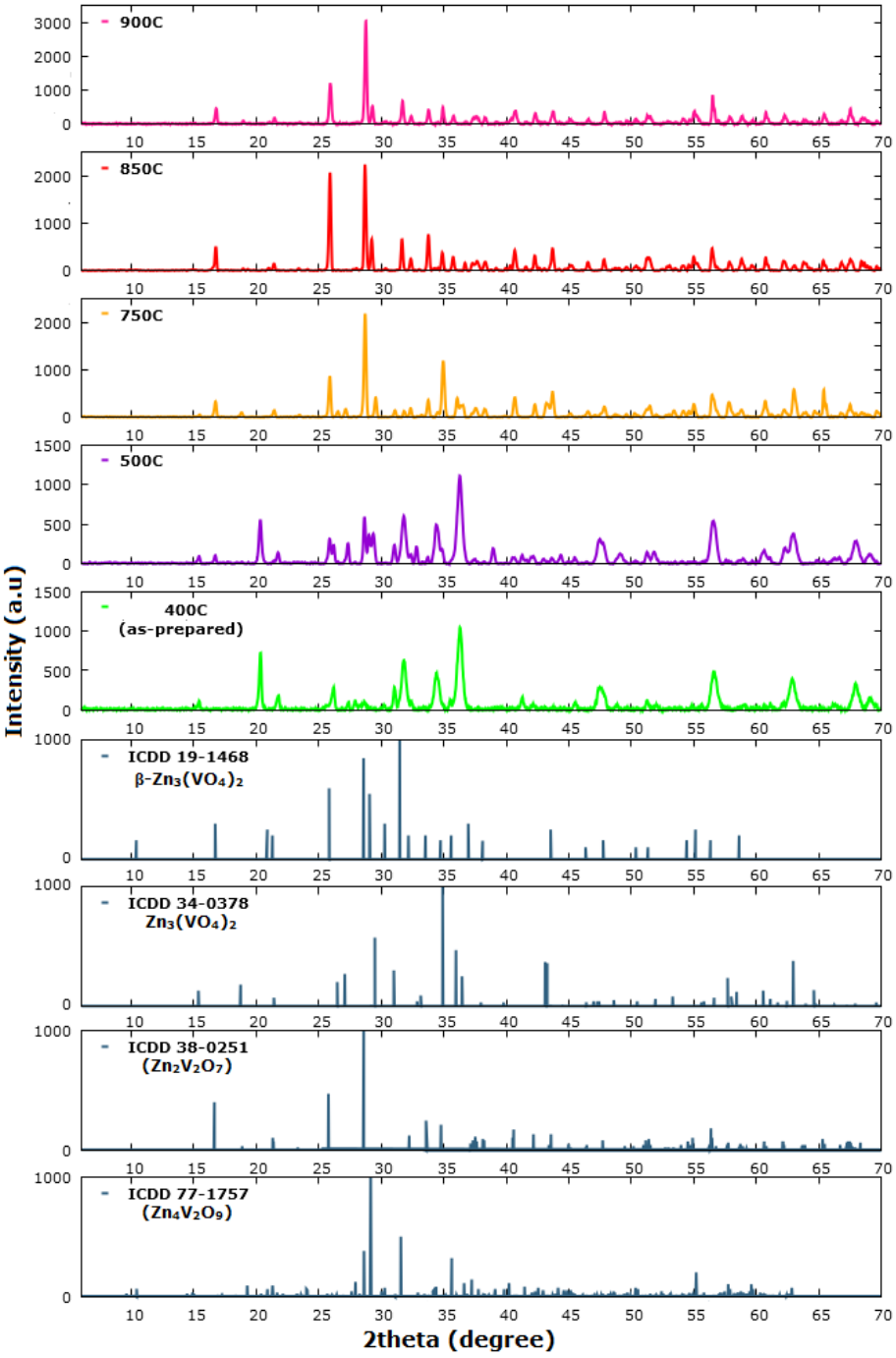

Figure 4.82. XRD patterns of $Zn_3V_2O_8$ product with glycine fuel.

The XRD patterns of **carbohydrazide and HMDA fuels** were presented in Figure 4.83 and 4.84. The same characterization was reported for all heating temperatures. At 400°C as-synthesized product and 750°C 1h, the products were monitored in multi phases of $Zn_3V_2O_8$ and $Zn_2V_2O_7$. Similar to the products obtained by urea and glycine fuels, the decomposion of $Zn_3V_2O_8$ was also occured at ≥850°C.

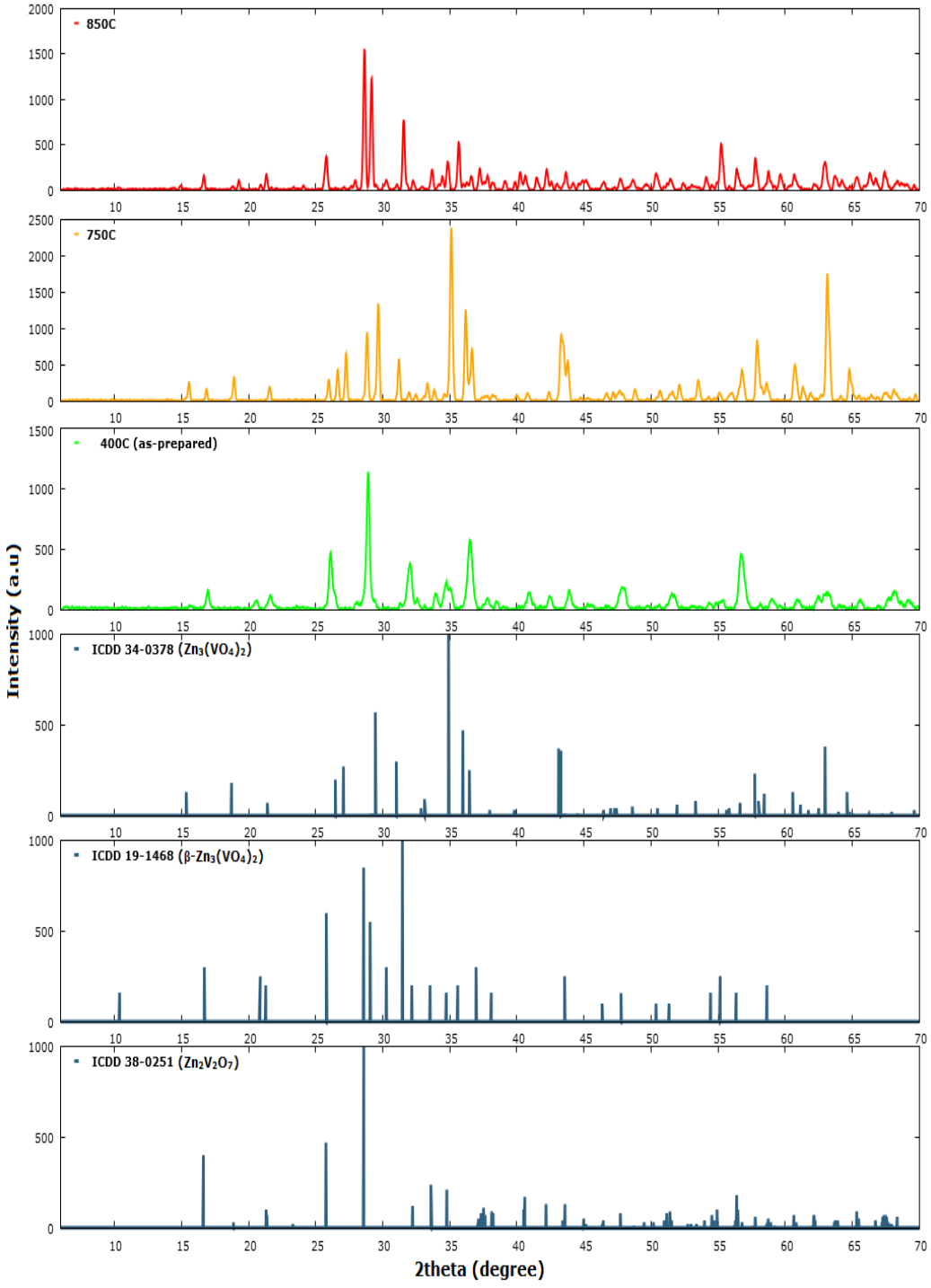

Figure 4.83. XRD patterns of $Zn_3V_2O_8$ product with carbohydrazide fuel.

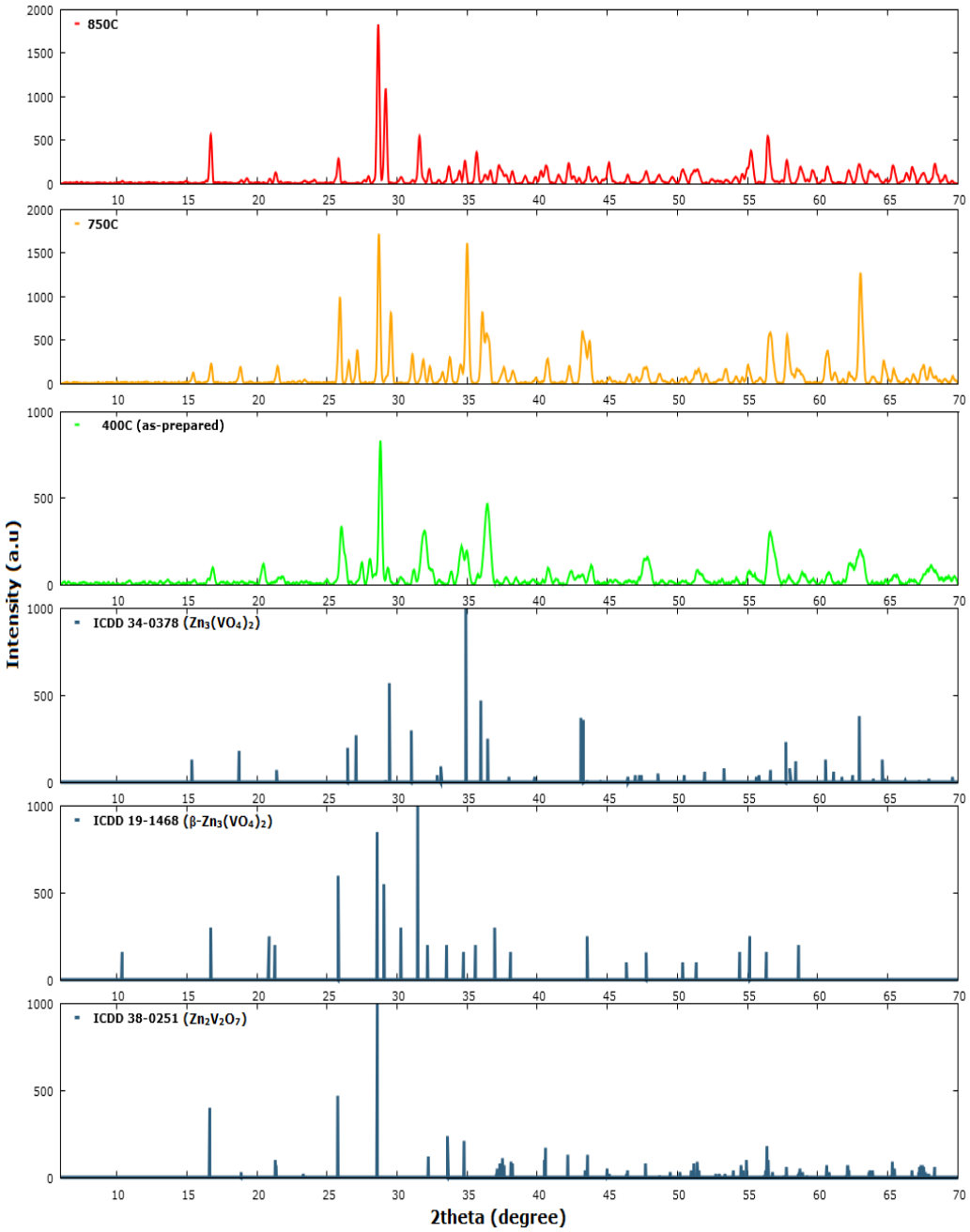

Figure 4.84. XRD patterns of $Zn_3V_2O_8$ product with HMDA fuel.

For all fuels, the synthesis of $Zn_3V_2O_8$ was fabricated at 530°C for 5 minutes as described in literature. The calcination process at 700°C were also carried out for the product acquired by **urea fuel** (Figure 4.85). The peaks that belongs to $Zn_2V_2O_7$ and $Zn_3V_2O_8$ were examined in their XRD pattern of the products as stated in literature [100].

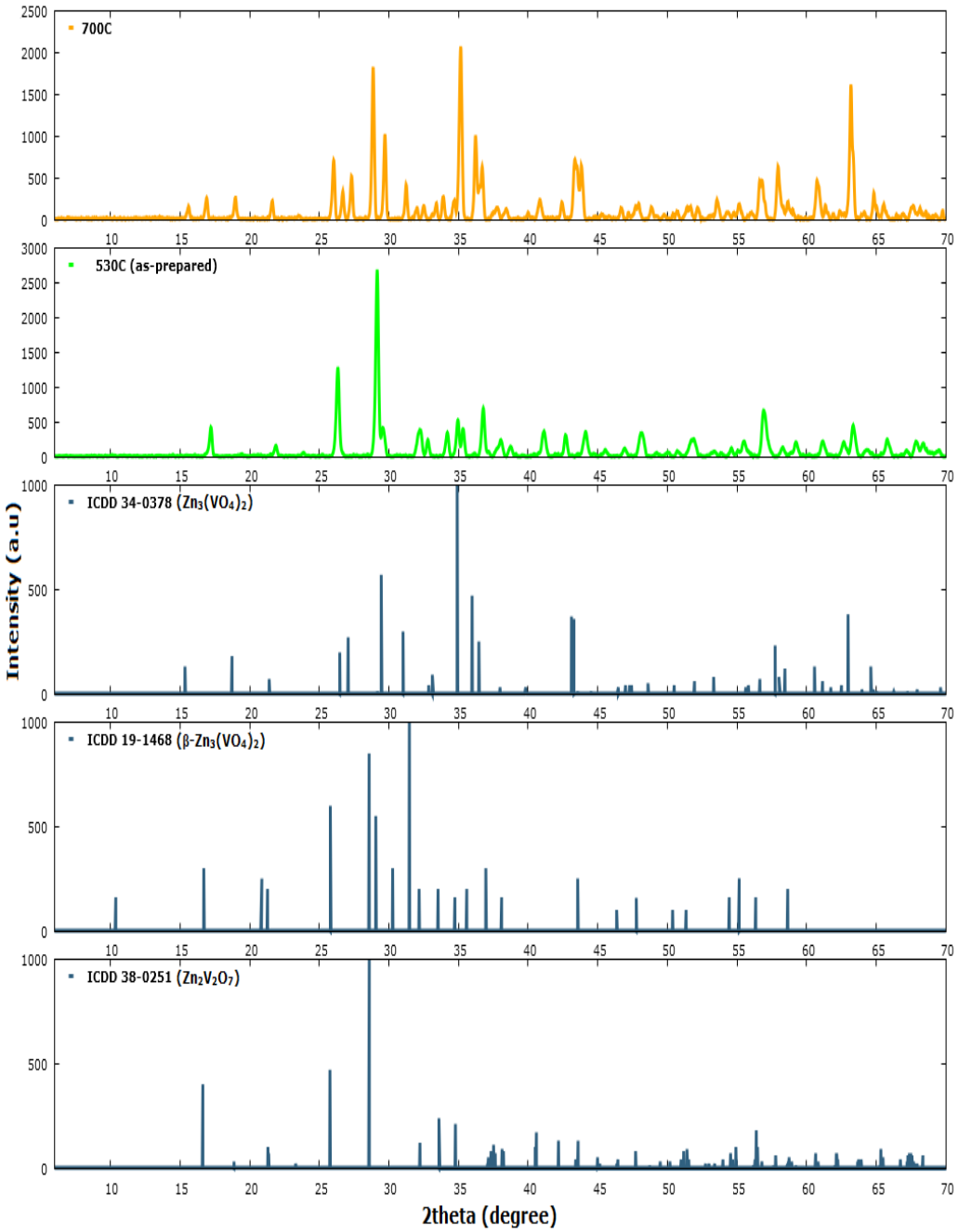

Figure 4.85. XRD patterns of $Zn_3V_2O_8$ as-synthesized and 700°C product with urea fuel.

Two different phase of $Zn_2V_2O_7$ and $Zn_3V_2O_8$ were observed in the XRD pattern of **glycine and HMDA fuels** at 530°C 5 minutes same as reported in literature. Hence, the XRD pattern of **carbohydrazide fuel** $Zn_2V_2O_7$, $Zn_3V_2O_8$, and $Zn_4V_2O_9$ mixture were detected (Figure 4.86).

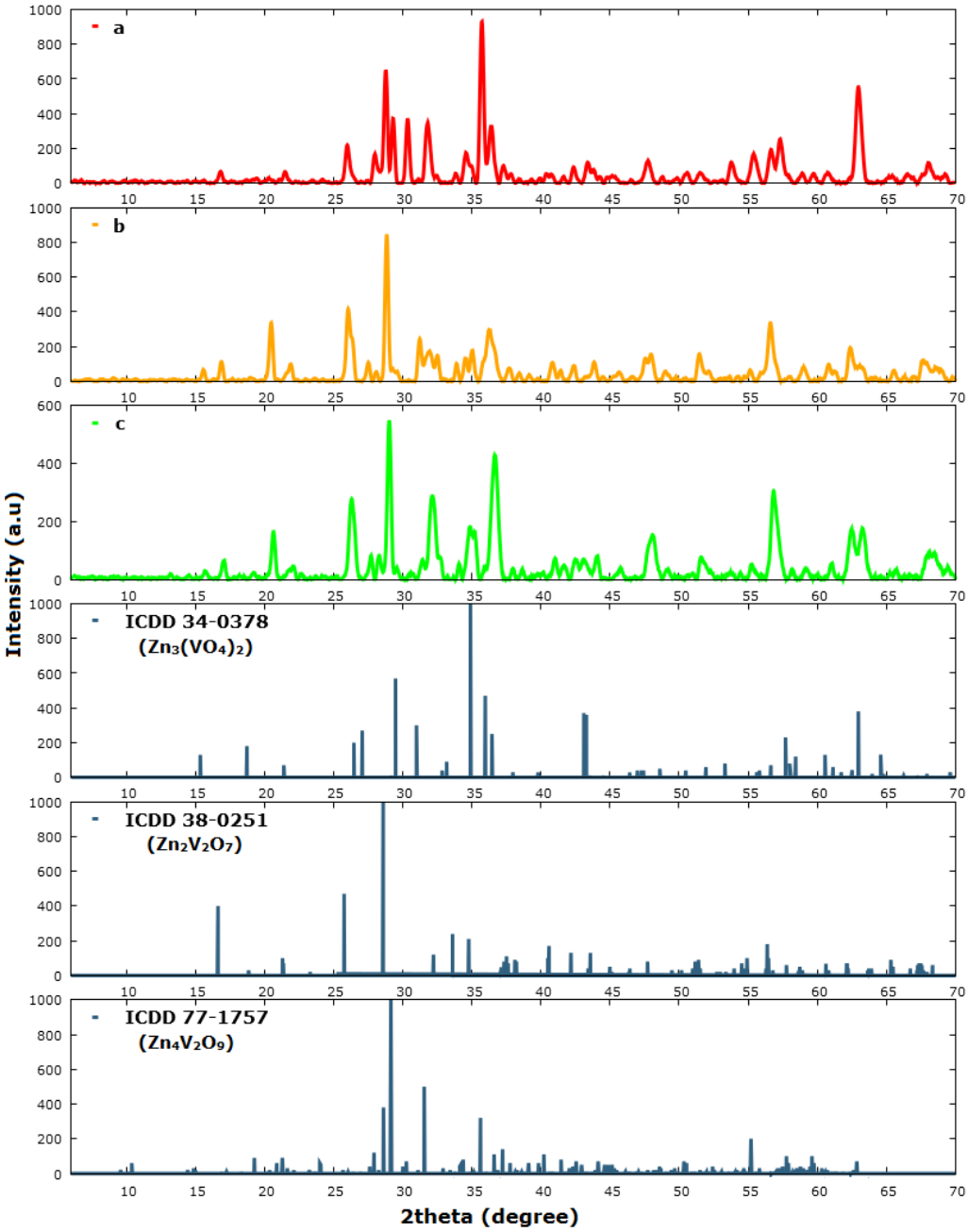

Figure 4.86. XRD patterns of $Zn_3V_2O_8$ as-synthesized product with different fuels (a=carbohydrazide, b=glycine, c=HMDA).

4.6.1.2 Infrared Spectroscopy Studies of Zinc Orthovanadate with Different Fuels (Urea, Glycine, Carbohydrazide and HMDA)

The FT-IR spectra of $Zn_3V_2O_8$ prepared with different fuels were presented in Figure 4.87 to 4.91. The characteristic band of orthovanadates were observed in all obtained products. The tetrahedral stretching vibration of VO_4 is assigned in the range of 900-420 cm^{-1}. The octahedral stretching vibration of ZnO_6 is attributed at around 418 cm^{-1}.

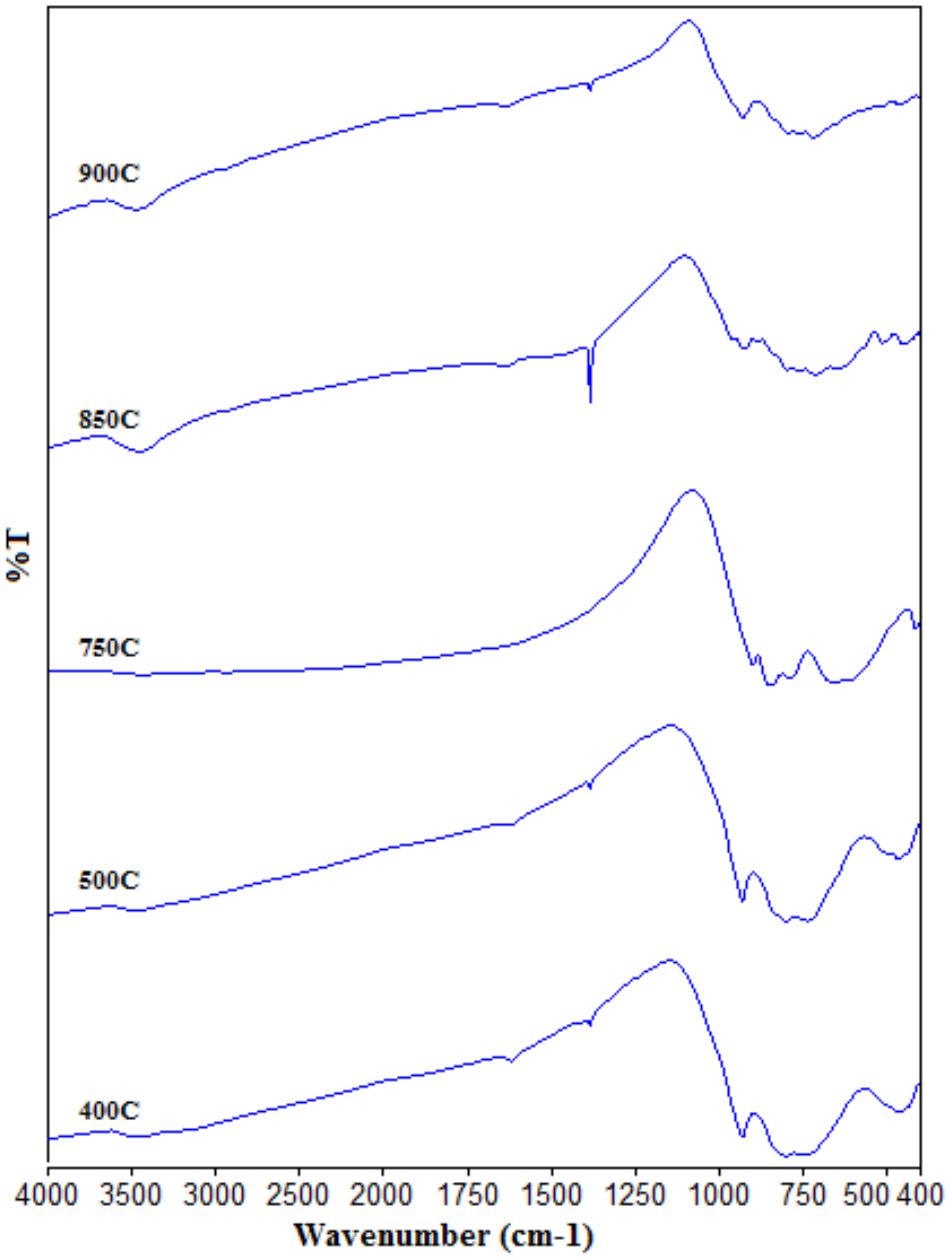

Figure 4.87. IR Spectra of $Zn_3V_2O_8$ product with urea fuel.

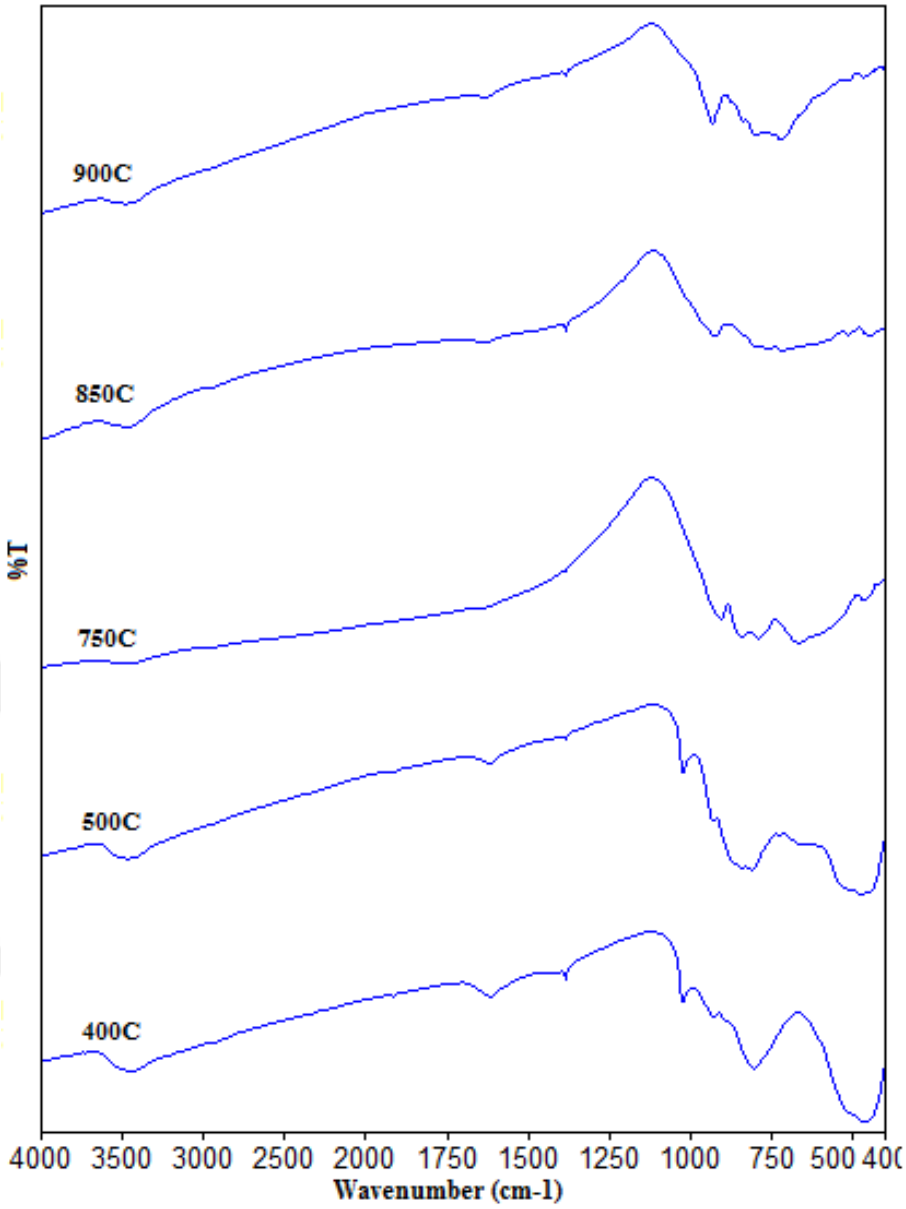

Figure 4.88. IR Spectra of $Zn_3V_2O_8$ product with glycine fuel.

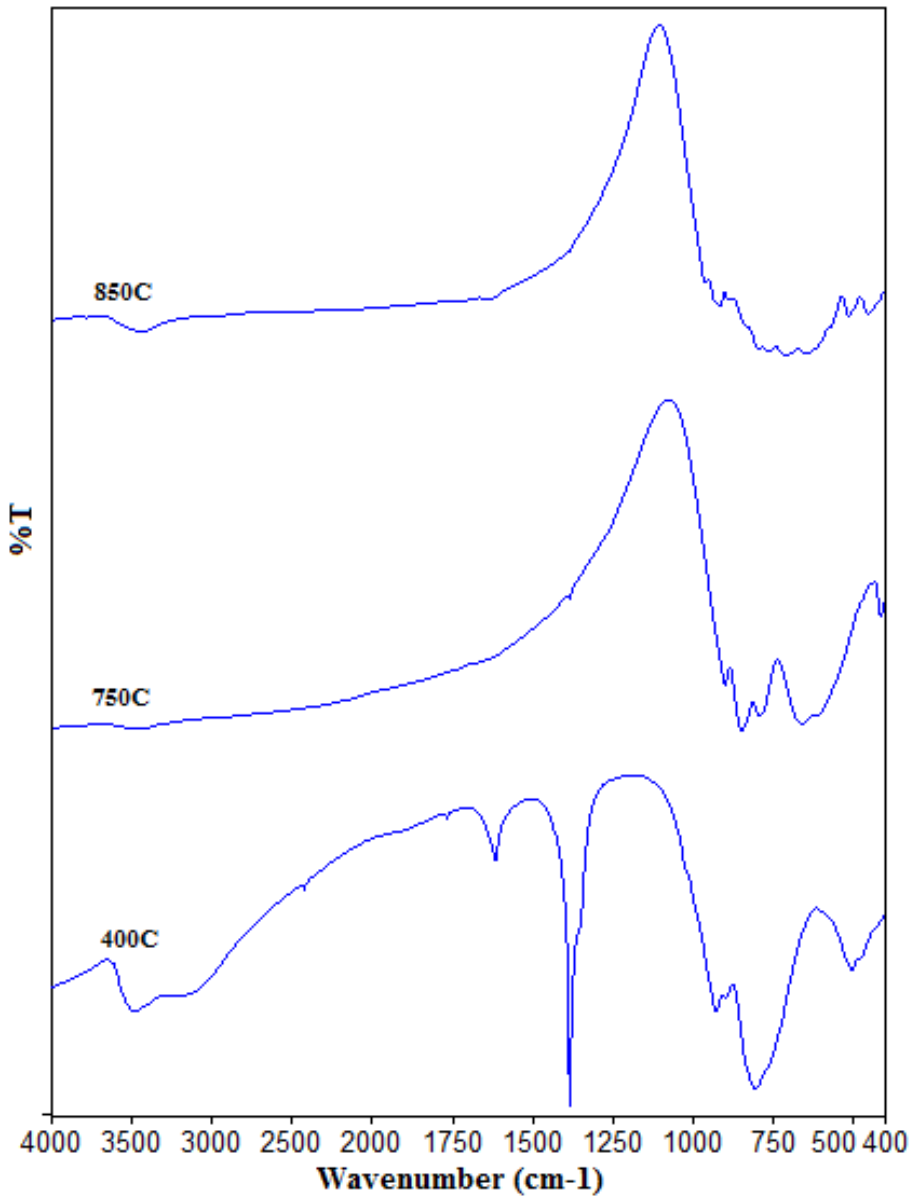

Figure 4.89. IR Spectra of $Zn_3V_2O_8$ product with carbohydrazide fuel.

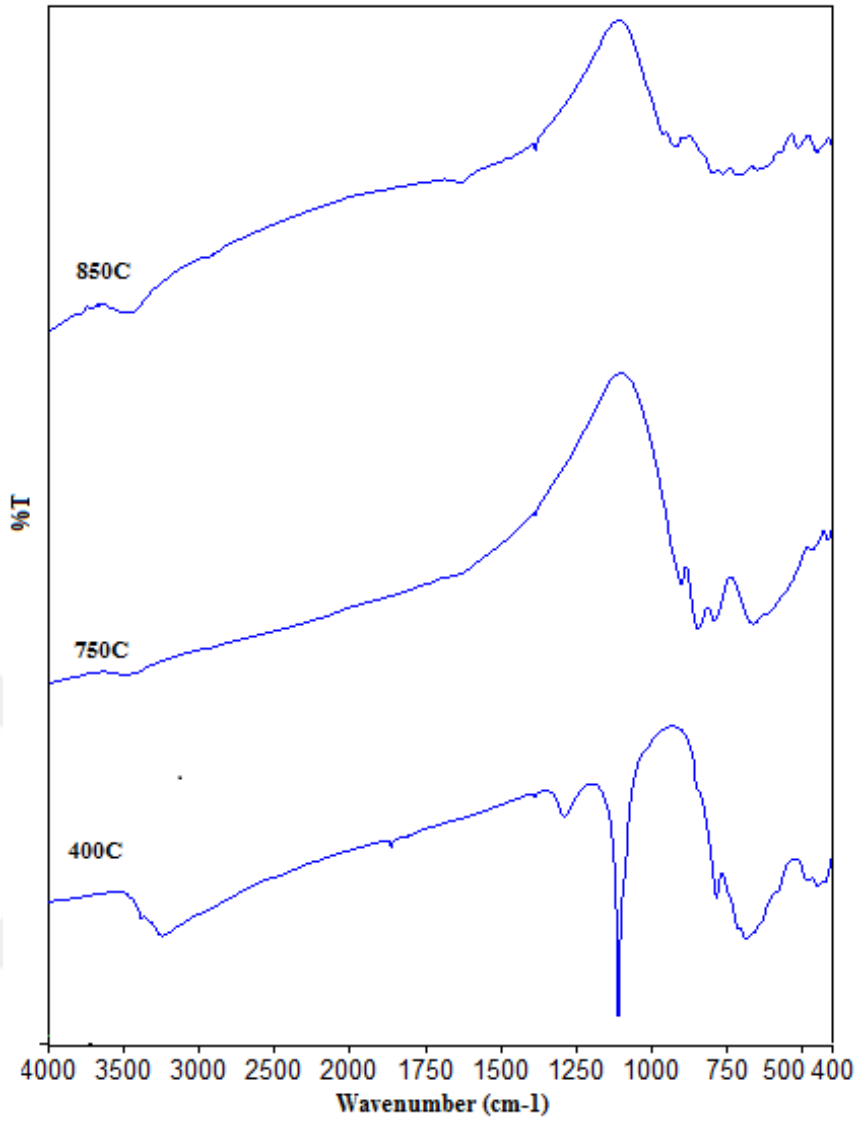

Figure 4.90. IR Spectra of $Zn_3V_2O_8$ product with HMDA fuel.

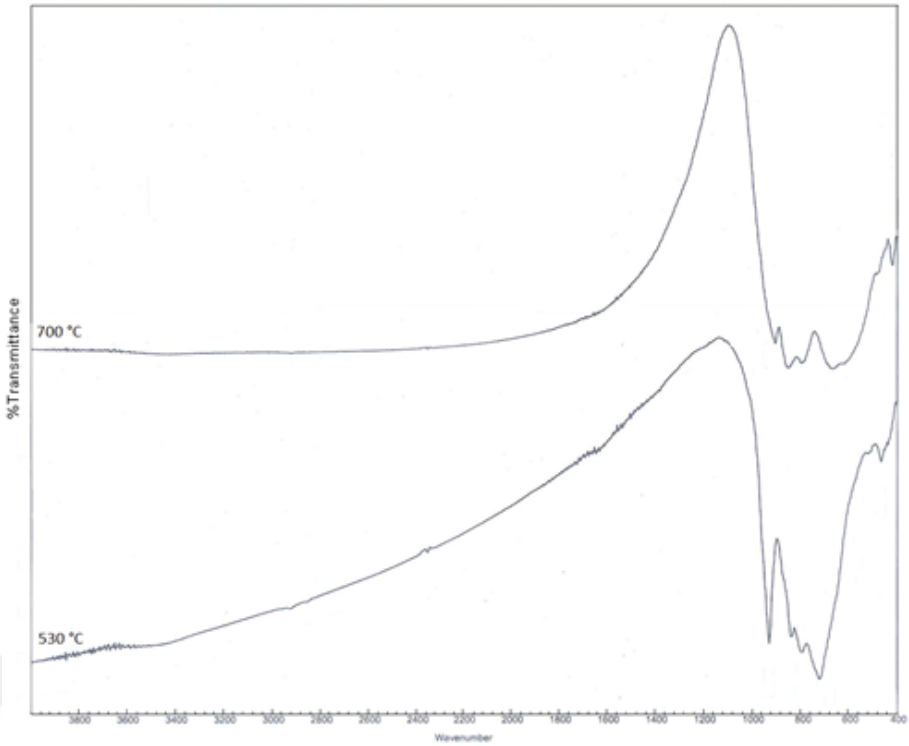

Figure 4.91. IR Spectra of $Zn_3V_2O_8$ as-synthesized and 700°C product with urea fuel.

4.6.1.3 TG/DTA Studies of Zinc Orthovanadate with Different fuels (Urea, Glycine, Carbohydrazide and HMDA)

To determine the thermal properties of $Zn_3V_2O_8$, the precursor gel of all fuels was used. The TG/DTA analysis was examined in the rate of room temperature up to 1300°C. The combustion reaction was started to take place approximately at 200°C. In DTA analysis, the decomposition of the products was identified at higher temperature, ≥850°C.

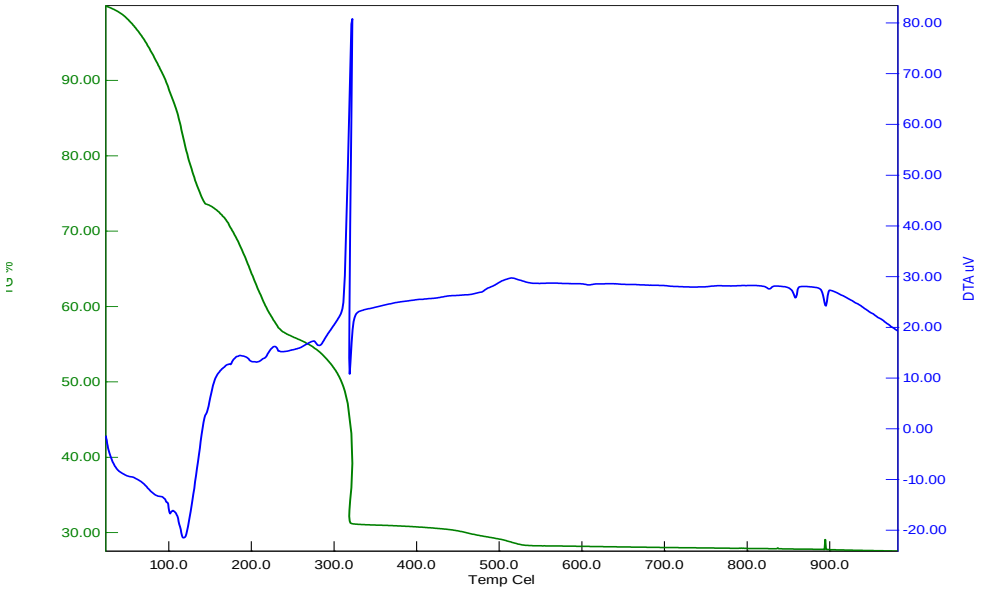

Figure 4.92. TG/DTA Curve of $Zn_3V_2O_8$ product with urea fuel.

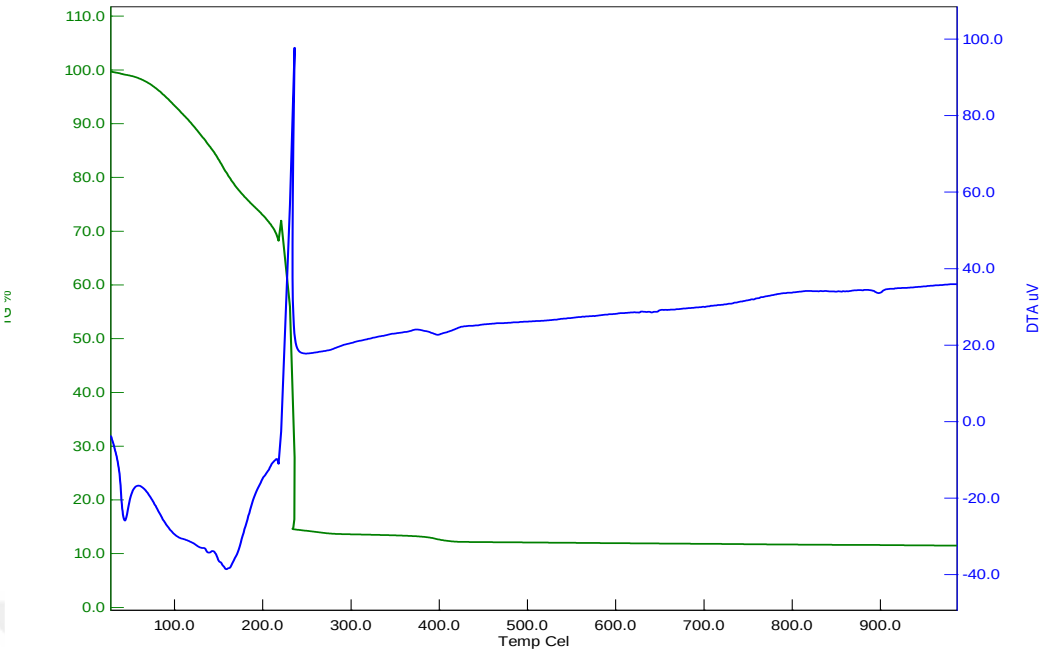

Figure 4.93. TG/DTA Curve of $Zn_3V_2O_8$ product with glycine fuel.

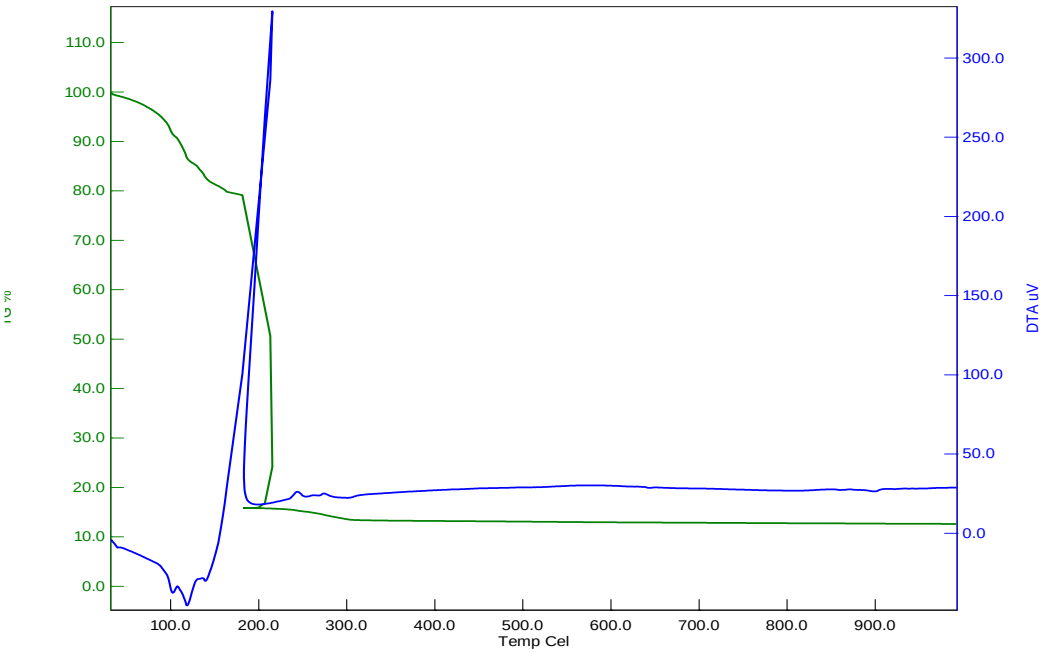

Figure 4.94. TG/DTA Curve of $Zn_3V_2O_8$ product with carbohydrazide fuel.

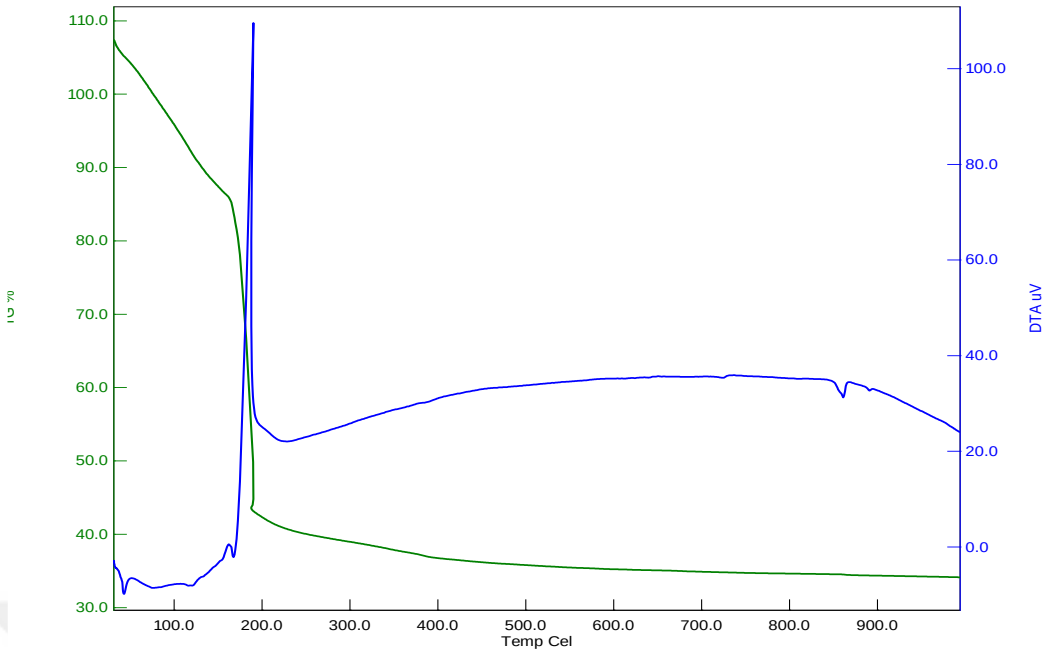

Figure 4.95. TG/DTA Curve of $Zn_3V_2O_8$ product with HMDA fuel.

4.3.9 Solution Combustion Synthesis Method for the Production of Manganese Orthovanadate with Different Fuels (Urea and Glycine)

The preparation of $Mn_3V_2O_8$ via solution combustion reaction was done by using two different fuels; glycine and urea. Stoichiometric amount of $Mn(NO_3)_2.4H_2O$ (oxidizer) and Fuels; urea and glycine (reducer), and V_2O_5 were weighed separately and dissolved in minimum volume of deionized water. The mixture evaporated under the uniform stirring until the gel-like solution was formed. The ignition process was done at 400^oC for 5 minutes and the as-prepared products were annealed at 900^oC and the characterization studies was done. The expected reactions are describe as:

With urea fuel;

$$6Mn(NO_3)_2.4H_2O + 2V_2O_5 + 10\ CON_2H_4 \rightarrow 2Mn_3V_2O_8 + 10CO_2 + 16N_2 + 44H_2O$$

With glycine fuel;

$$9Mn(NO_3)_2.4H_2O + 3V_2O_5 + 10\ C_2O_2NH_5 \rightarrow 3Mn_3V_2O_8 + 20CO_2 + 14N_2 + 61H_2O$$

The color changed of the powder products were observed from black powder into dark grey powder for urea and from dark brown into dark grey for product sythesized by glycine fuel.

4.7.1.1 X-Ray Powder Diffraction Studies of Manganese Orthovanadate with Different Fuels (Urea and Glycine)

The XRD patterns of the all obtained product were correlated with the ICDD card No: 31-0849 and 39-0091 which belongs to $Mn_3V_2O_8$. Single phase of $Mn_3V_2O_8$ could not be obtained as the peaks observe were not compatible with these ICCD data cards. For both products synthesized by **urea and glycine fuels**. The multiphase of α-$Mn_2V_2O_7$ (ICDD No: 89-0483) and β-$Mn_2V_2O_7$ (ICDD No: 89-0484) were clearly noticed at 900^oC as shown in Figure 4.96 and Figure 4.97.

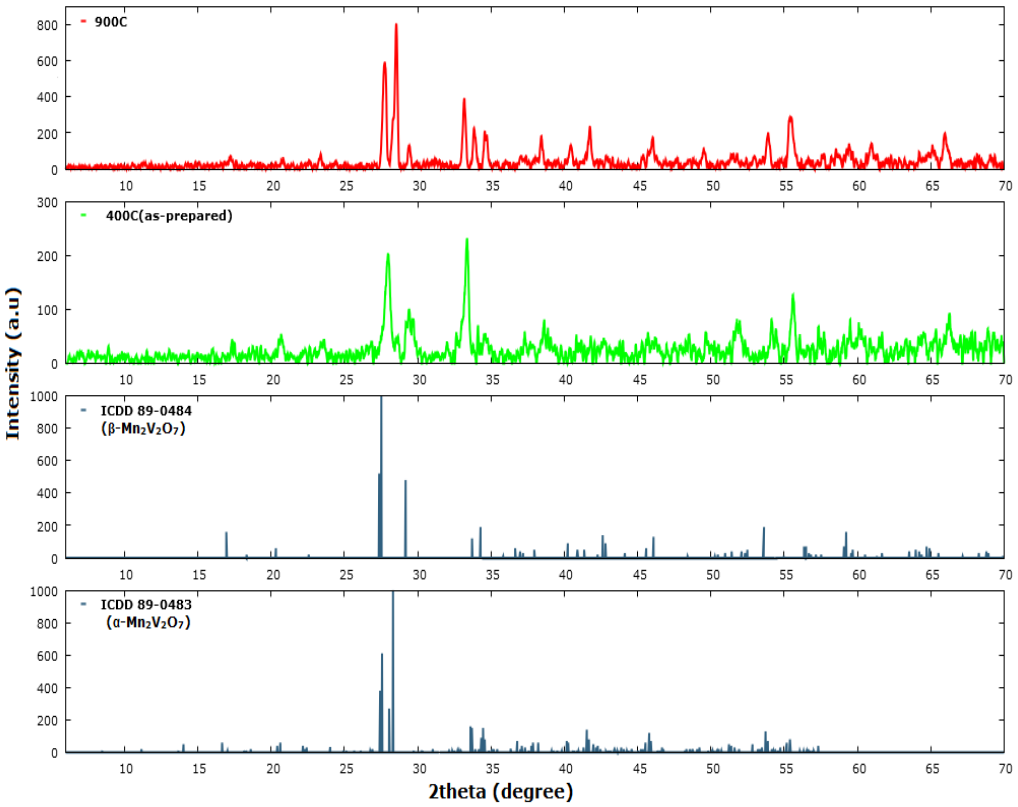

Figure 4.96. XRD patterns of $Mn_3V_2O_8$ product with urea fuel.

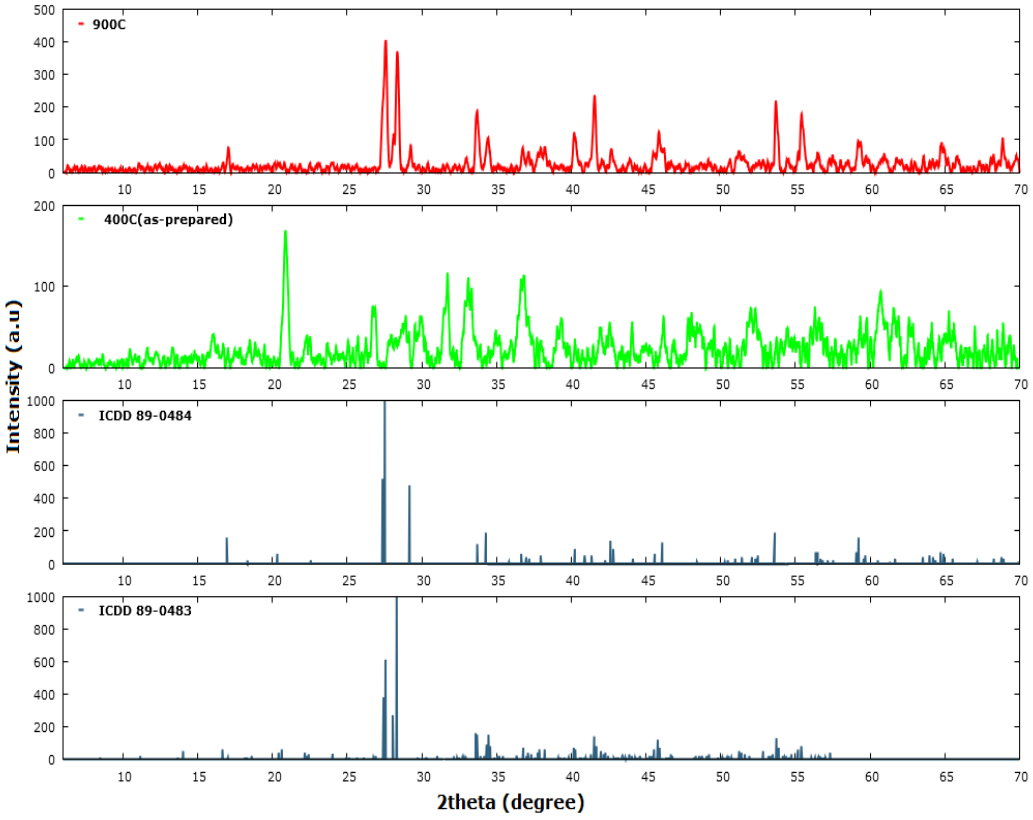

Figure 4.97. XRD patterns of $Mn_3V_2O_8$ product with glycine fuel.

4.7.1.2 Infrared Spectroscopy Studies of Manganese Orthovanadate with Different Fuels (Urea and Glycine)

The Fourier Transform Infrared (FT-IR) spectra of all products were recorded in the range of 4000-400 cm^{-1}. Since the mixture of α-$Mn_2V_2O_7$ and β-$Mn_2V_2O_7$ were obtained in both products, the band that assigned to asymmetric stretching of VO_3 at 944 cm^{-1} and symmetric stretching of V-O-V at 511 cm^{-1} were determined.

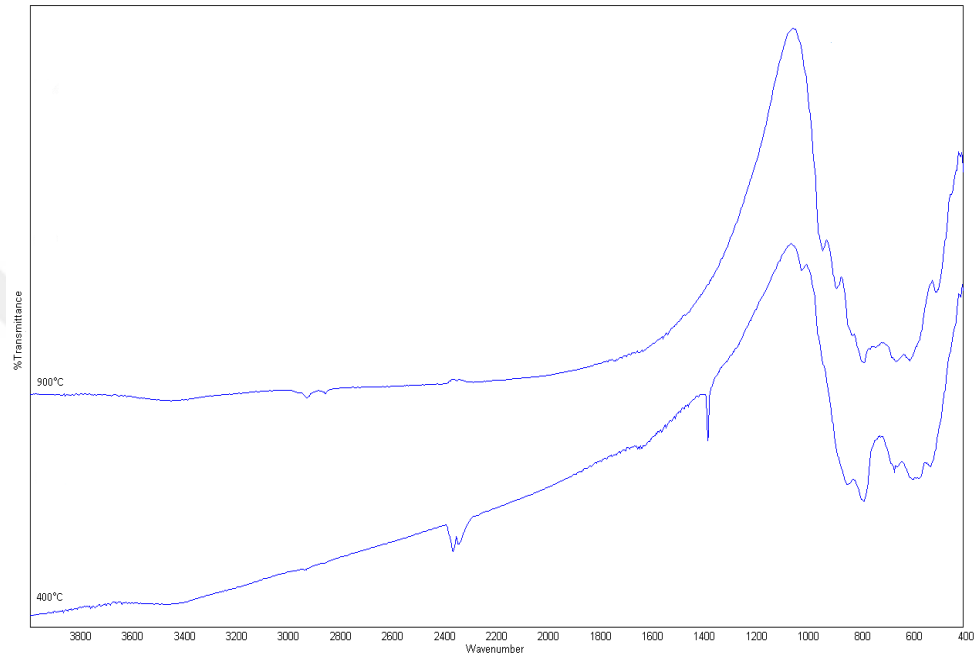

Figure 4.98. IR Spectra of $Mn_3V_2O_8$ product with urea fuel.

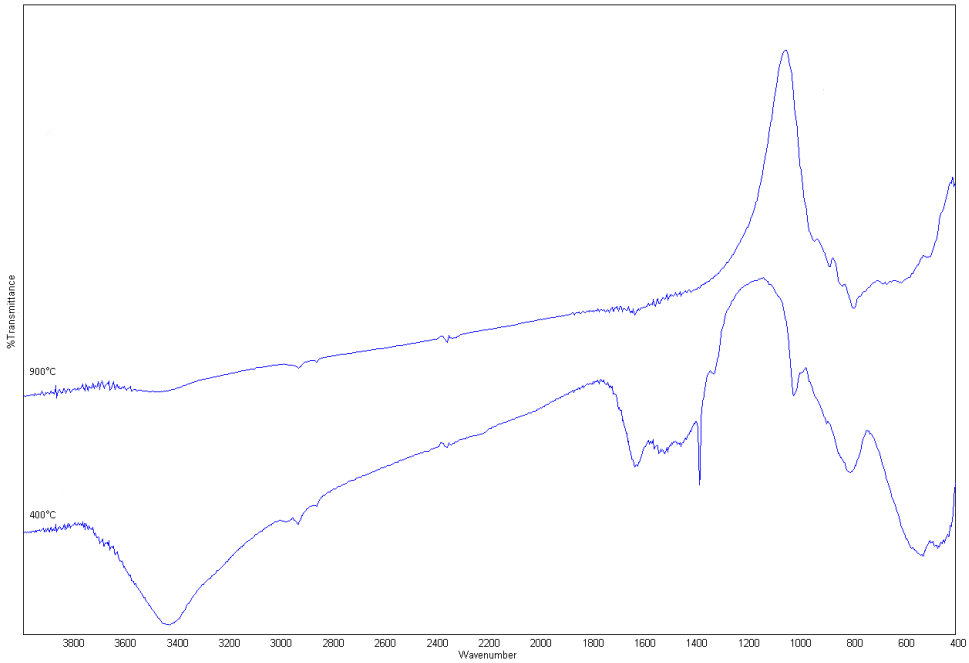

Figure 4.99. IR Spectra of $Mn_3V_2O_8$ product with glycine fuel.

4.3.10 Solution Combustion Synthesis Method for the Production of Magnesium Orthovanadate with with Different Fuels (Urea and Glycine)

Solution combustion method was applied in the synthesis of $Mg_3V_2O_8$. Stoichiometric amount of $Mg(NO_3)_2.6H_2O$, fuels (CON_2H_4, urea or $C_2O_2NH_5$, glycine) and V_2O_5 were dissolved in minimum quantity of distilled water. The homogeneous mixture was allowed to evaporate until the foamy gel was formed. Then the gel introduced to the preheated furnance at 400^oC for 5 minutes. The voluminous powder was ground and the further heating process was done at 900^oC for both products. The expected reactions are presented as:

With urea fuel;

$$6Mg(NO_3)_2.4H_2O + 2V_2O_5 + 10CON_2H_4 \rightarrow 2Mg_3V_2O_8 + 10CO_2 + 16N_2 + 56H_2O$$

With glycine fuel;

$$9Mg(NO_3)_2.4H_2O + 3V_2O_5 + 10C_2O_2NH_5 \rightarrow 3Mg_3V_2O_8 + 20CO_2 + 14N_2 + 79H_2O$$

The annealing process of product synthesized by **urea fuel** was done at 900^oC and the color changed from light yellow to white colour was seen. For **glycine fuel**, the khaki powder of as-synthesized product was turned into yellow colour after heated at 900^oC.

4.8.1.1 X-Ray Powder Diffraction Studies of Magnesium Orthovanadate with Different Fuels (Urea and Glycine)

The XRD Patterns of $Mg_3V_2O_8$ prepared with **urea fuel** was shown in Figure 4.100. Their XRD data were compared with the ICDD No: 73-0207 which belongs to orthorhombic $Mg_3(VO_4)_2$, ICDD No: 70-1163 ($Mg_2V_2O_7$) and ICDD No: 41-1426(V_2O_5). The multiphase of $Mg_3V_2O_8$, $Mg_2V_2O_7$ and V_2O_5 were detected at 400^oC. With further heating process all the peaks were found in a great agreement with the ICDD card of $Mg_3V_2O_8$ and only one small peak with very low intensity assigns to $Mg_2V_2O_7$ were detected at 2θ=28.750^o.

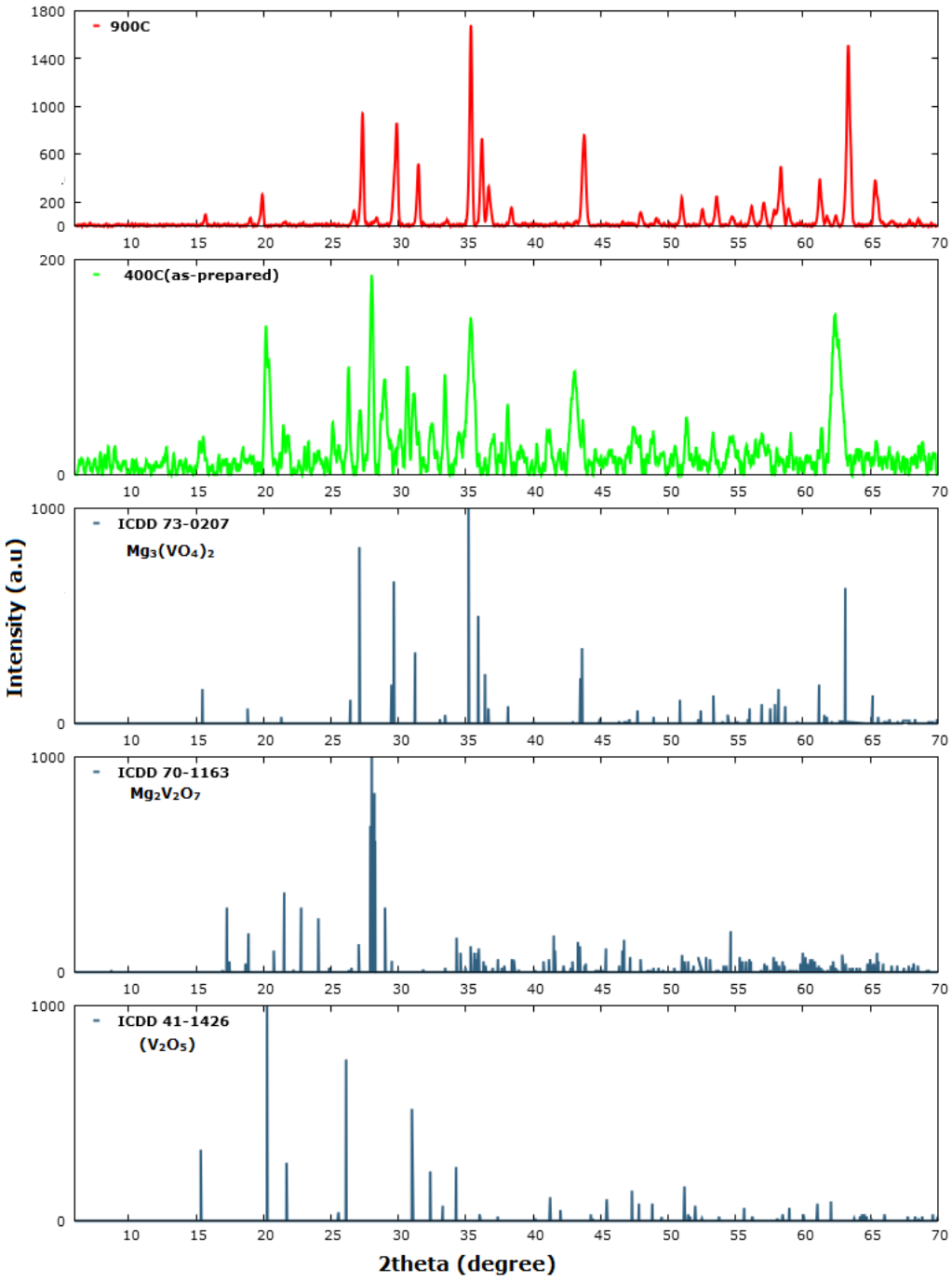

Figure 4.100. XRD patterns of $Mg_3V_2O_8$ product with urea fuel.

Figure 4.101 represent the XRD patterns of all product obtained by using **glycine fuel**. Due to the presence of V_2O_5 peaks, it can be reported that the combustion reaction was not completed at 400°C 5 minutes (ICDD No:41-1426). At 900°C, the peaks that assigned to triclinic $Mg_2V_2O_7$ were dominated and were compatible with ICCD No: 70-1163.

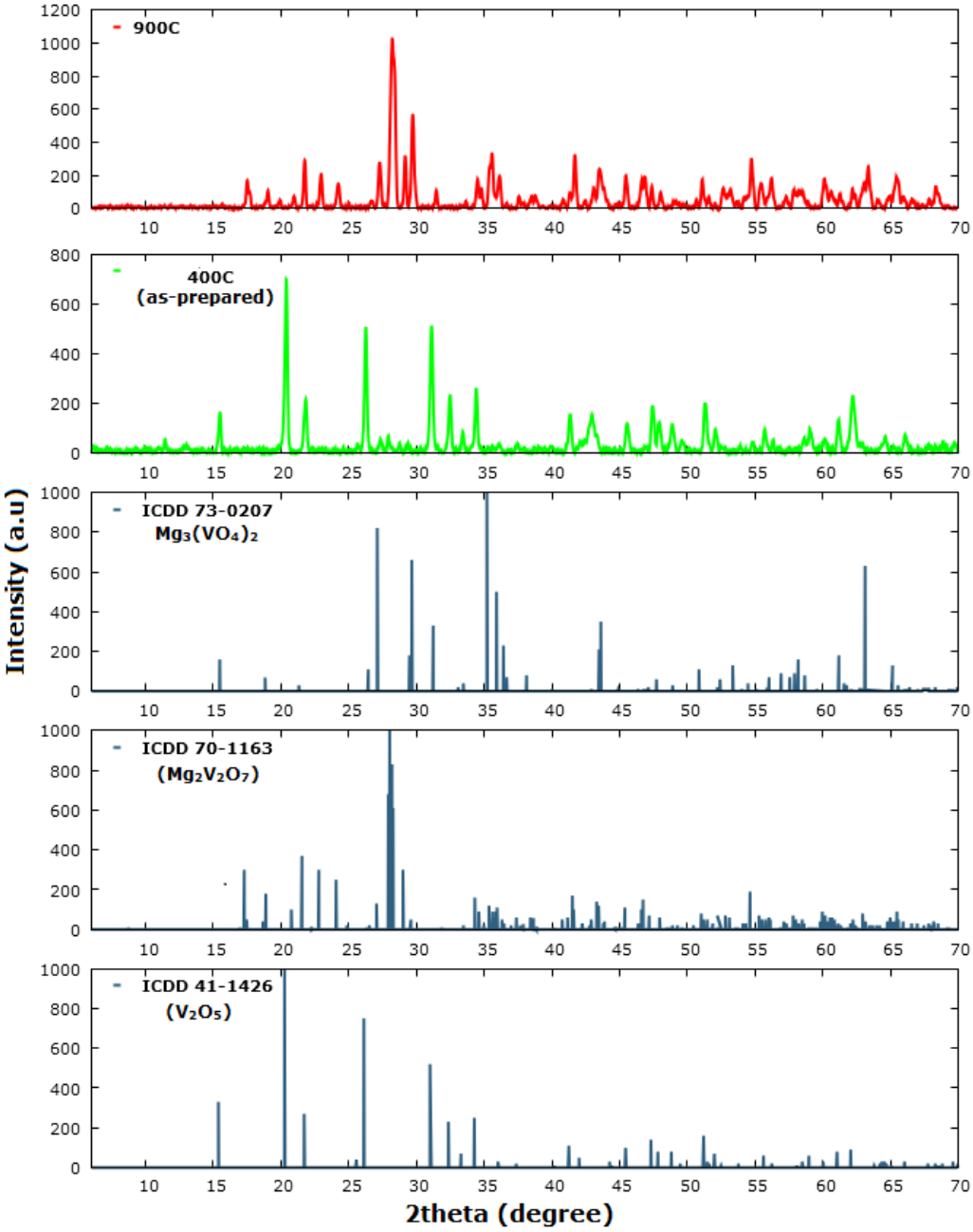

Figure 4.101. XRD patterns of $Mg_3V_2O_8$ product with glycine fuel.

4.8.1.2 Infrared Spectroscopy Studies of Magnesium Orthovanadate with Different Fuels (Urea and Glycine)

The FT-IR Spectra of magnesium orthovanadate synthesized with urea and glycine fuels were examined between 4000-400cm^{-1}. In the FT-IR spectra of product synthesized by **urea fuel**, the bands that associated to the vibration of tetrahedral stretching and the octahedral stretching of Mg-O were observed at 614 $cm^{-1}$and 450cm^{-1}, respectively (Figure 4.102).

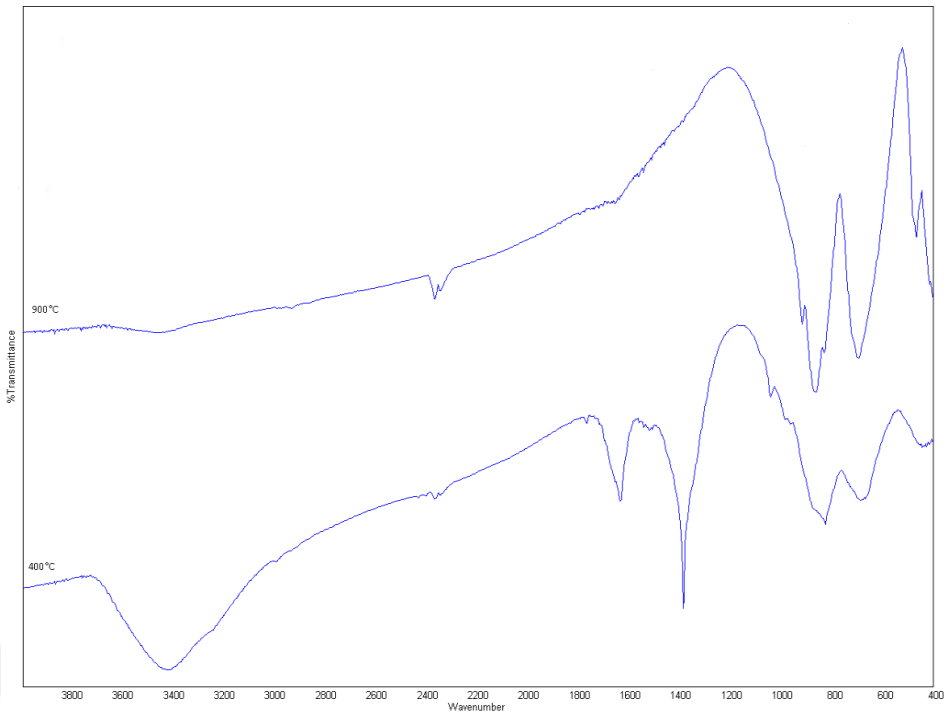

Figure 4.102. IR Spectra of $Mg_3V_2O_8$ product with urea fuel.

Supporting the XRD data of the products obtained with **glycine** fuels, the band that identified the asymmetric stretching of VO_3 at 916 cm^{-1} and symmetric stretching of VO_3 at 860 cm^{-1} were detected. Furthermore, at 700 cm^{-1} and 527 cm^{-1} the asymmetric and symmetric stretching of V-O-V were observed, respectively. Mg-O stretching vibration was also determined at 470 cm^{-1}(Figure 4.103).

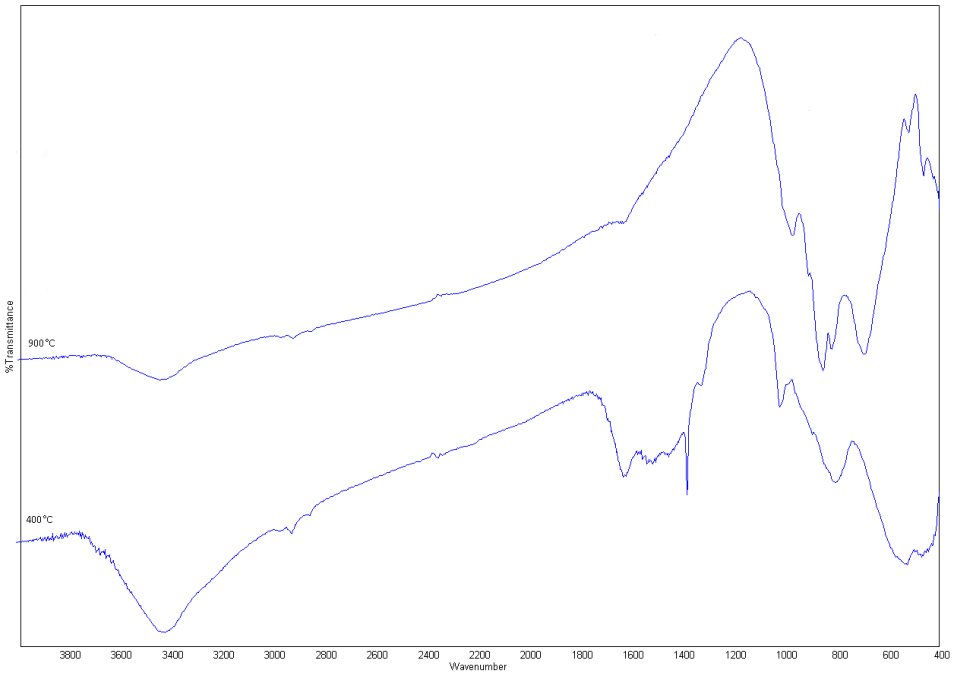

Figure 4.103. IR Spectra of $Mg_3V_2O_8$ product with glycine fuel.

5. DISCUSSION

The first part of this study presented the correlation between the synthesis of monazite and xenotime structure of borophosphate compounds, $LnB(PO_4)_2$ (Ln: Nd, Ce, Pr, Sm, Eu, Yb, Tb, Ho, Tm, Lu) with solid-state method. To determine the presence of boron compound in our products, different amounts of boric acid (0%, 25% 50%) were used in the preparation of monazite-$NdB(PO_4)_2$ and xenotime $YbB(PO_4)_2$. Since the evaporation of boron compound was not identified in all amount of boric acid, BPO_4 was formed at 1000^oC. For this reason, all the others rare earth borophophates compound were synthesized with non-excess of boric acid. The results indicate that at lower temperature in the range of 600-1000^oC the unreacted Ln_2O_3, $LnPO_4$ and $Ln(PO_3)_3$ were detected. For all synthesized $LnB(PO_4)_2$, the XRD patterns obtained at 1100^oC contributed the clearer understanding on formation of two different structures of lanthanide borophosphate as all the diffraction lines have a great aggreament to $LnPO_4$ (Ln: Nd, Ce, Pr, Sm, Eu, Yb, Tb, Ho, Tm, Lu). The borophosphate that synthesized with Ln =Nd, Ce, Pr, Sm and Eu were determined as monazite type structure whereas the synthesized with Ln=Yb, Tb, Ho, Tm and Lu known to be cystallized in xenotime type structure.

In the second part of this study, pyro ($M_2V_2O_7$, M=Cu, Ni, Co, Zn and Mn) and orthovanadates ($M_3V_2O_8$, M=Cu, Ni, Co, Zn, Mn and Mg) were fabricated via solution combustion synthesis method (SCS). In our study, this method was preferred in the preparation of vanadates compound because of its excellent energy and time effectiveness. As it is known that vanadate compounds have a low crystallinity which need a longer reaction time in their synthesis process. The pyro ($M_2V_2O_7$) and orthovanadates ($M_3V_2O_8$) with different metals and fuels were synthesized with this method. The metal nitrates were used as oxidizer and fuels (urea, glycine, carbohydrazide, HMTA and HMDA) was used as reducer. The synthesis of metal pyro and orthovanadates were carried out in shorter time compared to the other previous studies.

$M_2V_2O_7$ (M=Cu, Ni, Co, Zn and Mn) were synthesized and different polymorphs of $Cu_2V_2O_7$, $Zn_2V_2O_7$ and $Mn_2V_2O_7$ were discovered in this study.

$Cu_2V_2O_7$ were prepared by using urea and glycine. The results showed that, urea fuel was considered as the best fuel in the synthesis process of $Cu_2V_2O_7$ as two α-β phase transition were clearly seen. The formation of low temperature, α-

$Cu_2V_2O_7$ (blossite) was occurred at 670°C and its high temperature form, β-$Cu_2V_2O_7$ (ziesite) was observed at 800°C. The XRD data showed that single phase α-$Cu_2V_2O_7$ and β-$Cu_2V_2O_7$ crystallized in orthorhombic and monoclinic structure, respectively. By using glycine as fuel, pure β-$Cu_2V_2O_7$ was obtained at 800°C. Thus, multiphase of α-β-$Cu_2V_2O_7$ were detected at temperature below 600°C for products with urea and glycine fuels.

$Zn_2V_2O_7$ is known to has two crystallographic structure. The preparation of the compound was done by using urea fuel. Based on the result, the mixture of $Zn_2V_2O_7$ and $Zn_4V_2O_9$ were observed in as-prepared product obtained at 400°C and the formation of clear monoclinic α-$Zn_2V_2O_7$ were expected at 650°C. The further heating 900°C was also done to discover beta phase of $Zn_2V_2O_7$ and there is no distict changed on the diffraction line of the products were detected. All the data given in our result were compatiple with the ICDD No:70-1532 which belongs to monoclinic α-$Zn_2V_2O_7$.

α and β polymophs of $Mn_2V_2O_7$ were also observed in this study. Urea was applied as fuel in the synthesis. The results implied that at both phase of $Mn_2V_2O_7$ were found at lower temperature in the range of 400-650°C. by further annealing process at 900°C and 950°C, the d-line that belongs to β-$Mn_2V_2O_7$ was started to detect. The monoclinic β-$Mn_2V_2O_7$ (ICDD No: 89-0484) was successfully obtained at 1000°C.

The synthesis of $Co_2V_2O_7$ was also done by using urea fuel. The diffraction line observed in our results (600°C) were similar with the ICDD No: 70-1189 assigns to $Co_2V_2O_7$. Only one additional peak belongs to $Co_3V_2O_8$ were observed.

Due to low intensity and crystallinity of the product examined in the XRD results, the further heating was done. It found that the $Co_3V_2O_8$ lines were dominated at higher temperature, at 900°C. Based on the findings of single phase metal pyrovanadates with other metals, different annealing temperature and fuels might be attempted to acquire a pure $Co_2V_2O_7$.

The same fuel was also used in the fabrication of $Ni_2V_2O_7$. Reported in the results, the single phase $Ni_2V_2O_7$ could not obtained and the mixture with $Ni_3V_2O_8$ was examined at 600°C and 900°C. The usage of other fuels such as glycine or carbohydrazide etc. might be tried to obtain single phase $Ni_2V_2O_7$.

The Synthesis of various metal orthovanadates, $M_3V_2O_8$ (M= Cu, Ni, Co, Zn, Mn and Mg) was performed by solution combustion method. Two different

starting reagents, V_2O_5 and NH_3VO_3 were applied in the synthesis of $Ni_3V_2O_8$ and $Cu_3V_2O_8$.

For $Cu_3V_2O_8$ synthesized with urea and V_2O_5, the results specied that multiphase of $Cu_3V_2O_8$ and α-β-$Cu_2V_2O_7$ were detected at low temperatures. The formation of $Cu_3V_2O_8$ were discovered at 750^{o}C as the peaks of $Cu_3V_2O_8$ is dominated and has great accordance to ICDD No: 49-0689. Instead of single phase $Cu_3V_2O_8$, β-$Cu_2V_2O_7$ was determined at 850^{o}C. The analysis showed that the transformation of $Cu_3V_2O_8$ into β-$Cu_2V_2O_7$ was take placed at higher temperature. The preparation of $Cu_3V_2O_8$ using different starting reagent, NH_4VO_3 was also attempted. Rather than the formation of $Cu_3V_2O_8$, α-β $Cu_2V_2O_7$ were shown. Other fuel (glycine) was also applied to get the single-phase product with V_2O_5 but further characterization studies could not be done as the adhesion was observed.

The synthesis of $Ni_3V_2O_8$ with V_2O_5 was also done using various fuels (urea, glycine and HMTA). Among these fuels, better results were obtained with glycine. All the peaks detected at 900^{o}C verified the formation of orthorhombic $Ni_3V_2O_8$ (ICDD No: 74-1484). On the other hand, due to inseparable peak observed at around 2θ=44^o the formation of single phase $Ni_3V_2O_8$ with HN_4VO_3 was not entirely compatible with ICDD card. In the results of products synthesized with other fuels (urea with V_2O_5 and NH_4VO_3; HMTA with V_2O_5) two additional lines of $Ni_2V_2O_7$ were examined.

Three different fuels (urea, glycine and HMTA) were applied in the synthesis of $Co_3V_2O_8$ and better results were obtained by using glycine fuels. Compared to ICDD No: 70-1393, one characteristic line of $Co_3V_2O_8$ were not detected in the products obtained with urea and HMTA fuel.

In the preparation of $Zn_3V_2O_8$, four different fuels (urea, glycine, carbohydrazide and HMDA) were used. The results indicate that multiphase of $Zn_3V_2O_8$ and $Zn_2V_2O_7$ were identified at temperature up to 750^{o}C. At temperature higher than ≥850^{o}C, decomposition of $Zn_3V_2O_5$ to $Zn_2V_2O_7$ and $Zn_4V_2O_9$ were expected.

$Mn_3V_2O_8$ was also fabricated with urea and glycine fuels. Two phases of α-β-$Mn_2V_2O_7$ were found in the products of both fuels. The reflections of $Mn_3V_2O_8$ were not shown in the XRD patterns of our study. Further heating should be considered.

Urea and glycine were used in the formation of $Mg_3V_2O_8$ by solution combustion method. Rather than glycine, urea fuel gave better result as almost all d-line are compatible with ICDD No: 73-0207 except for one weak peak belongs to $Mg_2V_2O_7$ (ICDD No: 70-1163). For the glycine, the triclinic $Mg_2V_2O_7$ was defined at all heating temperatures.

6. CONCLUSIONS AND RECOMMENDATIONS

In the first part of this thesis, the lanthanide borophosphates, $LnB(PO_4)_2$ (Ln: Nd, Ce, Pr, Sm, Eu, Yb, Tb, Ho, Tm, Lu) were successfully synthesized by solid state reaction technique. The annealing process was done in the range of 600-1200^oC. Characterization of the products by XRD studies showed that LnB(PO4) was formed in monazite (Ln= Nd, Ce, Pr, Sm, Eu) and xenotime (Ln=Yb, Tb, Ho, Tm, Lu) crystal structures at temperatures above 1100 °C.From these compounds, $YbB(PO_4)_2$, $HoB(PO_4)_2$ and $LuB(PO_4)_2$ were indexed in tetragonal crystal system, space groups: $I4_1/amd$. Their refined unit cell parameters were calculated as a=6.820(3) c=5.975(2), V=277.945 for $YbB(PO_4)_2$, a=6.891(5) c=6.031(7), V=286.46 for $HoB(PO_4)_2$ and a= 6.798(9) c= 5.962(6) V= 275.62 for $LuB(PO_4)_2$, respectively. In addition, when the infrared spectra of the obtained borphosphate materials were examined, characteristic B-O and P-O vibrational bands of borophosphates were observed as symmetrical, asymmetrical stretching bands and bending frequencies.

In the second part of this study, the pyrovanadates ($M_2V_2O_7$, M=Cu, Ni, Co, Zn and Mn) were prepared by simple and time-efficiency solution combustion synthesis, SCS method. The products prepared by this synthesis process were characterized by XRD, FTIR and TG/DTA analysis. For $Cu_2V_2O_7$, urea and glycine were used as fuels, the better result was obtained by urea. The phase transition between orthorhombic α-$Cu_2V_2O_7$ (blossite) and monoclinic β-$Cu_2V_2O_7$ (ziesite) were observed. β-$Cu_2V_2O_7$ was found at higher temperature by glycine fuel. The other metal pyrovanadates were synthesized by using urea fuel. Monoclinic α-$Zn_2V_2O_7$ was acquired at 650^oC. Monoclinic β-$Mn_2V_2O_7$ was produced at 1000^oC. By Investigating of the XRD data of $Co_2V_2O_7$ the d-lines of $Co_2V_2O_7$ were mainly observed except only one small peak belongs to $Co_3V_2O_8$ During the preparation of $Ni_2V_2O_7$, as a result of structural analysis studies, it was determined that a binary phase containing a mixture of $Ni_2V_2O_7$and $Ni_3V_2O_7$ was formed.

In the last part of this work, the orthovanadates ($M_3V_2O_8$, M= Cu, Ni, Co, Zn and Mn) were fabricated by solution combustion synthesis method using various fuels (urea, glycine, carbohydrazide, HMTA and HMDA). Specifically, two different reagents (V_2O_5 and NH_4VO_3) were applied in the production of $Cu_3V_2O_8$

and $Ni_3V_2O_8$. All the products obtained in this study were also characterized by XRD, FT-IR and TG/DTA analysis.

In the comparison of all synthesized orthovanadate materials, $Ni_3V_2O_8$ and $Co_3V_2O_8$ compounds in which were prepared with glycine and V_2O_5 were identified as a single phase and crystallized in orthorhombic structures. Moreover, different fuels were also applied but single phase of these orthovanadates were not obtained. For $Ni_3V_2O_8$, two additional lines of $Ni_2V_2O_7$ were examined in the products synthesized with other fuels (urea with V_2O_5 and NH_4VO_3; HMTA with V_2O_5). In the synthesis of $Co_3V_2O_8$ with urea and HMTA one characteristic peak was missing according to the related ICDD card.

In the preparation of $Mg_3V_2O_8$, by the examining the structural data, urea was found to be better fuel than glycine. The XRD pattern showed all the peaks were compatible with the $Mg_3V_2O_8$ other than one minor peak of $Mg_2V_2O_7$. However, at all annealing temperature, d-lines belong to triclinic $Mg_2V_2O_7$ were observed during the synthesis process of $Mg_3V_2O_8$ by glycine fuel. In the fabrication of $Cu_3V_2O_8$ and $Zn_3V_2O_8$, the multiphase of products were observed and pyrovanadates of the related metal were identified. Single phase $Mn_3V_2O_8$ was also could not acquired. Rather than the desired $Mn_3V_2O_8$ product, the two polymorphs of $Mn_2V_2O_7$ as α and β were identified.

It has been also determined that the vibrational bands of the V-O bonds observed in the IR spectra of the products obtained during all processes performed by the solution combustion method of ortho and pirovanadate materials confirm the XRD data on whether the product is an ortho or pyrovanadate compound.

7. REFERENCES

Vancouver citation system was used in this thesis.

1. Kniep R, Gözel G, Eisenmann B, Röhr C, Asbrand M and Kizilyalli M, et al. Borophosphates-A Neglected Class of Compounds: Crystal Structures of $M^{II}[BPO_5]$ (M^{II}:Ca, Sr) and $Ba_3[BP_3O_{12}]$. Angewandte Chemie International Edition in English 1994;33:749-751.

2. Kniep R, Engelhardt H and Hauf C, et al. A first approach to borophosphate structural chemistry. Chemistry of materials 1998;10:2930-2934.

3. Ewald B, Huang Y-X and Kniep R, et al. Structural chemistry of borophosphates, metalloborophosphates, and related compounds. Zeitschrift für Anorganische und Allgemeine Chemie 2007;633:1517-1540.

4. Kniep R, Will H G, Boy I and Röhr C, et al. 61 Helices from Tetrahedral Ribbons $[BP_2O_8^{3-}]$: Isostructural Borophosphates $M^IM^{II}(H_2O)_2[BP_2O_8]\cdot H_2O$ (M^I= Na, K; M^{II}= Mg, Mn, Fe, Co, Ni, Zn) and Their Dehydration to Microporous Phases $M^IM^{II}(H_2O)[BP_2O_8]$. Angewandte Chemie International Edition in English 1997;36:1013-1014.

5. Kniep R, Schafer G, Engelhardt H and Boy I, et al. $K[ZnBP_2O_8]$ and $A[ZnBP_2O_8]$ (A= NH^{4+}, Rb^+, Cs^+): Zincoborophosphates as a new class of compounds with tetrahedral framework structures. Angewandte Chemie International Edition 1999;38:3641-3644.

6. Kang Q-Y, Song Q, Li S-Y and Liu Z-H, et al. Thermodynamic properties of microporous materials for two borophosphates, $K[ZnBP_2O_8]$ and $NH_4[ZnBP_2O_8]$. The Journal of Chemical Thermodynamics 2014;69:43-47.

7. Yilmaz A, Bu X, Kizilyalli M and Stucky G D, et al. $Fe(H_2O)_2BP_2O_8.H_2O$, a First Zeotype Ferriborophosphate with Chiral Tetrahedral Framework Topology. Chemistry of materials 2000;12:3243-3245.

8. Shi Y, Liang J, Zhang H, Yang J, Zhuang W and Rao G, et al. X-Ray Powder Diffraction and Vibrational Spectra Studies of Rare Earth Borophosphates, $Ln_7O_6(BO_3)(PO_4)_2$ (Ln= La, Nd, Gd, and Dy). Journal of Solid State Chemistry 1997;129:45-52.

9. Shi Y, Liang J, Zhang H, Liu Q, Chen X, Yang J, Zhuang W and Rao G, et al. Crystal Structure and Thermal Decomposition Studies of Barium Borophosphate, $BaBPO_5$. Journal of Solid State Chemistry 1998;135:43-51.

10. Baykal A, Kizilyalli M, Gözel G and Kniep R, et al. Synthesis of Strontium Borophosphate, $SrBPO_5$ by Solid State and Hydrothermal Methods and Characterisation. Crystal Research and Technology 2000;35:247-254.

11. Yilmaz A, Bu X, Kizilyalli M, Kniep R and Stucky G D, et al. Cobalt borate phosphate, $Co_3[BPO_7]$, synthesis and characterization. Journal of Solid State Chemistry 2001;156:281-285.

12. Kritikos M, Wikstad E and Walldén K, et al. Hydrothermal synthesis, characterization and magnetic properties of three isostructural chain borophosphates; $NH_4M(III)[BP_2O_8(OH)]$ with M= V or Fe and $NH_4(Fe(III)_{0.53}V(III)_{0.47})[BP_2O_8(OH)]$. Solid State Sciences 2001;3:649-658.

13. Schäfer G, Carrillo-Cabrera W, Schnelle W, Borrmann H and Kniep R, et al. Synthesis and Crystal Structure of $\{(NH4)_xCo_{((3-x)/2)}\}(H_2O)_2[BP_2O_8]\cdot(1-x)H_2O$ ($x\approx 0.5$). Zeitschrift für Anorganische und Allgemeine Chemie 2002; 628:289-294.

14. Ge M-H, Mi J-X, Huang Y-X, Zhao J-T and Kniep R, et al. Crystal structure of sodium cadmium diaqua *catena*-[monoborodiphosphate]-hydrate, $NaCd(H_2O)_2[BP_2O_8]\cdot 0.8H_2O$. Zeitschrift für Kristallographie-New Crystal Structures 2003;218:165-166.

15. Ge M-H, Liu W, Chen H-H, Li M-R, Yang X-X and Zhao J-T, et al. $NH_4Cd(H_2O)_2(BP_2O_8)\cdot 0.72H_2O$: a New Borophosphate with Abnormal Structure Changes Caused by Hydrogen Interactions. Zeitschrift für Anorganische und Allgemeine Chemie 2005;631:1213-1217.

16. Ewald B, Öztan Y, Prots Y and Kniep R, et al. Structural Patterns and Dimensionality in Magnesium Borophosphates: The Crystal Structures of $Mg_2(H_2O)[BP_3O_9(OH)_4]$ and $Mg(H_2O)_2[B_2P_2O_8(OH)_2]\cdot H_2O$. Zeitschrift für Anorganische und Allgemeine Chemie 2005;631:1615-1621.

17. Menezes P W, Hoffmann S, Prots Y, Schnelle W and Kniep R, et al. Preparation and characterization of the layered borophosphates $M^{II}(H_2O)_2[B_2P_2O_8(OH)_2]\cdot H_2O$ (M^{II}=Fe, Co, Ni). Inorganica Chimica Acta 2010;363:4299-4306.

18. Yilmaz A, Tatar Yildirim L, Bu X, Kizilyalli M and Stucky G D, et al. New zeotype borophosphates with chiral tetrahedral topology:$(H)_{0.5}M_{1.25}(H_2O)_{1.5}[BP_2O_8]\cdot H_2O$ (M= Co(II) and Mn(II)). Crystal Research and Technology: Journal of Experimental and Industrial Crystallography 2005;40:579-585.

19. Birsoz B, Baykal A, Toprak M and Koseoglu Y, et al. Synthesis, characterization and magnetic investigation of $(NH_4)_{0.5}Mn_{1.25}(H_2O)_2[BP_2O_8]\cdot_{0.5}H_2O$. Open Chemistry 2007;5(2):536-545.

20. Xiong D-B, Chen H-H, Yang X-X and Zhao J-T, et al. Low-temperature flux syntheses and characterizations of two 1-D anhydrous borophosphates: $Na_3B_6PO_{13}$ and $Na_3BP_2O_8$. Journal of Solid State Chemistry 2007;180:233-239.

21. Raskar D B, Eckert H, Ewald B and Kniep R, et al. Characterization of Local Environments in Crystalline Borophosphates Using Single and Double Resonance NMR. Solid State Nuclear Magnetic Resonance 2008;34:20-31.

22. Menezes P W, Hoffmann S, Prots Y, Schnelle W and Kniep R, et al. Synthesis and Crystal Structure of $SrFe[BP_2O_8(OH)_2]$. Zeitschrift für Anorganische und Allgemeine Chemie 2009; 635:1153-1156.

23. Zhao D, Cheng W-D, Zhang H, Huang S-P, Xie Z, Zhang W-L and Yang S-L, et al. $KMBP_2O_8$(M= Sr, Ba): A New Kind of Noncentrosymmetry Borophosphate with the Three-Dimensional Diamond-Like Framework. Inorganic Chemistry 2009;48:6623-6629.

24. Yang M, Chen P and Welz-Biermann U, et al. Synthesis, Crystal Structure, and Characterization of a New Metal Borophosphate: $Pb^{II}_4\{Co_2[B(OH)_2P_2O_8](PO_4)_2\}Cl$. Zeitschrift für Anorganische und Allgemeine Chemie 2010;636:1454-1460.

25. Zhang W-L, Lin C-S, Geng L, Li Y-Y, Zhang H, He Z-Z and Cheng W-D, et al. Synthesis and Characterizations of Two Anhydrous Metal Borophosphates: $M_2^{III}BP_3O_{12}$ (M=Fe, In). Journal of Solid State Chemistry 2010;183:1108-1113.

26. Zhou Y, Hoffmann S, Huang Y-X, Prots Y, Schnelle W, Menezes P W, Carrillo-Cabrera W, Sichelschmidt J, Mi J-X and Kniep R, $K_3Ln[OB(OH)_2]_2[HOPO_3]_2$ (Ln= Yb, Lu): Layered rare-earth dihydrogen borate monohydrogen phosphates. Journal of Solid State Chemistry 2011;184:1517-1522.

27. Yang W, Li J, Xu J, Xing H, Wang L, Yu J and Xu R, et al. Hydrothermal synthesis of isostructural open-framework manganese and iron borophosphates: Effect of the organic templates in determining the pore shapes. Solid State Sciences 2011;13:757-761.

28. Wang Y, Pan S and Shi Y, et al. Further Examples of the P-O-P Connection in Borophosphates: Synthesis and Characterization of $Li_2Cs_2B_2P_4O_{15}$, $LiK_2BP_2O_8$, and $Li_3M_2BP_4O_{14}$ (M=K, Rb). Chemistry–A European Journal 2012;18:12046-12051.

29. Duan R, Liu W, Cao L, Su G, Xu H and Zhao C, et al. A new copper borophosphate with novel polymeric chains and its structural correlation with raw materials in molten hydrated flux synthesis. Journal of Solid State Chemistry 2014;210:60-64.

30. Li H, Zhao Y, Pan S, Wu H, Yu H, Zhang F, Yang Z and Poeppelmeier K R, et al. Synthesis and Structure of $KPbBP_2O_8$ – A Congruent Melting Borophosphate with Nonlinear Optical Properties. European Journal of Inorganic Chemistry, 2013;2013:3185-3190.

31. Hasegawa T and Yamane H, Synthesis, Crystal Structure and Lithium Ion Conduction of $Li_3BP_2O_8$. Dalton Transactions 2014;43:2294-2300.

32. Liu W, Guo X-Q, Su G, Cao L-X, Wang Y-G and Duan J-R, et al. A new organically-templated cobalt borophosphate with a novel borophosphatic anionic partial structure. Journal of Solid State Chemistry 2011;184:2538-2542.

33. Hauf C, Yilmaz A, Kizilyalli M and Kniep R, et al. Borophosphates: Hydrothermal and microwave-assisted synthesis of $Na_5[B_2P_3O_{13}]$. Journal of Solid State Chemistry 1998;140:154-156.

34. Cotton F A, Wilkinson G, Murillo C A, Bochmann M, et al. Advanced Inorganic Chemistry (6^{th} ed.), New York: Wiley-Interscience 1999.

35. Touaiher M, Rissouli K, Benkhouja K, Taibi M, Aride J, Boukhari A and Heulin B, et al. Crystal Structures and Magnetic Properties of $M_2V_2O_7$ (M = Co, Ni and Cu) Compounds. Materials Chemistry and Phisics 2004;85:41-46.

36. He Z, Yamaura J, Ueda Y and Cheng W, et al. Magnetic properties of $Co_2V_2O_7$ single crystals grown by flux method. Journal of Solid State Chemistry 2009;182:2526-2529.

37. Liao J H, Leroux F, Payen C, Guyomard D and Piffard Y, et al. Synthesis, Structures, Magnetic Properties, and Phase Transition of Manganese(II) Divanadate: $Mn_2V_2O_7$. Journal of Solid State Chemistry 1996;121:214-224.

38. He Z and Ueda Y, Magnetic properties of $Mn_2V_2O_7$ single crystals. Journal of Solid State Chemistry 2008;181:235-238.

39. Salah A A, Benkhouja K, Jaafari K, Paz J R, Climent E and Puche R S, et al. Structural Characterization and Magnetic Properties of Divanadates $ZnMV_2O_7$ (M = Co, Ni and Cu). Journal of Alloys and Compounds 2005;402:213-218.

40. Krivovichev S V, Filatov S K and Cherepansky P N, et al. Crystal structure of γ-$Cu_2V_2O_7$ and its comparison to blossite (α- $Cu_2V_2O_7$) and ziesite (β-$Cu_2V_2O_7$). Canadian Mineralogist 2005;43:671-677.

41. Robinson P D, Hughes J M and Malinconico M L, et al. Blossite, α-$Cu_2^{2+}V_2^{5+}O_7$, a new fumarolic sublimate from Izalco volcano, El Salvador. American Mineralogist 1987;72:397-400.

42. Hughes J M and Birnie R W, Ziesite, β- $Cu_2V_2O_7$, A New Copper Vanadate and Fumarole Temperature Indicator. American Mineralogist 1980;65:1146-1149.

43. Brisi C and Molinari A, II Sistema Ossido Ramicoanidride Vanadica. Annali di Chimica, Roma, 1958;64:263-269.

44. Fleury P, Sur le Systeme CuO-V2O5. Comptes Rendus de l Academie des Sciences 1966;263:1375-1377.

45. Calvo C and Faggiani R, α Cupric Divanadate. Acta Crystallogr. B 1975;31:603-605.

46. Mercurio-Lavaud D and Frit M B, Crystal-Structure of High-Temperature Variety of Copper Pyrovanadate, Beta $Cu_2V_2O_7$. Comptes Rendus Hebdomadaires Des Seances De L Academie Des Sciences Serie C 1973;277:1101-1104.

47. Sivakumar V, Suresh R, Giribabu K, Manigandan R, Munusamy S, Praveen Kumar S, Muthamizh S and Narayanan V, et al. Copper Vanadate Nanoparticles: Synthesis, Characterization and its Electrochemical Sensing Property. Journal of Materials Science: Materials in Electronics 2014;25:1485-1491.

48. Buckley A M, Bramwell S T, Day P and Visser D, et al. The Magnetic Properties and Structures of the Transition Metal Pyroarsenates $M_2As_2O_7$ *(M=Ni, Co, Mn)*. Journal of Solid State Chemistry 1995;115:229-235.

49. Ponomarenko L A, Vasil'ev A N, Antipov E V and Velikodny Y A, et al. Magnetic Properties of $Cu_2V_2O_7$. Physica B 2000;284:1459-1460.

50. Kim E S, Noh S H, Kim S B, Kang S G and Kim P K, et al. Effect of $Cu_2V_2O_7$ on the Microwave Dielectric Properties of BiTaO4 Ceramics. Ferroelectrics 2001;257:181-188.

51. Hikazudani S, Kikutani K, Nagaoka K, Inoue T and Takita Y, et al. Anaerobic Oxidation of Isobutane I.Catalysis by Cu-V Complex Oxides. Applied Catalysis A: General, 2008;345:65-72.

52. Bhatia S N, Mohapatra N, Nirmala R and Malik S K, et al. The Effect of Spin Dilution on Magnetism of the Linear Chain System β-$Cu_{2-x}Zn_xV_2O_7$. Pramana-Journal of Physics 2010;74:833-843.

53. Sanchez-Andujar M, Yanez-Vilar S, Mira J, Biskup N, Rivas J, Castro-Garcia S and Senaris-Rodriguez M A, et al. Role of the magnetic ordering on the dielectric response of $M_2V_2O_7$ (M=Co and Cu). Journal of Applied Physics 2011;109:054106.

54. Camargo L P, Lucilha A C, Gomes G A B, Liberatti V R, Andrello A C, da Silva P R C and Antonia L H D, et al. Copper pyrovanadate electrodes prepared by combustion synthesis: evaluation of photoelectroactivity. Journal of Solid State Electrochemistry 2020;24:1935-1950.

55. Kar A K, Chattopadhyay B, Singha R, Barman A, Ahmed M A, Midya A, Bandyopadhyay S, Mukherjee D, Jana D and Mandal P, et al. Effect of Co and Mg doping at Cu site on structural, magnetic and dielectric properties of α-$Cu_2V_2O_7$. Journal of Physics: Condensed Matter 2022;34:075702(13pp).

56. Tsirlin A A, Janson O and Rosner H, et al. β-$Cu_2V_2O_7$: a spin -1/2 honeycomb lattice system. Physical Review B. 2010;82:144416

57. Schindler M and Hawthorne F C, Structural Characterization of the β-$Cu_2V_2O_7$ - α-$Zn_2V_2O_7$ Solid Solution. Journal of Solid State Chemistry 1999;146:271-276.

58. Kataev V, Pommer J, Choi K Y, Lemmens P, Lonescu A, Pashkevich Y, Lamonova K, Möller A, Freimuth A and Güntherodt G, et al. Magnetic exchange in a low-dimensional complex oxide (Cu, $Zn)_2V_2O_7$. Journal of Magnetism and Magnetic Materials 2004;272:933-934.

59. Baba Ali E, Bernede J C and Guyomard D, et al. $Ni_2V_2O_7$ thin films for negative electrode application of rechargeable microbatteries. Thin Solid Films 2002;402:215-221.

60. Schwendt P, Dudasova D, Chrappova J, Drabik M and Marek J, et al. Synthesis, Structure and Thermal Decomposition of $[Ni(NH_3)_6][VO(O_2)_2(NH_3)]_2$. Journal of Thermal Analysis and Calorimetry 2008;91:293-297.

61. Almukhlifi H A and Burns R C, Oxidative dehydrogenation of isobutane to isobutene by pyrovanadates, $M_2V_2O_7$, where M(II) = Mn, Co, Ni, Cu and Zn, and Co_2VO_4 and ZnV_2O_4: The effect of gold nanoparticles. Journal of Moleculer Catalysis A: Chemical 2015;408:26-40.

62. Baba Ali E, Bernede J C and Le Ray P, et al. Vanadium transition metal oxide films obtained by annealing under room atmosphere of metal layers sequentially deposited. Journal of Crystal Growth 2000;208:471-481.

63. He Z and Ueda Y, Flux growth of β-$Mn_2V_2O_7$ single crystals. Journal of Crystal Growth 2008;310:171-173.

64. He Z, Ueda Y and Itoh M, et al. Martensitic-like transition in $Mn_2V_2O_7$ single crystals. Solid State Communications 2008;147:138-140.

65. Krasnenko T I and Rotermel M V, Structural Modification of $Mn_2V_2O_7$: Thermal Expansion and Solid Solutions. Russian Journal of General Chemistry 2013;83:(9)1640-1644.

66. Sheetal, Taxak V B and Khatkar S P, et al. Synthesis and Luminescent Properties of $M_2V_2O_7$:Eu (M=Sr, Ba) Nanophosphors. Journal of Fluorescence, 2012;22:891-897.

67. Taxak V B, Sheetal, Dayawati and Khatkar S P, et al. Synthesis, Structural and Optical Properties of Eu^{3+}-doped $Ca_2V_2O_7$ Nanophosphors. Current Applied Physics 2013;13:594-598.

68. Nakajima T, Isobe M, Tsuchiya T, Ueda Y and Manabe T, et al. Photoluminescence property of vanadates $M_2V_2O_7$ (M=Ba, Sr and Ca). Optical Materials 2010;32:1618-1621.

69. Xiaoke H, Chenjun Z and Ding T, et al. The Structure, Vibrational Spectra and Thermal Expansion Study of AVO_4 (A=Bi, Fe, Cr) and $Co_2V_2O_7$. Materials 2020;13:1628.

70. Cowin P I, Lan R, Petit C T G, Zhang L and Tao S, et al. Conductivity and stability of cobalt pyrovanadate. Journal of Alloys and Compounds 2011;509:4117-4121.

71. Grzechnik A and McMillan P F, High pressure behavior of $Sr_3(VO_4)_2$ and $Ba_3(VO_4)_2$. Journal of Solid State Chemistry, 1997a;132:156-162.

72. Grzechnik A and McMillan P F, In Situ High Pressure Raman Spectra of $Ba_3(VO_4)_2$. Solid State Communications 1997b;102:569-574.

73. Merkle L D, Pinto A, Verdun H and McIntosh B, et al. Laser Action from Mn^{5+} in $Ba_3(VO_4)_2$. Applied Physics Letters 1992;61:2386-2388.

74. Buijsse B, Schmidt J, Chan I Y, and Singel D J, et al. Electron Spin-Echo-Detected Excitation Spectroscopy of Manganese-Doped $Ba_3(VO_4)_2$ – Identification of Tetrahedral Mn^{5+} as the Active Laser Center. Physical Review B 1995;51:6215-6220.

75. Zhuravlev V D and Fotiev A A, et al. Isomorphism of Calcium, Strontium and Barium Ortho-Vanadates. Zhurnal Neorganicheskoi Khimii 1980;25:2560-2562.

76. Qureshi N, Fuess H, Ehrenberg H, Ouladdiaf B, Carvajal J R, Hansen T C, Wolf T, Meingast C, Zhang Q, Knafo W and Löhneysen H, et al. Magnetic structure of the kagome mixed compound $(Co_{0.5}Ni_{0.5})_3V_2O_8$. Journal of Physics: Condensed Matter 2008;20: 235228(6pp).

77. Rogado N, Haas M K, Lawes G, Huse D A, Ramirez A P and Cava R J, et al. β-$Cu_3V_2O_8$: magnetic ordering in a spin-1/2 Kagome-staircase lattice. Journal of Physics: Condensed Matter 2003;15:907-914.

78. Rao N S and Palanna O G, Phase transitions in copper(II) orthovanadate. Bulletin of Materials Science 1993;16:261-266.

79. Arani M G, Arani M M and Niasari M S, et al. Facile synthesis, characterization and optical properties of copper vanadate nanostructures for enhanced photocatalytic activity. Journal of Materials Science: Materials in Electronics, 2016;27:4871-4878.

80. Rahni S Y and Kakhki R M, Facile and green synthesis of $Cu_3V_2O_8$ nanostructures via Moringa peregrina natural extract as a high performance photo catalyst. Applied Organometallic Chemistry 2019;e5392:1-8.

81. He Z, Ueda Y and Itoh M, et al. Crystal growth of $Ni_3V_2O_8$ by flux method. Journal of Crystal Growth 2006;297:1-3.

82. He Z, Yamaura J I, and Ueda Y, Morphologies of $Ni_3V_2O_8$ Single Crystals. Crystal Growth & Design 2008;8:799-801.

83. Sudakar C, Kharel P, Naik R and Lawes G, et al. Synthesis and characterization of thin film multiferroic $Ni_3V_2O_8$. Philosophical Magazine Letters 2007;87:223-229.

84. Balakrishnan G, Petrenko O A, Lees M R and Paul D M K, et al. Single crystals of the anisotropic Kagome staircase compounds $Ni_3V_2O_8$ and $Co_3V_2O_8$. Journal of Physics: Condensed Matter 2004;16:L347-L350.

85. Szymczak R, Baran M, Fink-Finowicki J, Krzymanska B, Aleshkevych P, Szymczak H, Barilo S N, Bychkov G L and Shiryaev S V, et al. Geometrically frustrated Kagome staircase lattice with chemical disorder. Journal of Non-Crystalline Solids 2008;354:4186-4188.

86. Celik G and Kurtulus F, Novel Route to Prepare Magnetic Material $Co_3V_2O_8$ and Structural Characterization. Acta Physica Polonica A 2012;121:203-204.

87. Fritsch K, Ramazanoglu M, Dabkowska H A and Gaulin B D, et al. Crystal growth and characterization of the magnetically dilute kagome staircase system $(Co_{(1-x)}Mg_x)_3V_2O_8$. Journal of Crystal Growth 2011;327:205-208.

88. Lin Z Q, Yang M, Wang H W, Guo Q, Liu Y J, Han X T, Han Y B, Wang J F, He Z Z and Kindo K, et al. High-magnetic-field phase transitions and H-T phase diagram of the Kagome-staircase compound $Ni_3V_2O_8$. Journal of Magnetism and Magnetic Materials 2015;382:7-9.

89. Qureshi N, Fuess H, Ehrenberg H, Hansen T C, Ritter C, Adelmann P, Meingast C, Wolf T, Zang Q and Knafo W, et al. The magnetic composition-temperature phase diagram of the kagome mixed system $(Co_xNi_{1-x})_3V_2O_8$. Journal of Physics: Condensed Matter 2008;20:095219 (5pp).

90. Sambandam B, Soundharrajan V, Song J, Kim S, Jo J, Pham D T, Kim S, Mathew V, Kim K H, Sun Y K and Kim J, et al. $Ni_3V_2O_8$ nanoparticles as an excellent anode material for high-energy lithium-ion batteries. Journal of Electroanalytical Chemistry 2018;810:34-40.

91. Wilson N R, Petrenko O A and Balakrishnan G, et al. Magnetic phase diagrams of the Kagome staircase compounds $Co_3V_2O_8$ and $Ni_3V_2O_8$. Journal of Physics: Condensed Matter 2007;19:145257 (6pp).

92. Kurzawa M and Blonska-Tabero A, Phase Equilibria In The System NiO-V_2O_5-Fe_2O_3 In Subsolidus Area. Journal of Thermal Analysis and Calorimetry 2004;77:65-73.

93. Salvia N D, Malavasi M P, Salvia G D and Vaccari A, et al. Formation of Ni and Mg vanadates during the flameless oxy-combustion of heavy fuels. Fuel Processing Technology 2015;138:534-539.

94. Liu M C, Kong L B, Kang L, Li X, Walsh F C, Xing M, Lu C, Ma X J and Luo Y C, et al. Synthesis and characterization of $M_3V_2O_8$ (M=Ni or Co) based nanostructures: a new family of high performance pseudocapacitive materials. Journal of Materials Chemistry A 2014;2:4919-4926.

95. He Z, Taniyama T, Itoh M and Ueda Y, et al. Flux Growth and Magnetic Anomalies of $Co_3V_2O_8$ Crystals. Crystal Growth & Design 2007;7:1055-1057.

96. Chai H, Wang Y, Fang Y, Lv Y, Dong H, Jia D and Zhou W, et al. Low-cost synthesis of hierarchical $Co_3V_2O_8$ microspheres as high-performance anode materials for lithium-ion batteries. Chemical Engineering Journal 2017;326:587-593.

97. Zhang Q, Pei J, Chen G, Bie C, Chen D, Jiao Y and Rao J, et al. $Co_3V_2O_8$ Hexagonal Pyramid with Tunable Inner Structure as High Performance Anode Materials for Lithium Ion Battery. Electrochimica Acta 2017;238:227-236.

98. Bellido N, Martin C, Simon C and Maignan A, et al. Coupled negative magnetocapacitance and magnetic susceptibility in a Kagome staircase-like compound $Co_3V_2O_8$. Journal of Physics: Condensed Matter 2007;19:056001(7pp).

99. Qureshi N, Fuess H, Ehrenberg H, Hansen T C and Schwabe D, et al. Magnetic phase transitions and structures of $Co_3V_2O_8$. Solid State Communications 2007;142:169-172.

100. Luitel H N, Chand R, Torikai T, Yada M and Watari T, et al. Rare Earth $Zn_3V_2O_8$ Phosphor with Controlled Microstructure and Its Photocatalytic Activity. International Journal of Photoenergy 2013;410613(9pages).

101. Sambandam B, Soundharrajan V, Song J, Kim S, Jo J, Pham D T, Kim S, Mathew V and Kim J, et al. $Zn_3V_2O_8$ porous morphology derived through a facile and green approach as an excellent anode for high-energy lithium ion batteries. Chemical Engineering Journal 2017;328:454-463.

102. Wang X, Liu Z, Ambrosini A, Maignan A, Stern C L, Poeppelmeier K R and Dravid V P, et al. Crystal growth, structure, and properties of manganese orthovanadate $Mn_3(VO_4)_2$. Solid State Sciences 2000;2:99-107.

103. Koc H, Palaz S, Mamedov A M and Ozbay E, et al. Electronic and elastic properties of the multiferroic crystals with the Kagome type lattices -$Mn_3V_2O_8$ and $Ni_3V_2O_8$: First principle calculations. Ferroelectrics 2019;544:11-19.

104. Clemens O, Rohrer J and Nenert G, et al. Magnetic structures of the low temperature phase of $Mn_3(VO_4)_2$ – towards understanding magnetic ordering between adjacent Kagomé layers. Dalton Transactions 2016;45:156-171.

105. Kesari S, Garg A B, Clemens O, Joseph B and Rao R, et al. Pressure-Induced Structural Behavior of Orthorhombic $Mn_3(VO_4)_2$: Raman Spectroscopic and X‑ray Diffraction Investigations. ACS Omega 2022;7:3099-3108.

106. Nakajima T, Isobe M, Tsuchiya T, Ueda Y and Kumagai T, et al. A revisit of photoluminescence property for vanadate oxides AVO_3 (A:K,Rb and Cs) and $M_3V_2O_8$ (M:Mg and Zn). Journal of Luminescence 2009;129:1598-1601.

107. Wang X, Zhang H, Sinkler W, Poeppelmeier K R and Marks L D, et al. Reduction of magnesium orthovanadate $Mg_3(VO_4)_2$. Journal of Alloys and Compounds 1998;270:88-94.

108. Xia Q, Obana Y, Nishiguchi H, Ito M, Ishihara T and Takita Y, et al. Oxidation of Isobutane over Complex Oxides Containing V and $Mg_2V_2O_7$ Catalysts Partially Substituted by Transition Metal Ions. Journal of the Japan Petroleum Institute 2003;46:87-92.

109. Soenen V, Herrmann J M and Volta J C, et al. *In Situ* Electrical Characterization of Magnesium Vanadate Reference Phases (meta-MgV_2O_6, pyro-$Mg_2V_2O_7$, and ortho-$Mg_3V_2O_8$) Used in Oxidative Dehydrogenation of Propane to Propene. Journal of Catalysis 1996;159:410-417.

110. Umemura R, Ogawa H, Yokoi A, Ohsato H and Kan A, et al. Low-temperature sintering-microwave dielectric property relations in $Ba_3(VO_4)_2$ ceramic. Journal of Alloys and Compounds 2006;424:388-393.

111. Parhi P, Manivannan V, Kohli S and McCurdy P, et al. Synthesis and Characterization of $M_3V_2O_8$(M=Ca, Sr and Ba) by a solid-state metathesis approach. Bulletin of Materials Science 2008;31:885-890.

112. Slobodin B V, Surat L L, Samigullina R F, Ishchenko A V, Cherepanov A N and Shul'gin B V, et al. Thermal Stability and Cathodoluminescence of Potassium Strontium Vanadates. Inorganic Materials 2009;45:428-431.

113. Zhang H, Lu M, Yang Z, Xiu Z, Zhou G, Wang S, Zhou Y and Wang S, et al. Effect of Processing Parameters on the Luminescence Intensity of $Sr_3(VO_4)_2$:Eu^{3+} Nanocrystals via Combustion Synthesis. Journal of Alloys and Compounds 2006;426:384-389.

114. Subramania A, Angayarkanni N, Karthick S N and Vasudevan T, et al. Combustion synthesis of inverse spinel $LiNiVO_4$ nano-particles using gelatine as the new fuel. Materials Letters 2006;60:3023-3026.

115. Bhatkar V B, Omanwar S K and Moharil S V, et al. Combustion Synthesis of the Zn_2SiO_4:Mn Phosphor. Physica Status Solidi 2002;191:(1) 272-276.

116. Ekambaram S and Patil K C, Synthesis and properties of Eu2+ activated blue phosphors. Journal of Alloys and Compounds 1997;248:7-12.

117. Tyagi A K, Combustion Synthesis: A Soft-Chemical Route For Functional Nano-Ceramics. Barc Newsletter 2007;285:39-48.

118. Altuntaş Öztaş N and Erdoğan H, Synthesis and Characterization of Magnesium Pyroborate by Solution Combustion and Conventional Ceramic Methods: A Comparative Study. Zeitschrift für Anorganische und Allgemeine Chemie 2009;635:1626-1632.

119. Bhatkar V B and Bhatkar N V, Combustion synthesis and photoluminescence study of silicate biomaterials. Bulletin of Materials Science 2011;34:1281-1284.

120. Benmokhtar S, Jazouli A E, Chaminade J P, Gravereau P, Menetrier M and Bouree F, et al. New process of preparation, structure and physicochemical investigations of the new titanyl phosphate $Ti_2O(H_2O)(PO_4)_2$. Journal of Solid State Chemistry 2007;180:2713-2722.

121. Hillel T and Ein-Eli Y, Copper Vanadate as Promising High Voltage Cathodes for Li Thermal Batteries. Journal of Power Sources 2013;229:112-116.

122. Slobodin B V and Samigullina R F, Thermoanalytical Study of the Polymorphism and Melting Behavior of $Cu_2V_2O_7$. Inorganic Materials 2010;46:196-200.

123. Arani M G, Arani M M and Niasari M S, et al. Size controllable synthesis of cobalt vanadate nanostructures with enhanced photocatalytic activity for the degradation of organic dyes. Journal of Molecular Catalysis A: Chemical 2016;425(15):31-42.

124. Frederickson L D and Hausen D M, Infrared Spectra-Structure Correlation Study of Vanadium-Oxygen Compounds. Analytical Chemistry 1963;35:7.

125. Clark, G. M., & Pick, A. N. (1975). Dta study of the reactions of V_2O_5 with metal (II) oxides. *Journal of thermal analysis*, *7*(2), 289-300.